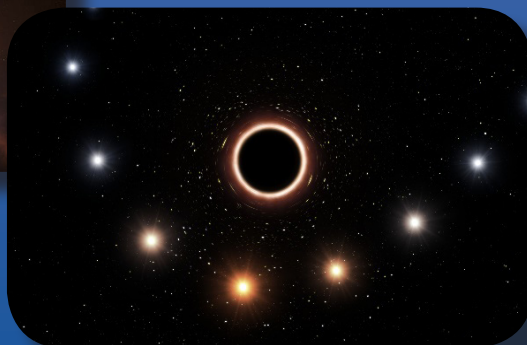
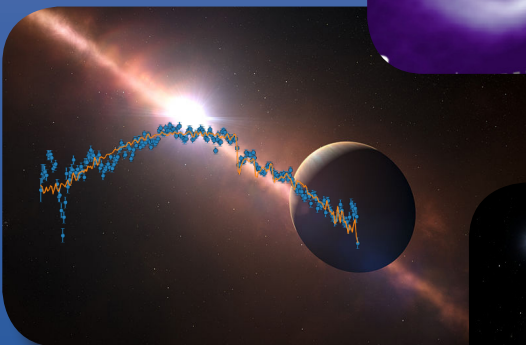
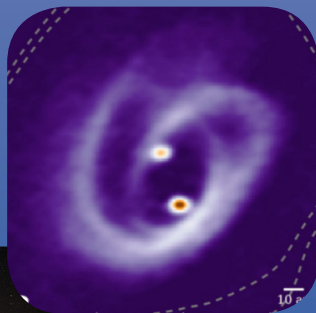


Science Report 2016 - 2018



Max Planck Institute for Extraterrestrial Physics



A photomontage of major instrumental developments - eROSITA (upper left) and NISP-Euclid (upper right) - and recent MPE science results - Galactic Center black hole, Active Galactic Nuclei, exoplanets, protoplanetary disks.



Report 2016 - 2018

MPE Science Report

Imprint

Responsible for contents: P. Caselli
Editors and Layout: W. Collmar, B. Niebisch
Text and Figure Contributions: MPE Science and Research Groups

1. Edition June 2019

Table of Contents

Preface	5
1 Research Areas and Institute Structure	9
2 Infrared and Submillimeter Astronomy	15
3 Optical and Interpretative Astronomy	55
4 High-Energy Astrophysics	81
5 Center for Astrochemical Studies	111
6 Independent Research Groups	139
7 The Institute	145

PREFACE

It is impressive to see the great scientific advances done at MPE in the past three years and I have the honor to present them this year. At MPE, large experiments are built for space and ground-based telescopes, allowing revolutionary new views in the fields of star and planet formation, galaxy structure and evolution, black holes, compact objects, dark energy.

During the last Scientific Advisory Board (SAB), the IR group presented GRAVITY in its astounding details; now, even more astounding results from this second-generation VLTI instrument are presented. GRAVITY has delivered precision tests of Einstein's General Theory of Relativity by measuring the motion of a star passing through the extreme gravitational field near the supermassive black hole at the center of our Galaxy. GRAVITY has also started to give spectacular contribution to the study of external galaxies, by unveiling their ionized gas and hot dust at sub-parsec scales. GRAVITY has recently provided high-quality atmospheric spectra of two young exoplanets, surpassing classical coronagraphic spectroscopy methods. The superb sensitivity of GRAVITY and its unsurpassed high precision astrometry, polarimetry and spectroscopy, makes it a highly versatile instrument, which can be used by different astrophysical communities for new detailed views of external galaxies, young stars and exoplanets.

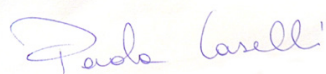
Meanwhile, the IR group is leading the design and construction of MICADO, the near-infrared first-light imager for the 39m European Extremely Large Telescope, expected to start operations around 2026. MICADO will be able to resolve stellar populations in the local universe and allow detailed studies of the very first galaxies at high redshift.

An exciting news from the HE group is the completion and upcoming launch of eROSITA, expected to fly on June 21st this year. eROSITA will perform the first imaging all-sky survey in the medium energy X-ray range with unprecedented spectral and angular resolution, allowing (among other things) detailed studies of the hot intergalactic medium, the Galactic X-ray source populations and the detection of all obscured accreting black holes in nearby galaxies. At the same time, the HE group is focusing on the completion of Athena, the next-generation X-ray observatory, due for launch in the early 2030s.

The OPINAS group has recently completed the optics for the EUCLID Near-Infrared Spectrometer and Photometer (NISP), surpassing the required specifications. EUCLID will be launched in 2022 and, by mapping the universe more accurately than ever before, it will allow scientists to get valuable insights on dark energy and dark matter.

In my CAS group, we have switched on most of our laboratory facilities, providing new insights on molecular species relevant for astrochemistry and starting to have a close look on the physical properties of interstellar-ice analogues. All this in close contact with CAS observers and theoreticians, with the final goal of unveiling the physical and chemical processes which drive interstellar clouds into stars like our Sun and planets like our Earth, where life is thriving.

I feel extremely fortunate to work at MPE, where excellent colleagues and bright young researchers and students make my every-day life an exciting experience.



Paola Caselli
Managing Director of the
Max Planck Institute for Extraterrestrial Physics

1 Research Areas and Institute Structure



1 Research Areas and Institute Structure

The Max Planck Institute for Extraterrestrial Physics (MPE, Fig. 1.1) is located on the University and Research Campus in Garching, near Munich, a vibrant environment with major research institutes in physics and astrophysics. Our Institute performs basic research in astrophysics, with particular emphasis on the following science areas:

- Astrochemistry, gas and dust processes in the Interstellar Medium
- Star and planet formation
- Compact Objects
- The Galactic Centre
- Active galactic nuclei
- Galaxy formation & evolution
- Galaxy-black hole co-evolution
- Galaxy clusters & large scale structure
- Cosmology and Dark Energy

To further our research aims, we combine hardware development with observations, data analysis, laboratory and theoretical work. Our experimental work in astrophysics is driven by our scientific interests and focuses on a relatively small number of key projects, spanning a broad range of the electromagnetic spectrum from the millimeter/submm, through infrared (IR) and optical-infrared wavelengths, to the X- and γ -ray bands (Fig. 1.2).

In many cases the observations must be made from space, and MPE has a proud history and reputation as Germany's premier space astrophysics Institute. Current satellites such as XMM-Newton, Chandra, Integral, Fermi and Swift feature MPE hardware contributions, as did the Herschel mission. We are preparing eROSITA for launch and are developing hardware for future space facilities, in particular Euclid and Athena. Most of these projects are implemented in collaboration with the Euro-

pean Space Agency (ESA), the German Space Agency (DLR), or NASA.

In parallel we build and use instruments on the ground. In the near infrared and optical bands MPE has developed and exploited ground-based instruments at the Very Large Telescopes (VLTs) of the European Southern Observatory (ESO), the Large Binocular Telescope (LBT) and others. MPE leads the development of MICAADO, one of the first-light instruments for ESO's Extremely Large Telescope (ELT). In the mm range we are very active users of the telescopes of the Institute for Radio Astronomy in the Millimetre Range (IRAM), located in the Alps and in Spain, and the Atacama Large Millimetre Array (ALMA), located at high altitudes in the Atacama desert in Chile. Our experimental and observational work is complemented by analytical, numerical and observation-related interpretational work and theory. Several laboratory astrophysics experiments study molecules and dust as part of the CAS group activities.

Our scientific activities are organised into four major research fields, each of which is led by one of the Directors: (1) Infrared- and Submillimeter Astronomy (IR, Prof. Reinhard Genzel), (2) Optical and Interpretative Astronomy (OpInAs, Prof. Ralf Bender), (3) High-Energy Astrophysics (HE, Prof. Kirpal Nandra), (4) The Centre for Astrochemical Studies (CAS, Prof. Paola Caselli). The main departments often host quasi-autonomous research groups concentrating on particular sub-fields, supported either by internal (MPG) or external, third party funds. The Institute also currently hosts a Max Planck Fellow, Prof. Joe Mohr. Close collaboration continues with the former Max Planck Fellowship holder Prof. Andreas Burkert.

While many of the major projects are driven at group

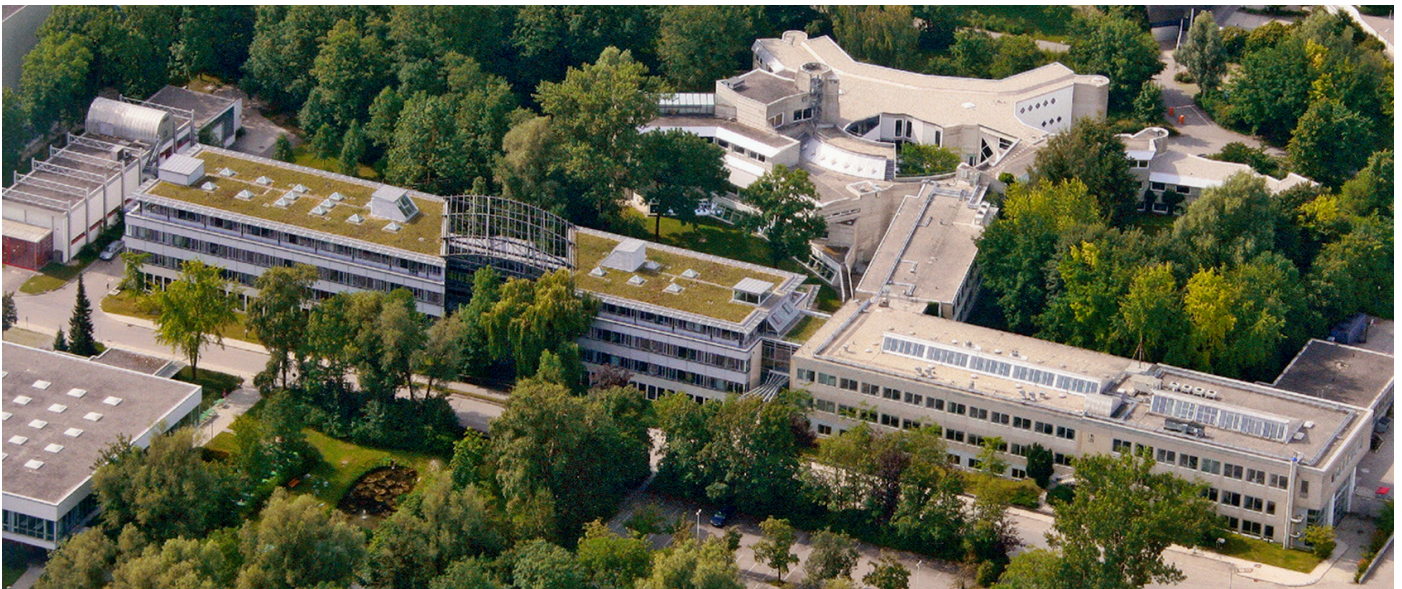


Fig. 1.1 MPE (front) and MPA (background) buildings in Garching. The MPE building houses the vast majority of our 350+ staff of scientists, engineers, and technical, administrative and support personnel.



Fig. 1.2 Scientists at MPE build and exploit state-of-the-art astronomical instruments and telescopes, both ground and space-based and across the whole span of the electromagnetic spectrum.

level, there are significant scientific synergies and collaborations in place between the different groups. The IR and OpInAs groups recently completed the KMOS3D galaxy evolution survey. Their joint instrument development continues with MICADO for the ELT. Star and planet formation processes and scaling laws from the smallest scales up to high redshift galaxies are being studied in the CAS group, the IR group, and the group of Ewine van Dishoeck. Andreas Burkert's group has a strong collaboration with the IR group, focussed on the dynamics of high redshift galaxies and gas clouds in the Galactic Center. The High Energy group and IR group have worked jointly on AGN hosts and their star formation properties, in particular during the Herschel mission, and study the multi-wavelength properties and physics of Galactic Center flares. Complementary routes to explore the nature of Dark Energy are pursued by HE (eROSITA

clusters, in collaboration with MPG fellow Joe Mohr) and OpInAs (Euclid weak lensing and baryonic acoustic oscillations), a synergy that extends to the collection of ancillary data and follow-up preparation for these missions. HE and OpInAs are also jointly studying AGN variability. Research programs at MPE are often organized into integrated project groups, which include scientists, post-docs, students from the main groups, and staff from the Institute's central support divisions. These central divisions play a key role in the development of our ambitious instruments and experiments and primarily consist of mechanical and electronic engineering staff and their associated work-shops. We are also engaged in the development of software packages for the analysis of large amounts of data yielded by our instruments, and for instrument control. A central IT division assists in these efforts, while also supporting our computer hardware and



Fig. 1.3 PANTER, a unique X-ray optics calibration and test facility, located in Neuried, South-West Munich. The eROSITA telescope is entering the PANTER vacuum chamber for the end-to-end test.

networking infrastructure. A highly efficient administration and a technical and building services team, which also serve the neighbouring Max Planck Institute for Astrophysics and the Max Planck Computing and Data Facility, complete the team on campus in Garching. Off-campus, a key facility of the High-Energy Astrophysics Group, is the PANTER X-ray test facility located in Neuried (Fig. 1.3).

The implementation of most of our experimental projects requires close cooperation with industry, both locally in the Munich area as well as all over Europe and worldwide. Our 50-year record of success in astrophysics and space research demonstrates the efficiency of such co-operations, primarily with space industry, speciality workshops and electronics companies.

In addition to the institutional support by the Max Planck Gesellschaft, which is the most important element of our funding for personnel and projects, our research is supported by government institutions such as the German Federal Ministries for Education and Research (BMBF) and for Economy (BMW), DLR and international organisation such as ESO, ESA, the European Research Council and the EU. Additional financial contributions for specific projects and fellowships come from the German Science Foundation (DFG) and the Alexander von Humboldt Foundation (AvH).

Our institute is strongly engaged in vocational and academic training. We co-operate closely with the major local Universities: Ludwig-Maximilians Universität (LMU)

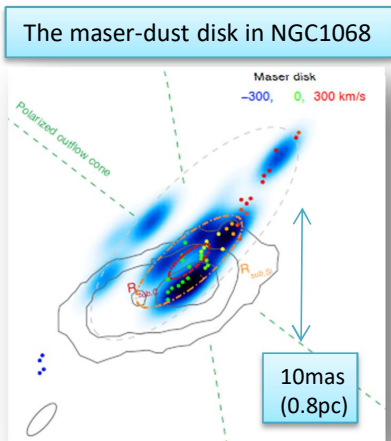
and the Technische Universität München (TUM). Staff at MPE supervise research students (Bachelor, Master and PhD), at both Munich Universities, as well as other German Universities and sometimes even further afield. Internships are offered to University, as well as high school students. The MPE Directors and many other senior staff have Professorial or Lecturer appointments at LMU, TUM and/or other Universities. The Institute hosts seminars, workshops and conferences in our own and adjacent research fields, often in cooperation with the Universities. Our very successful “International Max-Planck Research School on Astrophysics” at the LMU continues to attract many young motivated people to astrophysical research. We offer apprenticeships in our mechanical workshop, and incorporate refugees into these activities.

MPE is also active in public outreach. Our aim is to communicate our work specifically and interest in astrophysics in general to the local and national press, and the public. We achieve this in part via our web pages, press releases, and personal contacts. Our scientists regularly give public talks in schools, planetaria, and other forums, and write articles in popular astronomy publications.

School classes visit MPE regularly, facilitating awareness and inspiration in schools. Each year, around 50 girls visit MPE via the national “Girls' Day” initiative. Last but not least MPE hosts an Open House day every other year, where we typically welcome about 2000 visitors to the Institute, with programs of talks, extensive displays and interactive activities which serve to illustrate our work and astronomy in general.

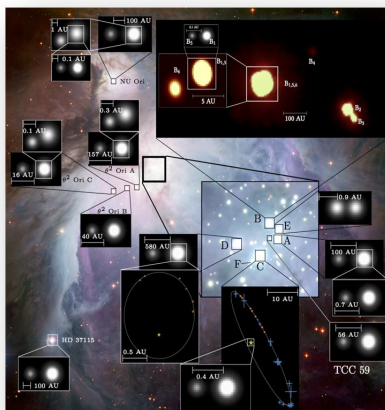
2 Infrared and Submillimeter Astronomy

GRAVITY's first 2 years

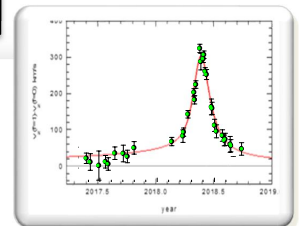
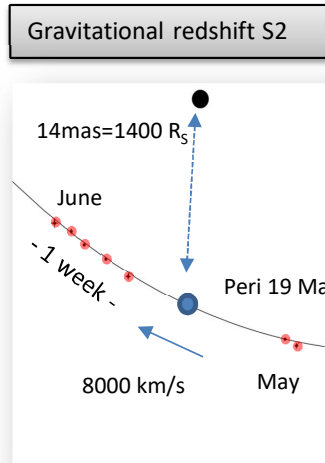


**19+ mag limiting
magnitude &
polarimetry**

Most Trapezium members
are multiple

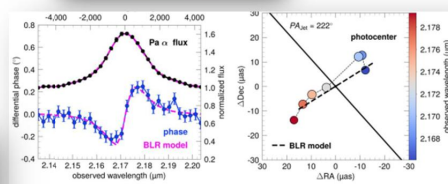


**2 x 4 milli-arcsec
resolution imaging**

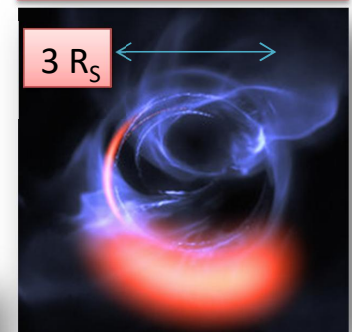


**<50 μ s imaging
astrometry**

Rotating BLR in 3C273

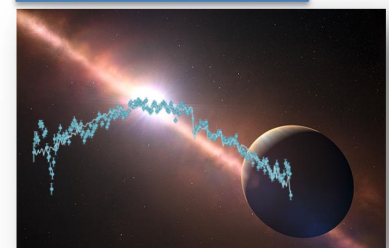


SgrA* Flare motion at ISCO



**Micro-arcsec spectral
differential astrometry**

Exoplanet spectroscopy



**High resolution
spectroscopy**

η Car & SS433 gas flows

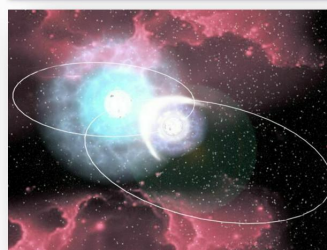


Fig. 2.1.1 Summary of the scientific results from the first two years of GRAVITY (2017-2018). This collage summarizes the remarkable depth and range of astronomy demonstrated with this new instrument, from circum-stellar gas and dust, to X-ray binaries and stellar black holes, to the detailed kinematics of dust and gas near the super-massive black hole in the Galactic Center, and then out to the circum-nuclear and broad-line regions around active galactic nuclei.

2. The MPE-Infrared/Submillimeter Group

2.1 Executive Summary

Without a doubt, **THE** Highlight of the last three years has been the rich harvest of science that has emerged already from the **GRAVITY** interferometric beam combiner instrument at the VLT (Fig. 2.1.1). **GRAVITY** has provided ground-breaking results covering a broad range of astrophysical science:

GRAVITY has delivered precision tests of Einstein's General Theory of Relativity and the so far strongest experimental evidence that the compact mass in the Galactic Center (SgrA*) is indeed a Schwarzschild-Kerr hole.

- **GRAVITY** has revealed that the ionized gas in the broad line region of the type 1 quasar 3C 273 is comprised of an ~ 0.1 pc turbulent rotating disk.
- **GRAVITY** has mapped the hottest dust in the nearby type 2 Seyfert galaxy NGC 1068 and unveiled a disk of about 1 parsec diameter associated with the H_2O masers. **GRAVITY** finds that this disk is not a thick torus, as postulated by the standard 'unified scheme' for AGN.
- **GRAVITY** has provided clear evidence that the majority of the massive stars in the Orion Trapezium region are multiple.
- **GRAVITY** has yielded milli-arcsec imaging spectroscopy of the gas in η Car and SS433 with remarkable detail and complexity.
- Finally and perhaps least expected, **GRAVITY** has provided outstanding, high quality atmospheric spectra of two young hot Jupiter exoplanets, en par or better than previous coronagraphic spectroscopy.

The key advance in **GRAVITY** is the superb sensitivity, which comes from the combination of novel low noise infrared detectors, external fringe tracking (phase-referencing), suppression of incoherent signals in single mode fibers, compact optics and high quality metrology. Together these features allow broadband imaging at $K\sim 19$ in the Galactic Center, almost 10 magnitudes fainter than previously), as well as high precision (20-50 μarcsec) astrometry, polarimetry and spectroscopy.

The IR group has continued to lead several efforts in galaxy evolution. Last year we successfully completed two ground-breaking surveys: the 75 night **KMOS^{3D}@VLT** spectroscopic survey of $\text{H}\alpha$ /[NII]/[SII] emission lines, and the 1500 hour **PHIBSS2@NOEMA** survey of CO in $z\sim 0.8$ -2.6 galaxies. These major surveys have provided quantitative ISM and kinematic properties of 750 (**KMOS^{3D}**) and 200 (**PHIBSS**) massive star forming galaxies at and after the peak of cosmic galaxy formation ten billion years ago, many with sub-galactic (a few to six kpc) resolution. **PHIBSS** has delivered statistically robust scaling relations of the relationship of (molecular) gas and star formation with redshift, stellar and baryonic mass, and vertical location in the stellar mass – star formation rate plane. **KMOS^{3D}** gives a detailed census of galactic outflows driven by stars and central black holes, and provides robust gas kinematics and velocity dispersions for over half of the full sample. Combining **SINFONI**, **KMOS** and **NOEMA** data sets we have high quality outer disk rotation curves for ~ 20 $z\sim 0.8$ -2.6 galaxies, providing the first test of the dark matter fractions during the assembly phase of massive halos at ~ 2 -3 R_e .

Group Philosophy, Instrumentation & Publications

Since the inception of the MPE-IR/submm group in 1986, our strategy has been to carry out group-wide research focused on selected major science themes. We have worked in Galactic and extragalactic star formation, studies of massive black holes and their environment and evolution, in the Galactic Center and in external galaxies, and in the physical properties driving galaxy evolution, from redshift ~ 3 to the present time. We often work with external collaborators to enhance our main observational efforts with interpretational and theoretical work.

To achieve our goals we develop innovative, state of the art, ground- or space-based instruments that address one or several of these themes. These instruments are built in house or in a consortium with MPE leadership (**3D**, **SINFONI**, **PACS**, **GRAVITY**), or with major MPE participation (**ISO-SWS**, **NACO**, **KMOS**). **GRAVITY** is

an obvious example, and perhaps the ultimate culmination of this philosophy. It took 13 years from initial vision to **GRAVITY's** shipment to Paranal in late 2016, with the first results emerging already in 2017 and 2018 (Fig. 2.1.1).

The upgraded successor of both **NACO** and **SINFONI**, called **ERIS**, is another example, which is currently in the final manufacturing and assembly stages. The first light astrometric imaging instrument **MICADO** for the next generation large ground-based optical/IR telescope, the ESO **ELT**, under MPE PI-ship, passed PDR at the end of 2018.

Finally, we are deeply engaged at the Institute for Radio Astronomy in the mm-Range (**IRAM**, Grenoble). We have led the MPG-effort of expanding the Plateau de Bure Interferometer, now called **NOEMA**, by factors of two to five each in sensitivity, resolution and spectral bandwidth. As

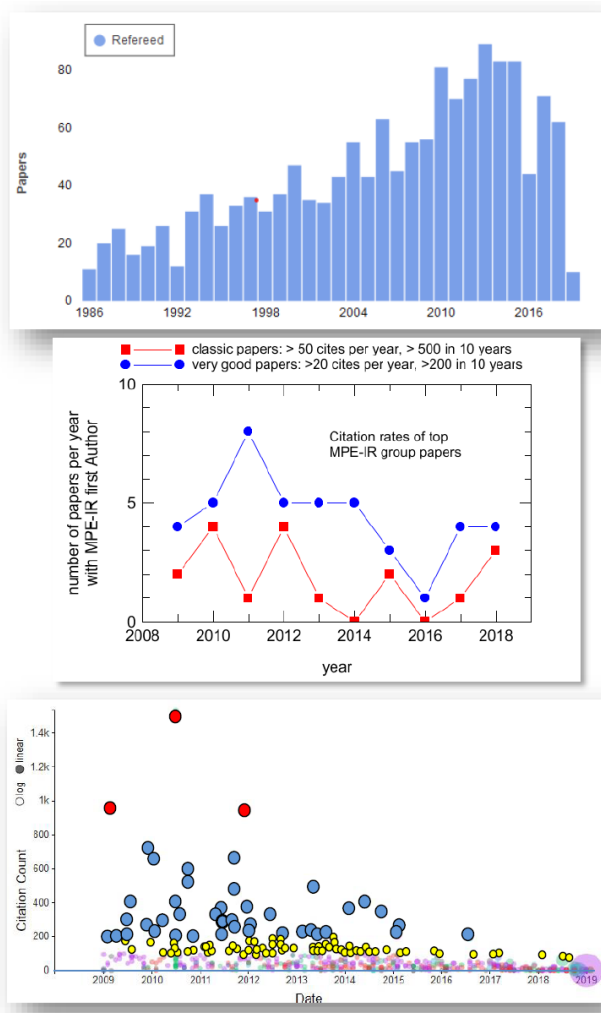
of this report Antenna 11 is being assembled and tested on the mountain, and Antenna 12 construction will begin in about one year from now, thus concluding Phase 2 of the upgrade. With its 12x15m antennas and their state of the art receivers (factor 2 broader bandwidth and lower noise temperature than ALMA), two software correlators for dual-band operation and an expanded 1.6 km baseline, **NOEMA** will soon have 60-80% of the sensitivity of ALMA in the 3, 2 and 1 mm bands.

We are grateful for the support and positive recommendations the Visiting Committee has given to the experimental program of the MPE-IR group over the years, which has been extremely helpful in getting additional resources from the MPG, such as recently for NOEMA and MICADO.

A very positive development of the last decade has been the overall increase in the fraction of women in the group to ~34% (at all levels, from students, postdocs to senior

scientists (38%). The IR group currently hosts the only two W2 female scientists at MPE, and enjoys the part-time presence of Prof. Ewine van Dishoeck. About half of the group's scientists are German, the other half come from a dozen countries world-wide. Because of the ending of the **PACS** effort and attached DLR funding, the size of the group has decreased somewhat in the last few years from 57 to about 48 now (of these 38 scientists, postdocs and PhD students).

The IR group also hosts the research group "Star and Planet Formation" of Prof. Ewine van Dishoeck (External Scientific Member of MPE), a Sofia-Kovalevskaja Awardee of the Alexander von Humboldt Foundation (Jason Dexter), and (just completed) an ERC starting grant (Stefan Gillessen). Prof. Amiel Sternberg, long-standing collaborator of the MPE-IR group and initiator of a strong scientific tie between MPE-IR and several groups in Israel, was appointed External Scientific Member of the MPE in 2018.

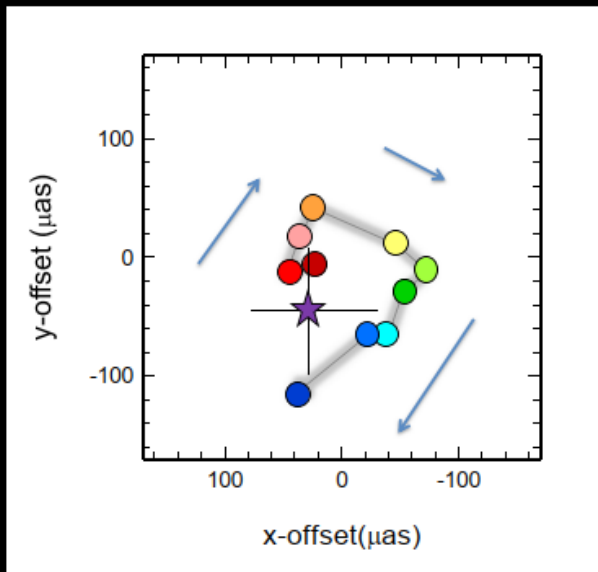


Topic	Authors	Year	Citations
Herschel-PACS Instrument	Poglitsch et al.	2010	1545
GC stellar orbits	Gillessen et al.	2009	979
SINS high-z IFU survey	Förster Schreiber et al.	2009	742
High-z molecular gas	Tacconi et al.	2010	673
High-z gas-SF relation	Genzel et al.	2010	599
GC black hole and cluster	Genzel et al.	2010	528
High-z gas scaling relations	Tacconi et al.	2013	505
Galaxy structure and SF to z~2	Wuyts et al.	2011	396
SINS: star-forming clumps	Genzel et al.	2011	378
ULIRG outflows and feedback	Sturm et al.	2011	345
Cold gas accretion	Bouche et al.	2010	344
Local gas scaling relations	Saintonge et al.	2011	289
Herschel PEP deep survey	Lutz et al.	2011	281
S2 orbit around SgrA*	Gillessen et al.	2009	265
SFR and SFH of high-z galaxies	Wuyts et al.	2011	258
Molecular gas scaling relations	Genzel et al.	2015	252

Topic	Authors	Year	Cit. rate
GC SMBH gravitational redshift	Gravity Coll. / Eisenhauer	2018	121.5
Molecular gas scaling relations	Tacconi et al.	2018	88.6
High-z gas scaling relations	Tacconi et al.	2013	86.6
Molecular gas scaling relations	Genzel et al.	2015	61.7
SINS/zC-SINF high-z AO survey	Förster Schreiber et al.	2018	55.2
KMOS ^{3D} survey	Wisnioski et al.	2015	52.2
GC stellar orbits	Gillessen et al.	2017	49.8
Dark matter in high-z galaxies	Genzel et al.	2017	40.5
Flare motion near GC SMBH	Gravity Coll. / Pfuhl, Dexter	2018	38.4
Herschel-PACS deep survey	Magnelli et al.	2013	38.2
GRAVITY first light	Gravity Coll. / Eisenhauer	2017	31.8
High-z outflows	Genzel et al.	2014	29.3
High-z bulge growth and quenching	Lang et al.	2014	28.4

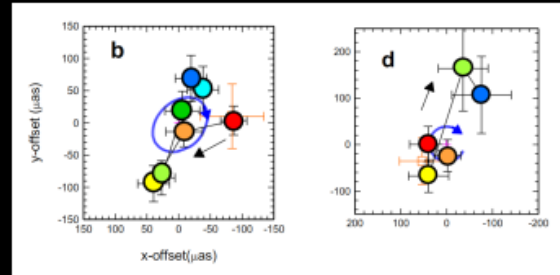
Fig. 2.1.2 Left top and middle: Publication statistics of the MPE-IR group; total number of papers and integrated total citation count (per year) of the group since its inception in 1986. **Bottom:** citations of individual papers as a function of time since 2009. Filled red, blue and yellow circles denote papers with >1000, 200-1000, and 100-200 citations, respectively. While the epoch between 2009 and 2012 was truly an overall high point of our research on several fronts (combination of GC, SINS, PHIBSS and PACS-PEP and SHINING), much of the apparent drop in the highest cited papers is owed to time. A number of the more recent papers can be expected to rise to the same level of 200-300 cites in a few more years. **Four of the group members (Förster Schreiber, Genzel, Lutz & Tacconi) belong to the top cited researchers in Clarivate Analytics Web of Science Highly Cited Researchers (of 121 space scientists in that group worldwide, and 12 in the MPG).** **Top right:** Frequently cited (>250 cites) 2009-2018 papers with IR group first author. **Bottom right:** High citation rate 2013-2018 papers with IR group first author. In the mid term, these are likely to enter the frequently cited group, or have already done so.

GRAVITY Flare 22 July 2018



- Clockwise, looped motion
 - 150 μas scale
 - few ten minutes
- Corresponding to 30% speed of light

And again on 28 July and back on 27 May



GRAVITY collaboration+18

Fig. 2.1.3 Left: motion of the emission centroid of SgrA* during a bright flare on 22 July 2018 (relative to its median relative to S2, and with time running from dark red to blue), with the purple asterisk and cross marking the position of the mass, as inferred from S2's orbit. The centroid follows a clockwise loop with a radius of 100 μarcsec and an estimated period of 40 minutes. **Right:** two further flares on July 28 and May 27 with similar clockwise loops. The data can be well fit by near-face one (<20 degree inclination) circular orbit at $6\text{--}10 R_g$ for a Schwarzschild hole, consistent with or just outside its innermost stable circular orbit (ISCO).

The Galactic Center: testing the massive black hole paradigm

We have been studying the Galactic Center and the star cluster around the massive black hole (candidate) SgrA* for the past three decades. During the reporting period we were able to achieve a breakthrough, in exploiting the Galactic Center 'laboratory' for precision tests of the black hole paradigm. We used the peri-passage at $\sim 1400 R_s$ of the bright star S2 in May 2018 with **NACO**, **SINFONI** and **GRAVITY** for a precision measurement of the orbital parameters and the mass and distance of SgrA* (Fig. 2.1.1). **GRAVITY's** $\sim 50 \mu\text{arcsec}$ astrometry (an order of magnitude better than **NACO**) is critical for determining and reducing the degeneracies of all relevant parameters to $\sim 0.2\text{--}0.6\%$ precision. As a first result, we were able to detect with ~ 20 rms significance the gravitational redshift in the Doppler shift of S2's orbit, as predicted by General Relativity (GR, Fig. 2.1.1). While the gravitational redshift occurs solely in redshift/wavelength space observed with **SINFONI**, the high astrometric precision of **GRAVITY** decisively excludes other Kepler orbits that are degenerate with the best fitting GR orbit. With the same data we also confirmed the validity of the positional invariance and the weak Einsteinian equivalence principle. Next, we hope to be able to detect in the next one or two years the Schwarzschild in-plane prograde precession of the S2 orbit, predicted by GR to be $11.9'$.

In more than 90% of the **GRAVITY** images we detect infrared emission from SgrA* itself, which is continuously variable, polarized synchrotron emission. Following our discovery of SgrA*-IR about 15 years ago, it became clear that the emission must come from a small fraction of the virialized electrons in the inner most accretion zone that may have been accelerated to high energy ($\gamma \sim 10^3$) by magnetic reconnection or shocks. Theoretical studies suggested that such 'hot spots', while short-lived, might be useable for kinematic studies of the hot gas near the innermost particle orbits. While this theoretical interpretation appeared plausible, it nevertheless came as a great surprise when we detected on three occasions in 2018 looped motions of the emission of SgrA* on a scale of 100 μarcsec when the source was in a 'high state' of emission, such that **GRAVITY** enabled the possibility of 20–40 μarcsec relative astrometry between S2 and SgrA*, in short integration times of a few minutes. The data are well fit by near-face-on, clockwise circular orbits on or slightly outside the innermost stable circular orbit (ISCO) of a 4 million solar mass black hole (Fig. 2.1.3). Interestingly, these orbital motions appear to be accompanied by similar rotations of the direction of polarization of the emission. Analysis suggests that the polarization patterns require again a face-on geometry and a poloidal field geometry. If so, the near ISCO plasma may be magnetically dominated.

35 years progress: GC mass distribution

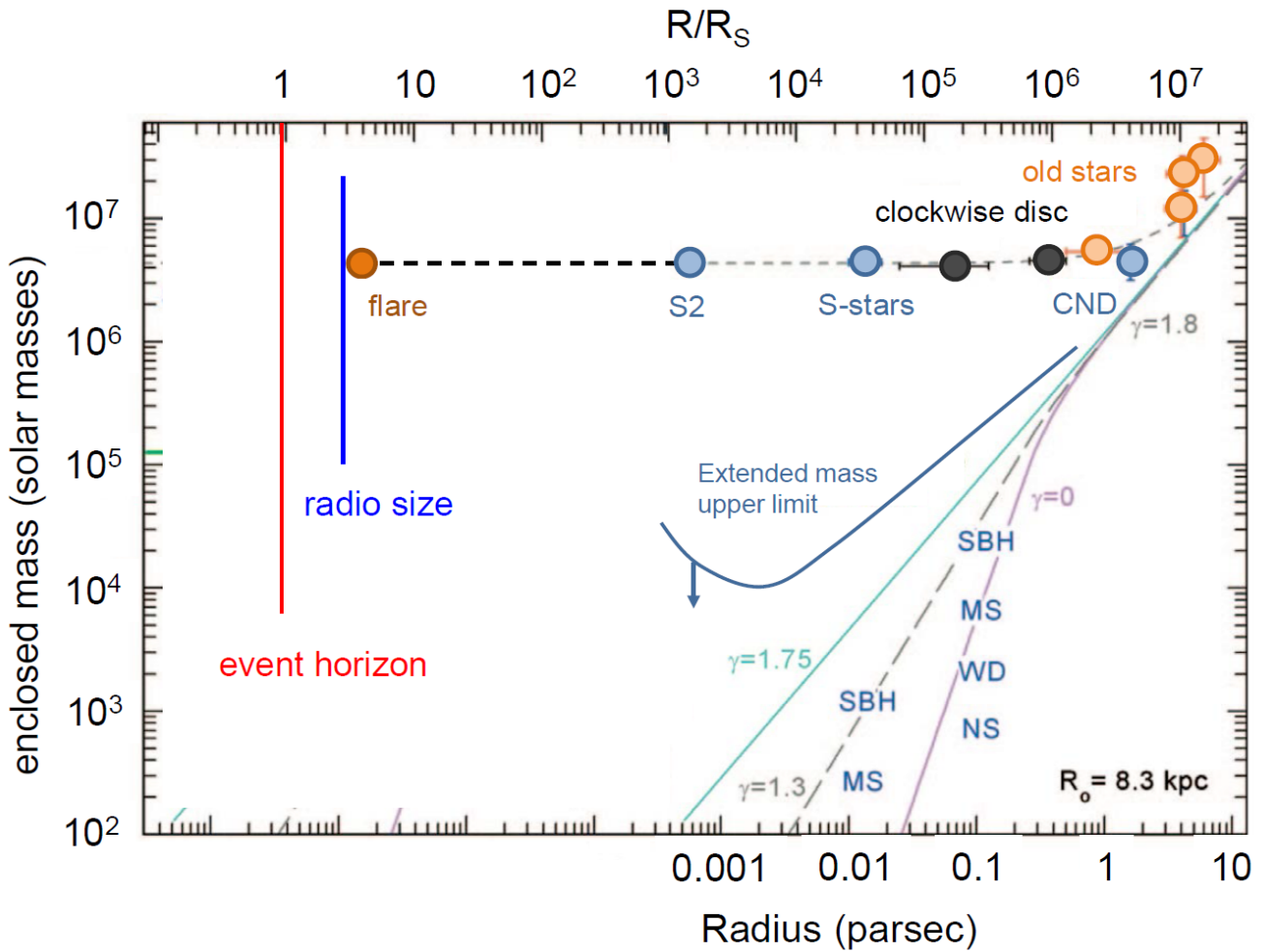


Fig. 2.1.4 The mass distribution in the Galactic Center, as established from gas and stellar dynamical measurements. Compared to the 1980s when the first evidence for a central mass emerged, 35 years later the data now sample the gravitational potential over 6 orders of magnitude and establish that the same mass is contained within 1 μ parsec (or 3 R_S of a 4 million solar mass black hole) as at the outer sphere of influence of this object, ~ 1 pc. While the compact mass associated with SgrA* is located in a very dense star cluster, including the enigmatic S-stars, which probably have been captured by the central object during their flyby on near loss-cone orbits, the extended mass within the S2 orbits is $<0.3\%$ of the central mass. Although fainter stars within the S2 orbit have not yet been detected by **GRAVITY** imaging to $K < 19$, some tens of stars and stellar black holes are expected there from numerical simulations. If we detect such stars in the future, they will be used to measure the spin of the black hole. In terms of other tests of General Relativity near a super-massive black hole, we expect to be able to detect the Schwarzschild precession of the S2 orbit within the next two years.

Fig. 2.1.4 summarizes the progress in our empirical determination of the Galactic Center mass distribution since the mid-80s, at which time measurements of the Doppler velocities of ionized and neutral gas clouds around SgrA* for the first time indicated the presence of a spatially concentrated central mass. Since the start of our MPE high resolution stellar orbit (especially the star S2) monitoring program in 1991, and that of Andrea Ghez and team at the Keck in 1995, we have built a convincing case that this concentrated mass of 4.1 million solar masses is coincident with the compact radio source SgrA*. With the detections of gas motions near ISCO discussed in the last section, this mass must be concentrated within 7-10 R_g of a 4 million solar mass Schwarzschild-Kerr hole. By resolving the sphere of influence of the central mass over 6 orders of magnitude, the Galactic Center provides by far the best case for the existence of super-massive black holes as predicted by General Relativity, although

more speculative configurations, such as massive boson or gravastars, cannot yet be unequivocally excluded. In a broader comparison, the ‘Kerr-ness’ of SgrA* is now confirmed to a level of rigor en par or not far behind that of the 30 M_\odot stellar black holes by **aLIGO**.

Inward Bound in Galactic Nuclei

GRAVITY also provides long awaited near-IR dust continuum and differential spectroscopic imaging of iconic bright AGNs and quasars on spatial scales of <0.1 to a few parsec. We resolve the Broad Line Region (BLR) in the famous quasar 3C273 and detect a clear spatially resolved (40 μ parsec), continuous velocity gradient across the 4000 km/s wide Pa α line. This indicates that the BLR is a thick, turbulent rotating disk, seen near face-on and perpendicular to the prominent radio jet (top center in Fig. 2.1.1). While rotation was previously suspected to

be present in a number of QSO BLRs on the basis of their spectral and reverberation properties, the **GRAVITY** data (in 3C273 and NGC3783) for the first time resolve the gas dynamics in differential spectral imaging, and yield a few ten percent precision determination of the black hole mass. We will come back to this when discussing prospects for the future below.

In the nearby archetypal Seyfert 2 galaxy NGC 1068, **GRAVITY** for the first time has imaged the nuclear hot dust distribution at <0.1 parsec resolution. The dust is in a parsec scale, highly inclined and clumpy dust disk (top left in Fig. 2.1.1). The H_2O maser spots appear to delineate the lower right side of this clumpy disk. Since at least the brightest maser spots are thought to be amplifying the somewhat extended nuclear radio continuum source, this lower right side must be the front side of the disk, while there are naturally no masers on the upper left, backside of the disk, behind the nucleus. It was known for some time that the somewhat cooler dust at $5\text{--}10\ \mu\text{m}$ predominantly comes from the walls of the jet emerging perpendicular to the parsec scale maser and dust disk. Neither the hottest dust just outside the sublimation radius detected with **GRAVITY**, nor this cooler dust seem to come from an optically and geometrically thick torus, as predicted by the standard unified model of type 1 and 2 AGN. If NGC 1068 is indeed archetypal, the dust obscuration cone of opening angle ~ 40 degrees differentiating the optical/UV types 1 and 2 may originate in a moderate column but geometrically thick structure, perhaps associated with a dusty nuclear wind, while the

very high gas columns inferred from X-ray observations ($\sim 10^{25}\ \text{cm}^{-2}$ in NGC 1068) may come from the ionized, dust free accretion and wind zone very close to the black hole.

These first spectacular results raise the question of how many AGN are accessible to **GRAVITY** now, or would be accessible with additional upgrades of the instrument. Data for 3 further AGN are in hand, and a large program of ~ 11 type 1 AGN spanning 4 orders of magnitude in luminosity has been granted time for this year by the ESO OPC. It will hopefully delineate a first census of the frequency of spatially resolved rotation in type 1 AGN.

GRAVITY*

We have started to investigate the possibilities for further upgrading the capabilities and sensitivity of **GRAVITY**. We will present the very promising results of this study in a white paper to ESO and the MPG. In summary, upgrades of the throughput of gratings and several optical components (factor 2-3), and still lower read noise in the infrared detectors (factor 2-2.5) are possible and are partly already under way. A more costly upgrade is the implementation of Na-laser guide stars on all four UTs, which will improve Strehl ratios and coherent fluxes injected into the fibers by a factor of typically 4 for faint AGN, which at the same time can serve as fringe tracking targets. Higher Strehl ratios also yield a very valuable increase in the stability of fringe detection (factor 2), which reduces the demand on the very best atmos-

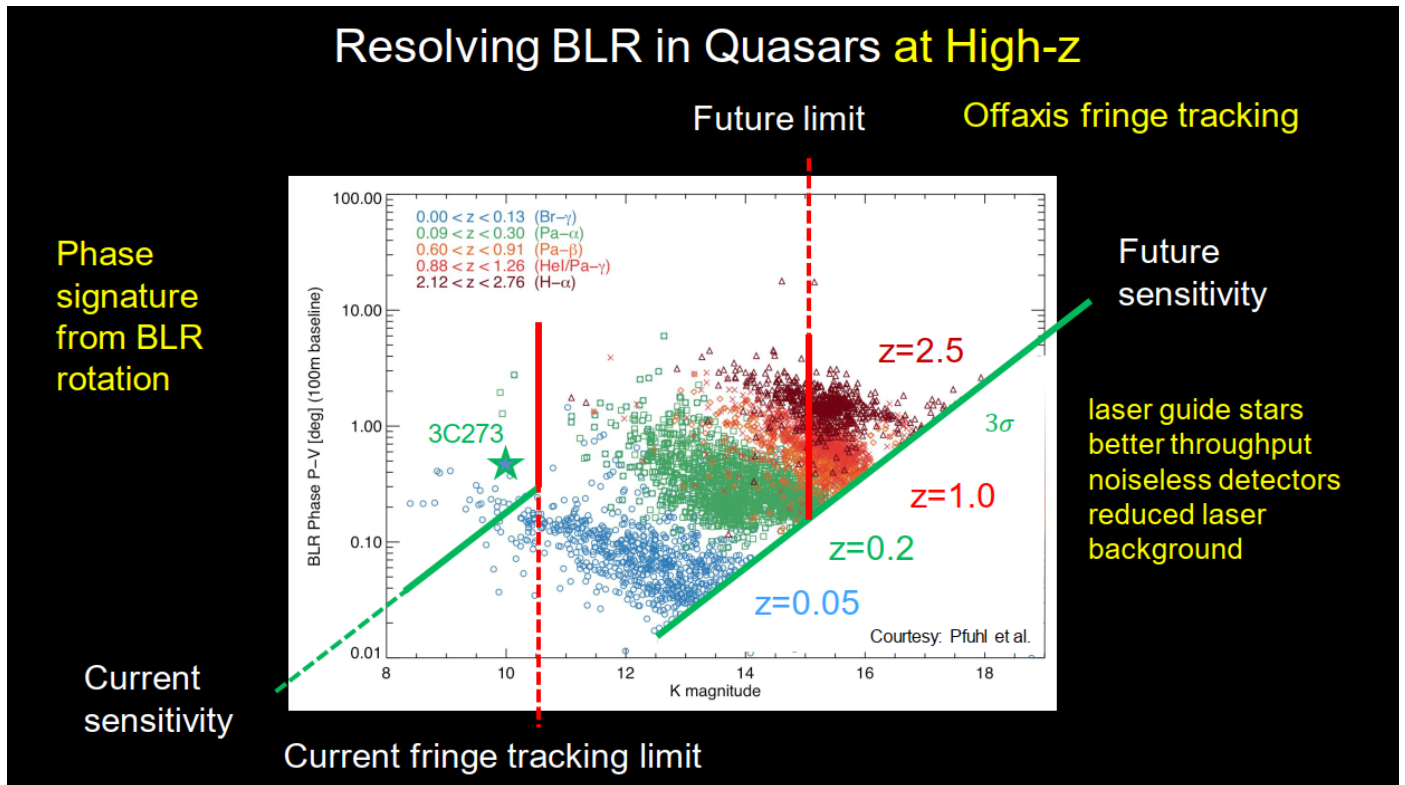


Fig. 2.1.5 Impact of the proposed 4.5 -5 mag upgrades to **GRAVITY*** to the availability of type 1 QSOs for resolved BLR work. The current limit of on-axis tracking are AGNs with $K < 10.5$ (vertical red line), and the requirement of the detectability of a spatially resolved blue-red phase shift due to rotation is given by the green line. There are about 20 or so BLR AGN detectable at current sensitivity. With the upgrades to $K \sim 15$ the number of accessible AGN increases dramatically, to hundreds of $z < 0.3$, ~ 100 $z \sim 0.8\text{--}1$, and 20 $z \sim 2$ QSOs. With $30''$ external fringe tracking the number of $z \sim 2$ targets increases to ~ 100 .

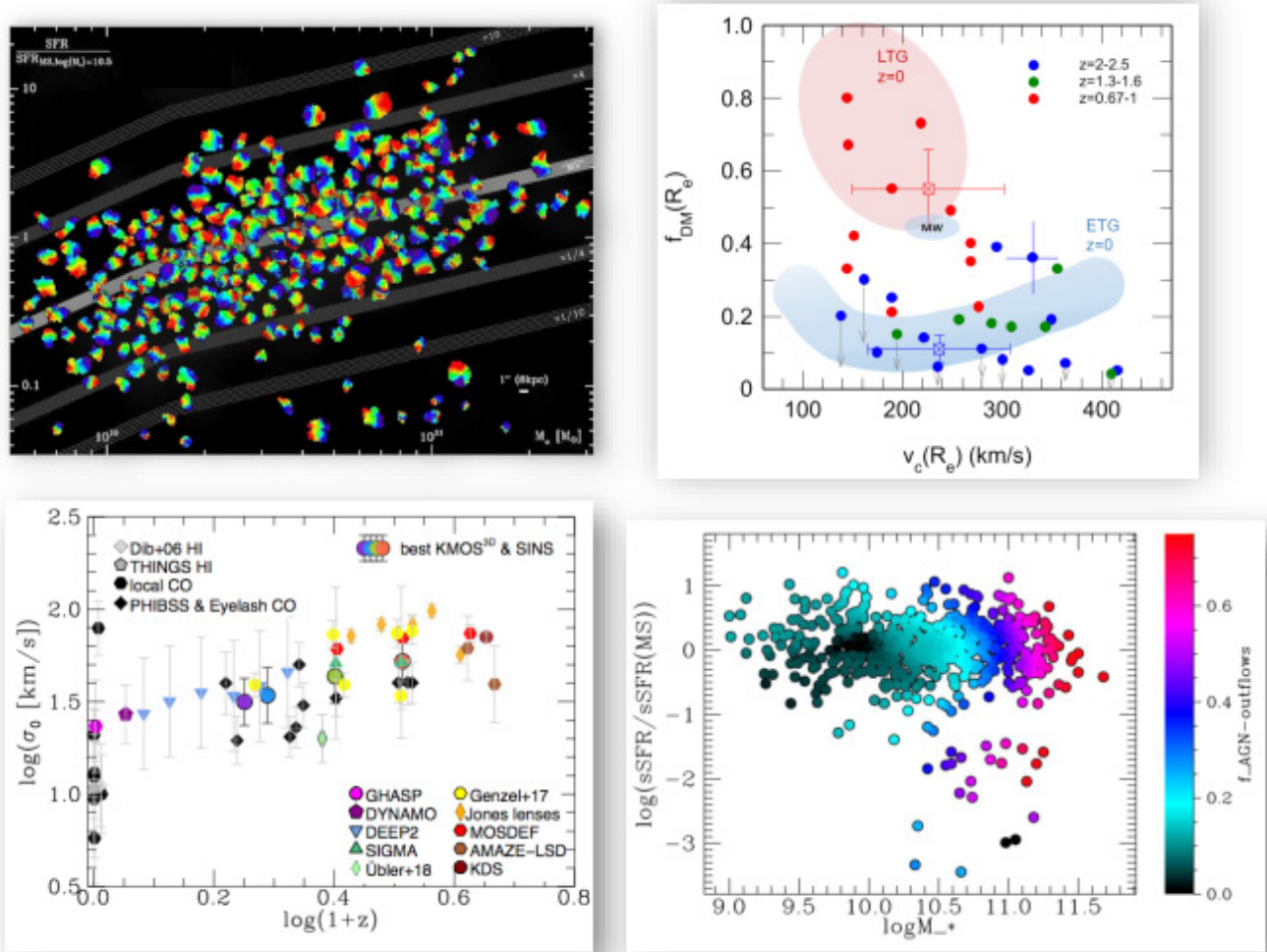


Fig. 2.1.6 Selected key results of **KMOS^{3D}** and **NOEMA**. **Top left:** ~70% of all near main-sequence (MS) star forming galaxies with $\log(M/M_\odot) > 9.7$ at $z=0.8-2.6$ are rotating disks, albeit with a large component of random motions. Remarkably 10-15% of $z \sim 1-2.5$ galaxies far below the M_S also exhibit H α emission, some from AGN activity, some from fresh, low metallicity gas in rotating disks indicative of rejuvenation. **Bottom left:** These velocity dispersions σ_0 appear to be approximately constant within galaxies on sub-galactic scales, and appear to depend mostly on redshift and gas fraction, with substantial scatter but few other significant parameter dependencies. There appears to be a continuous drop of galaxy wide velocity dispersion from ~45-50 km/s at $z \sim 2.6$ to 10 km/s at $z=0$. Molecular gas dispersions are comparable to the H α dispersions at $z \sim 1-2$. Recent theoretical work suggest that low- z dispersions are driven by feedback, while the large high- z dispersions are driven by release of gravitational energy due to radial gas transport. **Bottom right:** **KMOS^{3D}** detects both extended, star formation driven and nuclear, AGN driven outflows. The star formation driven outflow incidence scales with star formation rate and surface density but not mass, while the AGN-outflows depend only on mass. 70-90% of all near-MS galaxies near and above the Schechter mass with $\log(M/M_\odot) > 10.8$ exhibit powerful, high velocity nuclear outflows, strongly suggesting that these outflows indeed are causally related to the star formation quenching at that mass. **Top right:** Very deep integrations (as well as stacking) of **SINFONI**, **KMOS** and **NOEMA** p - v diagrams are delivering high quality rotation curves to $2.5-4 R_e$. From modeling with a combination of an exponential disk, a bulge and an NFW halo with a concentration parameter that decreases with redshift, we find that the most massive and highest redshift galaxies have very low dark matter fractions at R_e , comparable to local massive Early Type Galaxies, which are the likely descendants of these massive SFGs. SFGs at lower mass and lower redshift have higher dark matter fractions, comparable to the Milky Way and the more massive $z=0$ late type galaxies. We propose that the fast baryonic processes and angular momentum transport in the gas rich high- z SFGs allow rapid buildup of baryon dominated massive bulges and inner disks.

pheric conditions for faint interferometry. Finally, a more invasive upgrade would be to revive the PRIMA project for the UTs to allow fringe detection on external stars within 20-30" instead of 1". This would allow observations of non-AGN and high- z extragalactic targets. Even without the latter these upgrades would sum up to 4.5-5 magnitudes improvement for on-axis fringe detection, allowing interferometry of $K \sim 15$ targets (instead of 10-10.5 currently) even in the self-referenced mode, and fainter for external fringe tracking. Fig. 2.1.5. gives a first assessment of the increase in AGN samples, facilitated by these changes. Based on this assessment the number of accessible type 1 AGN increases dramatically, to hundreds of $z < 0.3$, ~100 $z \sim 0.8-1$, and 20 $z \sim 2$ QSOs. With

30" external fringe tracking the number of $z \sim 2$ targets increases to 100. This includes a number of compact binary radio AGN. Mass measurements on such a large sample of AGN are highly desirable, especially at high masses, where reverberation mapping has not been successful because of the long time scales needed, and would allow dramatically more robust studies of galaxy-AGN co-evolution.

Evolution of star forming galaxies at the peak of galaxy formation

KMOS^{3D}. While the emphasis of this summary report so far has been on the very recent developments with

GRAVITY, much of the IR-group's research during the past years has focused on in-situ observations of the physical, dynamical and gas properties of massive star forming galaxies near the peak of the cosmic galaxy formation epoch, about 10 billion years ago.

In close collaboration with the MPE OPINAS group we have carried out in the last six years a major, and highly successful spectroscopic survey (**KMOS**^{3D}, following on from the earlier **SINS** and **zC-SINF** surveys with **SINFONI**). **KMOS**^{3D} has delivered a robust census of the sub-galactic scale dynamics and H α /[NII]/[SII] line ratios in ~ 750 mainly mass selected main-sequence SFGs in three redshift slices at $z \sim 0.6-1.1$, $1.3-1.7$ and $2-2.7$, and probing for the first time with near-IR IFU observations into the regime of passive galaxies. In contrast to other ongoing **KMOS** and **MOSFIRE** spectroscopic programs **KMOS**^{3D} excels by depth (typical integration time per target of 8 hours, and up to ~ 25 hours) and quality of spectra at seeing limited scales. **KMOS**^{3D} exploits the unique multiplexing capabilities of the **KMOS** spectrometer (24 IFU units), in whose development the OPINAS and IR groups have been involved in.

Strengthening the **SINFONI** work of the past decade, **KMOS**^{3D} has now robustly shown that $>70\%$ of massive star forming galaxies (SFGs) are clumpy, thick and turbulent rotating disks, with a minority of mergers (Fig. 2.1.6 upper left). The level of sub-galactic scale turbulence seems to mainly depend on redshift and gas fraction, with large scatter, and drops from about 45-50 km/s at the peak of galaxy formation activity to 10 km/s in $z \sim 0$ galaxies (Fig. 2.1.6 bottom left). Recent theoretical work strengthens our earlier conclusions that the source of the stirring of the ISM at high- z is not stellar feedback, as is likely the case at low- z but the release of gravitational potential energy, as matter is rapidly transported inward through efficient angular momentum re-distribution in high gas fraction, clumpy disks.

KMOS, **SINFONI**, **HST** and **PACS** observations show that more than 90% of the cosmic star formation activity between $z=2.5$ and $z=0$ occurs in a well-defined 'Main Sequence' (MS) of star forming disks in the stellar mass - star formation plane. With **KMOS**^{3D} we have been able to extend the coverage to quiescent galaxies below the MS. We find that about 10% of these passive, compact galaxies have H α disks with non-negligible star formation rates, suggestive of 'rejuvenation' processes reigniting star formation in quenched galaxies. Another key recent discovery with **SINFONI/KMOS**^{3D} is powerful nuclear outflows of ionized gas (Fig. 2.1.6 bottom right). The incidence of these outflows is strongly mass dependent, and increases to about 70-90% near and above the Schechter mass. This suggests that nuclear outflows may play a significant role in the quenching of star formation activity. **KMOS**^{3D} also has permitted statistically robust studies of metallicities, metallicity gradients and the specific angular momenta of the high- z star forming galaxy population.

Very deep integrations (as well as stacking) of **SINFONI**, **KMOS** and **NOEMA** p-v diagrams are delivering high

quality rotation curves as far out as $2.5-4 R_e$. From modeling with a combination of an exponential disk, a bulge and an NFW halo with a concentration parameter that decreases with redshift, we find that the most massive and highest redshift galaxies have very low dark matter fractions at R_e (Fig. 2.1.6 upper right panel). Low dark matter fractions in fact are also inferred in $z \sim 0$ massive Early Type Galaxies, which are likely the descendants of the massive SFGs we study at $z \sim 1-2.6$. SFGs at lower mass and lower redshift have higher dark matter fractions, comparable to the Milky Way and the more massive $z \sim 0$ late type galaxies. We propose that the fast baryonic processes and angular momentum transport in the gas rich high- z SFGs allow rapid buildup of baryon dominated massive bulges and inner disks.

NOEMA. With CO data from the galaxy-integrated **PHIBSS2** survey on the expanded **IRAM NOEMA** array and from dust data with **PACS/SPIRE** on Herschel, we have been able to significantly improve the robustness and statistics of the scaling of molecular gas properties with redshift, star formation rate and stellar mass. Our data strongly support the interpretation that most main-sequence galaxies undergo 'equilibrium growth' regulated by the replenishment of fresh gas on the one hand, and by consumption of the gas by star formation and powerful galactic winds on the other. The more than one order of magnitude increase in galactic star formation rates, for constant stellar mass, between $z=0$ and $z=2$ thus is mostly due to the large gas accretion rates (and larger gas fractions), rather than more efficient star formation rates per free fall time.

Further improvements of the capabilities of **NOEMA** in the next years, thanks to the excellent support of the MPG (and CNRS), along with detailed follow-up observations with the **ALMA** facility, promise to give further detail in this key story on the growth and quenching of galaxies at high redshifts. We are about to start a major new survey (**NOEMA**^{3D}, ~ 1500 hours over 4 years), which will emphasize spatially resolved studies of the molecular dynamics at $z \sim 0.5-2$. The main science goals include outer rotation curves, the exploration of molecular outflows, the central molecular distributions and kinematics, and the detection of density dependent molecular transitions (to test for local volumetric dependencies in the molecular gas-star formation relation).

Next steps in galaxy evolution and looking toward the ELT

While these observations, along with increasingly powerful simulations of our collaborators at LMU (Burkert), MPA (Naab), Israel (Dekel @ Hebrew, Sternberg @ Tel Aviv) and New York (Genel @ CCA), give us a first direct glimpse of the key physical processes operating at the peak of galaxy formation, the next big step will be to cast the qualitative picture sketched above into an increasingly firm quantitative form. **KMOS**^{3D}@VLT and **NOEMA**^{3D} are the first examples of these next generation surveys, with 300-1000 galaxies in the redshift range leading up to and dropping down from the $z \sim 1-2$ peak. Starting in

2020 we will take the next step in AO-scale studies of the optical emission and perhaps absorption features with GTO time from the upgraded **ERIS** imager/spectrometer. We are also actively pursuing programs during the open time of **JWST**. The biggest step will come from the next generation extremely large telescopes. MPE is the PI institute for the **MICADO** astrometric imager/spectrometer, which is slated to be the first light instrument for the 40 m European ELT on Armazones/Chile, which is expected to go into operation in 2025.

The MPG President Prof. Martin Stratmann has extended my tenure as Director of the group by another 3 years to spring 2026 (7 years from now), hopefully allowing the **MICADO** development to be brought to a successful conclusion during my term as Director and starting its scientific exploitation at the **ELT**. **Prof. Stratmann has also been very supportive of the recommendation of the 2016 Visiting Committee to continue experimental IR/submm astronomy at MPE beyond 2026, when both Ralf Bender and I retire. To achieve a smooth**

transition between now and >2026 the MPE directorate have agreed to carry out an early hire already in 2022/2023. The personnel and financial resources for this early hire will in part be coming from a ramping down of the IR group beyond 2022.

While the science plans for the exploitation of **MICADO** are already being discussed now in the **MICADO** science team and will become finalized well before 2025, it is almost certain that the GTO phase of **MICADO** will not come before my retirement as Director of the MPE-IR group. **As the outgoing Director, I am naturally keen to ensure that MPE's science exploitation of such a high profile project as MICADO can be carried out smoothly and that the science plans drawn up now by the younger generation of scientists at MPE-IR and in the MICADO consortium can be executed as planned in the next few years. I very much hope that the Visiting Committee will support me in this vision and pledge.**

Reinhard Genzel

& MPE-IR Senior Team



2.2 In-situ Surveys of Galaxy Evolution

Spatially- and spectrally-resolved observations of the rest-frame optical and submm line and continuum emission are very powerful in exploring galaxy formation and evolution 5–10 billion years ago, around the peak epoch of cosmic star formation. Our major near-IR and (sub)mm spectroscopic mapping programs of galaxies at $z \sim 1\text{--}3$ with **KMOS** and **SINFONI** at ESO's Very Large Telescope (VLT) and with the **IRAM/NOEMA** interferometer are probing the life cycle of distant galaxies through the cold molecular gas, warm ionized gas, and stellar components. Our in-situ studies have 1) revealed the central role of the cold gas reservoirs and the importance of internal galaxy dynamics in growing early disks and bulges, 2) unveiled the strong dominance of baryons on galactic scales at higher mass and redshift, 3) established the demographics and energetics of feedback via outflows, and 4) brought unique new insights into star formation quenching at high galaxy masses. These multi-year, synergetic surveys provide comprehensive and resolved views of galaxies, essential to pin down the main drivers of galaxy evolution. They paved the way for the next major steps forward with **ERIS** at the VLT, the fully upgraded **NOEMA** array, **ALMA** and **MICADO** at the Extremely Large Telescope (ELT).

Our programs in context:

In the “equilibrium growth model,” young star-forming galaxies (SFGs) are fed by fairly smooth accretion from their halos, and minor mergers, continuously replenish-

ing their gas reservoirs and fueling star formation. The balance between accretion, star formation, and outflows maintains the bulk ($\sim 95\%$) of SFGs over most of the Universe's history on a narrow observed “main sequence” (MS) relation between star formation rate (SFR) and stellar mass (M_*). The MS comprises mainly disk-like systems, and its zero-point evolution reflects the decrease in cosmic SFR and galactic molecular gas fractions since $z \sim 2\text{--}3$. The growth of galaxies thus appears to be tightly regulated until they reach $\sim 10^{11} M_\odot$, where their star formation is rapidly quenched. While the statistical census of deep look-back surveys has played an important role in establishing the broad scope of the equilibrium growth model, detailed spatially-resolved studies of individual galaxies, well sampled from the parent populations, are critical for understanding the physical processes at play. Building on our initial pioneering studies with SINFONI at the VLT and the IRAM Plateau de Bure Interferometer (PdBI, now NOEMA), our recently completed multi-year programs at the VLT and IRAM have placed our earlier results on a firm statistical footing, expanded the galaxy parameter space explored, and led to several breakthroughs highlighted below.

The SINS/zC-SINF and KMOS^{3D} surveys:

SINS/zC-SINF was the first and largest survey of spatially-resolved ionized gas kinematics, star formation, and physical properties at $z \sim 2$ with the single-object near-IR integral field spectrometer unit (IFU) SINFONI. The survey used 60 nights of MPE IR/Submm group Guar-

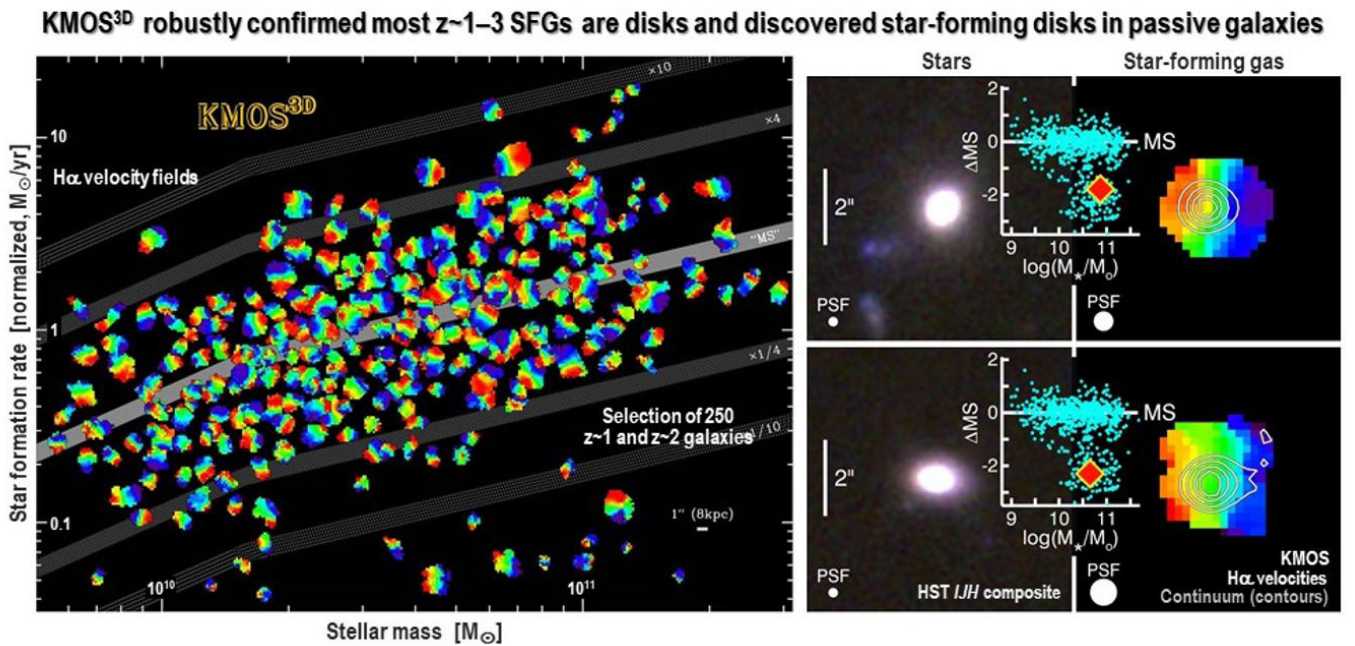


Fig. 2.2.1 KMOS^{3D} observed 740 $0.6 < z < 2.7$ galaxies over wide ranges in stellar mass, SFR, and colors, with typical integration times of 8h, and up to 28h. The survey covers homogeneously the MS, where 90% of the targets are detected, and 78% are rotation-dominated disks (left panel: H α velocity fields of 125 $z \sim 1$ and 125 $z \sim 2$ targets). KMOS^{3D} also detected 25% of the targets well below the MS ($\Delta MS = \log(\text{SFR}/\text{SFR}_{\text{MS}}) < -0.8$ dex), confirming very low SFRs from the H α luminosities and revealing extended disks around the dense passive stellar cores in 1/4 of them (right panels, highlighting two cases); low [NII]/H α ratios suggest rejuvenation events in several of these objects through accretion of external, low metallicity gas.

anteed Time Observations (GTO, for the SPIFFI spectrometer of SINFONI and PARSEC for the VLT Laser Guide Star Facility) and 50 nights via several Open Time programs. The observations focused on $H\alpha$ + $[NII]$ + $[SII]$ emission of 110 $z \sim 1-3$ MS SFGs, in seeing-limited mode (4–5 kpc resolution) and with adaptive optics (AO) for a sharper view of 40 of the targets (1–2 kpc resolution). Taking advantage of the new and efficient near-IR 24-IFU KMOS instrument, built by a consortium involving MPE, we carried out the **KMOS^{3D}** survey, an ambitious and highly successful 75-night GTO program jointly led by the IR/Submm and OPINAS groups. KMOS^{3D} mapped the $H\alpha$ + $[NII]$ + $[SII]$ emission of 740 mass-selected galaxies at $z \sim 0.6-2.7$. Fulfilling its design, KMOS^{3D} provides a largely unbiased census from deep integrations ($\sim 5h-28h$) of the same spectral diagnostics resolved on seeing-limited scales of ~ 4 kpc, over a wide range of galaxy parameters and 5 Gyrs of cosmic time. The strategy uniquely enabled faint line emission mapping in individual objects out to large galactocentric radii, and pushed into the regimes well below/above the MS that were unexplored by IFU studies. Altogether, KMOS^{3D} and SINS/zC-SINF span >2 orders of magnitude in stellar mass ($\log[M_*/M_\odot] \sim 9.0-11.7$) and >3 orders of magnitude in SFR relative to the MS ($-3 \leq \Delta MS = \log[SFR/SFR_{MS}] \leq 1$).

The PHIBSS and PHIBSS2 surveys:

We have recently completed the **PHIBSS** and **PHIBSS 2** surveys, which have provided ~ 200 individual CO detections of $z \sim 0.5-3$ SFGs, and spatially resolved maps the molecular in ~ 12 of these systems. PHIBSS/PHIBSS2 cover the massive MS population over a comparable redshift range as KMOS^{3D} and SINS/zC-SINF, and were largely carried out in the 3D-HST/CANDELS fields accessible from IRAM, thus also benefitting from extensive multi-wavelength ancillary data. By targeting normal SFGs at $0.5 < z < 3$, rather than rare star-bursting outliers, our PHIBSS/PHIBSS2 surveys at IRAM bridge the gap between conventional molecular gas studies and optical-to-infrared deep look-back surveys. PHIBSS has also provided the first glimpse of the kinematics of the cold, star-forming molecular component of the ISM, which we can then use to compare with the ionized gas kinematics derived from the above near-IR surveys.

The prevalence of disks and gravity-driven gas turbulence at $z \sim 1-3$:

With the statistical power of KMOS^{3D} and the exquisite sensitivity and resolution of SINS/zC-SINF+AO, we robustly confirmed that the majority ($\sim 75\%$) of high- z SFGs are rotating disks (Fig. 2.2.1). The data also confirmed the elevated gas turbulence of high-redshift disks, with typical intrinsic disk velocity dispersions $\sigma_0 \sim 45$ km/s at $z \sim 2.3$ and ~ 30 km/s at $z \sim 0.9$ (Fig. 2.2.2). Our deep observations of CO with NOEMA reveal a comparable evolution of the cold gas dispersion, demonstrating that the turbulence is a characteristic of the entire ISM. The amount and increase with redshift of the velocity dispersions is in line with expectations for gravity-driven turbulence in marginally-stable gas disks and the cosmic evolution in gas fractions, where heating is caused by

rapid gas flows onto and within the galaxies, with only a minor contribution by stellar feedback.

The disk angular momentum and early bulge formation:

Dissipative processes should be particularly efficient in $z \sim 1-3$ disks given their gas-richness and elevated turbulence. Our spatially-resolved studies provided important clues that the associated inward mass transport and angular momentum loss could lead to bulge formation on $\leq 10^9$ -year timescales. Massive stellar bulges are in place, and large nuclear concentrations of molecular gas have been uncovered as early as $z \sim 2.5$ in massive star-forming disks. Measurements of the disk angular momenta further support bulge formation via disk-internal mechanisms. The specific angular momenta of the disks anti-correlate with their galaxy-wide stellar and gas mass surface densities, but exhibit no significant trend with stellar mass surface densities in the inner 1 kpc, suggesting that accumulation of low angular momentum material to form bulges in the disk centres is decoupled from the mechanisms that set disk structure and angular momentum on global galactic scales. The inferred halo scale angular momentum distribution of the galaxies is consistent with the theoretical prediction for their dark matter halos in terms of mean spin parameter $\langle \lambda \rangle \sim 0.037$ and dispersion $\sigma(\log \lambda) \sim 0.2$. Our data empirically support the long-standing assumption that, on average and independently of redshift, the global specific angular momentum of disks reflects that of their dark matter halos ($j_d = j_{DM}$). This result implies conservation of the *net* angular momentum of baryons as they settle from the cosmic web and halo onto the central ~ 10 kpc-scale disks, which may be mediated by the strong galactic outflows that are observed in high- z SFGs.

Baryon dominance in $z \sim 1-3$ disks:

Our studies strengthened in important ways the key finding from smaller samples that $z \sim 1-3$ SFGs are not only gas-rich but also strongly baryon-dominated on $\sim 10-15$ kpc scales (Fig. 2.2.2). Kinematic modelling of 240 well-resolved disks with high S/N data showed that gas and stars dominate the total dynamical mass budget, making up $\sim 55\%$ on average and reaching $\sim 85\%$ at $z \sim 2.3$, leaving little room for dark matter within the disk's half-light radius $R_{1/2}$ at $z > 2$. The baryonic mass fraction at fixed redshift also positively correlates with mass surface density. These effects are reflected in the evolution of the Tully-Fisher relation, connecting the disk circular velocity and mass. Three factors can explain the trends in mass budget and Tully-Fisher relation: the gas and baryonic fractions of the disks increase with lookback time as enhanced cosmic accretion promotes high baryon concentrations at the centre of dark matter halos, these halos have shallow profiles, and more compact disks probe less far into their host dark matter halo.

Our exploration of the outer rotation curves of high- z disks, thanks to our sensitive KMOS, SINFONI, and NOEMA observations, led to the most compelling evidence of the lesser role of dark matter on disk scales at high masses and redshifts (Fig. 2.2.2). The method

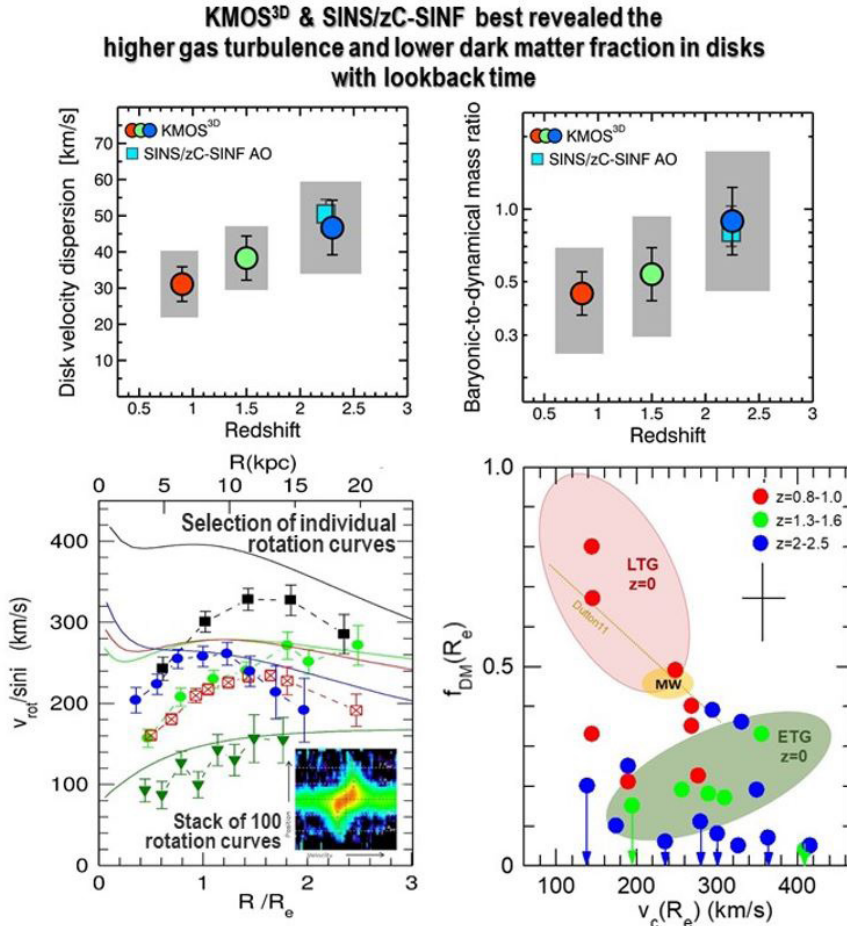


Fig. 2.2.2 Our KMOS^{3D} and SINS/zC-SINF H α data trace consistently the evolution of disk properties across 5 Gyrs of cosmic time between $z=0.6$ and $z=2.7$ from the same observational approach and analysis methods. The disk velocity dispersion and inner disk baryonic-to-dynamical mass ratio both increase with redshift (top row), reflecting higher accretion rates and efficient internal dynamical processes in the increasingly gas-rich disks at earlier times. In the deepest observations of >20 individual, and stacked data of ~ 100 disks, the rotation curves are measured beyond the peak, out to ~ 2.5 half-light radii (bottom left). Detailed modeling of these rotation curves, incorporating baryonic + dark matter components and the effects of pressure support, reveal most robustly the decrease in DM mass fractions towards higher redshift and galaxy masses (bottom right); high- z disks have similar galactic-scale DM fractions as their present-day descendants.

relies on rotation curve shapes, making it independent of (uncertain) assumptions on light-to-baryonic mass conversions involved in the other approaches above. Data of an initial set of six high-mass SFGs probing out to $2-3xR_{1/2}$ led to the exciting discovery of velocity falloffs beyond a peak at radius $r \sim 1.3xR_{1/2}$, with slopes as steep or steeper than a Keplerian decline ($v_{rot} \propto r^{-1/2}$). Detailed modelling implies dark matter fractions of $\leq 20\%$ within a half-light radius. KMOS^{3D} substantiated this breakthrough by showing, through a novel stacking technique, that dropping outer rotation curves to $3-4xR_{1/2}$ are likely a widespread feature of $\log(M_*/M_\odot) \geq 9.5$ star-forming disks around cosmic noon. In local spiral galaxies, the typically flat or slightly rising rotation curves are the hallmark of dominant dark matter in outer disk regions. At high redshift, however, the dominance of baryons within the shallower inner dark matter potential leads to declining rotation curves, with the considerable dynamical support from random motions further steepening the falloff and possibly implying disk truncation.

These findings also link massive $z \sim 1-3$ SFGs to their descendants — high-mass early-type galaxies and strongly bulged disks at $z \sim 0$ — which also have low central dark matter fractions. Our most recent efforts are substantially expanding the set of galaxies with best constraints on their resolved mass budget to probe a wider range in galaxy mass and redshift. With now detailed models for over 20 galaxies covering circular velocities of $\sim 100-400$ km/s across $z \sim 0.6-2.7$, a trend is emerging of increasing galactic-scale dark matter fractions towards lower masses and later cosmic epochs. This result further strengthens the evidence that baryons are incorporated early in disk galaxies, in line notably with the recent cosmological simulations from the Illustris/TNG project.

Outflow demographics and physical properties at $z \sim 1-3$:

Galactic winds have long been observed in distant SFGs and luminous quasars through high-velocity, blueshifted absorbing gas detected in integrated rest-UV spectra. In rest-optical nebular line emission, outflows manifest themselves through a broad component in H α + [NII]+[SII] underneath a narrower component from star formation, whose separation is greatly facilitated by IFU data. Our studies based on ~ 600 galaxies spanning very wide mass and MS offset ranges, mostly from KMOS^{3D} and SINS/zC-SINF, have revealed the distinct launching sites, demographics, and physical properties of outflows (Fig. 2.2.3). Winds powered by star formation (SF), characterized by

broad emission with FWHM ~ 450 km/s closely associated with bright star-forming clumps across the disks, are increasingly prevalent in galaxies above the MS and at SFR surface densities $\geq 1 M_\odot \text{yr}^{-1} \text{kpc}^{-2}$, reaching incidences up to $\sim 30\%$. In contrast, faster AGN-driven winds (FWHM ~ 1500 km/s) originate from the nuclear regions and their incidence correlates strongly with stellar mass: they are rare below $\log(M_*/M_\odot) \sim 10.7$ and rapidly become ubiquitous above this mass, being present in $\sim 75\%$ of $\log(M_*/M_\odot) > 11.2$ galaxies. The outflows, along with the elevated disk turbulence, could efficiently redistribute metals within the galaxies and explain the typically flat radial metallicity gradients inferred from SINS/zC-SINF+AO + KMOS^{3D} maps of the diagnostic [NII]/H α flux ratio.

The high quality and S/N achieved in stacked spectra enabled a first reliable measurement of the electron density of the outflowing ionized gas from the [SII] $\lambda\lambda 6716, 6731$

KMOS^{3D} & SINS/zC-SINF pinned down the roots and established the demographics of high-*z* galactic winds

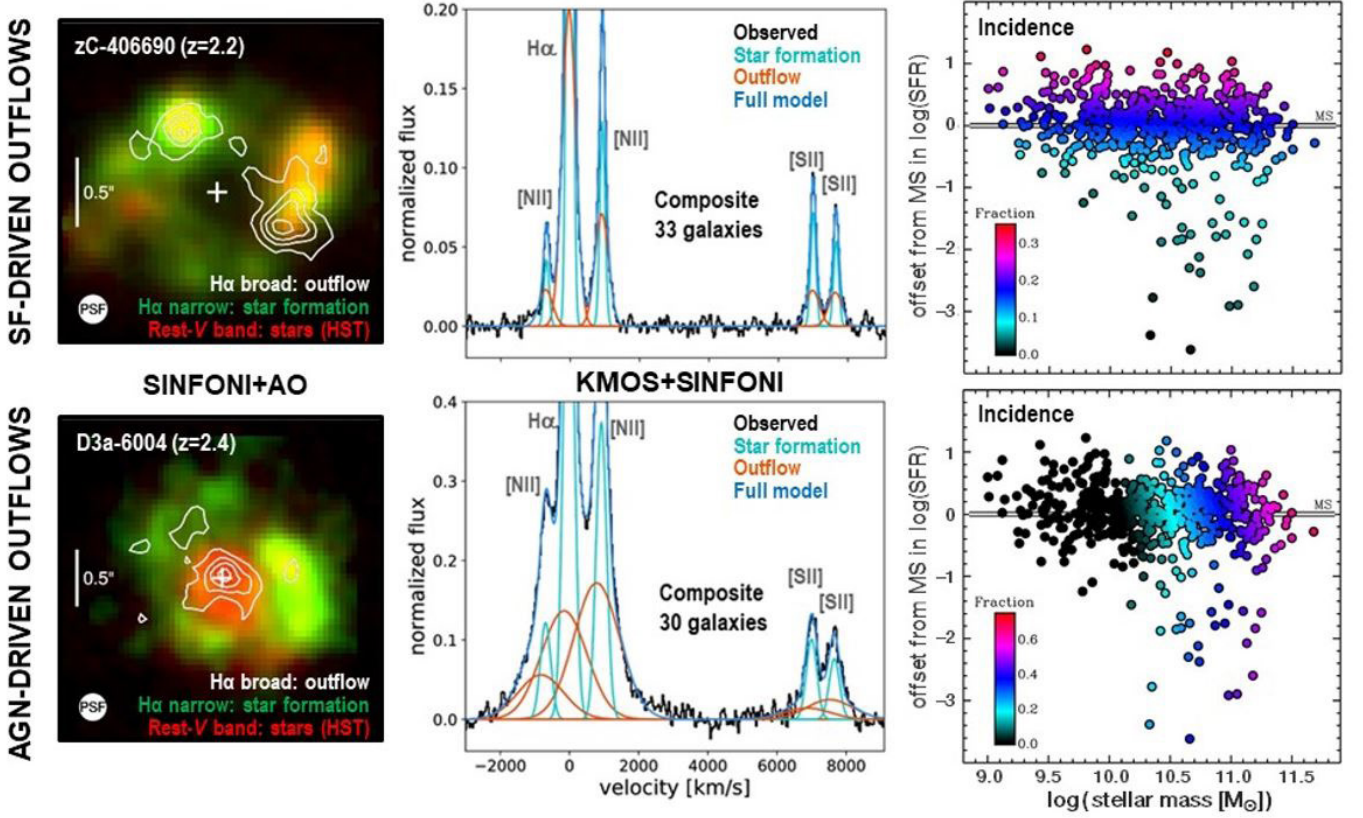


Fig. 2.2.3 Spatial distribution, spectral properties, and demographics of galactic winds driven by star formation (SF) and AGN. Maps of two example galaxies from SINFONI+AO and HST (FWHM physical resolution of ~ 1.8 kpc), composite spectra from our KMOS+SINFONI samples, and the fraction of galaxies exhibiting the broad $H\alpha$ + $[NII]$ + $[SII]$ outflow signature as a function of galaxy stellar mass and MS offset in SFR illustrate key results uniquely enabled by our studies. SF-driven winds are launched near bright star-forming clumps, have typical speeds ~ 450 km/s below the hosts' escape velocity except at $\log(M_*/M_\odot) \leq 10.3$; the prevalence of these winds depends on SF properties, not mass. AGN-driven winds originate from the nuclear regions, are ubiquitous in $\log(M_*/M_\odot) \geq 10.7$ galaxies hosting a massive bulge but rare at lower masses, irrespective of SF activity; with velocities of ~ 1500 km/s, they can escape the galaxies where their energy input ($\sim 1\%$ that of the AGN) may heat halo gas, thereby contributing to quenching. The high S/N spectra constrain for the first time the density in high-*z* SF-driven winds from the broad $[SII]$ doublet ratio, yielding $n_e \sim 400$ cm $^{-3}$; for AGN-driven winds, a higher $n_e \sim 1000$ cm $^{-3}$ is inferred. The high densities lead to modest mass outflow rates $\sim 0.1\text{--}0.4 \times \text{SFRs}$ in the warm ionized gas phase.

doublet ratio in SF-driven winds, yielding $n_e \sim 400$ cm $^{-3}$, and possibly as high as $n_e \sim 1000$ cm $^{-3}$. These new determinations are a factor of several higher than previously assumed values, and lead to correspondingly lower mass outflow rates. The velocity of SF-driven winds varies little with galaxy mass, implying that the bulk of expelled gas escapes only from $\log(M_*/M_\odot) \leq 10.3$ systems while more massive galaxies drive so-called “fountains.” The inferred mass outflow rates \dot{M}_{out} are only $\sim 0.1\text{--}0.2$ times the SFRs at all galaxy masses, at odds with theoretical work that requires mass loading factors $\eta = \dot{M}_{\text{out}}/\text{SFR}$ above unity and $\propto 1/M_*^{0.35-0.8}$ to reproduce the observed slope of the galaxy mass–metallicity and galaxy mass – halo mass relationships at $\log(M_*/M_\odot) < 10.7$. This tension could be alleviated if substantial amounts of mass, momentum, and energy are contained in much hotter and/or colder wind phases than the $\sim 10^4$ K ionized gas probed by $H\alpha$

The faster, high duty cycle AGN-driven winds at high masses have comparable mass loading factors as the SF-driven winds but carry ~ 10 times more momentum and ~ 50 times more energy, such that they can escape

the galaxies, contribute to heat halo gas, and help prevent further gas infall. Results from EAGLE and Illustris/TNG numerical simulations suggest that such a mechanism, acting also at the modest AGN luminosities and Eddington ratios of a majority of the KMOS^{3D} AGN, may be more effective at widespread and long-term quenching than ejective “QSO mode” feedback in rare, high luminosity, high Eddington ratio AGN. The sharp increase in incidence of AGN-driven winds near the transition mass above which passive galaxies become prevalent and both galactic molecular gas fractions and specific SFRs drop steeply, strengthens the notion of a connection between AGN activity and quenching. Our first observations with NOEMA and ALMA of a handful of MS massive galaxies indicate that the total mass outflow and energy deposition rates could be higher when accounting for a possible outflowing component in cold molecular gas, as inferred in the local Universe, highlighting the role of feedback through outflows in galaxy evolution.

Star-forming disks and rejuvenation in compact galaxies:

The KMOS^{3D} strategy allowed a systematic exploration

of the emission line properties in rarer subsets of galaxies, with consistent comparisons to the underlying population. Massive compact SFGs at $z \sim 1-3$ have received much attention in recent years as potential immediate progenitors of dense massive quiescent galaxies. In 2/3 of 35 compact SFGs observed in KMOS^{3D}, spatially resolved line emission reveals rotating gas disks with up to twice the extent of the compact stellar cores. The rotation observed in the compact SFGs, and the emerging evidence from stellar morphologies and kinematics that high- z passive galaxies often are disk-like systems, support an evolutionary link between these populations. Pushing into a regime so far unexplored with IFUs at $z > 1$, we discovered line emission in $\sim 1/4$ of the targets classified as quiescent (Fig. 2.2.1). Half of them exhibit spectral signatures revealing the persistence of AGN activity and gas outflows well into quenching. In the other sources, the $H\alpha$ luminosities confirm the low star formation activity with $SFR(H\alpha) \sim 0.2-7 M_\odot \text{ yr}^{-1}$ but, surprisingly, their average $[NII]/H\alpha$ ratio indicates ~ 3 times lower metallicities than MS SFGs of the same mass, and half also exhibit resolved gas disks. These properties sug-

gest rejuvenation, where the low-level star formation is fuelled by recent accretion of metal-poor gas via cosmic flows or minor mergers rather than being associated with advanced stages of disk fading.

Gas content and scaling relations $z \sim 0-3$:

By targeting normal SFGs at $0.5 < z < 3$, rather than rare star-bursting outliers, our PHIBSS/PHIBSS2 surveys at IRAM bridged the gap between conventional molecular gas studies and optical-to-infrared deep look-back surveys. PHIBSS/2 revealed molecular gas mass fractions as high as 1/2 at $z \sim 1-2$, quantified galaxy-integrated star formation – molecular gas scaling relations at high redshift, and established that the rapidly declining SFRs since $z \sim 1$ are mainly controlled by a reduction of cold gas reservoirs (Fig. 2.2.4, top left). Higher resolution follow-up of selected galaxies revealed gas complexes with sizes akin to those of star-forming clumps traced by stellar and ionized gas light at rest-UV and optical wavelengths, and showed that the bulk of molecular gas is similarly turbulent as the ionized gas layer (Fig. 2.2.4, bottom 3 panels).

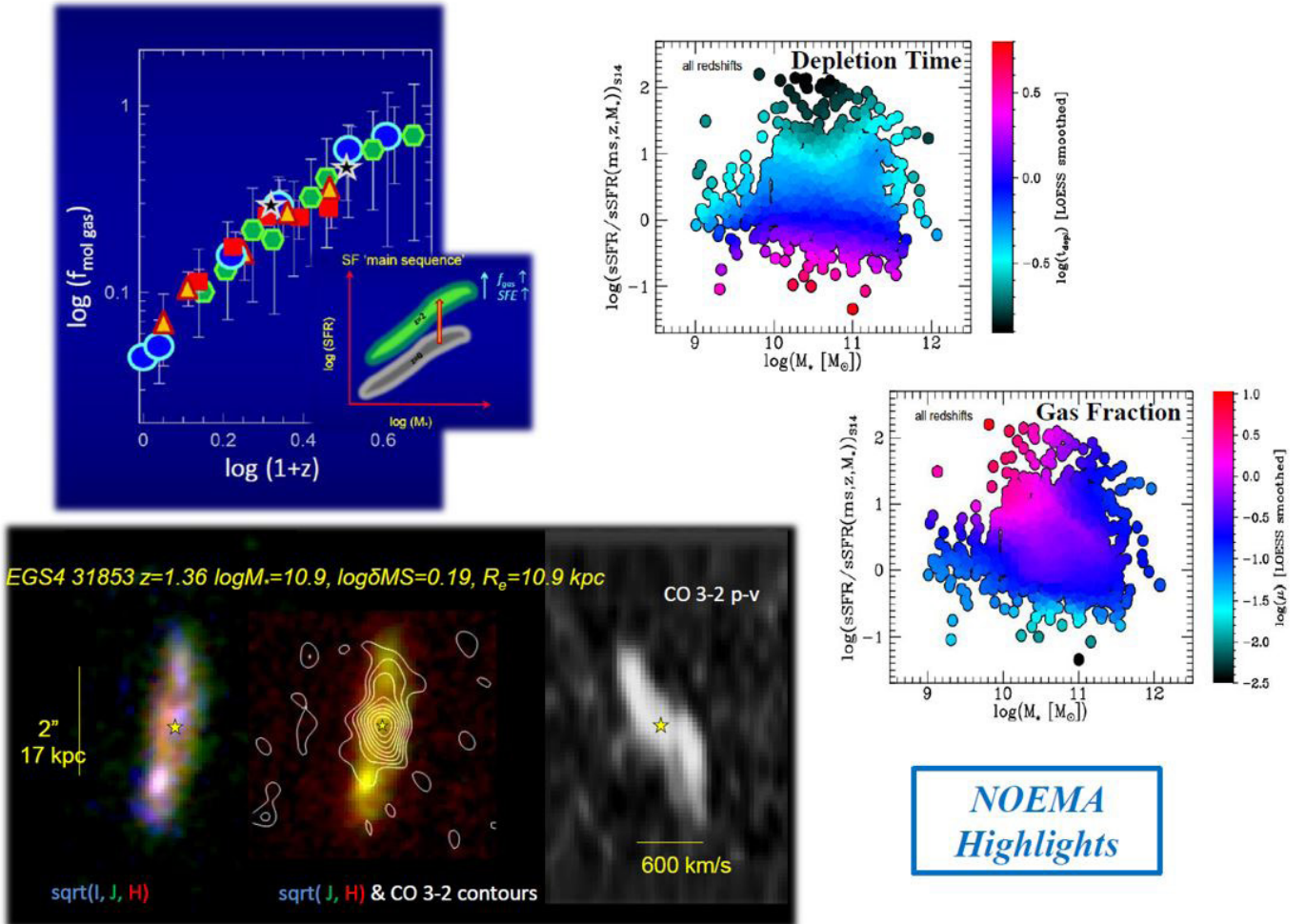


Fig. 2.2.4 Main results from our PHIBSS surveys and outlook to NOEMA^{3D}. **Clockwise from top left:** 1) the evolution of molecular gas fraction with redshift. The symbols are averages in redshift of molecular gas measurements from CO (blue circles), Herschel FIR-SED stacks (green hexagons, red squares and gold triangles), and submm continuum fluxes (black stars). The inset shows how the evolution of gas fraction tracks the evolution of the star formation rate; 2) two-dimensional distributions of depletion time scale t_{depl} (top) and molecular gas to stellar mass ratio, μ_{gas} (bottom) in the stellar mass – specific SFR, taking data at all redshifts, after removing the redshift dependencies. The color-coding is shown in the bars to the right of each plot; 3) CO 3-2 observations with NOEMA (20 hr in D+A configuration and 9 antennas), of a massive, $z \sim 1.4$ SFG, together with our best-fit kinematic model. **Left to right:** HST color-composite image; CO integrated intensity map (contours) and HST JH-band composite (color); CO position-velocity map.

We have combined our PHIBSS1&2 CO molecular gas measurements with the low redshift xCOLDGASS CO survey, smaller high- z CO samples from the literature, gas masses derived from > 500 Herschel far-IR galaxy stacks, and gas masses derived from single band submm continuum flux measurements to provide a total sample of 1444 individual measurements. With these data, we have established statistically robust scaling relations of molecular gas depletion time scale (t_{depl}) and gas to stellar mass ratio (M_{molgas}/M_*) of SFGs near the star formation ‘main-sequence’ with redshift, specific star formation rate sSFR, and stellar mass (Fig. 2.2.4, right panels). The steep redshift dependence of $M_{\text{molgas}}/M_* \propto (1+z)^3$ mirrors that of the sSFR evolution and likely reflects the gas supply rate. Decreasing gas fractions at high M_* are driven by the flattening of the SFR– M_* relation at all redshifts. Throughout the redshift range probed, a larger sSFR at constant stellar mass is due to a combination of an increasing gas fraction and a decreasing depletion time scale, in approximately equal measure. Future spatially resolved gas and dust maps with NOEMA and ALMA will enable us to determine accurate molecular gas size distributions and dynamical properties, which will elucidate the underlying physics driving the scatter in the relations.

Taking the next steps with NOEMA, VLT/ERIS+AO, ELT/MICADO:

With large samples in hand from KMOS^{3D} and PHIBSS, we are planning the next big steps with new or upgraded instruments and facilities. Later this year we will start a comprehensive, spatially resolved (few kpc) CO and dust imaging program of ~ 50 $z \sim 0.5$ – 2 SFGs with NOEMA. **NOEMA^{3D}, an MPG-IRAM GTO program**, will run for 4–5 years, and aims to provide deep, $\sim 0.4''$ FWHM resolution observations of CO 4–3, [CI] 1–0 and dust continuum for a representative galaxy sample. The program will fully utilize the increased bandwidth, sensitivity and spatial resolution provided by the 32 GHz bandwidth receivers, 11–12 antennas, and the extended 1.5 km baselines of the upgraded NOEMA facility. With NOEMA^{3D} we will explore the critical role that cold dense gas plays in galaxy disk and bulge formation by: 1) measuring the inner and outer disk rotation curves and velocity dispersion distributions; 2) searching for evidence for molecular outflows; 3) determining the relative distribution of gas/dust and optical/UV/IR emission; and 4) establishing how commonly they exhibit concentrated nuclear gas and dust distributions.

Our galaxy evolution programs will further capitalize on the novel opportunities afforded by two new state-of-the-art near-IR instruments built under the leadership of our MPE IR/submm group. **ERIS, the next-generation AO-assisted near-IR IFU and imager at the VLT** to be commissioned in 2020, will feature more than two-fold improvements in sensitivity, AO performance, and spectral resolution across the entire $\lambda = 1$ – $2.5 \mu\text{m}$ window compared to SINFONI, while keeping its versatility in the combination of three pixel scales and fields of view for diffraction- to seeing-limited observations. These capabilities will greatly facilitate studies of distant galaxies

resolved on ~ 1 kpc scales from $z \sim 3$ to later epochs around $z \sim 1$ when the decline of cosmic star formation and SMBH accretion is well underway. With an instantaneous field of view of up to $8'' \times 8''$, ERIS will remain the instrument of choice for mapping the faint outskirts of high- z disks. With our GTO, we expect to triple the existing SINS/zC-SINF AO sample and outer rotation curves sets, over wider ranges in redshift, mass, and SFR by drawing targets notably from KMOS^{3D}. Key science goals entail (1) detailed inner disk dynamics to characterize mass and angular momentum transport from signatures of non-circular motions on ~ 1 kpc scales, (2) outer disk kinematics to > 15 – 20 kpc to strengthen the emerging DM fraction trends, (3) ionized gas outflows mapping to constrain accurately their typical extent and geometry, critical in estimating wind mass, energetics, and evolution.

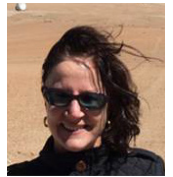
Around 2025, the **first-light MICADO imager and spectrograph on the 40m ELT** will be a game-changer: optimized for diffraction-limited operations, it will provide a 10-fold gain in angular resolution over AO at 8–10m telescopes and HST, and even a 6-fold increase compared to JWST. Together with its sensitivity and $R \sim 20000$ spectroscopic capabilities, MICADO will provide unprecedented views of the structure, stellar populations, and kinematics of substructure down to ~ 100 pc at $z \geq 1$, comparable to individual star-forming complexes such as 30 Doradus in the Large Magellanic Cloud. With MICADO, we plan to take our studies of galaxy evolution to the next level through detailed properties of sub-galactic components from disk clumps and bulges to globular cluster progenitors to determine their formation mechanisms and time-scales, reach into the dwarf galaxy mass regime and the first galaxies and SMBHs towards reionization, resolve the stellar structure and kinematics of compact passive galaxies out to $z \sim 3$. We are undertaking major efforts to set up an ambitious and coherent MPE/IR GTO program in anticipation of the new and transformative discovery space that MICADO will bring to our physical understanding of galaxy evolution.

Selected References:

- Belli, S., Genzel, R., Förster Schreiber, N.M., et al. 2017, *ApJ*, 841, L6
 Burkert, A., Förster Schreiber, N.M., Genzel, R., et al. 2016, *ApJ*, 826, 214
 Davies, R.L., Förster Schreiber, N.M., Übler, H., et al. 2019, *ApJ*, in press (arXiv:1808.10700)
 Förster Schreiber, N.M., Renzini, A., Mancini, C., et al. 2018, *ApJS*, 238, 21
 Förster Schreiber, N.M., Übler, H., Davies, R.L., et al. 2019, *ApJ*, 875, 21
 Genzel, R., Förster Schreiber, N.M., Übler, H., et al. 2017, *Nature*, 543, 397
 Genzel, R., Tacconi, L.J., Lutz, D., et al. 2015, *ApJ*, 800, 20
 Herrera-Camus, R., Tacconi, L.J., Genzel, R., et al. 2019, *ApJ*, 871, 37
 Lang, P., Förster Schreiber, N.M., Genzel, R., et al. 2017, *ApJ*, 840, 92
 Tacconi, L.J., Neri, R., Genzel, R., et al. 2013, *ApJ*, 768, 74
 Tacconi, L.J., Genzel, R., Saintonge, A. et al. 2018, *ApJ*, 853, 179
 Übler, H., Förster Schreiber, N.M., Genzel, R., et al. 2017, *ApJ*, 842, 121
 Übler, H., Genzel, R., Tacconi, L.J., et al. 2018, *ApJ*, 854, L24
 Wisnioski, E., Förster Schreiber, N.M., Wuyts, S., et al. 2015, *ApJ*, 799, 209
 Wisnioski, E., Mendel, J.T., Förster Schreiber, N.M., et al. 2018, *ApJ*, 855, 97
 Wuyts, E., Wisnioski, E., Fossati, M., et al. 2016, *ApJ*, 827, 74
 Wuyts, S., Förster Schreiber, N.M., Wisnioski, E., et al. 2016, *ApJ*, 831, 149



Natascha Foerster Schreiber



Linda Tacconi

(Other MPE members include: R. Genzel, E. Wisnioski, A. Beifiori, S. Belli, R. Bender, A. Burkert, R.I. Davies, R.L. Davies, M. Fabricius, M. Fossati, A. Galametz, R. Herrera-Camus, D. Lutz, J.T. Mendel, S.H. Price, R. Saglia, S. Seitz, T. Shimizu, A. Sternberg, H. Übler, D. Wilman)

2.3 Massive Black Holes and Black Hole-Galaxy Co-Evolution

Many open questions concerning AGN and their environment are best addressed by our tools of high spatial and spectral resolution NIR and mm spectrometry and interferometry. Among other aspects, our projects have dealt with the characterization of circum-nuclear starbursts, the distribution and dynamics of circum-nuclear gas, and the properties of obscuring material. Key aspects of our research in this area are the feeding of and the feedback from BHs: We map the distribution, kinematics, and properties of gas on scales of < 100 pc to understand how gas flows in from large scales to fuel the AGN, and how gas is ejected out as a result of energy released from accretion onto the SMBH, ultimately leading to powerful large-scale galactic winds. The advent of the 2nd generation near-infrared interferometer GRAVITY has led us to major recent breakthroughs. One of the most remarkable results has been the spatial resolution of the broad-line region (BLR) in 3C273. The discovery not only confirmed the long-standing hypothesis of a coherent rotation of the BLR, but also provided a unique kinematic measurement of the mass of a supermassive black hole (SMBH) - at a distance of 550 Mpc. In an approved ESO/VLTI Large Program we will extend this study to a sample of local AGN, and we are exploring options to expand it to larger samples and higher redshifts with potential upgrades of GRAVITY.

LLAMA: our project to study Local Luminous AGN with Matched Analogues is, for the first time, systematically addressing gas flows on circumnuclear scales in nearby active galaxies using spatially resolved observations. Awarded 195 hrs of time on the VLT to observe a complete volume limited sample of 14-195 keV selected AGN as well as a matching sample of inactive galaxies, the data are enabling us to better understand a variety of different aspects about AGN. Following up on our earlier results, we have confirmed that the role of the environment in fuelling AGN does depend on the host galaxy: for lenticular galaxies which have little gas, AGN are found only in smaller groups where pre-processing strips gas that can then be accreted from the environment to fuel the AGN; in spiral galaxies, which are much more common, environment plays little role in fuelling AGN, which is instead dominated by secular processes within the host galaxy itself (Davies et al. 2017). As the gas flows in, a nuclear stellar disk is formed on scales of 10-100 pc, although its kinematic signature is often masked due to the underlying radial dependence of the pseudo-bulge kinematics (Lin et al. 18). Our stellar population synthesis shows that, in contrast to inactive galaxies, in AGN this region is typified by stellar ages of a few tens of Myrs but no longer actively forming stars – as expected for episodic star formation, with the most recent episode occurring shortly before inflowing gas reaches the AGN. In terms of the central obscuration, we have identified a population of AGN that were hinted at in our initial exploration of the sample. These AGN have little

dust obscuration so are optically type 1, but exhibit very significant gas columns absorbing the X-rays. Related to the few well known sources with variable X-ray columns caused by Broad Line Region clouds crossing the line of sight to the accretion disk, this population of objects suggest that our line of sight to about 15% of Seyfert 1s is through relatively dust-free gas (Shimizu et al. 2018). The LLAMA project is helping us quantify the impact of outflows through the combination of different spatially resolved datasets. In a case study of NGC 5728 (Shimizu et al. 2019), we have used the weak trans-auroral lines to derive the density in the outflowing gas, avoiding the implicit bias associated with the usual tracers. Within 500 pc, it remains above 1000 cm^{-3} , an order of magnitude higher than often assumed. As a result the derived outflow rate is much lower than previously estimated, only $0.1 M_{\odot} \text{ yr}^{-1}$. In this object, the outflow is bisecting the host galaxy's disk. Yet, although it changes the excitation in the disk, the outflow does not disrupt the disk. Hence in this AGN, which has a luminosity $L_{\text{AGN}} \sim 10^{44} \text{ erg s}^{-1}$, feedback has little impact on the host galaxy even in the circumnuclear regions. Our next steps in this respect will be to apply a similar analysis to the other AGN in our sample to ascertain whether the high density in the outflow is typical of Seyfert galaxies.

Spatially resolving the inner structures of AGN with GRAVITY: One of the most exciting opportunities offered by GRAVITY, the new VLTI beam combiner, is to directly resolve the broad line region of active galactic nuclei on scales of tens of μarcsec , using spectro-astrometry, and to image the hot dust (aka torus) structures.

Resolving the Broad Line Region: Broad lines in AGN spectra can be used to measure the mass of the black hole (assuming that the motions are due to gravity), and to constrain accretion and outflow models. However, because of its small radius it has been impossible to resolve the structure of the BLR directly, which introduces uncertainties in derived black hole (BH) mass measurements. Studies of the BLR structure have relied mostly on reverberation mapping (RM). Reverberation techniques use the time variability observed in the AGN continuum emission and the subsequent response of the gas in the BLR or of the hot dust located at the sublimation radius (inner torus rim). These RM programs established a size-luminosity relation ($R_{\text{BLR}} \sim L^{\alpha}$) which allow black hole mass estimates from a single AGN spectrum. This is the only available method for measuring black hole masses in large surveys and out to high redshift and plays a key role in our understanding of black hole growth over cosmic time. However, recent velocity-resolved RM studies are starting to indicate a variety of BLR geometries and a previously unknown dependence on the Eddington ratio. Spectro-astrometry with GRAVITY provides a new, direct probe of the BLR spatial and velocity structure which can independently test and break degeneracies in these studies.

Imaging the innermost hot dust: Another long-standing issue of AGN models is the size and structure of the obscuring, dust-emitting region: is it a torus or disk, inflowing or outflowing? The near and mid infrared luminosity associated with AGN originates in dust surrounding the AGN and heated by it. However, like the BLR, circum-nuclear dust in AGNs is unresolved in single-dish images. In the past decade infrared interferometry has begun to shed light on the physical structure of this component. Tens of AGN have been observed in the mid-IR with MIDI. Detailed results from Circinus and NGC 1068 show evidence for an inner disk, but have also revealed dust in the polar regions indicative of outflow. The presence of multiple components could have a severe impact on dust-RM methods which assume a torus origin. The NIR is thought to trace hot dust just beyond the sublimation limit at the inner edge of the torus. Measuring the emission size can therefore test the assumptions on which dust-RM methods are based. GRAVITY observations provide the first resolved view of the shape and structure of the hot dust emission region whose size and orientation can be compared directly with that of the BLR.

Our team has observed several Type 1 and Type 2 AGN with GRAVITY in commissioning and open time programs in the past two years. We have now, for the first time, spatially resolved (10 μ arcsec or ~ 0.03 parsec for a distance of 550 mega-parsecs) a velocity gradient across the broad line region of the quasar 3C 273 (Gravity Collaboration et al. 2018). The gradient reveals rotation perpendicular to the jet, and is consistent with line emission from a thick disc of gravitationally bound material around a black hole of 3×10^8 solar masses. We infer a disc radius of 150 light-days (compared to 100-400 light-days found previously from reverberation mapping - RM). Thus, GRAVITY provides both a confirmation of RM (at least for this one object) as the main previous method to determine black hole masses in quasars and a new and highly accurate, independent method to measure such masses.

The GRAVITY AGN Large Programme:

We have recently been granted (in open time) a Large Program by ESO (17 nights over 4 semesters, starting in April 2019). In a sample of 11 AGN spanning 4 orders of magnitude in luminosity we aim to constrain questions like: How reliable are RM-based BLR sizes and black hole masses? Are BLR kinematics always dominated by ordered rotation? What is the size and shape of the obscuring structure? Further examples of what data and insights can be expected from such a study are shown in Fig. 2.3.1: the Seyfert 1 galaxy NGC 3783 (upper middle) is another Type I AGN where we have detected a velocity gradient (coloured circles). While deeper integration is still needed, the signature is consistent with a thick disk, rotating BLR at the size found by RM. (ii) NGC 3783 shows extended, asymmetric structure (upper middle, the first reconstructed mas scale image of an AGN “torus”). The core minor axis size is compatible with the sublimation radius, but it is extended a factor ~ 2 and there is a second component offset by ~ 2 mas. The BLR

velocity gradient appears to follow the elongated axis of the hot dust continuum, suggesting a possible physical connection between the two structures. (iii) The K-band hot dust continuum sizes we have measured so far generally agree with the empirical relation between hot dust radius and AGN luminosity, but with the QSO sources more compact than expected. (iv) We have also detected the hot dust core in the Seyfert 2 galaxy NGC1068. The dust is in a parsec scale, highly inclined ($i \sim 75^\circ$) and clumpy ring-like structure, aligned with the H_2O maser spots (see Figure 2.1.1). This hot dust does not appear to come from an optically and geometrically thick torus that the standard unified model of type 1 and 2 AGN predicts. The overall goal of our Large Program is to establish a new and independent BLR size – AGN Luminosity relation which is essential to derive black hole masses in larger samples and at high redshifts (lower right).

GRAVITY+: Evolution of Supermassive Black Holes and their Host Galaxies over Cosmic Time:

This pilot study demonstrated the great potential of near-infrared interferometry in the study of supermassive black holes and their immediate environments. The present sensitivity, however, only allows targeting relatively few, bright AGN in the local universe. Observational and theoretical work indicate that SMBHs play an important role in the early evolution of their host galaxies. The M-sigma relation over six orders of magnitudes (Ferrarese et al. 2006), the similar integrated star formation rate and BH growth over cosmic time (Madau & Dickinson 2014; see also Fig. 2.3.1 lower right) as well as the correlation of star formation history and BH mass seen in individual galaxies (Martin-Navarro et al. 2018) are likely the result of AGN regulated gas feeding and quenching. In order to bring the most active phase of BH growth at redshift 1-2 into reach and to be able to probe the coevolution of high redshift galaxies and their SMBHs, we started to investigate possible upgrade paths and projected performance improvements to unlock the full potential of near-infrared interferometry with the European VLTI facility.

We identified a large margin for improvement for the adaptive optics (AO). The current AO achieves in case of AGN a Strehl of only 10-15%. This comparably low Strehl not only reduces the injected flux but also results in a significantly reduced fringe-tracking performance. This leads to a multiplicative loss of coherent signal on the stabilised science channel. Between high Strehl and low Strehl science integrations we find a loss of coherence of a factor ~ 2.2 . State-of-the art Na-laser guided AO systems have demonstrated a factor 4.5 better performance in the K-band. An upgrade of the AO facility with lasers therefore has the potential to improve the coherent sensitivity by a factor 10. A factor 2-3 better instrument throughput can be achieved with new grisms (science grade grisms have already been purchased from CANON) and by upgrading key optical components. Zero noise (photon-counting) detectors, currently under development, will lead to a factor ~ 2 better sensitivity. Furthermore, noiseless detectors will fundamentally change the concept of optical interferometers. They

will remove the necessity to split the object light in two channels; one channel for high bandwidth, low resolution fringe-tracking and a second stabilised channel for spectrally dispersed long science integrations. Overall, we estimate a total margin for sensitivity improvements of a factor 80-100 compared to the current GRAVITY performance. This increases the accessible magnitude limit from $m_K \sim 10.5$ to $m_K \sim 15-15.5$. Another very promising upgrade path is to make use of the dual-feed capability of the VLTI. This allows using an external, throughput optimised fringe-tracker locking on a guide star, which corrects atmospheric perturbations and enables long integration times on the faint science objects. The accessible field of view (isopistonc angle) and the corresponding sky coverage, under good atmospheric conditions, is $\sim 30''$ at the site of the VLTI. The probability to find a

suitable guide star ($m_K < 15$) within the isopistonc angle from a potential science target is about 20% for large galactic latitudes and $>90\%$ for low galactic latitudes. With a large enough sample size this allows to pick the most promising candidates. Fig. 2.3.1 (lower right) shows selected AGN (with suitable guide stars) of different redshifts and their expected phase signal. With the proposed sensitivity upgrades of GRAVITY+ we will be able to obtain accurate BH masses for a thousand local AGN, few hundred AGN at $z \sim 0.6-1.3$ and order 100 AGN at $z \sim 2-2.8$, effectively covering the most active phase of black hole growth. Support of this vision by the Visiting Committee would be most helpful in our attempt to realize this upgrade of GRAVITY.

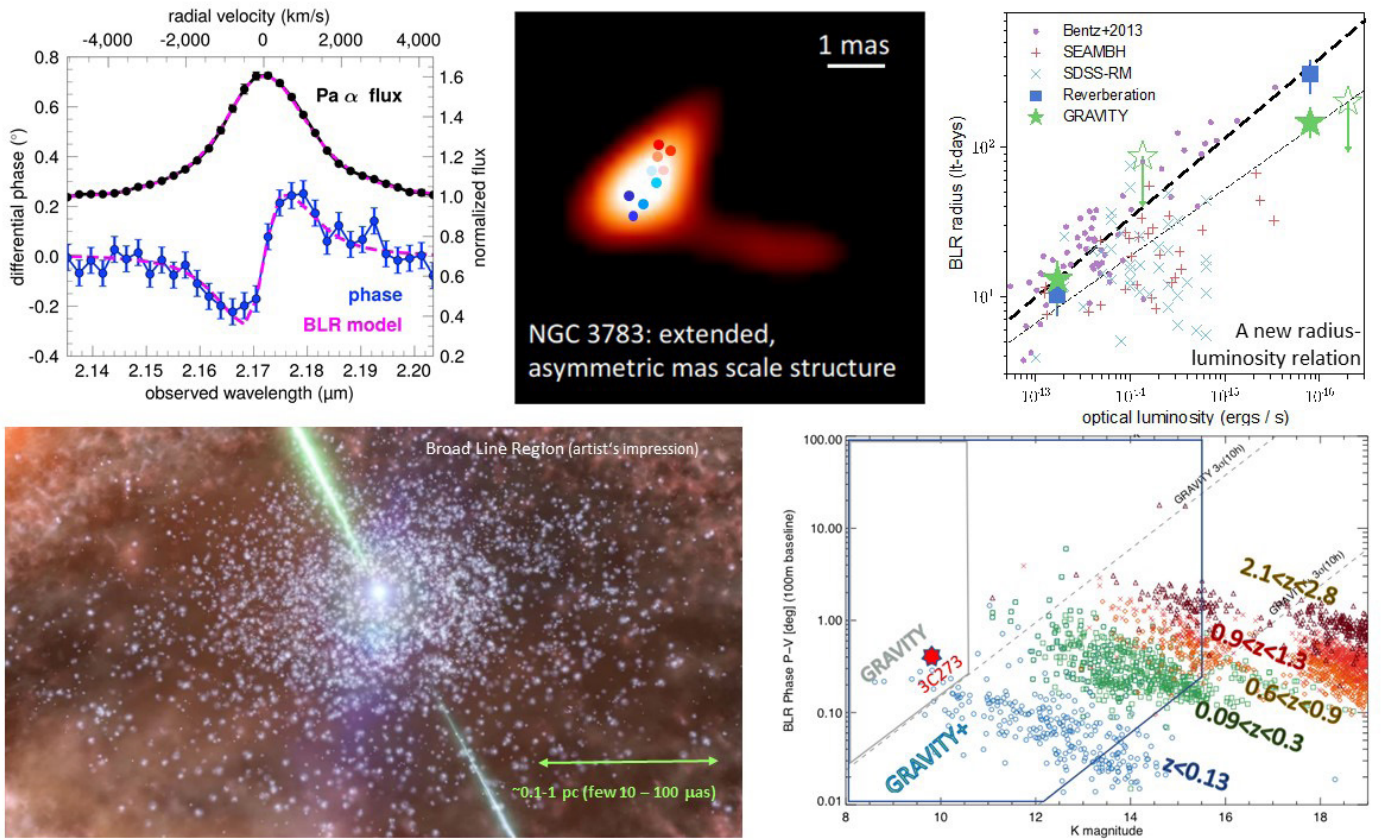


Fig. 2.3.1 Upper Row: left: Measured astrometric phase and radial velocity of the BLR in 3C273; **middle:** the first reconstructed mas scale image of the hot dust structure (torus?) in a type 1 AGN - NGC 3783 shows extended, asymmetric structure. The core minor axis size is compatible with the sublimation radius, but it is extended a factor ~ 2 and there is a second component offset by ~ 2 mas. The BLR velocity gradient (circles) aligns with the elongated hot dust; **right:** BLR size – AGN luminosity relation; in our accepted Large Program we will build up a small sample to establish a new radius-luminosity relation from interferometric data. **Lower Row: left:** artist's impression of the BLR in 3C273 as derived from our GRAVITY measurements (upper left); **right:** Extrapolated astrometric phase signal of type I AGNs and QSOs at different redshifts. All targets have a suitable guide star within $30''$. The colours indicate the BLR line shifted into the observable K-band (blue: Br-γ, green: Pa-α, orange: Pa-β, red: Pa-γ, brown: H-α). The grey area indicates the current GRAVITY detection parameter space assuming a 10h exposure. The blue outlined area shows the detection parameter space for GRAVITY+. Hundreds of AGN at low redshift and order 100 AGN up to redshift 2.8 will be in reach with GRAVITY+.

Selected References:

Davies, R., et al. 2017, *MNRAS*, 466, 4917
 Ferrarese et al. 2006, *ApJ*, 644, L21
 GRAVITY Collaboration: Sturm, E. et al. 2018, *Nature*, 563, 657
 Lin, M.-Y., et al. 2018, *MNRAS*, 473, 4582
 Madau & Dickinson 2014, *ARAA*, 52, 415
 Martin-Navarro et al. 2018, *Nature*, 553, 307
 Shimizu T., et al. 2018, *ApJ*, 856, 154
 Shimizu T., et al. 2019, *submitted*

(Other MPE team members include: J. Dexter, F. Eisenhauer, N. M. Förster Schreiber, R. Genzel, S. Gillessen, R. Herrera-Camus, D. Lutz, T. Ott, J. Shangguan, T. Shimizu, A. Sternberg, L. J. Tacconi, I. Waisberg, F. Widmann)

Richard Davies



Eckhard Sturm



Oliver Pfuhl



2.4 The Galactic Center

Since 2017 our team has a fantastic, new tool available to study in unprecedented detail the center of the Milky Way: The NIR interferometer GRAVITY, coherently combining the light of the four 8m telescopes of the VLT and synthesizing a virtual telescope of 120m diameter. This improved the imaging resolution by a factor 15, and the astrometric precision by a similar factor compared to what was possible before. This advance sharpened very much the arguments for SgrA* being a massive black hole (MBH). The superb astrometry from GRAVITY of the star S2 as it passed the pericenter of its orbit in May 2018 determined the mass of SgrA* to 0.5% precision: $M_{\text{SgrA}^*} = (4.15 \pm 0.02) \times 10^6 M_{\odot}$. Further, the triple observation of orbital motion of a flaring, hot spot close to the innermost stable orbit shows unambiguously that this mass is confined to within a region of < 0.35 AU. Previously, the spatial constraint needed to come from the combination of the intrinsic size of SgrA* measured at 1.3mm with the VLBI work showing that SgrA* moves linearly and thus exceeds the surrounding objects in mass by a large factor.

2.4.1 Emission from SgrA*

GRAVITY detects orbital motion of flares from SgrA*:

On July 22nd, 2018, we observed a NIR flare from SgrA* with GRAVITY. Our data show continuous positional and polarization changes. The position exhibits 3/4 of a clockwise loop with a diameter of $\approx 100 \mu\text{as}$ within 40 minutes, a speed corresponding to 30% speed of light (Fig. 2.4.1, left). At the same time, the polarization angle rotates. Together, these data point towards a near face-on, circular orbit of a compact polarized hot spot at $\approx 6 - 10 R_{\text{g}}$ moving in a poloidal magnetic field. Further, for at least two more flares observed in 2018 we find qualitatively and quantitatively the same. Notably, the flares

match the relation between radius and period expected for a Kerr-Schwarzschild black hole (Fig. 2.4.1, middle, GRAVITY collaboration 2018b).

NIR flares thus constitute dynamical probes deep down in the potential of SgrA*, a regime in which relativistic effects are expected to be significant. In particular, this opens up prospects for measuring the spin parameter a of SgrA*. If a flare on an orbit smaller than $3 R_{\text{g}}$ ($\approx 30 \mu\text{as}$) can be observed, a lower limit on a can be given (Fig. 2.4.1, middle). Also, the apparent flare centroid position is affected by lensing, and a suitable flare might show a characteristic kink in its orbit (Fig. 2.4.1, right).

Polarization swings yield strong constraints on the SgrA* system:

We developed fully relativistic models and used them to interpret GRAVITY flare data. This 'NERO' code combines a fully relativistic treatment of particle orbits in a Kerr spacetime with relativistic ray tracing to calculate observed snapshots and movies at a distant observer. The code includes out of plane motion in such calculations for the first time.

The hot spot model produces polarized synchrotron radiation whose time variability traces the spatial structure of the background magnetic field. All GRAVITY flares to date show polarization behavior consistent with a continuous rotation of the polarization angle. The time for one polarization-angle rotation matches the astrometric orbital period. Naively, one would expect for a fixed toroidal magnetic field two polarization rotations per orbit - the spot runs through alternating vertical and horizontal linear polarization every $1/4$ of an orbit. Our data rule this out. A single rotation is obtained when the field is predominantly poloidal. Overall, astrometry, polarization period, the number of polarization loops and the mod-

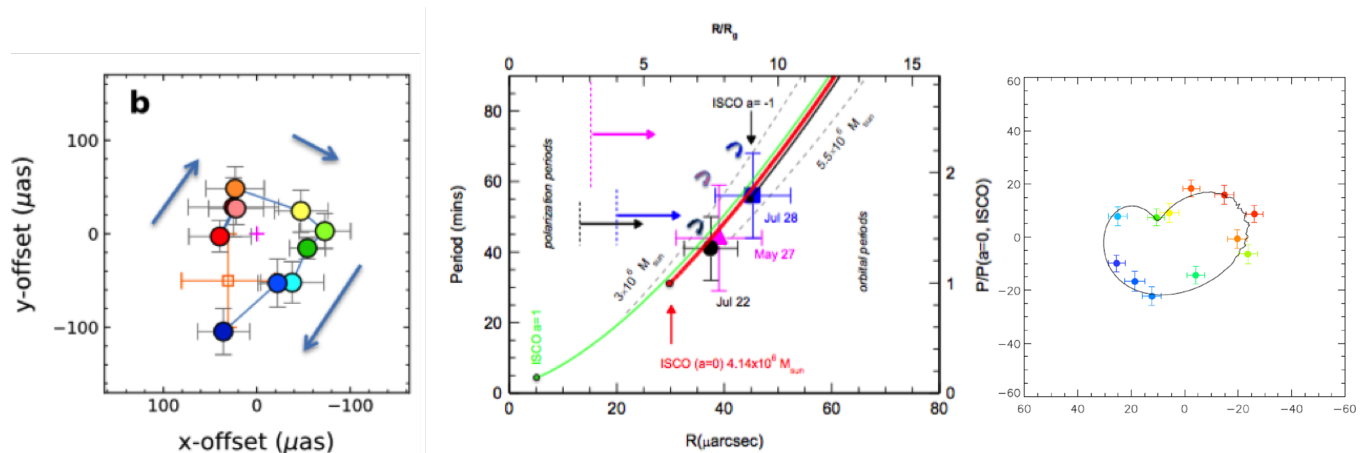


Fig. 2.4.1 Left: Observed on-sky motion of SgrA*'s flaring emission in the NIR obtained with GRAVITY on July 22, 2018. The emission exhibits 3/4 of a clockwise loop within 40 minutes. **Middle:** Relation between radius and period for orbital motion around SgrA*. The three GRAVITY flares lie on the relation, but do not yet allow constraining the spin. **Right:** A 13-year old figure from the science proposal for GRAVITY, dreaming at the time about resolving the flares' motions in a simulation. The centroid track shows a kink due to the secondary image of an orbiting hot spot. Will GRAVITY be able to see that in a future flare?

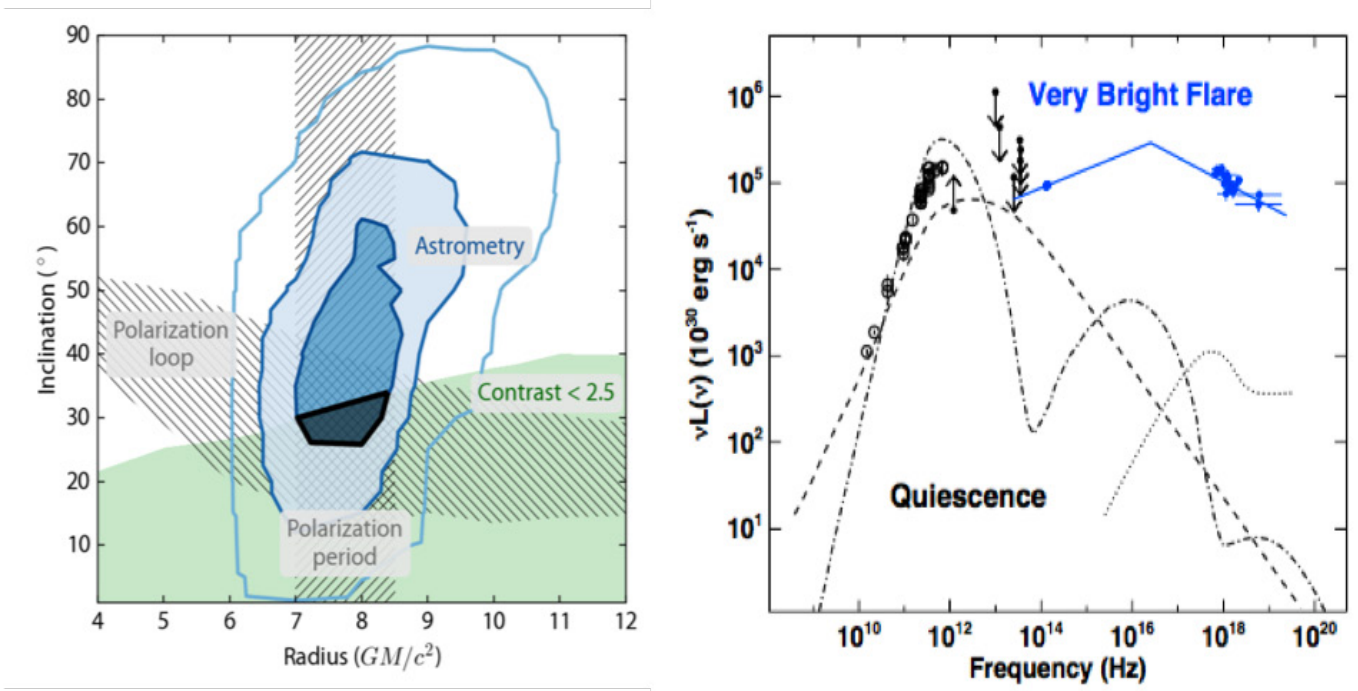


Fig. 2.4.2 Left: Combined constraints for the flare orbit radius and the inclination, using the astrometry, the polarization period, the number of polarization loops and the contrast of the light curve. **Right:** Spectral energy distribution of SgrA* from Yuan et al. (2003). The blue data are for the powerful flare observed simultaneously with SINFONI and XMM/Newton. The blue line is the best-fit synchrotron with cooling break model.

erate light curve contrast constrain the orbit radius and inclination to a small region (Fig. 2.4.2, left) around $i = 25^\circ$ and $r = 8 R_g$.

- Further we constrain the size of the flare emission region. A large region should shear due to differential rotation. A small region should produce a linear polarization $\sim 70\%$, much larger than the average $\sim 20\%$ observed. Further, both the near-infrared flux density and more strictly energetics constraints from X-ray flares set a lower limit on the size needed to power the flare from the energy density contained in the accretion flow. Combined, these constraints

lead to a spot radius of ~ 2 -3 Schwarzschild radii.

- It is possible to fit the astrometry of all three flares simultaneously under the assumption that the radius, inclination, and orientation of the orbit do not change between flares.

Flares are synchrotron emission:

On August 30, 2014, we observed a very bright flare from SgrA* simultaneously with SINFONI and XMM/Newton, allowing us for the first time to determine the spectral indices of the emission at NIR and X-ray wavelengths simultaneously. The average multi-wavelength spectrum

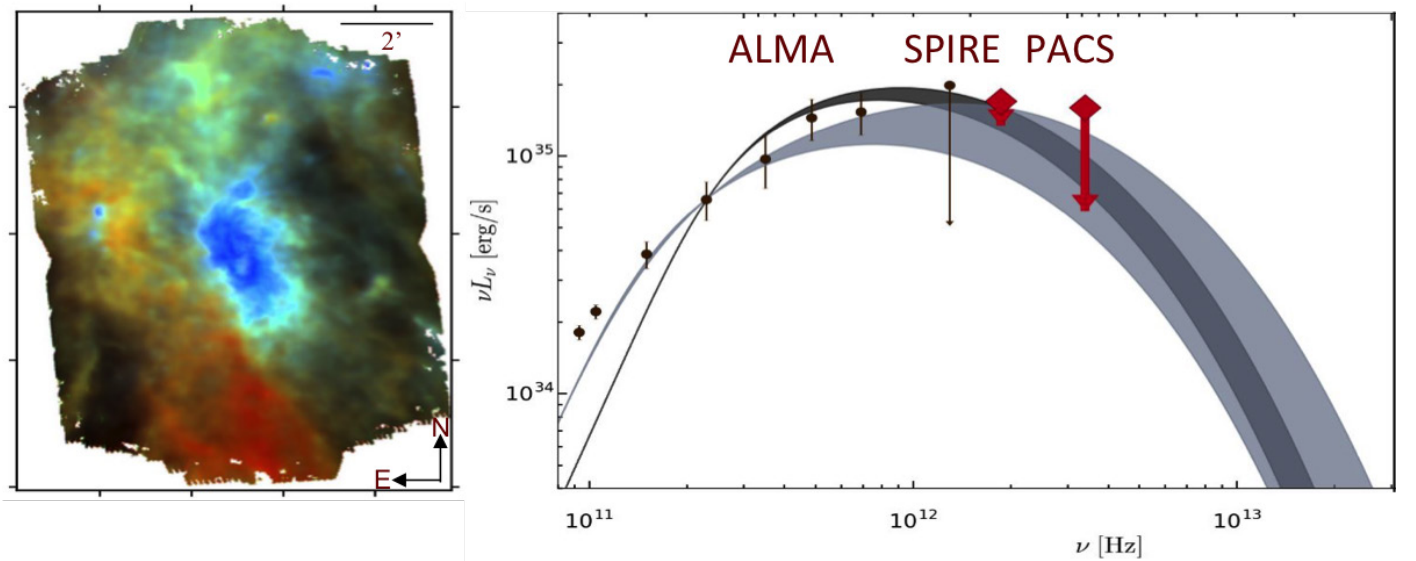


Fig. 2.4.3 Left: Color-composite PACS-image of the Galactic Center region using the images at $70\ \mu\text{m}$, $100\ \mu\text{m}$ and $160\ \mu\text{m}$. **Right:** Our PACS variability measurement of SgrA* converted to flux (red data) in comparison with other data and 1D zone models of the hot electron population. In the favored models one has $T_e \approx 10^{11}\text{K}$, the accretion flow is optically thin at the peak frequencies, and the peak position is set by the critical frequency. This modifies the previous picture, in which the peak position was set by optical thickness effects.

is well reproduced by a broken power-law with $\gamma_{\text{NIR}} = 1.7 \pm 0.1$ and $\gamma_x = 2.27 \pm 0.12$. The difference in spectral slopes strongly supports that the flare is synchrotron emission in both wavebands with a cooling break (Fig. 2.4.2, right, Ponti et al. 2017). This model already had been favored in our previous work, but here for the first time we can present a simultaneous measurement of the spectral indices, which is the smoking gun sign for the emission model.

Assuming variability of 25% in the FIR, we can convert this to an upper limit for the flux, which is consistent with modern ALMA and VLA observations (Fig. 2.4.3 right) and the SPIRE/Herschel detection. Our upper limit provides further evidence for a broad spectral peak at $\approx 10^{12}$ Hz and constrains the number density of electrons with a relativistic $\gamma \approx 100$ in the hot electron bulge to be such that the plasma is optically thin throughout the submm regime (von Fellenberg et al. 2018).

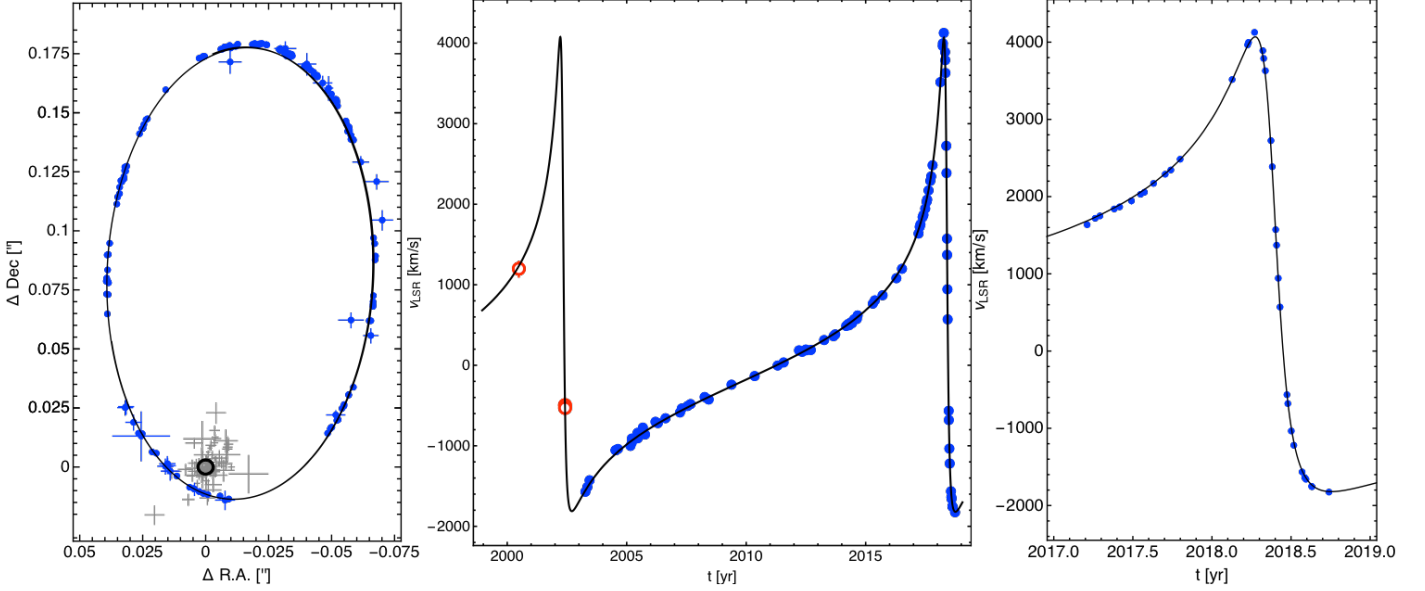


Fig. 2.4.4 The orbit of the star S2 around SgrA*. **Left:** The on sky motion of S2. The black line is the best fitting orbit to the astrometric and radial velocity data (middle panel). The gray crosses mark the measured positions of flares from SgrA* (black circle). S2 passed the pericenter twice during our observing window (1992 to 2018): In 2002 and 2018. **Middle:** The radial velocity data. Blue data are from the VLT, red from the Keck. **Right:** Zoom into the radial velocity curve, showing the quick swing-by in spring 2018, when the radial velocity changed within weeks from +4000 km/s to -2000 km/s. The error bars are not visible on this scale.

A detection of SgrA* at 100 μm and 160 μm :

Using PACS on board the Herschel satellite, we were able to detect for the first time the emission of SgrA* at 100 μm and 160 μm . While the warm dust in the Galactic Centre is too bright to allow for a direct detection of SgrA* (Fig. 2.4.3 left), we measured a significant and simultaneous variation of its flux of $\Delta F_{\nu, 160\mu\text{m}} = 0.27 \pm 0.06$ Jy.

These findings have important implications for horizon scale models of SgrA* which we carry out using general relativistic MHD simulations and fully relativistic, polarized, ray tracing radiative transfer (Dexter 2016). Around 1 mm, VLBI observations using the Event Horizon Telescope can study the spatial structure of the emission. We have shown that non-thermal electrons lead to a

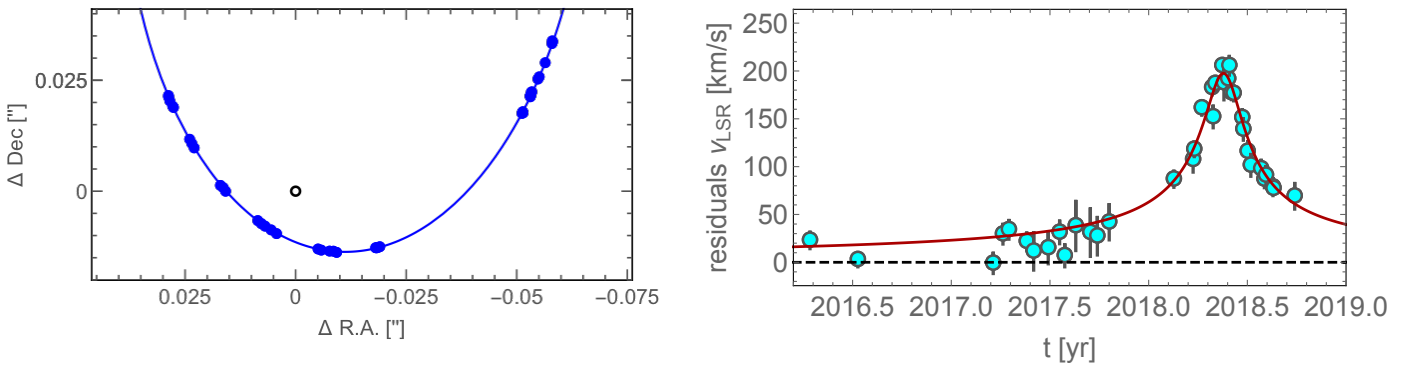


Fig. 2.4.5 Left: Astrometric data from GRAVITY of S2 in 2017 and 2018, as the star passed the pericenter of its orbit. The black circle marks the position of the MBH. **Right:** The radial velocity data from SINFONI show the combined redshift and transverse Doppler effect. The black line at zero corresponds to the underlying Keplerian orbit; the blue line is the model including the two relativistic effects. Clearly, the data favor general relativity.

large-scale “halo” of radiation. Further we have shown that the electron temperature is sensitively constrained by the degree of order in the polarization map (Jiménez Rosales & Dexter 2018). The mm-VLBI observations will therefore be sensitive to plasma physics (electron heating) in the accretion flow as well as to relativistic effects.

2.4.2 Fundamental Physics with SgrA*

Detection of the gravitational redshift from SgrA*:

Due to its brightness the star S2 orbiting SgrA* on an $e = 0.88$, 16-year orbit is by far the best probe for the gravitational potential of SgrA*. Fig. 2.4.4 shows the orbit, which we have followed for more than 1.5 revolutions since 1992. In May 2018, S2 passed the pericenter of its orbit, reaching then a speed of almost 8000 km/s and passing by the MBH at a distance of 16.4 light hours.

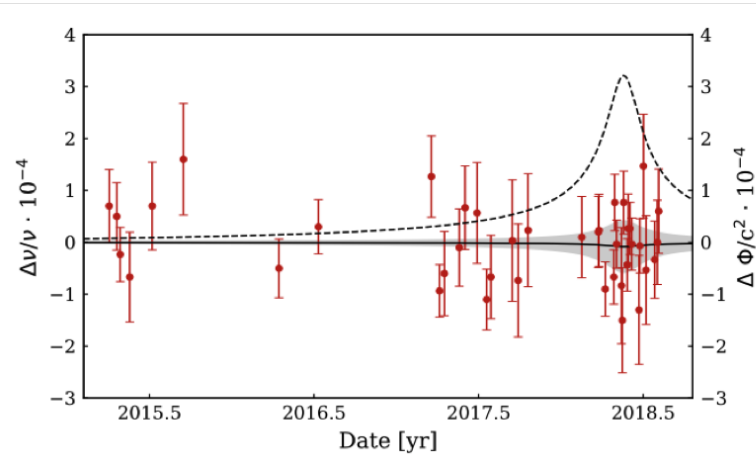


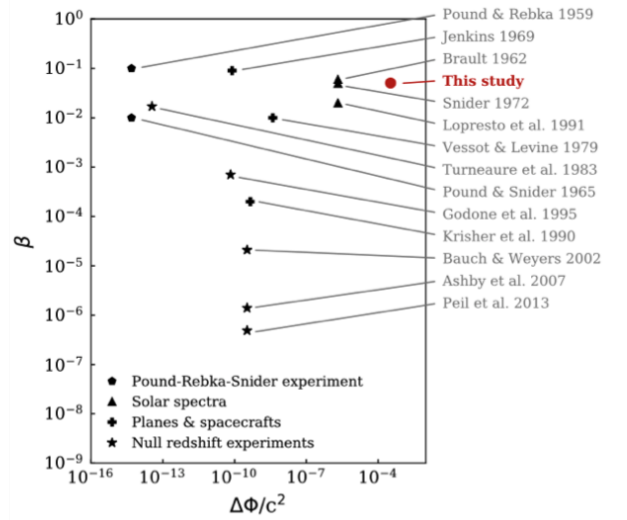
Fig. 2.4.6 Left: The difference in redshift between the He- and the H-line from the S2 SINFONI spectra as a function of time. If LPI would be violated, the residuals should be a function of the gravitational potential (dashed line, right axis). **Right:** Comparison of our constraint with other measurements. While our limit is not (yet) particularly constraining, we tested a regime of much stronger gravitational fields compared to other tests.

During the closest approach the gravitational redshift from SgrA* notably affects S2's light: Einstein's theory predicts an apparent shift of 100 km/s, occurring together with the transverse Doppler effect amounting also to 100 km/s. Fig. 2.4.5, right, shows that we detected the relativistic terms with very high significance. Parameterizing the GR effects with a factor f , where $f = 0$ is the purely Keplerian model and $f = 1$ relativistic version allows quantifying the significance. We find (including all 2018 data, i.e. more than in the discovery paper) $f = 1.04 \pm 0.05$. GRAVITY also here was key (Fig. 2.4.5, left, GRAVITY collaboration 2018a). While the two relativistic effects are affecting the radial velocities, one needs to determine at the same time and from the same data the underlying (Keplerian) orbit. In order to predict the radial velocities with sufficient accuracy, precise astrometry is needed as well. GRAVITY allowed us to see the effect at the 10σ level just a month after pericenter passage.

Using GRAVITY data for an orbit fit turned out to be easier than what one might have feared. We detect in almost all frames S2 and SgrA* within the same interferometric beam - such that a binary fit to the complex visibilities gives us directly the separation vector between S2 and the central mass. Also note that we detect SgrA* in more than 90% of the frames. This will yield a flux distribution, probably allowing us to determine a characteristic NIR flux of SgrA*.

Testing the Einstein equivalence principle with SgrA*:

During its orbit, S2 experiences significant changes in gravitational potential. Since we can measure the gravitational redshift separately from hydrogen and helium absorption lines, we can compare the two for testing the local position invariance (LPI), one of the pillars of the



Einstein equivalence principle. We can report a limit on a violation of the LPI of $|\beta_{\text{He}} - \beta_{\text{H}}| = (2.4 \pm 5.1) \times 10^{-2}$ (Fig. 2.4.6, left). The variation in potential that we probe is six magnitudes larger than possible for measurements on Earth, and a factor ten larger than in white dwarfs. We are therefore testing the LPI in a regime where it has not been tested before (Fig. 2.4.6, right, GRAVITY collaboration 2019).

Our GRAVITY data have impact on the galactic structure:

Our orbital data also make for an exquisite measurement of the distance to the Galactic Center, R_0 . We find $R_0 = 8.180 \pm 0.013_{\text{stat}} \pm 0.021_{\text{sys}}$ kpc (GRAVITY collaboration 2019 in prep.). Together with the angular rotation speed of the Milky Way as estimated from SgrA* our data imply $\Theta_0 + V_0 = 247.4 \pm 1.4$ km/s. Our R_0 is also consistent with the best combined estimate of R_0 when using all measurements that don't involve SgrA*.

Another result of the S2 orbit fit is that the radial motion offset ($v_{z,0}$, one of the free fit parameters) is consistent with 0: $v_{z,0} = -2.5 \pm 1.6$ km/s. This parameter absorbs the sum of the radial motion of the local standard of rest (LSR) and a radial motion of the MBH itself. Given that we find a value consistent with zero, the most likely explanation is that both of these numbers actually are small.

We conclude that the GRAVITY S2 data imply that the LSR is on a tangential orbit and that the MBH is at rest in the center of the Milky Way bulge.

Outlook:

What is next? As S2 moves now outward again, we should be able to detect the relativistic prograde Schwarzschild precession. For the highly eccentric S2 orbit, the precession term essentially acts during pericenter passage, giving the star a little kick, which leads to a rotation of the orbital ellipse in its plane amounting to $\Delta\omega = 12'$ for S2. With the accuracy of GRAVITY, we hope to detect the effect by the end of 2019 at the 5σ level.

function, and the eccentricity distribution. Down to mK = 19, one expects ≈ 1 such star.

The prospects for seeing the spin effects might though be much better spectroscopically, using faint stars within the central 100 μ s. One would not necessarily need to spatially resolve these stars, since their spectra would be highly red- or blue-shifted, avoiding confusion on the spectral axis. Such stars likely are giants (Habibi et al. 2019), showing thus a wealth of spectral features in the K-band. This would help measuring their radial velocities with errors < 1 km/s. Clearly, this is a topic for the next generation extremely large telescopes, such as for MICADO at the ELT.

Potential caveats for all these future measurements are the unknown Newtonian perturbations from so far unseen and unknown mass components.

2.4.3 A gaseous scherzo in the Galactic Center

In 2011 our team discovered the gas cloud G2 flying

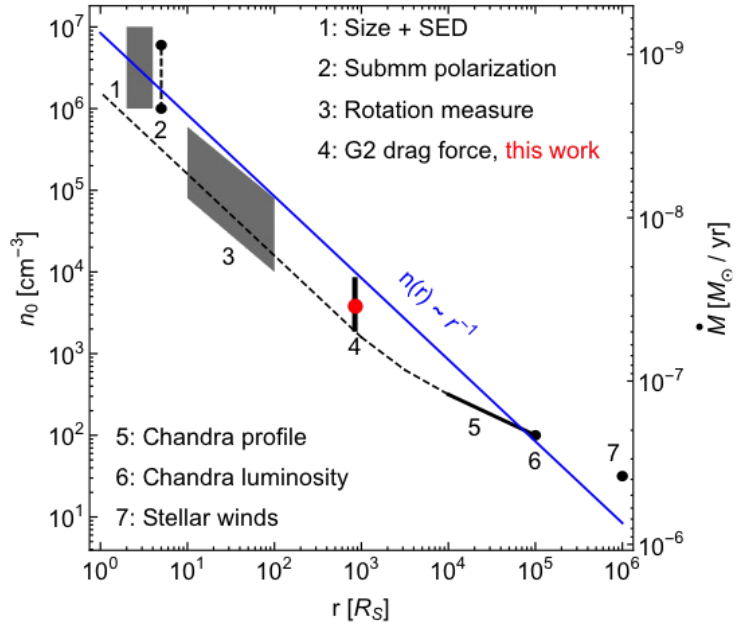
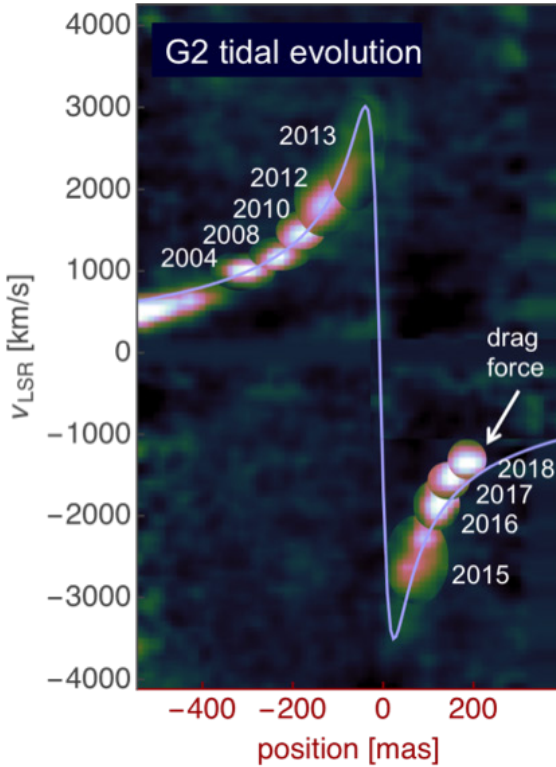


Fig. 2.4.7 Overlay of position-velocity-diagrams (slit along the orbital trace) of the gas cloud G2 from the He- and H-lines in K-band. The blue line is the best fit, Keplerian orbit. The initially compact cloud gets stretched ever more, swings around the MBH from 2013 to 2015, and then became more compact again, as expected by purely tidal evolution. Further, G2 shows a systematic slow-down after pericenter passage. Adding a drag force to the orbit fit can explain this, and yields an estimate of the ambient medium density. Right: Compilation of measurements of the accretion flow density. Our new value is in the intermediate regime at around 10^3 RS.

A further goal would be measuring the spin of SgrA* from a stellar orbit. This is difficult, owed to the strong radial decay of the spin effects. For typical observation setups and a spin parameter of 0.9, the orbit needs to fulfill a $\times (1 - e^2)^{3/4} \leq 300 R_S$, in order for the spin to show up astrometrically (Waisberg et al. 2018). We estimate the number of such stars from the density profile, the luminosity

on a very eccentric orbit ($e \approx 0.98$) around SgrA* with a pericenter passage in 2014. While the nature of G2 has been discussed widely, it is clear that it has a gaseous component that for the last 15 years dynamically evolved as an unbound gas cloud. This is not surprising, since for the measured size of G2 the binding mass is $\approx 10^4 M_\odot$. Fig. 2.4.7, left, shows how the object has stretched out

more and more, before it swung around SgrA* from 2013 to 2015 - a pericenter passage lasting for two years. The evolution can be very well described by an ensemble of non-interacting test particles moving along (roughly) the same orbit (Plewa et al. 2017). In 2018, we detected at 10σ significance level that G2 left its initial orbit and lost energy during the pericenter passage - an effect we suspected to happen by comparing the orbits of G1 and G2 (Pfuhl et al. 2015). For G2, the effect is now directly visible in the radial velocities, which are less blue than what we would have expected (Fig. 2.4.7, left, Gillessen et al. 2019).

Measuring a drag force together with the size of G2 leads to an estimate of the density of the medium through

dial velocities. As soon as we can measure an acceleration (on-sky or as a change of radial velocity) we have enough data to determine an orbit. This has been possible for 40 stars so far. For 17 stars we have data good enough that they actually constrain the gravitational potential of SgrA*, and we can perform a combined orbit fit. The gain compared to an S2-only fit was only moderate before GRAVITY already and has since the availability of GRAVITY decreased further of course. Yet, such a fit is important for determining the potential further out - it can answer the question how far out and to what extent does the central mass dominate the potential. Eight of our orbits are for stars belonging to the clockwise stellar disk confirming their disk membership explicitly. The other 32 stars appear to have randomly oriented orbits and a ther-

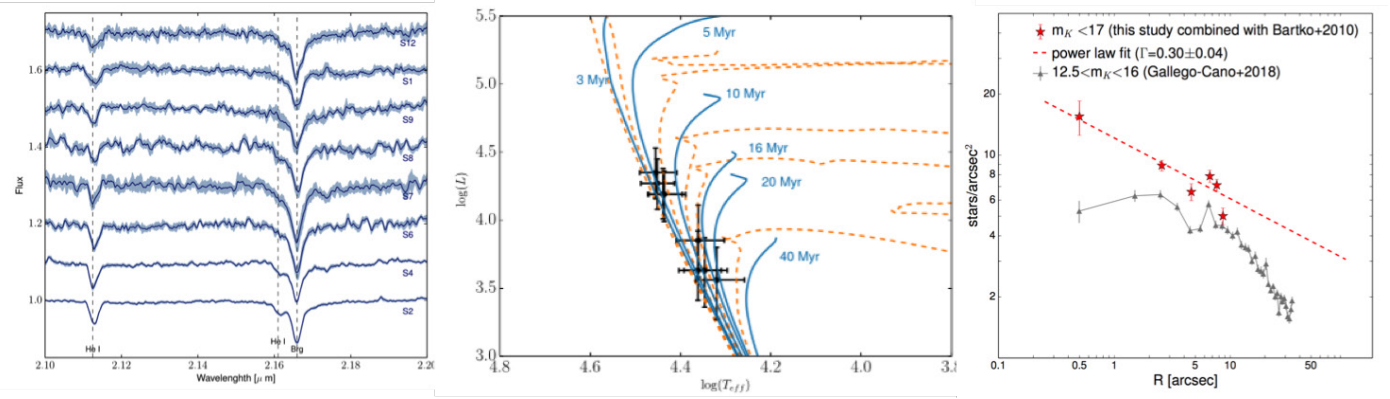


Fig. 2.4.8 **Left:** Collection of deep S-star K-band spectra from multi-year SINFONI data. Note the extremely low noise level for S2. **Middle:** Hertzsprung-Russell-diagram of the young S-stars together with evolutionary tracks, hinting at very young ages for these stars. **Right:** Density profile of the old population, defined by spectroscopically identified stars. The innermost data point yields strong evidence for a cusp.

which G2 is plowing - the accretion flow of SgrA*. Using a ram pressure model and assuming a constant cross section, we obtain a measurement of the particle density at around $10^3 R_s$, a regime not accessible at all before (Fig. 2.4.7, right). At $10 R_s$ submm data constrain the density to values around $10^6 - 10^5 \text{ cm}^{-3}$, at $10^5 R_s$ X-ray data from Chandra point to values around 10^2 cm^{-3} . Our value nicely fills the gap, and matches the overall $1/r$ behavior of the accretion flow density. Using high-resolution simulations together with analytical arguments we were able to reproduce the observed constancy of the Br γ flux. We find that for too large an ambient density, G2 would fragment. The survival of G2 thus sets another limit on the ambient density: The value of $\approx 500 \text{ cm}^{-3}$ is consistent with and at the lower bound of our drag force based number (Steinberg et al. 2016).

2.4.4 The Dance of Stars

The number of stellar orbits determined has reached 40:

Beyond S2, we track many more stars in the vicinity of SgrA* with adaptive optics based imaging, and in the central most area also with integral field spectroscopy. For all stars we have positions and proper motions, and for most of the ones in the central arcsecond also ra-

mal eccentricity distribution (Gillessen et al. 2017).

We have built up ultra-deep spectroscopy for the stars in the central arcsecond:

As a side effect of tracking the stellar radial velocities with SINFONI, we have been able to compile very deep spectra for many stars. Co-adding the spectra obviously requires correcting the orbital Doppler shifts, and has lead to an effective integration time on S2 in excess of 100 hours (Fig. 2.4.8, left).

The deep spectroscopy of the young stars together with atmosphere modeling yielded surprisingly young ages for these S-stars - less than ≈ 15 Myr. For S2, the age estimate is even as low as 7 Myr (Fig. 2.4.8, middle). These young ages challenge the established standard picture that the origin of the young S-stars is a field binary-disruption scenario (Habibi et al. 2017). Other than the young age, the S-stars appear to be normally rotating, young main sequence stars of spectral type B0-B3V.

A cusp of giants in the central arcsecond:

Using our multi-epoch spectroscopy, we also identified spectroscopically 16 late-type stars in the regime of the S-stars. This includes the first five warm giants (G2-G8I-II), within the central arcsecond. The spectroscopically identified number counts establish a cusp within 0.02 -

0.4 pc described by a single power law with an exponent $\Gamma = 0.34 \pm 0.04$ (Fig. 2.4.8, right, Habibi et al. 2019). For future work with GRAVITY and MICADO this is an important key, what to expect in terms of stellar content when zooming in further onto SgrA*.

10000 proper motions, 2500 radial velocities:

Looking at the larger field we compiled a sample of 10000 stellar proper motions and 2500 radial velocities from our AO data sets. We cleaned this sample of stars to contain only old stars, i.e. a population that is expected to be relaxed. These data show that the nuclear cluster of the Milky Way slightly flattened (axis ratio of $q = 0.80 \pm 0.04$) and has a half-light radius of 7 ± 2 pc. An isotropic spherical Jeans model for the cluster yields a cluster mass inside of 100" of $M = (6.1 \pm 0.5) \times 10^6 M_{\odot}$ (Fritz et al. 2016). Applying a dynamically flattened model, we fitted simultaneously cluster mass, R_0 and the mass of the MBH. The constraints are consistent, although not quite competitive with the stellar orbit based values (Chatzopoulos et al. 2014).

Pinpointing SgrA*:

We have improved our astrometric reference frame for the adaptive optics based imaging data. The coordinates are tied to (radio-)SgrA* via a set of red giant stars, which are also detectable at radio wavelengths through SiO maser emission in their envelopes. By modeling and correcting the optical distortion in the VLT/NACO imager, we improved the definition and stability of the reference system by roughly a factor five. SgrA* is in the coordinate system at rest at the origin, within 170 μas in position and 70 $\mu\text{as/yr}$ in proper motion (Plewa et al. 2015).

Massive binaries in the Galactic Center:

From our long-term spectroscopic and photometric data set, we detected two new binary stars in the Galactic Center, besides the well-known star IRS16SW. IRS16NE is a binary with a period of 224 days with a moderate eccentricity of $e \approx 0.3$, and an eclipsing Wolf-Rayet binary with a period of 2.3 days (Pfuhl et al. 2014). This brings the binary fraction in the Galactic Center to a regime similar to other young clusters. The presence of IRS16NE could in principle set a lower bound on the 2-body relaxation timescale at $t_{\text{relax}} \geq 10^7$ yr, and correspondingly, an upper bound on the stellar number density. However, other dynamical estimates are more constraining for t_{relax} , such that the most massive binaries in the Galactic Center are too short-lived to constrain an underlying dark cusp. Fainter, longer-lived binaries would yield such constraints (Alexander & Pfuhl 2014).

Selected References:

- Alexander, T. & Pfuhl, O. 2014, *ApJ*, 780, 148
 Chatzopoulos, S. et al. 2015, *MNRAS*, 447, 948
 Dexter, J. 2016, *MNRAS*, 462, 115
 Fritz, T.K. et al. 2016, *ApJ*, 821, 44
 Gillessen, S. et al. 2017, *ApJ*, 837, 30
 Gillessen, S. et al. 2019, *ApJ*, 871, 126
 GRAVITY collaboration 2017, *A&A*, 602, 11
 GRAVITY collaboration 2018a, *A&A*, 615, L15
 GRAVITY collaboration 2018b, *A&A*, 618, L10
 GRAVITY collaboration 2019, *arXiv/1902.04193*
 GRAVITY collaboration 2019 in prep.
 Habibi, M. et al. 2017, *ApJ*, 847, 120
 Habibi, M. et al. 2019, *ApJ*, 872, L15
 Jiménez-R., A. & Dexter, J. 2018, *MNRAS* 478, 1875
 Pfuhl, O. et al. 2014, *ApJ*, 782, 101
 Pfuhl, O. et al. 2015, *ApJ*, 798, 11
 Plewa, P.M. et al. 2015, *MNRAS*, 453, 3234
 Plewa, P.M. et al. 2017, *ApJ*, 840, 50
 Ponti, G. et al. 2017, *MNRAS*, 468, 2447
 Steinberg, E. et al. 2018, *MNRAS*, 473, 1841
 von Fellenberg, S. et al. 2018, *ApJ*, 862, 129
 Waisberg, I. et al. 2018, *MNRAS*, 476, 3600



Stefan Gillessen

(Other MPE team members include: M. Bauböck, J. Dexter, F. Eisenhauer, F. Gao, R. Genzel, M. Habibi, A. Jiménez Rosales, T. Ott, O. Pfuhl, O. Straub, S. von Fellenberg, I. Waisberg, F. Widmann)

2.5 GRAVITY

In 2015, just in time for the last visiting committee, we could proudly report the first light observation of the GRAVITY interferometer. Since then GRAVITY excelled all expectations with breakthrough discoveries and measurements at the frontier of astrophysics, including spectra of exo-planets, probing Einstein's theory of general relativity and the black hole paradigm in the Galactic Center, and zooming in to supermassive black holes in the distant universe (see section 2.3.). GRAVITY outperforms earlier interferometers by factors 100-1000 in sensitivity and accuracy, now offering milli-arcsecond resolution imaging for objects as faint as 19 magnitude, and astrometry with ten micro-arcsecond accuracy.

The Genesis of GRAVITY:

The development of GRAVITY was triggered by the discovery of stellar orbits and flares around the Galactic Center black hole in the early 2000s. The "laboratory" was set up for the direct detection of general relativistic effects and for probing physics close to the last stable orbit – if we could only measure to a precision of the Schwarzschild radius, corresponding to ten micro-arcsecond. At the same time the first interferometry with ten meter class telescopes at the Very Large Telescope Interferometer and the Keck observatory were giving promise to this kind of precision, but the sensitivity was far too low for the Galactic Center.

Why Infrared Interferometry is so More Difficult than at Radio Wavelengths:

Charles Townes – the pioneer of heterodyne infrared interferometry – already noted in his "Multiple telescope infrared interferometry" conference proceedings (1981siha. conf..199T): "However, if a sufficiently accurate optical delay line is built and very careful work is done, it should

be practical under some conditions to make direct detection more sensitive than heterodyne by approximately 5 magnitudes. In the case of weak sources this can, of course, be exceedingly important". There is no doubt, the large bandwidth of the direct detection wins. So why took it so long to arrive at GRAVITY? Let us define a "difficulty of coherent detection" to demonstrate the scale of the problem when comparing infrared and radio interferometry:

Difficulty $\sim 1/(\lambda \tau T N) \approx 10^4 10^5 10^2 10^{-6} \approx 10^5 \times$ harder at IR vs. radio

where λ is the wavelength, τ the (atmospheric) coherence time, T the throughput, and N the photon flux per bandwidth. In infrared interferometry, the wavelength is 10^4 smaller, the coherence time is 10 millisecond rather than minutes, i.e. 10^5 smaller, and the throughput, because of the complex mirror train, a factor 10^2 smaller than for a radio receiver. The 10^6 times more photons available at infrared wavelengths when observing a 10,000K hot star ($N \propto \nu^2 T$) compensate part of the difficulty, but all together, the problem at remains a hundred thousand times harder, at least.

Only the combination of robust fringe-tracking, a dual-star mode to decouple the kilohertz fringe-tracking from the minute long science exposures, a laser metrology to measure the optical path lengths in the observatory to nanometer accuracy, and an infrared wavefront sensor for the highly obscured Galactic Center region will do the job – the idea of GRAVITY was born, and proposed to ESO in 2005.

The Key to Success:

The success of GRAVITY results from a clear science vision, the development of transformational technology,

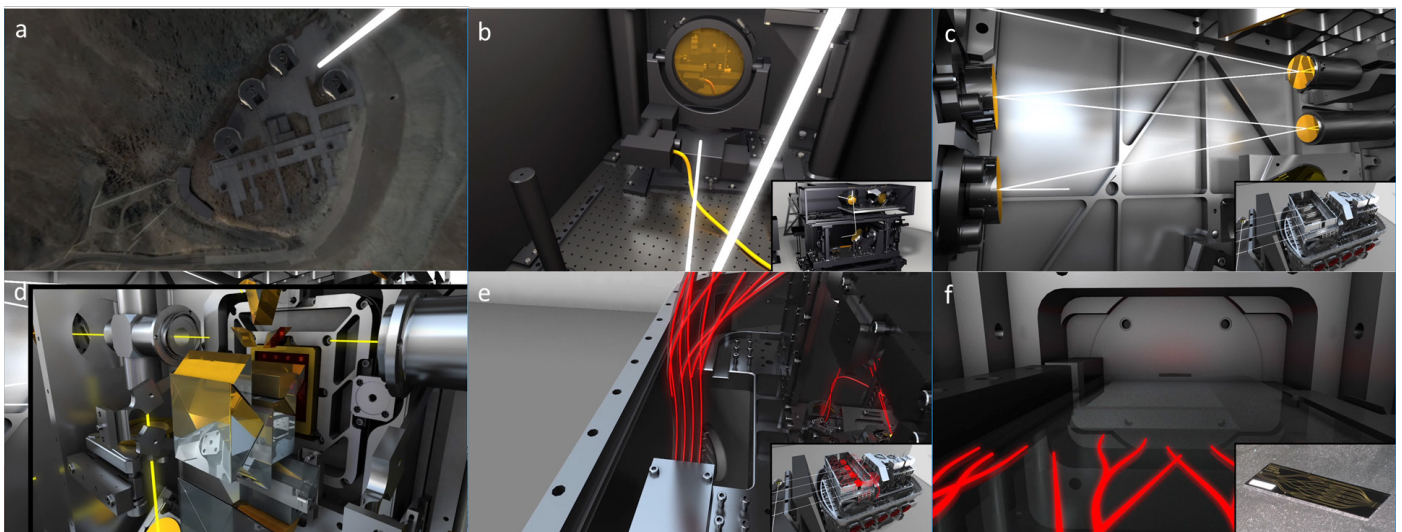


Fig. 2.5.1 Flight through GRAVITY. In the online version of this document, clicking on the figure links to a video stream. a) arriving at the VLT on mount Paranal in Chile; b) adaptive optics in the basement of each telescope; c) active optics coupling the light to single mode fibers; d) acquisition and guiding camera; e) optical fibers; f) integrated optics beam combiner.

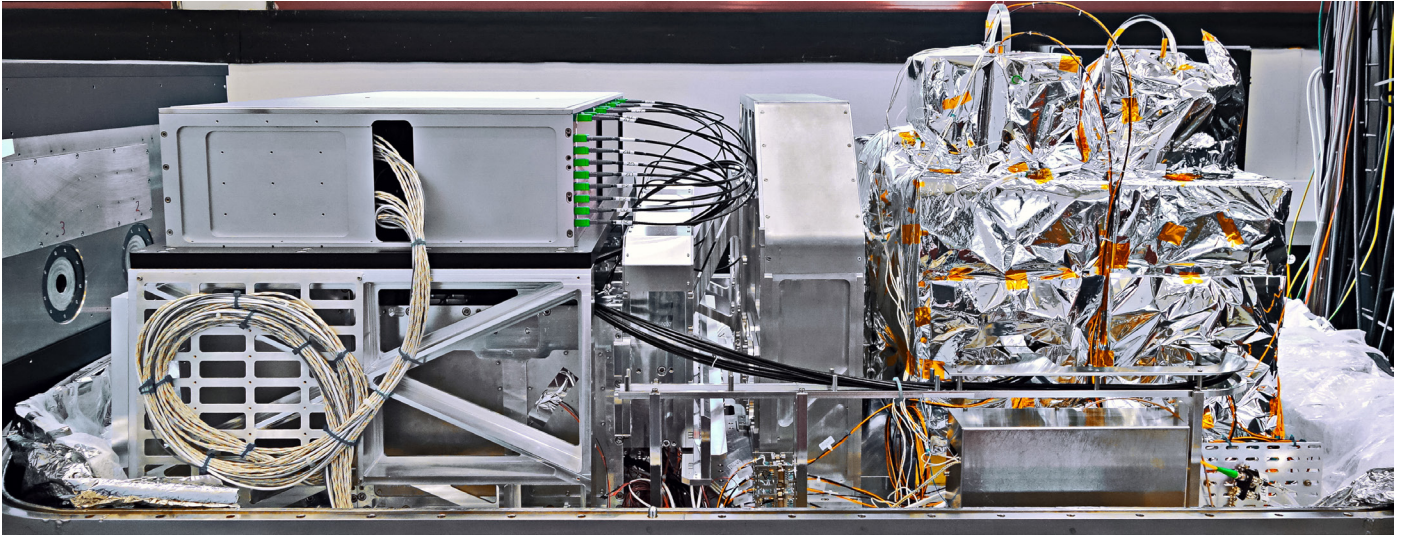


Fig. 2.5.2 GRAVITY: The heart of the GRAVITY experiment is the beam combiner instrument. It is located in the center of mount Paranal, where it combines the light of the four 8m ESO Very Large Telescopes. The picture shows the interior of the instrument, which is evacuated, and cooled with liquid nitrogen, for optimum stability and background suppression. The light from the telescopes enters from the left. It is coupled to single mode fibers, combined in integrated optics, and finally analyzed in a high resolution spectrograph. Laser beacons are launched from the telescopes down to the instrument to control pupil and field aberrations, and from the instrument up to the telescopes to measure to optical path lengths to nanometer precision. The beam combiner instrument is about two meter in size.

and continued tuning at the observatory. With the goal of following the peri-passage of the star S2 in 2018, the schedule was set from the beginning. On the way, we made technical breakthroughs on several fronts. A few examples: Together with ESO and SELEX we developed the quasi-noiseless SAPHIRA infrared avalanche photodiode detector array for wavefront sensing and fringe tracking. With the Paris and Grenoble Observatories we ported the integrated optics technology to the 2 – 2.5 micrometer wavelength range, and developed supra-balanced (in dispersion and length) Fluoride glass fibers. And especially at MPE, we developed a revolutionary laser metrology, measuring the optical path from the beam combiner up to the telescopes with nanometer precision. And last but not least, GRAVITY includes a highly sophisticated control system, including wavefront and pupil control at the telescope and instrument level, optical path length control for fringe tracking and astrom-

etry, metrology based fiber control, vibration compensation as part of the adaptive optics and fringe-tracking, etc.

The other key to success was the continued tuning of the system after installation at the Observatory in 2015. The GRAVITY team was traveling to Paranal almost every month in 2016/17/18 for technical activities, commissioning and science observations. E.g. together with the observatory, we could hunt down and eliminate the vibrations from the telescopes and infrastructure down to a level of several hundred nanometer, and we now routinely achieve fringe tracking residuals as low as 200 nm rms for the 8m VLTs, and below 100 nm rms for the smaller 1.8m Auxiliary telescopes.

Performance Increase of Factor up to 1000:

The resulting performance has transformed optical interferometry. A few examples: Before GRAVITY, the limiting

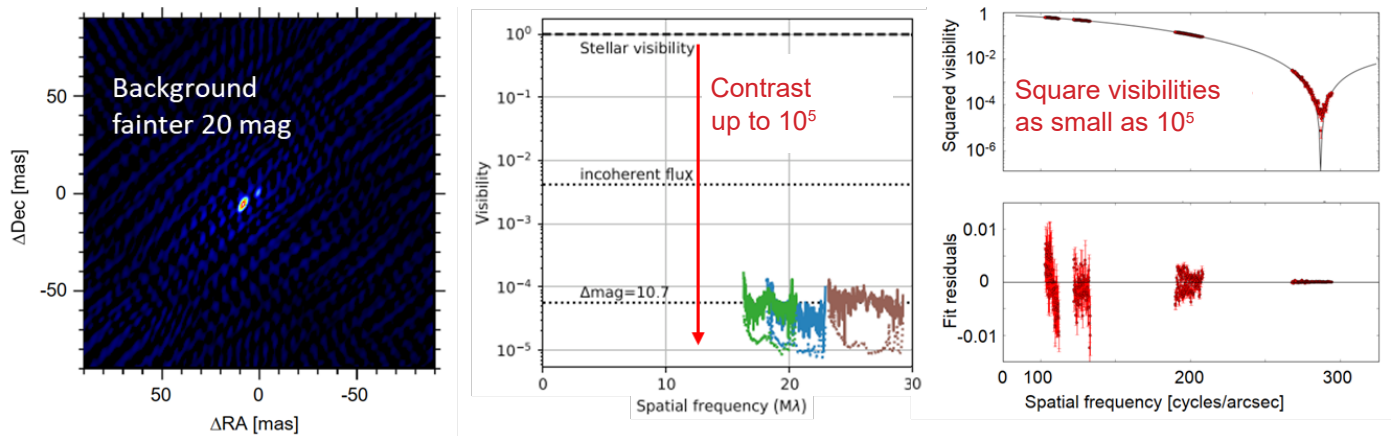


Fig. 2.5.3 GRAVITY performance: Image of the Galactic Center around the S2 peri-passage in May 2018 (left). The bright object is the star S2, the faint object in the center is the black hole SgrA*. The image is reconstructed from a single night of observing. The rms of the background in this image is below 20 mag. First detection of an exo-planet by optical interferometry (middle). The contrast between the planet HR8799e and its host star is 11 mag. High precision interferometry of the fully resolved giant star 24 Cap (right). The depth of the null of the first minimum is 8×10^{-6} , probably caused by the granulation in the star's surface.

magnitude for near-infrared interferometry was typically around $K \sim 10$ mag, with a one-time record of $K = 12.5$ mag for technical observations. Now with GRAVITY, the background in images of the Galactic Center combining several nights has a noise of 21 mag. For fringe-tracking – the prerequisite for long-exposures and high spectral resolution interferometry – GRAVITY has increased the sensitivity of the VLTI by a factor of several ten to hundred compared to what was possible before. The astrometric precision during the July 2018 flare of SgrA* (about 14 mag) was about 20 micro-arcsecond in 5 minutes (Fig. 2.4.1). Our monitoring of the 2 arcsecond separation M-star binary GJ65 measures the relative position of the stars to a level of 3×10^{-5} . In our first detection of a planet by optical interferometry, we have achieved a contrast of 11 mag between the planet HR8799e and its host star at 390 mas separation. For bright objects, we have measured the visibilities to an accuracy better than 0.25%. GRAVITY is ushering a new epoch.

Hundred Times Better to Come

And we will do even better. High-performance, laser-guide star AO and improved optics and grating-prisms will boost the detective transmission by a factor few ten, and avalanche photodiode IR detectors will offer quasi-noiseless long exposures. The new Germanium and Indium Phosphide grisms – developed together with Canon Inc. – are already in house, and with Leonardo Inc. and ESO – as part of our joint development of a next generation eAPD Saphira detector – we have already demonstrated seconds long exposures with $< 1e^-$ readnoise. Together with large-separation off-axis fringe tracking, interferometry will then open up the “extragalactic sky” at milli-arcsecond resolution, a regime completely out of reach even for the next generation 30-40 m telescopes.

Selected References:

GRAVITY collaboration: Abuter et al. 2017, *First light for GRAVITY: Phase referencing optical interferometry for the Very Large Telescope Interferometer*, *A&A*, 602, A94



Frank Eisenhauer

(MPE GRAVITY team: A. Agudo Berbel, M. Bauböck, A. Buron, S. Czerniack, R. Davies, C. Deen, S. Dengler, J. Dexter, P.T. de Zeeuw, F. Eisenhauer, N.M. Förster Schreiber, F. Gao, R. Genzel, S. Gillessen, M. Habibi, O. Hans, F. Haußmann, D. Huber, A. Jiménez-Rosales, M. Karl, S. Lacour, M. Lippa, D. Lutz, T. Ott, O. Pfuhl, P.M. Plewa, S. Rabien, C. Rau, R. Stock, O. Straub, E. Sturm, L.J. Tacconi, S. von Fellenberg, I. Waisberg, F. Widmann, E. Wieprecht, E. Wiezorrek, S. Yazici, J. Zanker-Smith)

2.6 The ARGOS GLAO Facility at the LBT

Having completed its commissioning phase, the Advanced Rayleigh guided Ground-layer adaptive Optics System (ARGOS) facility will now be handed over for scientific observations at the Large Binocular Telescope (LBT). With six Rayleigh laser guide stars in two constellations and the corresponding wavefront sensing, ARGOS corrects the ground-layer distortions for both LBT 8.4 m eyes with their adaptive secondary mirrors. Under regular observing conditions, this set-up delivers a point spread function (PSF) size reduction by a factor of ~ 2 -3 compared to a seeing-limited operation. With the two LUCI infrared imaging and multi-object spectroscopy instruments receiving the corrected images, observations in the near-infrared

can be performed at high spatial and spectral resolution. Imaging with ground-layer adaptive optics (GLAO) is enhancing several scientific programmes, from cluster colour magnitude diagrams and Milky Way embedded star formation, to nuclei of nearby galaxies or extragalactic lensing fields. In the unique combination of ARGOS with the multi-object near-infrared spectroscopy available in LUCI over a 4×4 arcmin field of view, the first scientific observations have been performed on local and high- z objects. Being open now for general scientific programs highly enhanced spectroscopic and imaging capabilities are now at hand with ARGOS at the LBT.

The Advanced Rayleigh guided Ground-layer adaptive Optics System (ARGOS) has been implemented by a MPE led international consortium of institutes to deliver a ground-layer adaptive optics (GLAO) correction

to both of the 8.4 m 'eyes' of the Large Binocular Telescope (LBT). GLAO is a technique used to correct the atmospheric induced optical distortions over a large field of view, enhancing the image quality homogeneously. To



Fig. 2.6.1 The ARGOS system propagating a bundle of laser beams on each side of the large binocular telescope. This wide-angle photograph was taken in 2017 with a 25s exposure time. Each visible green beam in this image consists of three individual laser rays forming the wide-field constellations of guide stars in the atmosphere. The light pulses from the high-power lasers are subject to Rayleigh scattering by air molecules in the Earth's atmosphere. Having the wavefront sensors gated and adjusted to receive the photons only from a distance of 12 km, a sharp reference beacon constellation is formed. Measuring the wavefronts and correcting the atmospheric ground-layer distortions with the two adaptive secondary mirrors yields a wide-field correction for imaging and spectroscopy.

conduct this correction, ARGOS utilizes two constellations of multiple guide stars, generated artificially above the LBT with Rayleigh backscattering of high-power pulsed green lasers. Fig. 2.6.1 shows the ARGOS binocular laser beams when propagated to sky. With range-gated wavefront sensing systems for the laser beacons and the LBT's adaptive secondary mirrors, the correction yields an improved point spread function (PSF) for imaging and spectroscopic observations.

Enhancing the image quality with GLAO has several advantages. Increasing the spatial resolution gives insights into the details of an object's structure. Additionally, the signal-to-noise ratio (S/N) in spectroscopy benefits strongly from sharpening the image. With the required integration time to reach a given S/N being inversely proportional to the square of the PSF diameter, observations can be carried out in a much shorter time. Due to the smaller PSF size the spectroscopic slit width can be decreased accordingly, enhancing the spectral resolution and allowing spatially resolved spectroscopic observations. With GLAO delivering a wide field-of-view correction, science cases benefit from adaptive optics that cannot be done with single-conjugate systems or in seeing-limited mode. With a factor 2 to 3 PSF size reduction, ARGOS can be considered a 'seeing enhancer' beneficial for the two facility instruments LUCI1 and LUCI2

offering imaging and multi-object spectroscopy (MOS) in the near-infrared (NIR) wavelength regime. A multitude of science cases will benefit from the enhanced resolution and encircled energy that ARGOS delivers. Amongst others, scientific topics that can be addressed with the aid of GLAO span a wide range, from extragalactic cases such as high- z galaxy dynamics, active galactic nuclei, and Quasar host galaxies, to Galactic astrophysical questions about planets, Cepheids, or stellar clusters. To summarize briefly, ARGOS with LUCI at the LBT offers the following benefits:

- Binocular observations, using the two 8.4 m telescopes of LBT at once. With a GLAO correction over the full 4×4 arcmin field of view, delivering a $0.25''$ to $0.3''$ resolution;
- A fairly homogeneous PSF shape over this full field;
- A large 2×3 arcmin field for the tilt star selection;
- NIR imaging of the full field at the GLAO spatial resolution;
- GLAO corrected NIR multi-object spectroscopy with custom cut slit masks and high spectral resolution.

The last bullet emphasizes one of the unique capabilities that ARGOS provides. Currently this combination is only

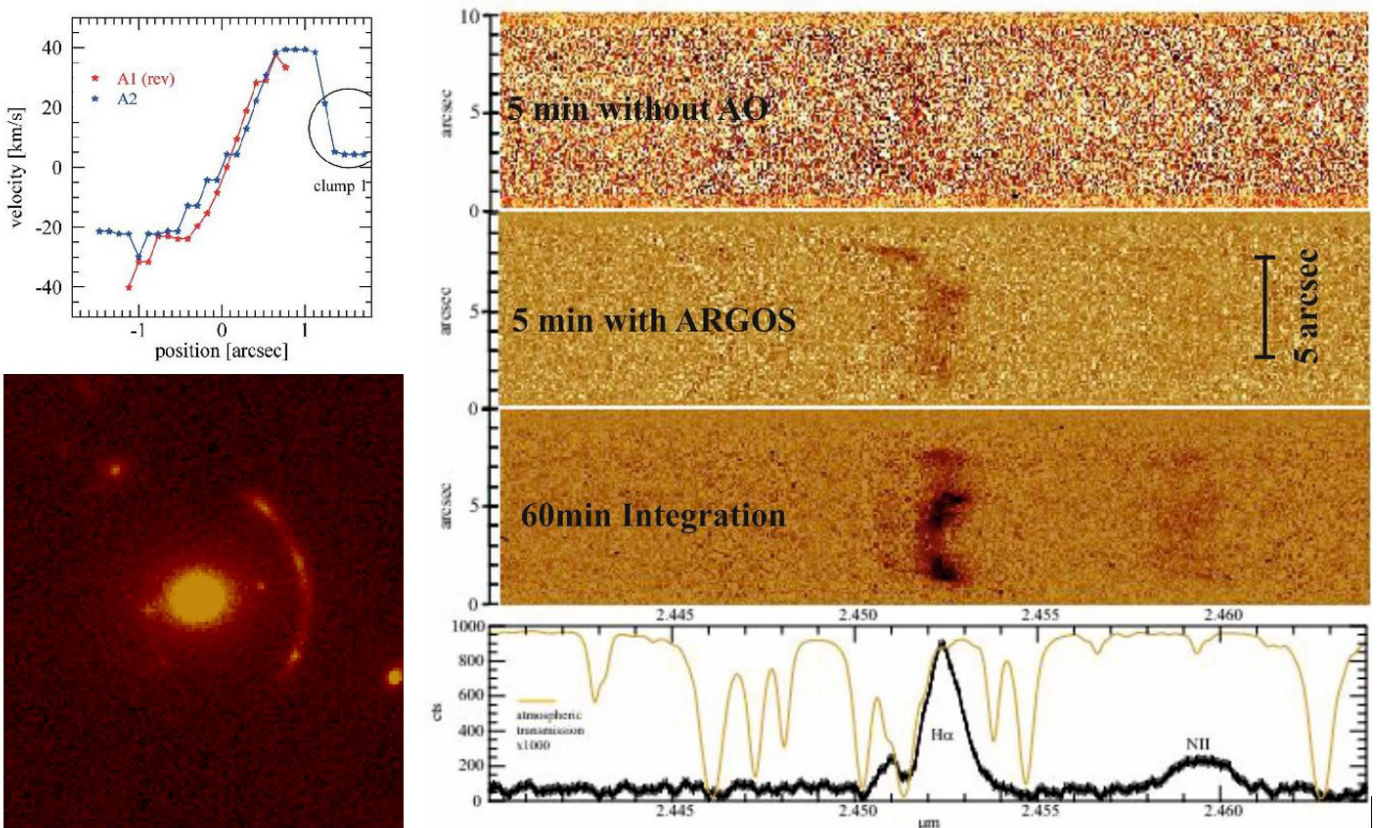


Fig. 2.6.2 The 8 o'clock arc. **Lower left:** an image taken with ARGOS in K-band at high spatial resolution, comparable to HST. **Right panel:** Emission lines H α and [NII] detected from the 8 o'clock arc. **From top to bottom:** A 5min integration with the ARGOS loop open; the emission is barely visible, due to the small slit width. A 5min integration with the adaptive optics loop on; all the flux from the object is nicely squeezed into the curved slit. Combining multiple nodded integrations for an hour of observation and removing the slit curvature; the velocity distribution and a richness of details can be seen. In the bottom panel a 1d spectrum is shown, formed by collapsing the 2d spectrum from above along the spatial axis.

available at the LBT, enabling spectroscopic observations at high spatial and spectral resolution with slits cut to the object's shape. The high spatial resolution allows the spectroscopic slits to be cut as narrow as $0.25''$ to pushing the spectral resolution up to $R \sim 10000$, enabling the detection of structures in the velocity distribution of high- z galaxies in great detail, and reducing the fraction of atmospheric bands for which the spectra are disturbed by the OH night sky emission lines.

Highlighting the ARGOS capabilities, we show here an example of a demanding spectroscopy target, a high- z galaxy, the gravitationally lensed 8 o'clock arc. Gravitational lensing offers a great opportunity to study objects at high redshift, due to the flux enhancing effect of the lens, which makes dim objects appear brighter. Due to the mass distribution of the lensing clusters or massive galaxies, many lensed objects appear as small, extend-

ed arcs on sky. In some cases these arcs extend over tens of arcseconds in length, but only over $0.2 - 0.3''$ in width. In that respect LUCI-ARGOS offers an ideal facility for detailed studies of those arcs. With LUCI we can make curved matched shape slits over the full extent of the arcs, while with ARGOS we sharpen the object, such that it concentrates all the light through the narrow $0.3''$ slit to resolve velocities spatially un-smeared at $R \sim 10000$. The spectrum shows details of the velocity distribution and dispersion, at a level that has not been seen in previous observations due to the lack of spectral resolution and signal-to-noise ratio. The resulting average 1D spectrum of the 8 o'clock arc is shown in the lowest panel of Fig. 2.6.2, reaching a H α peak flux-to-noise ratio of ~ 50 within 1h of observation. Compared to the previous observations with other instruments, the lines are better resolved and the S/N reaches a magnitude higher.

Selected References:

S. Rabien, et al., ARGOS at the LBT, A&A 621, A4 (2019)

Sebastian Rabien
for the ARGOS consortium



(MPE ARGOS team: L. Barl, A. Contursi, R. Davies, M. Deysenroth, F. Eisenhauer, H. Gemperlein, R. Genzel, T. Ott, M. Rosensteiner, J. Ziegeleder)

2.7 MICADO: First Light Imager for the Extremely Large Telescope

MICADO, the adaptive optics imaging camera for the ELT being developed under MPE leadership, successfully concluded its Preliminary Design Review at the end of 2018, and is on track to be ready for the first light of the ELT at the end of 2025. The instrument will exploit the most unique features of the ELT, enabling major advances in many key topics of modern astrophysics. It will enable a dual view of galaxy evolution at high redshift. On the one hand it will directly resolve small galaxies and sub-structures of larger galaxies on scales < 100 pc; on the other, it will provide star formation histories over cosmic time by spatially resolving the relic stellar populations in local galaxies. In the Galactic Center, it will lead to the characterization of main sequence stars with masses $< 1 M_{\text{sun}}$, and trace orbits that lie within light hours of Sgr A*. And it will transform our knowledge of intermediate mass black holes by tracking the proper motions of stars in globular clusters and dwarf spheroidals anywhere within the Galactic halo.

MICADO, the Multi-AO Imaging Camera for Deep Observations, will address a wide range of science topics including the dynamics of dense stellar systems, the centre of the Milky Way, black holes in galaxies, the star formation history of galaxies through resolved stellar populations, the formation and evolution of galaxies in the early universe, planets and planet formation, and the solar system. To do so, it is being designed with a focus on sensitivity and resolution, capabilities which are central to its observing modes of imaging, astrometry, coronagraphy, and spectroscopy.

Diffraction limited imaging at wavelengths in the range $0.8\text{--}2.4 \mu\text{m}$ will exploit the 30-50% Strehl ratio provided by MCAO across the whole field in K-band, and the 60-70% Strehl ratio delivered by SCAO on axis. With a point-source sensitivity comparable to JWST and a factor 6 better resolution, MICADO is well suited to studies of galaxy evolution over cosmic time. We now have a fairly robust outline of this evolution for global galaxy properties, and hence the first pieces of evidence about how galaxies assembled and transformed into the present day Hubble sequence. An obvious next step is to resolve the faint distant galaxies on sufficiently small scales to assess their sub-galactic components including disk structures, nascent bulges, clumps, and globular cluster progenitors. The current view is limited by spatial resolution of ~ 1 kpc even in the best cases. Relatively unexplored regimes include lower mass galaxies, comprising the bulk (by number) of the galaxy population, and galaxies at early cosmic times, when they were building their first stars. Fig. 2.7.1 illustrates the type of detailed structure on 100 pc scales that MICADO might be able to detect in high redshift galaxies.

Astrometry over the full field reaching a precision better than $50 \mu\text{as}$, is one of the most challenging requirements for MICADO. It is a factor 5-10 better than possible with MCAO on ground-based 8-m class telescopes, or space telescopes such as HST, and is similar to that reachable with dedicated astrometry space missions such as Gaia. Developing a methodology for doing so on the ELT, in which every mirror is shifting with respect to the others, has made a promising start.

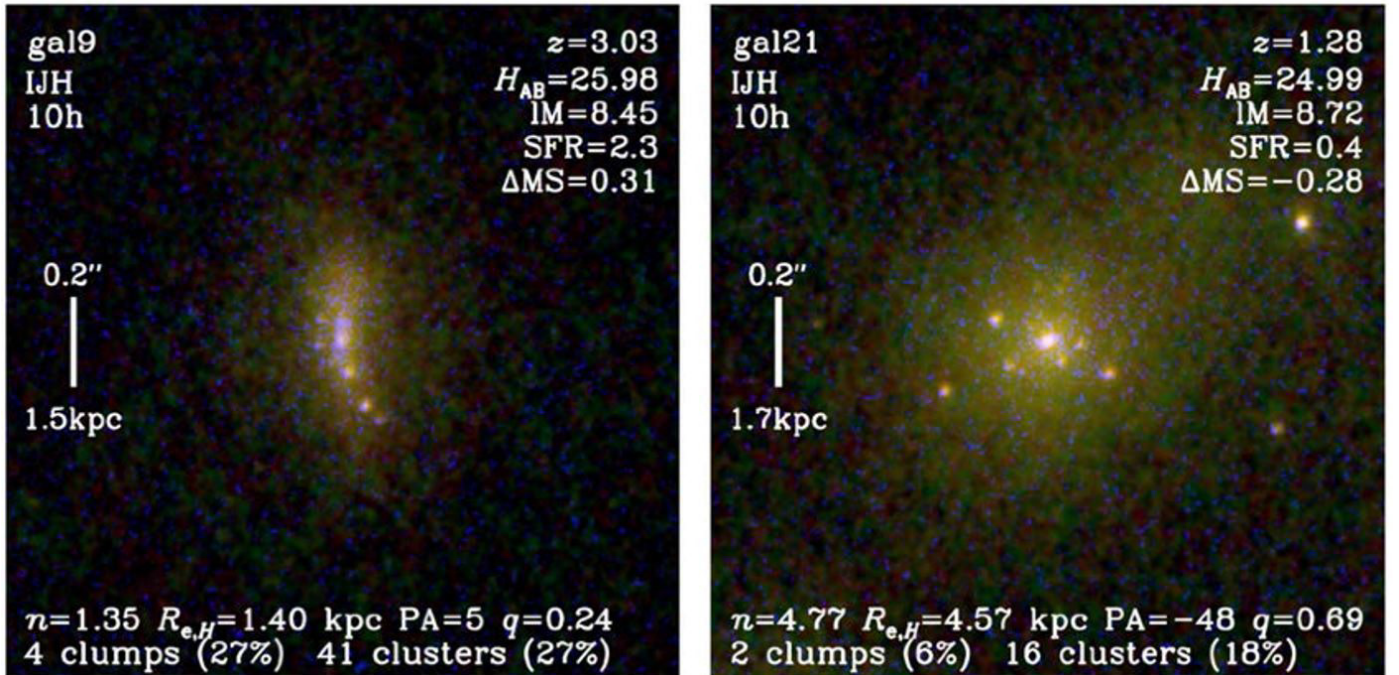


Fig. 2.7.1 Simulations of galaxies above and below the main sequence at $z \sim 2$. These composite IJH colour maps are based on known galaxies in the Hubble Ultra Deep Field, to which additional inferred structure (in particular a star cluster and clump population) has been added.

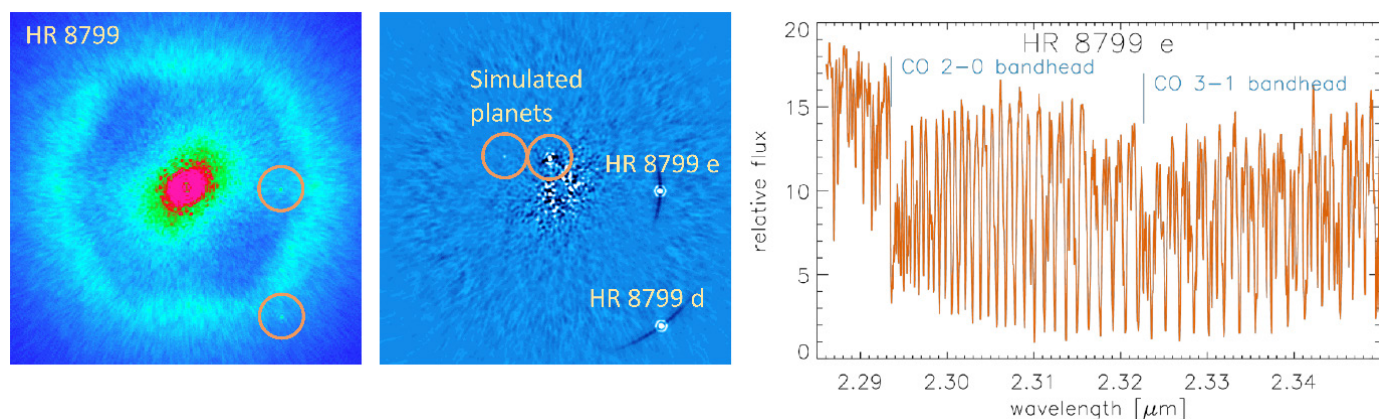


Fig. 2.7.2 **Left:** simulation of a 30 sec integration with MICADO reveals the two known inner planets of the HR 8799 system (the structure in the image arises from the optical configuration of the telescope and AO system and its wavefront correction). **Centre:** with basic processing of a series of such ADI exposures, one will be able to detect other fainter and cooler planets at smaller radii. **Right:** a 30 min spectroscopic integration of the innermost known planet easily detects the individual CO lines, enabling a precise measurement of the radial velocity as well as details of the atmospheric properties.

High contrast imaging of planets around other stars is one of the fundamental science drivers for the ELT. Now that a large number of exoplanets are known, we are entering a phase driven by the need to characterise these planets, in particular the atmospheres of giant exoplanets. Direct imaging of exoplanets provides an opportunity to do this through the use of intermediate band filters that cover molecular absorption bands, enabling one to distinguish models with different temperatures, surface gravities, and clouds. As illustrated in Fig. 2.7.2, MICADO on the ELT offers a multiple gain for such work: the small inner working angle, the increased contrast between the PSF core and the speckles in the halo, and the elongation of the speckles when imaged through a broad or intermediate band.

Spectroscopy in MICADO will cover a wide wavelength range simultaneously at a resolution $R \sim 20000$, for faint compact or unresolved objects. It aims to emulate the success of Xshooter, while addressing a complementary role to the spatial resolution afforded by integral field spectroscopy. MICADO achieves this with a pair of cross-dispersing gratings in a fixed configuration, that exploit the large number of detectors to provide spectral traces covering $0.84\text{--}1.48\ \mu\text{m}$ and $1.45\text{--}2.4\ \mu\text{m}$ depending on the order-sorting filter selected. As an example, spectroscopy of exoplanets with the ELT will be radically different from what is possible today. The short spectral segment in Fig. 2.7.2 shows that individual molecular lines will be detected, leading to vast gains both in the planet's atmospheric characterisation as well as radial velocity measurements.

Technical Development: Since the Agreement for MICADO was signed in September 2015, the MICADO team at MPE have been fully engaged in developing all aspects of the instrument design. This culminated in a week-long Preliminary Design Review which ESO considered highly successful. The project has now entered its Final Design Phase, and remains on track to be ready for the ELT first light. One of the biggest challenges of MICADO is its size: the total height in Fig. 2.7.3 is over 6 m in order to reach the ELT optical axis, which has led to a 2-phase integration strategy that first sees the cryostat assembled and tested at MPE, before mounting the full structure together in ESO's Integration Hall.

Key features of the instrument include a catoptric design providing a $19''$ FoV sampled at 1.5mas and a $50''$ FoV sampled at 4mas . The single exchange mechanism can also move in a grating module for spectroscopy or a pupil imager for alignment and calibration. Folding the optical path from the telescope downwards allows the cryostat to rotate in a gravity invariant orientation and hence minimizes flexure. Using the same support structure both when MICADO is mounted with MAORY and in the stand-alone mode, means that MICADO is free-standing on the Nasmyth Platform, improving both accessibility and maintainability. Integrating both SCAO and the low order reference sensors for MCAO in a single module means that one can change seamlessly between the two adaptive optics modes. And it provides the capability to use SCAO in an initial stand-alone phase before MAORY is available. In terms of procurement, the science detectors have already been ordered, and MPE is now beginning the process that will enable the order for the cold optics, the heart of the instrument, to be placed later in 2019.



Fig. 2.7.3 A rendering of MICADO in its initial 'stand-alone' configuration, when it will operate with its own SCAO system and interface directly to the ELT pre-focal station. The calibration assembly and optical relay at the top (red) feed the light through the NGS wavefront sensor module (green) and into the cryostat (silver). The co-rotating platform underneath supports most of the electronics (blue).



Richard Davies

(Other MPE team members include: E. Sturm, S. Rabien, V. Garrel, M. Rosensteiner, M. Hartl, N. Förster Schreiber, S. Gillessen, R. Genzel, R. Bender, M. Fabricius, J. Thomas, F. Grupp, J. Schubert, V. Hörmann, J. Ziegler, L. Barl, N. Geis, H. Gemperlein, M. Plattner)

2.8 Star- and Planet Formation

The overarching goal of our program is to constrain the physics and chemistry of star- and planet-forming regions and follow the evolution of molecules from clouds to disks and planets, using combined observations (ALMA, NOEMA, Herschel, VLT) and models. Highlights over the past 3 years include (a) revealing planet construction sites in transitional disks through dust and gas cavities, rings and traps with ALMA; (b) determining disk demographics with ALMA showing that typical dust masses are not enough to form a giant planet core and that much of the CO is sequestered into other species; (c) demonstrating that gas disk sizes are much larger than those of the dust due to a combination of optical depth difference and radial drift of large dust grains; (d) characterizing the temperature of the warm surface layers of disks through observations and by including grain growth and evolution into our thermo-chemical disk code DALI; (e) following the trail of water, O_2 and complex organic molecules from collapsing cores to disks and comets, (f) quantifying the far-IR cooling budget of low-mass protostars and revealing a new class of UV-irradiated shocks; (g) resolving the gas-star cycle in nearby galaxies at molecular cloud scale. Interactions with the IR group occur on the galactic-extragalactic relation, and with CAS on astrochemistry (i.p. water, ammonia) and selected planet-forming disks.

Revealing planet construction sites in transitional disks:

Planets are found around nearly every star, but it is still not understood how they form. With ALMA, our team has continued to study a special class of disks with large dust cavities, the transitional disks. A beautiful example of an asymmetric dust trap imaged by ALMA by PhD student Cazzoletti is shown in Fig. 2.8.1; other examples include a multi-gap system in HD 169142 by Fedele and the dust ring in the HD 100546 disk with Pineda/CAS. In all cases, the gas cavity is smaller than that of dust. These observational facts are most plausibly explained by the scenario in which newly formed massive planets

have cleared the gas as they travel around their orbits, but trap the dust particles in pressure bumps further out. Hydrodynamical simulations have been coupled with the group's physico-chemical code DALI including dust evolution by Facchini to predict observables. The model results demonstrate how differences between gas and dust cavities can be used to constrain the masses of planets several times that of Jupiter.

ALMA survey of disk demographics:

An ALMA snapshot survey of ~ 100 disks in the Lupus star-forming region (1 min each) was carried out at 230 and 345 GHz in 2015-2017 (PI J. Williams, EvD co-PI). Surprisingly, at 1-3 Myr the medium dust disk mass is only that of Neptune with only 25% of disks having enough mass to form a giant planet core (Ansdell et al. 2016, 150 cit.). Also, gas emission was found to be unexpectedly weak, and thus gas/dust ratios are very low even when full thermo-chemical DALI disk models by Miotello are used (see below). The data either imply more rapid disk evolution than predicted by models, or volatile carbon being locked up in other species than CO, a scenario that has been modeled in detail with the Leiden part of the group. The CO data also allow sizes of gas disks to be determined, a further test of viscous evolution, which are found to be a factor 2-3 larger than the dust disks (with extreme cases up to 5, see Fig. 2.8.1). Detailed models of gas versus dust sizes including grain growth have been developed by Facchini within DALI demonstrating that a combination of difference in line vs continuum optical depth together with inward radial drift of mm-sized grains can explain the observations. Similar demographic studies have been performed with ALMA for other regions, most notably for Corona Australis by Cazzoletti, showing even weaker dust and gas emission.

Other fascinating and often surprising disk structures are seen in the data such as the huge V1094 disk in Lupus with a 'fried egg' structure (bright core with rings at large radii that are not related to snowlines) (see Fig. 2.8.1). Equally important, the unbiased and complete Lupus survey allows to put these large disks (van Terwisga et al. 2018) as

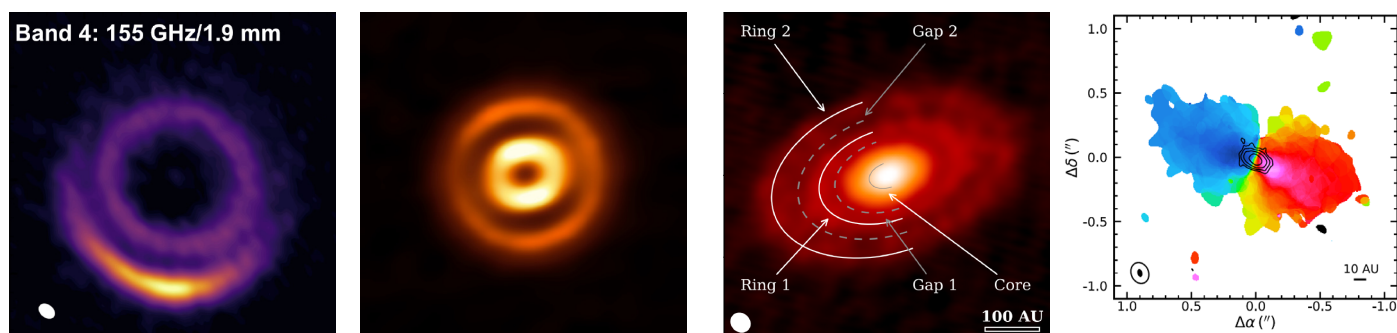


Fig. 2.8.1 Collection of ALMA observations of disks. **From left to right:** a) The transitional disk around HD 135344B revealing a symmetric ring at 50 au together with a major asymmetric dust trap at 80 au, both likely caused by a single companion (Cazzoletti et al. 2018). b) The HD 169142 disk with multiple rings out to 70 au (Fedele et al. 2017); c) The huge V1094 Sco disk showing a bright central core with rings out to 220 au unrelated to snowlines (van Terwisga et al. 2018); d) The CX Tau disk showing a very large ratio of gas (color) vs dust (black contours) disk size of ~ 5 (Facchini et al. 2019).

well as the transitional disks (van der Marel), in the context of the general disk population for the first time. They comprise typically 2% and 10% of the disks, respectively. Other molecules detected in the Lupus data include CN and HNC. Cazzoletti, van Terwisga and Visser have developed detailed models for these N-bearing species (including isotopologs) which explain the ring-like structure seen for CN and point to small gas disk sizes ($R_c < 15$ au) for the bulk of the Lupus population.

Deriving gas masses of disks:

The amount of gas in disks is a crucial parameter that determines its ability to form giant planets and that affects the dynamics of dust and its growth to planetary embryos. There are few reliable determinations of gas masses in disks, however. Miotello computed a grid of models which properly treats the freeze-out and isotope selective photodissociation of CO isotopologs in a full disk model using DALI (developed originally by Bruderer) and applied it to the Lupus disk survey. Using unique Herschel-PACS data on the HD J=1-0 line at $112\ \mu\text{m}$ analyzed with McClure et al., independent disk mass determinations have been obtained for a few sources that serve as benchmarks. These data lead to high gas masses and gas/dust ratios suggesting that transformation of CO to less volatile molecules can be significant and/or that these molecules are locked up in large pebbles early on.

Characterizing the temperature of protoplanetary disk atmospheres:

The surface layers of disks are heated by the UV radiation from the young star resulting in high gas temperatures > 1000 K. By combining velocity resolved CO J=16-15 line profiles from Herschel-HIFI with the CO ladder data from PACS, the distribution and temperature structure of warm molecular gas has been directly constrained. Including grain growth in DALI models, Facchini has shown that the gas and dust components thermally decouple much deeper in the disk resulting in colder gas and less mid-J CO emission.

Herschel far-IR surveys of protostars: UV-irradiated shocks:

Far-infrared spectroscopy reveals gas cooling and the physical processes near protostars. Karska et al. presented a summary of Herschel-PACS spectroscopy of 90 embedded low-mass protostars from the WISH, DIGIT (with Evans), and WILL surveys. CO rotational temperatures are universally ~ 300 K, with some sources showing additional components with temperatures as high as ~ 1000 K. The $\text{H}_2\text{O} / \text{CO}$ and $\text{H}_2\text{O} / \text{OH}$ flux ratios are low compared to stationary shock models, suggesting that UV photons may dissociate some H_2O and decrease its abundance. Cooling by molecular lines (CO, H_2O) dominates in

the early deeply embedded stages, with OH and atomic lines ([O I]) becoming more significant in the later phase.

Other projects:

The water deuterium fractionation is often used to infer the amount of water brought to Earth by comets. Using ALMA and IRAM NOEMA observations of H_2^{18}O , HDO and D_2O the HDO/ H_2O ratio is determined on 150 AU scales in several protostars, and found to be similar to comets, suggesting that planetesimals are formed early. The fact that $\text{D}_2\text{O}/\text{HDO} \gg \text{HDO}/\text{H}_2\text{O}$ supports this picture. Modeling with Taquet demonstrated that the surprisingly high cometary O_2 abundance is 'primordial', but that the pre-solar cloud must have been warmer (20-30 K) than typical dense cores (10 K). Complex organic molecules have been studied on solar-system scales through the ALMA PILS 345 GHz line survey of IRAS16293-2422 (PI J. Jørgensen, EvD co-I), with a dozen papers published.

Resolving the gas-star cycle in nearby galaxies at molecular cloud scale:

To understand the growth and evolution of galaxies requires understanding of the physics that regulate the gas-star cycle within galaxies. For the first time, multi-wavelength observations of the interstellar medium and stellar population are becoming available that resolve the fundamental scale of star formation - individual star-forming molecular clouds - for entire nearby galaxies (Fig. 2.8.2). These observations allow to relate the small-scale physics of gas and star formation - as studied inside our Milky Way - with galactic structure and galaxy evolution. Schruba, Bialy & Sternberg used high resolution maps of atomic (HI) gas in 70 nearby galaxies to show that the maximal HI columns saturate for large total gas surface density, with values that vary inversely

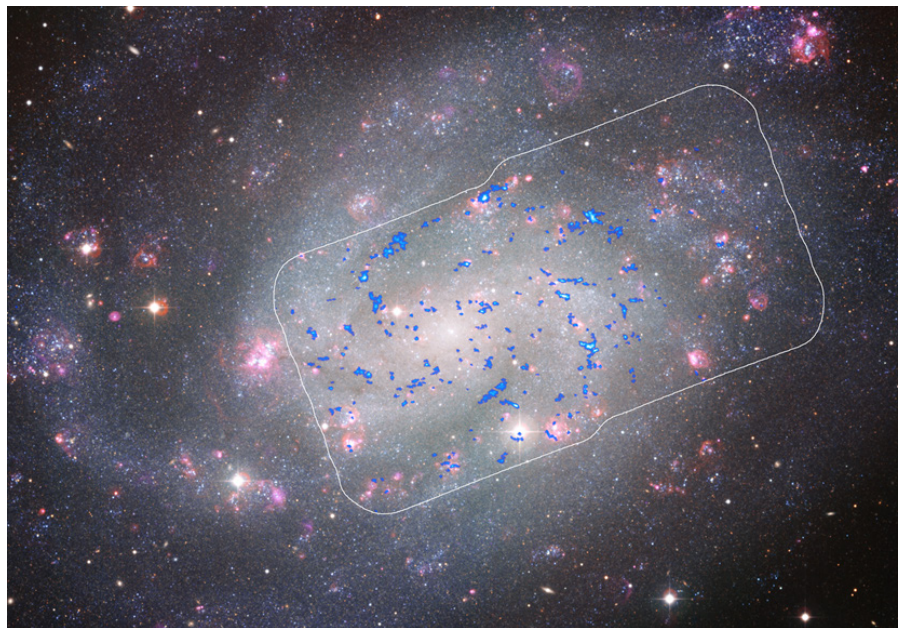


Fig. 2.8.2 Cloud-scale view of molecular gas (traced by ALMA CO, blue) and young stellar emission (traced by H α , red) in the nearby flocculent spiral NGC 300. Such observations allow to study the small-scale physics of gas and star formation - as studied inside our Milky Way - within the context of galactic structure and become now available for a large sample of nearby galaxies.

with metallicity. Such behavior is naturally reproduced by metallicity dependent shielding theories for the HI-to-H₂ transition in star-forming galaxies developed for galactic clouds.

The importance of shielding from dissociating radiation for the formation of cold molecular gas has also become apparent from today's finest (2 pc) ALMA CO observations in the low ($\sim 1/5$ solar) metallicity dwarf galaxy NGC 6822. CO emission emerges from compact clumps of only a few parsec in size which are embedded in large (~ 100 pc) complexes of atomic (HI) and molecular (H₂) gas. The CO-bright clumps have similar macroscopic properties as clumps in the outer Milky Way and another dwarf galaxy, WLM ($\sim 1/8$ solar metallicity). This suggests that their dynamical evolution and star formation process does not significantly change despite the 8x variation in metallicity. More generally, molecular gas in massive, near solar metallicity galaxies is arranged such that dense structures can have column densities and turbulent velocities spanning a wide dynamic range while their turbulent and gravitational energies remain in virial equilibrium. Also, they contain a significant fraction of molecular gas in diffuse structures; their turbulent energies are in pressure equilibrium with the weight of the atomic and stellar disk.

Based on samples of nearby galaxies, the (average) star formation rate per unit molecular gas mass and its efficiency per unit free-fall time are found to be similar within their molecular disks but systematically deviate in galaxy centers and atomic-dominated outer disks, demonstrating the role of environment. To improve our interpretation of H/H₂ and C⁺/C/CO transitions, Bisbas, Schruba and vD have developed a new PDR model which self-consistently determines the thermal and chemical composition of hierarchically structured (based on observed PDFs of galactic clouds), unresolved gas structures.

The study of samples of star-forming clouds reveals large variations between a cloud's star formation activity and gas mass indicative of capturing clouds in various evolutionary stages. With Kruijssen, a model has been developed that links the observed de-correlation of gas and star formation tracers as function of spatial scale to the evolutionary stage of individual clouds, thus constraining the underlying timescales and efficiencies of star formation. First application to ALMA observations of the nearby spiral NGC 300 indicate that star formation in molecular clouds is fast and inefficient (Nature in press).

In NGC 300, molecular clouds live for about one dynamical time scale (~ 10 Myr) until the formation of massive stars whose feedback quickly disperses the parent cloud. The slow conversion of gas into stars on galactic scales thus stems from the repeated cycling of gas between a diffuse, non-star-forming and a dense, star-forming state. The above studies have been a key contribution that enabled the "Physics at High Angular resolution in Nearby GalaxieS" (PHANGS; <http://phangs.org>) initiative, that is currently executing four Large Programs at ALMA, VLT-MUSE, HST, and the VLA to obtain multi-wavelength observations of the interstellar medium and stellar population at the scale of individual star-forming regions across a representative sample of 74 nearby galaxies. This survey will enable a comprehensive observational census of the interplay of the small-scale physics of gas and star formation with galactic structure and differentiate between competing theories of star formation.

Selected References:

- Cazzoletti et al. 2018, A&A 619, A161
 Bisbas, Schruba, van Dishoeck, 2019 MNRAS accepted
 Kruijssen, Schruba et al. 2019 (including van Dishoeck, Tacconi), Nature accepted
 Facchini, Birnstiel, Bruderer, van Dishoeck 2017, A&A 605, A16
 Facchini, Pinilla, van Dishoeck, de Juan Ovelar 2018, A&A 612, A104
 Karska et al. 2018, ApJS 235, 30
 Miotello et al. 2017, A&A 599, A113
 Schruba et al. 2017 (including van Dishoeck, Tacconi), ApJ 835 278 (ESO POTW)
 Schruba, Bialy, Sternberg 2018, ApJ 862 110
 Schruba, Kruijssen, Leroy 2019, ApJ, resubmitted

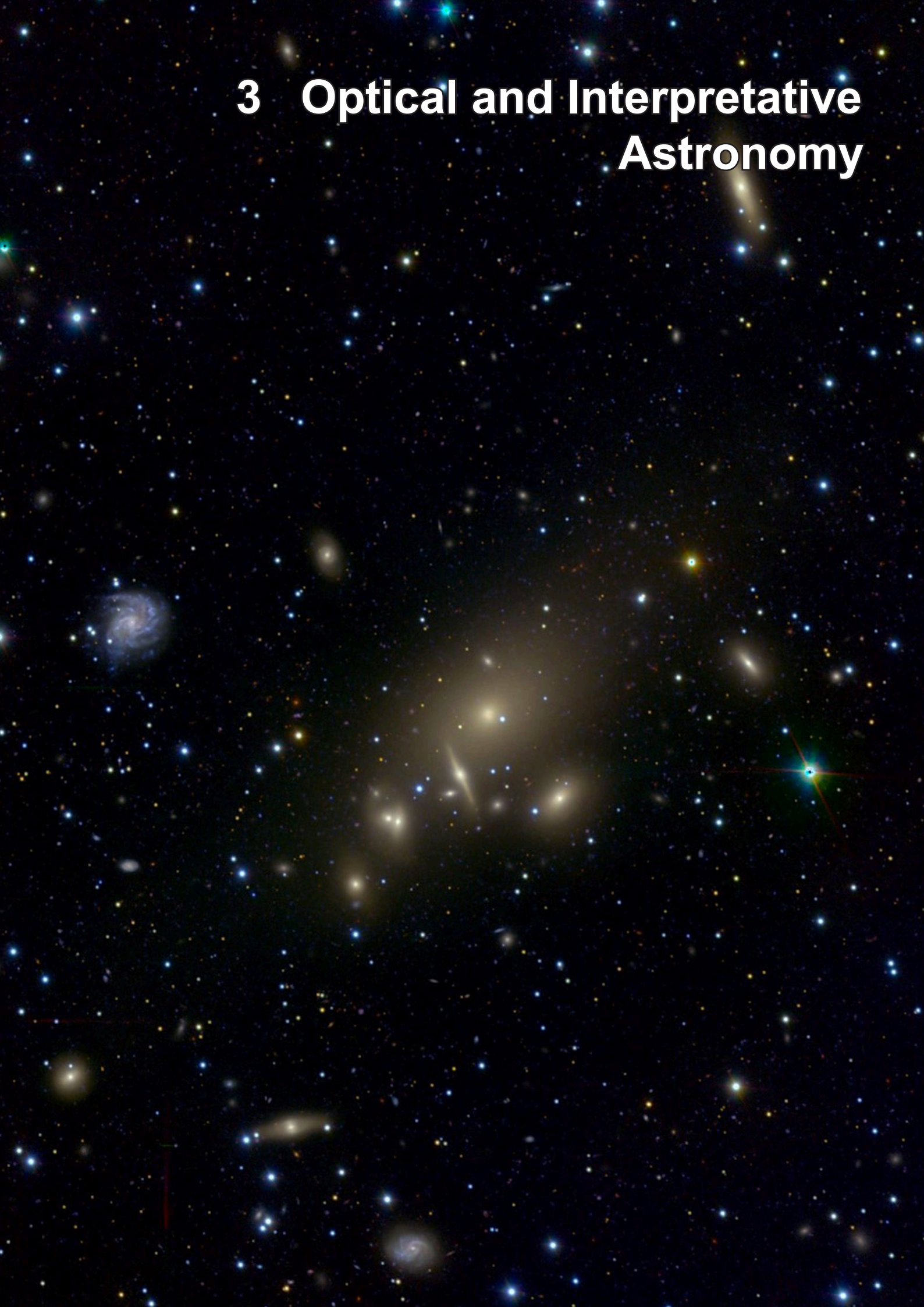
(About 140 refereed papers with MPE affiliation have been published in this period, $\sim 30\%$ of which have a significant MPE involvement.)



Ewine van Dishoeck

(Other MPE team members include: P. Cazzoletti, S. Facchini, and A. Schruba. Collaborations with former members: S. Bruderer, T. Bisbas, D. Fedele, A. Karska, A. Miotello, N. Murillo)

3 Optical and Interpretative Astronomy



Deep real-color u'g'r'-image of the galaxy cluster Abell 262, obtained with the Wide-Field Imager of the 2m Fraunhofer Telescope of the Wendelstein Observatory.

3. Optical and Interpretative Astronomy (OPINAS)

3.1 Overview

Research in the OPINAS group revolves around two central topics:

1. **Passive Galaxies.** We study their internal structure and dynamics, their stellar populations, their dark matter halos and their central supermassive black holes. We made influential contributions to the analysis of the scaling properties of galaxies (Fundamental Plane), the formation of massive ellipticals (they form their stars earlier and faster than lower mass ellipticals and spirals), the co-evolution of central black holes with galaxy host properties (e.g. black hole - velocity dispersion relation) and their dark matter properties (their halos are more massive and more concentrated than those of spiral galaxies at the same mass). Our current activities are aiming for a deeper and more refined understanding of the formation of passive galaxies and bulges, including their central black holes and dark halos, a goal which we pursue along a variety of directions with deep integral-field spectroscopy and ultra-deep imaging of local galaxies, with spectroscopy of high redshift objects (up to $z \sim 2$) and with improved modelling techniques (e.g. a new triaxial Schwarzschild orbit superposition method).
2. **Dark Matter and Dark Energy.** Complementing the dynamical studies, we investigate the dark matter properties of passive galaxies with gravitational lensing. The lensing method is further employed to study dark matter in galaxy clusters (e.g. with HST CLASH) and on larger scales (e.g. with the Dark Energy Survey). The new method of density split statistics was developed by our group. We have also led key elements of the analysis of the large-scale distribution of passive galaxies in SDSS BOSS by employing so-called clustering wedges for the first time. This has provided tight new constraints on Dark Energy properties and cosmological parameters. Understanding Dark Matter and Dark Energy are also key science goals of the Hobby-Eberly-Telescope Dark Energy Experiment (HETDEX) and the ESA Space mission EUCLID in which we have leading roles.

The organizational structure of OPINAS is different from those of the other MPE departments. OPINAS is hosted both at MPE and the University Observatory Munich as Ralf Bender is Director at MPE and holds a chair at the Ludwig-Maximilians-University. About half of the group is located at the Observatory, the other half at MPE. Our science projects are carried out distributed over both places, as is the education of graduate students. The group members at the observatory are also heavily involved in undergraduate teaching. Ortwin Gerhard's Dynamics Group is an independent MPE group associated with OPINAS (see separate report in section 3.8) and

we collaborate with them, e.g., in an extensive modeling project of M31.

Our research is profiting substantially from the hardware we have built and the software we have written. Instrument development for ground-based observatories is primarily taking place at the University Observatory. We had PI or leading roles in the VLT-instruments FORS, OmegaCAM, and KMOS and we contributed to HET and HETDEX with hardware and software. We also have a prominent role in MICADO, the first-light camera for the ESO Extremely Large Telescope. Last but not least, the instrument group at the University Observatory is also providing all instruments for the University Observatory's 2m telescope on Mt. Wendelstein in the Bavarian Alps (to which we have privileged access). Our hardware contribution to the ESA mission EUCLID is instead hosted at MPE, as is the German Science Data Center for EUCLID.

The most important OPINAS highlights of recent years have been:

1. We discovered the most massive black hole ($4 \cdot 10^{10} M_{\text{sun}}$) in the local universe in the central cluster galaxy Holm 15a. This galaxy also has one of the lowest density and largest cores known and probably formed in a merger of two massive ellipticals which already had large cores.
2. We surveyed a large sample of local Brightest Cluster Galaxies (BCG) to the unprecedented depth of 30 mag/arcsec² and showed that many BCGs show distortions at faint levels. Unlike previous shallower studies we show that the scaling relations of BCGs differ from normal bright ellipticals which is related with their often smooth transition into the Intra-Cluster-Light.
3. Our KMOS GTO surveys culminated with a series of papers on the evolution of massive galaxies up to $z \sim 2$. For the first time we studied the Fundamental Plane in galaxy clusters at $1.2 < z < 1.8$ showing that the most massive objects are evolving passively and are 1 Gyr to 2 Gyr old. In parallel we studied a sample of passive field galaxies in the same redshift range. We found evidence that the stellar initial mass function (IMF) is more similar to the Milky Way than to local massive galaxies at the same velocity dispersion (i.e. not bottom-heavy). We also participated in the KMOS^{3D} Survey led by Natascha Foerster-Schreiber (see the section 2.2 of the Infrared-Group) and showed that the growth in size and mass with time of star forming disks cannot be explained by star formation alone.
4. To extract maximal information on the large-scale density field with gravitational lensing, we developed the so-called density split statistics method. This new method allows to measure structure growth be-

tween linear and highly non-linear regimes by sorting the sky in different density quantiles. The density split statistics is now used in the Dark Energy Survey to improve the constraints on cosmological parameters and measure, e.g. how the skewness of the density field develops when structures become slightly non-linear.

5. We have made key contributions to SDSS BOSS. From the 12 core papers of BOSS, members of OPINAS have first-authored 4. We successfully employed clustering wedges to improve constraints on cosmological parameters and are now deeply involved in the analysis of eBOSS. We designed the methodology to obtain (and computed) the final cosmological consensus constraints from the survey, which were published in Alam et al. (2017) (the final alphabetical paper). At the same time, we started to prepare for HETDEX and EUCLID, which will be supported and accompanied by smaller participations in other surveys (DESI, PFS).
6. We have completed the optics for the EUCLID Near-Infrared Spectrometer and Photometer (NISP) much better than specifications required and delivered it for integration to LAM in Marseille. We are running the German EUCLID Science Data Center, participate in EUCLID Science Working Groups, have a key role in the so-called 'Organisational Unit' on Photometric Redshifts, lead the Joint Likelihoods Analysis and are represented on the EUCLID Board.
7. We have established a key role in the development of MICADO, the first light imager for the ESO Extremely Large Telescope. We will provide the main selection mechanism, an optomechanical component allowing to switch with high precision between different instrument modes, and we provide the instrument control electronics and instrument and observing preparation software.

The longer term strategy of the OPINAS group continues to rely on the successful combination of three components: construction of instrumentation serving our science goals, participation in large surveys where preferable, and the development of sophisticated modelling techniques for the optimal exploitation of the data we obtain. With the mix of projects described above, we believe we are well-positioned for a scientifically successful future.

Ralf Bender



3.2 Dynamics of Local Galaxies

The OPINAS group is the world-wide leader in dynamical studies of the centers of early-type galaxies. In the last years, we discovered the most massive black hole ever directly measured from the motion of the stars around it: the 40-billion solar mass black hole at the center of Holm 15A, the brightest cluster galaxy in Abell 85. We also successfully continued to push the limits of current state-of-the-art dynamical modelling techniques: We developed SCHERPA, a triaxial implementation of the Schwarzschild orbit superposition method. During the testing phase of our new triaxial implementation of the Schwarzschild orbit superposition code on N-body models with a central black hole, we have found previously unnoticed long-lived intermediate axis rotation, a kinematic behaviour that was believed to be unstable on short time scales. We embedded SCHERPA and our existing axisymmetric modelling code into an adaptive-mesh-search framework, allowing us to efficiently explore the multi-dimensional triaxial parameter space, to fit stellar population gradients and even non-parametric mass profiles – advancements necessary to solve the current issue about the stellar initial mass function in massive galaxies. We systematically studied the luminous envelopes of 171 local brightest cluster galaxies (BCGs) down to an unprecedented depth of 30 mag/arcsec² (g-band). Differing from previous shallower surveys, our data show that scaling relations for BCGs differ from those of luminous ellipticals.

Schwarzschild orbit superposition models provide fully general solutions of the collisionless Boltzmann equation, free of anisotropy assumptions which are required, for example, in Jeans models. The OPINAS group is world-wide leading in modelling the centers of elliptical galaxies with stellar orbits. With our work on black holes and stellar orbits in core galaxies in the last years we presented the first solid evidence, that the diffuse cores of massive galaxies are the result of scouring by binaries of supermassive black holes. More massive black holes produce larger and fainter cores. An extreme case is Holm 15A, the brightest cluster galaxy of Abell 85 at a distance of 221 Mpc. The central surface brightness of the galaxy is 2 mag fainter than in any core galaxy with a measured black hole and the cusp-radius is 4x larger than in other core galaxies. In accordance with these extreme properties, we found a black hole at the center of this core that is at least 2x more massive than any other other black hole in the local universe: it has a mass of 40 billion solar masses (Fig. 3.2.1). A detailed analysis of the central light profiles shows that Holm 15A's core is exponential, while "classical" cores follow a shallow power-law profile. However, the stars in the center of Holm 15A are mostly found on tangential orbits, similar as in other elliptical galaxies with "classical" cores (Fig. 3.2.2). High-resolution N-body merger simulations suggest that remnants of mergers between core galaxies are less tangentially anisotropic than remnants of

coreless progenitors (Fig. 3.2.2). Holm 15A falls into this core-core merger regime. A merger between two galaxies like NGC4874 and NGC4889 at the center of the Coma cluster would produce a galaxy with similar stellar mass, black-hole mass and, probably, similar anisotropy as Holm 15A (→ K. Mehrgan).

These high-resolution N-body simulations (collaboration with the Max-Planck-Institute for Astrophysics) provide, for the first time, a formation scenario for kinematically decoupled cores in massive slowly rotating ellipticals: when the progenitor black holes drift towards the center of the remnant galaxy, the angular momenta of their orbits experience several "spin flips" which induce the kinematically distinct features in the collective motion of the stars. These simulations also confirm that gas-poor mergers, even with very massive central black holes, lead to triaxial remnant galaxies (→ J. Thomas).

In the last decade it had been state-of-the-art to model stellar orbits in elliptical galaxies in axial symmetry. Earlier work has shown that this can bias the measured stellar and black hole masses. To reduce the systematics in dynamical mass measurements, we developed SCHERPA in the last years. SCHERPA is a triaxial orbit-superposition code based on a newly developed adaptive orbit sampling technique. We tested and optimised SCHERPA on realistic mock observations obtained from the high resolution N-body merger simulations with black holes mentioned above. (Fig. 3.2.3).

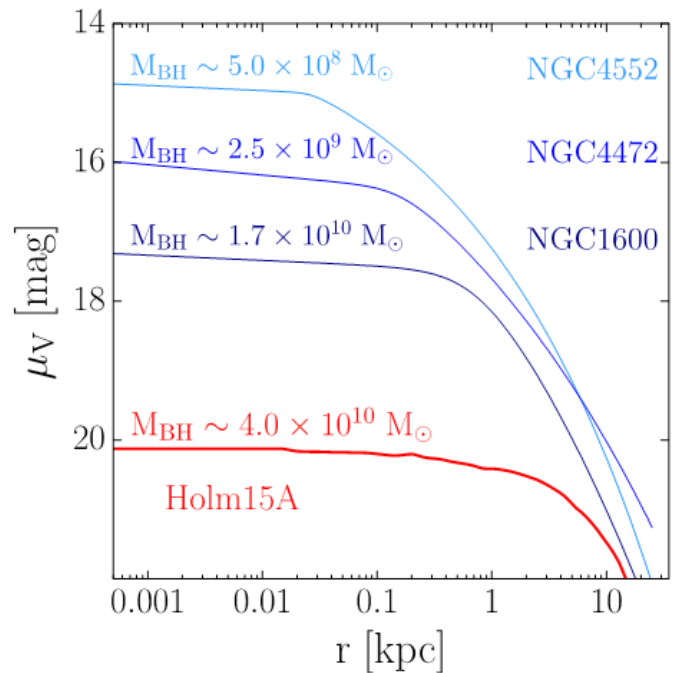


Fig. 3.2.1 The surface brightness profile of Holm 15A and other elliptical galaxies with classical cores. Size and brightness of the cores correlate with the mass of the central black hole. Holm 15A fits into this homology.

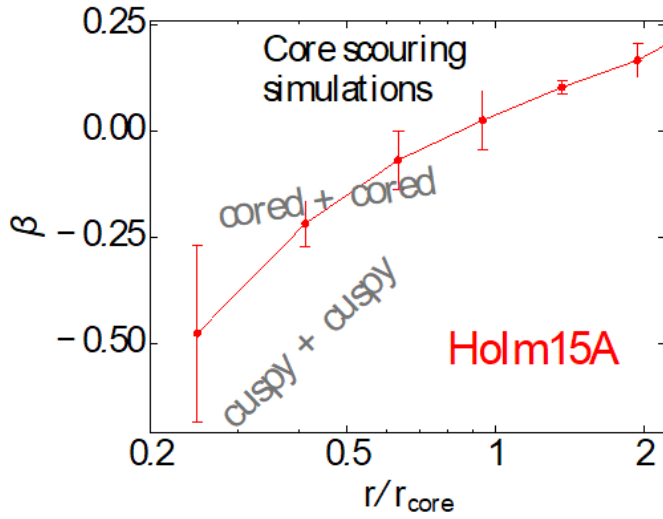


Fig.3.2.2 The orbital anisotropy β of Holm 15A is similar to the anisotropy of other elliptical galaxies with a classical core: outer radial anisotropy ($\beta > 0$) changes to central tangential anisotropy ($\beta < 0$). N-body merger simulations with central black holes predict less central tangential anisotropy when the progenitors already had cores, similar to what we observe in Holm 15A.

With SCHERPA's adaptive orbit sampling technique we could construct near-equilibrium distribution functions with rotation around the intermediate axis which arises from intrinsically chaotic orbits (Fig. 3.2.4). Transient rotation about the intermediate axis on time scales of Gyrs could have important consequences for modelling real galaxies. Reconstructions of the intrinsic shape distribution of early-type galaxies typically assume rotation only about the long and/or about the short axis, possibly leading to biased results. In general, SCHERPA is able to reconstruct the intrinsic velocity moments of the N-body simulation with better than 5% accuracy (\rightarrow F. Finozzi, B. Neureiter; R. Bender, R. Saglia, J. Thomas).

We embedded our axisymmetric and triaxial Schwarzschild codes into the NOMAD framework (NOMAD = non-linear optimisation using mesh-adaptive direct search). In this way, we managed to reduce the computing-time requirements by more than an order of magnitude opening new doors for dynamical modelling: we can now (i) fully explore the multi-dimensional parameter space of triaxial galaxies, (ii) explore dynamical consequences of stellar population gradients, (iii) fit multi-parameter dark-matter halo profiles or (iv) reconstruct even non-parametric mass distributions. The NOMAD master process launches several individual Schwarzschild models simultaneously, each running as a multi-core slave process, to build up a common cache where all the model results are stored and analysed to optimise the next

search steps. This new level of model complexity is crucial to accurately determine the intrinsic scatter of black-hole scaling relations, determine the spatial distribution of dark matter and measure the stellar initial mass function (\rightarrow F. Finozzi; R. Saglia, J. Thomas).

Already in axial symmetry, the deprojection of a given light distribution is not unique unless a galaxy is seen exactly edge-on. So-called conus-densities exist, which are invisible in projection above a critical inclination. Tri-axial deprojections are more complex due to so-called funnel densities, the triaxial analogues to conus densities. To be able to systematically investigate triaxial deprojections and to overcome the limitations of the sometimes used Multi-Gaussian-Expansion method, we developed a fully non-parametric deprojection code, generalising the axisymmetric Metropolis Code of Magorrian (1999). The isophote shapes of real galaxies and the remnants of N-body simulations suggest that the stellar densities in elliptical galaxies are ellipsoidal. We therefore also implemented an ellipsoidal triaxial deprojection where the free parameters are (1) the densities at a set of (typically 80) radial grid points; (2) the intermediate-to-long axis ratio p at the same radii; (3) the short-to-long axis ratio q at the same grid points. Fig. 3.2.3 shows the ellipsoidal reconstruction of a triaxial Jaffe model with varying axis ratios. The figure suggests that the ellipsoidal triaxial deprojection is very useful to separate physically plausible deprojections from mathematically allowed but unphysical ones (\rightarrow Stefano de Nicola; R. Saglia, J. Thomas).

As part of the MASSIVE survey, we systematically studied the radially resolved stellar populations and kinematic features of early-type galaxies above a stellar mass of $M^* = 3 \times 10^{11} M_{\odot}$. As expected, the angular momentum λ_e decreases towards the high-mass end of early-type galaxies and the fraction of slow rotator galaxies, f_{slow} ,

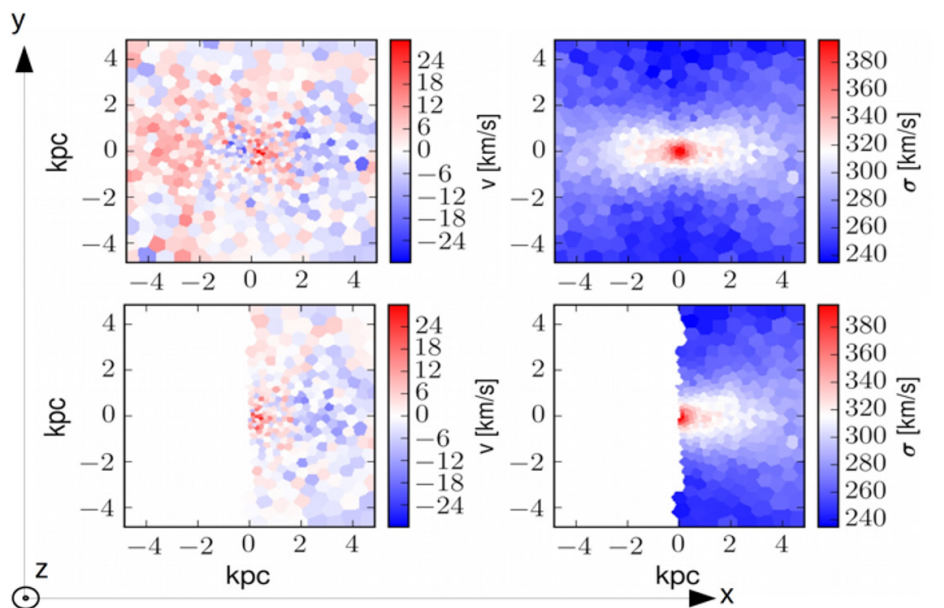


Fig. 3.2.3 Kinematic maps of an N-body merger between two elliptical galaxies with central black holes (top row) and a model fit with SCHERPA. The line-of-sight was near the short axis of the triaxial remnant.

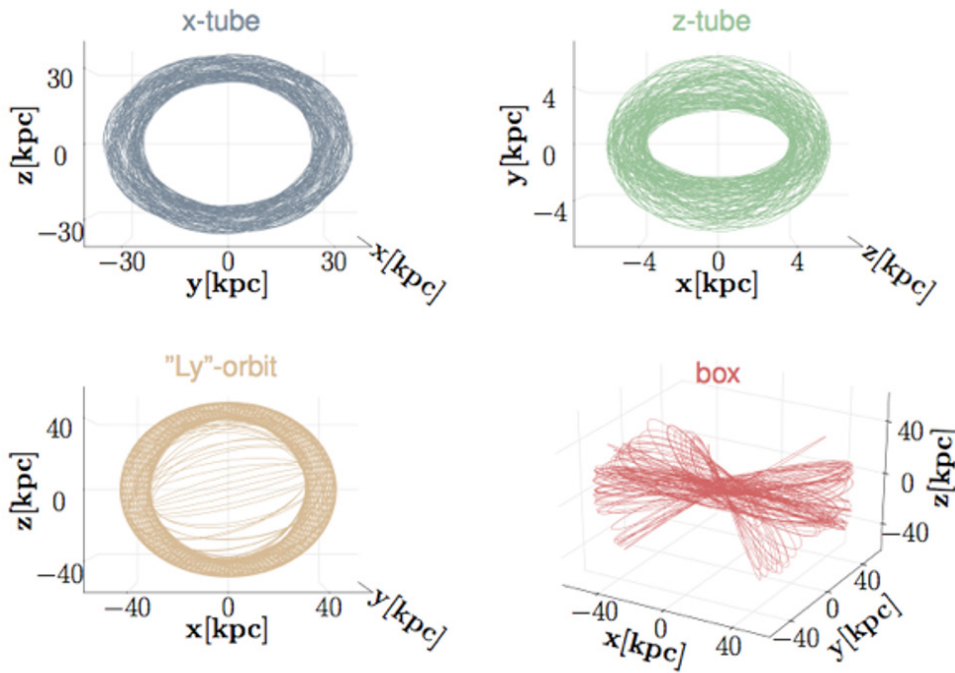


Fig. 3.2.4 SCHERPA can produce intermediate-axis rotation by populating “Ly”-orbits. In the model they coexist with classical families of tube, box or other orbits. “Ly”-orbits are mostly chaotic, but maintain intermediate-axis rotation for several Gyrs.

increases from 10% at $M^* < 10^{10} M_{\text{sun}}$ to 90% at $M^* = 10^{12} M_{\text{sun}}$. At a fixed stellar mass, there is almost no dependency of the angular momentum content with galaxy environment. The apparent kinematic morphology-density relation of ETGs is primarily driven by galaxy mass. Of the fast-rotating galaxies in MASSIVE, 90% have their rotation aligned with the light distribution. The slowly rotating galaxies fall into two subcategories: about 1/3 of the galaxies have no detectable rotation signal. In the remaining galaxies kinematic and photometric axes are misaligned with an almost flat distribution of the misalignment angle. MASSIVE galaxies show a variety of different velocity dispersion profiles. Galaxies with rising outer dispersion are found in the densest environments and have stars with low metallicity $[\text{Fe}/\text{H}] = -0.25$ and large $[\alpha/\text{Fe}] = 0.3$ their outer parts. The rising velocity dispersion is indicative of an accreted halo. Galaxies with falling dispersion profiles show a strong correlation between the kurtosis of their line-of-sight velocity distributions (LOSVDs) and chemical composition of their stars: LOSVDs characteristic of a radially anisotropic orbit distribution likely related to stellar accretion come again along with metal-poor and α -enhanced stars. Our findings support the two-phase scenario in which central stars are formed in situ while outer stars are accreted in massive early-type galaxies (\rightarrow J. Thomas and MASSIVE).

We systematically study the structure of local ($z < 0.08$) BCGs and their surrounding intracluster light (ICL). Using novel background subtraction techniques, we carefully measured BCG+ICL light profiles down to a g-band magnitude of 30 mag/arcsec². This unprecedented photometric depth means that we can follow the ICL out to ~ 400 kpc from the galaxy. 39% of the 171 observed BCGs

are better described by a double Sersic function than a single one, indicating that the BCG-ICL transition is often very smooth. The outer Sersic component does not correlate with cluster properties. On average, the ICL’s position angle is better aligned with that of the satellite distribution, the ICL center is shifted towards the satellite galaxy number peak and the BCG+ICL brightness correlates with cluster mass, radius and richness, in agreement with an accretion scenario for the ICL. The photometric depth of our new sample clearly shows that the size-luminosity relation for BCGs is steeper than previously known (\rightarrow M. Kluge; R. Bender).

We study dwarf elliptical galaxies to measure the central dark-matter density slopes: are they “cuspy” as expected in a Λ CDM universe, or are they “cored” as suggest by previous gas obser-

vations? Preliminary results for VCC2048 suggest a central logarithmic halo slope lower than 0.5, flatter than the canonical value of unity for Navarro-Frenk-White dark-matter halos. We have completed observations for a sample of 11 galaxies in total (\rightarrow G. Pentaris, G. Murrell, X. Mazzalay).

Finally, we continued our work on black hole masses in disk galaxies. For the S0 galaxy NGC307 we showed

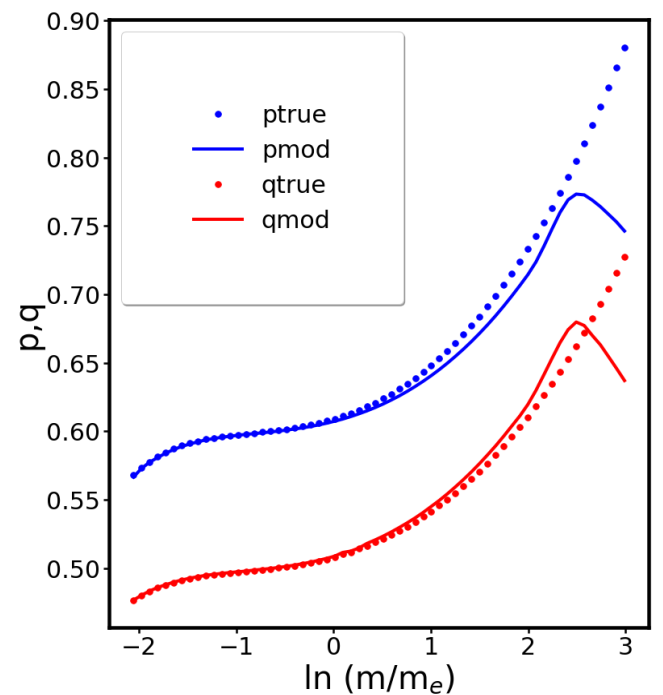


Fig. 3.2.5 Ellipsoidal deprojection of a triaxial Jaffe toy model. The variation of the short-to-long axis ratio q and the intermediate-to-long axis ratio p with the radial coordinate m of the Jaffe model (dots) is well reproduced by the triaxial deprojection (lines).

that measuring SMBH masses in disk galaxies using just a single stellar component and no dark matter halo has the same drawbacks as it does for elliptical galaxies: it can cause the central stellar mass to be biased high and the black-hole mass to be biased low. Reasonably accurate SMBH masses and bulge M/L ratios can be recovered (without the added computational expense of modelling dark-matter haloes) by using separate bulge and disk components, though the disk M/L may contain some of the dark halo mass. The mass of the galaxy's black hole is $3 \times 10^8 M_{\text{sun}}$.

Jens Thomas



Roberto Saglia



Selected References:

Chaturvedi, A., 2018, *Master Thesis, Marseille University*
 Ene, I., Thomas, J., et al. 2018, *MNRAS*, 479, 2810
 Erwin, P. et al. 2018, *MNRAS*, 473, 2251
 Finozzi, F., 2018, *PhD Thesis, LMU*
 Goullaud, C., Thomas, J., et al. 2018, *ApJ*, 856, 11
 Greene, J., Thomas, J., 2019, *ApJ*, in press
 Kianusch, M., 2018, *Master Thesis, TUM*
 Murrell, G., 2018, *Master Thesis, Dublin University*
 Neureiter, B., 2018, *Master Thesis, LMU*
 Pandya, V., Thomas, J., et al. 2017, *ApJ*, 837, 40
 Rantala, A., Thomas, J., et al. 2019, *ApJ*, 871, L17
 Veale, M., Thomas, J. et al. 2017, *MNRAS*, 464, 356
 Veale, M., Thomas, J. et al. 2017, *MNRAS*, 471, 1428
 Veale, M., Thomas, J. et al. 2018, *MNRAS*, 473, 5446

(Other OPINAS team members include: R. Bender, M. Fabricius, M. Kluge, K. Mehrgan, B. Neureiter, S. de Nicola, G. Pentaris. Former team members: A. Chaturvedi, P. Erwin, F. Finozzi, X. Mazzalay, G. Murrell)

3.3 Constraining Large Scale Structure and Cosmology with Gravitational Lensing

One focus of our work is to measure the mass distributions of clusters of galaxies using the strong and weak lensing effects and to study implications on cosmology. Another goal is to measure the properties of the galaxy halos within the clusters and compare them with field galaxies. Depending on the nature of dark matter the details of this effect will be different. With “cosmic shear” we measure the growth of dark matter density fluctuations with cosmic time on scales that can be treated in the linear regime. In this way we determine the basic parameters of our standard model universe or can find hints for inconsistencies. With the so-called “density split statistics” we recently also developed a method which measures structure growth between the linear and the highly non-linear regimes, by sorting the sky in different density quantiles as traced by galaxy density and analysing lensing effects therein. This allows to measure, e.g., how the skewness of the density field develops, when structures become slightly non-linear.

1. Clusters of Galaxies:

Regarding the frequency of background galaxies lensed into giant arcs by massive foreground clusters we showed in Xu et al. 2016 that there is no conflict to the standard LCDM model prediction, when the statistics of observed arcs towards CLASH clusters is compared to predictions based on simulated clusters with realistic “mock observations” and correct cluster selection function. This means that a long-standing question (Meneghetti et al. 2013, SSRv, 177, 31) was answered. With the Planck Cluster PLCK287 we identified the second strongest lensing cluster discovered so far (Gruen et al. 2014, MNRAS, 442, 1507), followed it up with HST and obtained a mass model based on the strong lensing effect (Zitrin et al. 2017). Our most recent work (Furtak et al. in prep.) measures an Einstein radius of 50.5 arcsec. PLCK287 will be further analysed (with more spectroscopic data) because it is the second best magnifying lens for studying $z > 6$ galaxies (first results in Salmon et al., 2017, astro-ph-171008930) and because its existence adds to the potential tension with LCDM universes regarding the observed order-statistics of Cluster Einstein radii (Redlich et al. 2014, A&A, 569, 34).

Analysing CLASH clusters we showed (Monna et al. 2017a, Caminha et al. 2016, A&A, 606, 93) that with 30-50 multiple image positions used for the strong lensing models, one can achieve an image position reproduction accuracy down to 0.4-0.3”. This equals the minimum contribution of light deflection by uncorrelated line-of-sight structures (Caminha et al. 2016, Host et al. 2012, ApJ, 420, L18), and means that the cluster mass components related to the cluster galaxies and the overall dark matter distributions are well separable and each of them is well constrained in our models. In Monna et al. 2017b we showed that using the cluster members’ stellar velocity dispersions improves the modelling quality and allows

to measure their halo truncation radii more precisely. For galaxies close to giant arcs and for models where the arcs’ overall surface brightness distributions are reconstructed, the halo size constraining power increases by a factor of 10. According to our measurements cluster galaxy halos with 100km/s stellar velocity dispersions have half mass or truncation radii of only a few kpc, indicating that they are stripped relative to field galaxies.

Measuring cluster mass profiles and properties of cluster galaxy sub haloes on larger scales relies on analysing the weak lensing effect. We have played a leading role in measuring the mass profiles for optical richness selected clusters with Dark Energy Survey data (Melchior et al. 2016, McClintock et al. 2019, Varga et al. 2019), see posters. The excess surface mass density was measured with an unprecedented precision, for the largest cluster sample ever. This was possible because of the high precision we reached for the photometric redshift estimates for the weak lensing background sample (Hoyle et al. 2018) but needed a large additional effort, since cluster lines of sights are not representative for the universe, and the redshift distribution in these directions is changed by unavoidable contaminations due to cluster members and correlated structures. This problem was solved with the so-called “boost-factor-calibration” (Varga et al. 2019) – see poster. Our cluster mass richness relation is currently used to constrain cosmology from cluster mass vs. number count statistics. In addition, since we now have better understood the mass properties of the DES cluster sample as a whole, we can start to investigate the cluster sub halos traced by the cluster members.

For some special Xray and SZ clusters we measure the weak lensing mass distribution with our Wendelstein 2m Telescope (Rehmann et al. 2019, see poster). This will be used to contribute to the calibration of the mass versus gas-mass relation for relaxed clusters, and to derive cosmological constraints for such a sample (in collaboration with D. Gruen, S. Allen and A.v.d.Linden).

2. Weak Cosmic Shear results & Covariance modelling:

Using weak lensing and galaxy clustering, the DES collaboration (Abbott et al. 2018, PhysRevD, 98, 043526) has published constraints (see Fig.3.3.1) on the LCDM and Λ CDM parameters for which the precision for the first time rivals that of Planck-CMB analyses. Our contribution to this work was photometric redshift estimates (Hoyle et al. 2018) and a substantial contribution to the analysis methods of the multi-probes (Krause et al. 2017, 2017arXiv170609359K) and expertise in performances of internal covariance estimators (Friedrich et al. 2016). In addition, Friedrich & Eifler 2018 developed a method to expand the precision matrix around a known analytic covariance model and to estimate the leading order

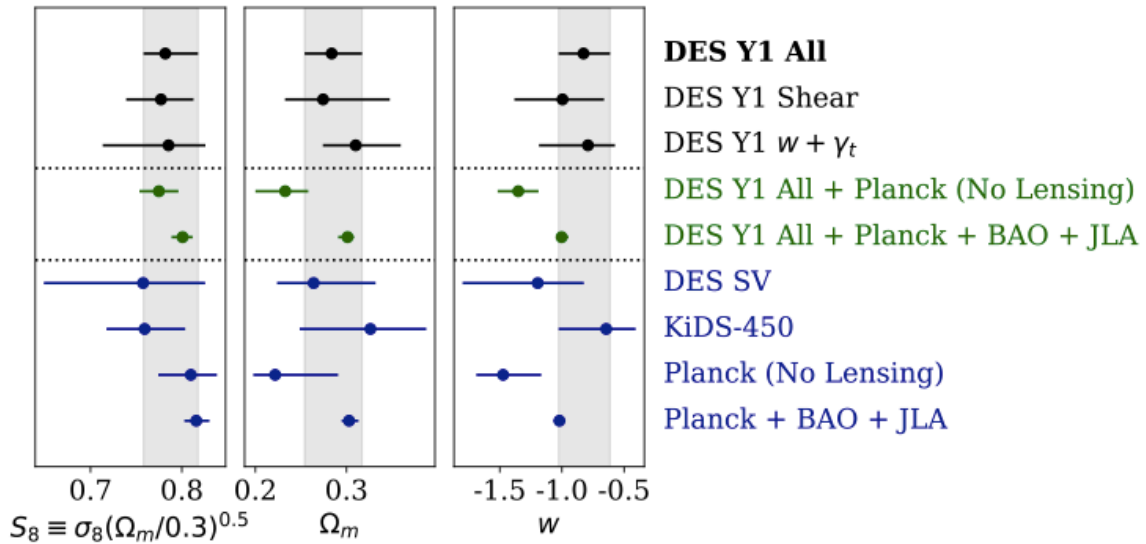


Fig. 3.3.1 DES-Year-1 constraints on w CDM parameters from weak lensing and galaxy clustering vs literature (Figure 9 from Abbott et al. 2018)..

terms for this expansion with simulations in an efficient way. This will allow to increase the dimensionality of further combined probes analyses without having the number of required “simulated Universes” becoming ridiculously high.

3. Density Split Statistics:

Up to now most analysis methods and most recent weak lensing measurements study only the rms-fluctuations of the density field. This is at most a sufficient description of the Large Scale Structure in the very early Universe (and when assuming gaussian initial conditions). Later on, non-linear gravitational collapse of the most evolved structures turns the cosmic density field into a non-gaussian, “skewed” field and significant information about the growth history of structures is transferred to higher order moments of that field. To recover this information our group has developed the so-called “Density Split Statistics” (Gruen, Friedrich et al. 2016, Friedrich, Gruen et al. 2018, Gruen, Friedrich et al. 2018), see also the poster. Galaxy counts in cells are used to sort the sky in different galaxy density quantiles and the weak lensing effect is analysed relative to these regions. The lensing effect is modelled by describing the density field with perturbation theory and by using a galaxy bias model. In addition to the classical cosmological parameters, one can then measure this galaxy biasing and the skewness of the density field. Applying the model to SDSS and DES data it was shown that the ratio of the skewness to the squared variance (called S3) agrees with the value derived by Peebles J. in 1980 in his book “The large-scale structure of the universe”. This is based on gaussian initial conditions and perturbation theory and is nearly independent of the matter and energy content of the universe. We currently develop further analysis methods to analyse the cosmic density field beyond either just measuring its variance (classical cosmic shear) or analysing its highest peaks (i.e. clusters of galaxies).

Selected References (2016-2019):

- Friedrich, O., Seitz, S., Eifler, T.F., Gruen, D. 2016, *MNRAS*, 456, 2662
 Friedrich, O., Eifler, T.F. 2018, *MNRAS*, 473, 4150
 Friedrich, O., Gruen, D. et al. 2018, *PhRvD*, 98, 023508
 Furtak, L., Seitz, S. et al. in prep.
 Gruen, D., Friedrich, O. et al. 2016, *MNRAS*, 445, 3367
 Gruen, D., Friedrich, O. et al. 2018, *PhRvD*, 98, 023507
 Hoyle, B., Gruen, D., Bernstein, G., Rau, M.M. et al. 2018, 478, 592
 Monna, A., Seitz, S. et al. 2017a, *MNRAS*, 466, 4094
 Monna, A., Seitz S. et al. 2017b, *MNRAS*, 465, 4589
 Melchior, P., Gruen, D., McClintock, T., Varga, T. N. et al. 2017, *MNRAS* 469, 4899
 McClintock, Varga, T. N., Gruen, D. 2019, *MNRAS*, 482, 1353
 Rehmman, R., Gruen, D., Seitz, S., Bender, R. et al. 2019, 2018arXiv180610614R, *MNRAS* in press
 Varga, T.N., DeRose, J., Gruen, D. et al. 2019, 2018arXiv181205116V, *MNRAS* in press
 Xu, B., Postman, M., Meneghetti, M., Seitz, S. et al. 2016, *ApJ*, 817, 85
 Zitrin, A., Seitz, S., Monna, A. et al. 2017, *ApJ*, 839, 11L



Stella Seitz

(Other team members: A. Halder, A. Monna, R. Rehmman, T. N. Varga. Former members are: O. Friedrich, L. Furtak, D. Gruen, M. M. Rau)

3.4 The Evolution of Star Forming and Passive Galaxies from $z=0.7$ to 2.7

Our KMOS GTO surveys came to an end with the publication of several papers. We found that the growth in size and mass with time of star forming disks cannot be explained by star formation alone. We constrained the evolution with redshift of color gradients of passive cluster galaxies; we pushed the study of the evolution of the Fundamental Plane up to redshift 1.8 and we characterized the galaxy environment in this redshift range. Our final investigations revealed that the amount of dark matter in passive field galaxies up to redshift 2 is low.

In March 2019 the last 3-night run of GTO observations with KMOS at the VLT was executed, closing our 6 years effort to study star-forming and passive galaxies in the redshift range $0.7 < z < 2.7$ with this instrument. In the context of the KMOS^{3D} project in collaboration with the Near-Infrared group, we mapped the distribution and kinematics of the ionized gas in ~ 600 relatively massive star forming galaxies, studying their dynamics, dark matter and metallicity content. An exhaustive description of the recent KMOS^{3D} results is given by Förster Schreiber et al. in this book. Here we focus on our study of the H α distribution of 281 representative star-forming galaxies of the KMOS^{3D} sample up to redshift 2.7, aiming to explain the growth in mass and size of star forming galaxies reported in the past. Fig. 3.4.1 shows that H α sizes ($r_{\text{H}\alpha}$, derived from exponential disk model fits) are a mean 1.26 times larger than those (r_{F160W}) of the stellar continuum in the F160W band. This ratio does not vary with redshift, stellar mass, star formation rate or morphology. It could possibly be an upper limit: the presence of a dust component embedded in the star forming disk will cause regions of higher star formation to be more absorbed and the half-light radius of the observed emis-

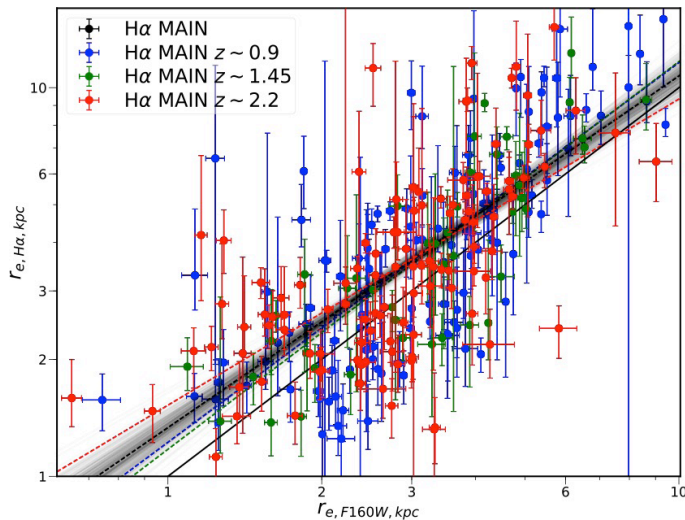


Fig. 3.4.1 H α galaxy sizes as a function of galaxy size measured in the F160W CANDELS band ($\sim H$ band). The best fit and sample fits are shown with the black line and fainter grey lines. Galaxies are divided in three redshift bins with data points colour-coded and fits to each redshift bins also shown (coloured lines).

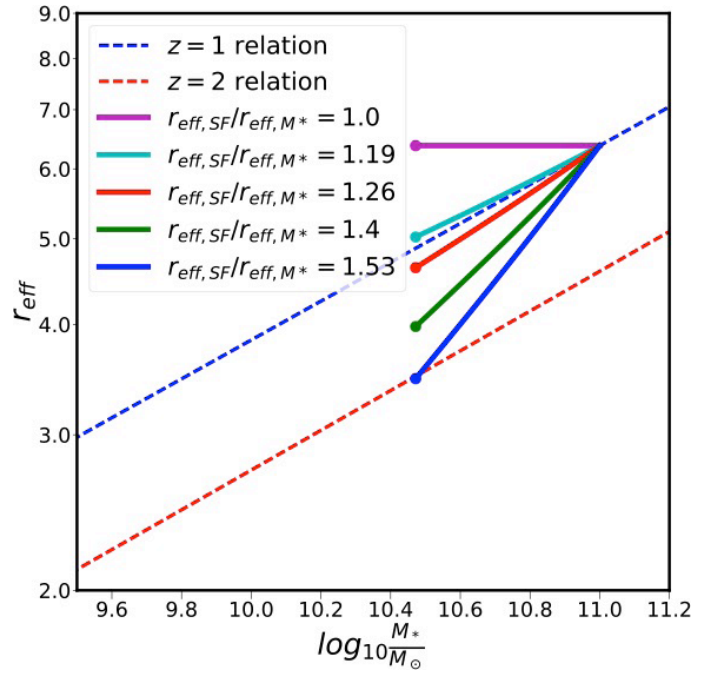


Fig. 3.4.2 The galaxy growth from $z=2$ to $z=1$ on the size-mass plane. Galaxies grow in mass through star formation following the mass-star formation relation determined from previous observations (van der Wel et al. 2014, solid red and blue lines at redshift 2 and 1, respectively). They grow in size following a fixed $r_{\text{eff,SF}}/r_{\text{eff},*}$.

sion to be overestimated. On the other hand, the ratio between the half-mass ($r_{\text{eff},*}$ given by Lang et al.) and r_{F160W} is ~ 0.8 and also approximately constant with redshift. This would give us (again as an upper limit due to the dust) $r_{\text{H}\alpha}/r_{\text{eff},*} = 1.57$. We constructed a model to study the evolution in the size-mass plane implied by these observations, assuming that the scale length of star formation $r_{\text{eff,SF}}$ is given by $r_{\text{H}\alpha}$. We find (see Fig. 3.4.2) that if we assume that $r_{\text{eff,SF}}/r_{\text{eff},*} = r_{\text{H}\alpha}/r_{\text{F160W}} = 1.26$ we can explain the evolution of galaxies along a non-evolving size-mass relation. However, we need $r_{\text{eff,SF}}/r_{\text{eff},*} = 1.66$ to explain the evolution with redshift of the size-mass relation. Given the uncertainties connected to the role of dust, we conclude that other mechanisms (such as progenitor bias, secular dynamical evolution and minor mergers) are probably at work to produce the redshift evolution of the mass-size relation of star forming galaxies. Important contributions to this study came from the PhD Thesis of Matteo Fossati (2016, LMU).

In the context of the KCS, our KMOS cluster survey, we measured the central velocity dispersions of 26 (19 published by Beifiori et al. 2017, 7 by Prichard et al. 2017) quiescent galaxies in 4 galaxy clusters up to redshift 1.8. Coupled with the photometric analysis we performed in Chan et al. (2018), this allowed us to study for the first time the evolution of the Fundamental Plane up to redshift 1.8. We found that the derived evolution of the mass-to-light ratio is consistent with passive evolution and a formation age between 1 and 2 Gyr, broadly agreeing with stellar population fitting of the stacked spectra. The

colour gradients we observe in these galaxies are twice the local value and are best reproduced by a combination of age and metallicity gradients (Chan et al. 2018). Major contributions to these studies came from the PhD Thesis of Jeffrey Chan (2016, LMU).

Finally, we measured 60 massive passive galaxies in the field up to redshift 2.1 (Mendel et al. 2019). We constructed dynamical models to study total masses, dark matter fractions and possible variations of the stellar initial mass function (IMF). Under the assumption that a Navarro-Frank-White dark matter halo is present, we find that a Milky Way like IMF is preferred for massive galaxies at these epochs. Moreover, the fraction of dark matter within the effective radius has increased by a factor of more than 2 since $z \sim 2$ (see Fig. 3.4.3). Local galaxies show a correlation between the velocity dispersion σ and the IMF offset parameter α , the ratio between the

measured mass-to-light ratio and the one obtained assuming a Milky Way IMF. High z -redshift galaxies (see Fig. 3.4.4) show a similar correlation, albeit with an offset towards higher σ at fixed α . The magnitude of this offset is consistent with the expectations for dynamical evolution driven by minor merging, which can systematically decrease σ by up to 0.15 dex.

Selected References:

- A. Beifiori et al. 2017, *ApJ*, 846, 120-144
- J. Chan et al. 2018, *ApJ*, 856, 8-46
- M. Fossati et al. 2017, *ApJ* 835, 153-189
- T. Mendel et al. 2019, to be submitted to *ApJ*
- L. Prichard et al. 2017, *ApJ*, 850, 203-224
- D. Wilmann et al. 2019, submitted to *ApJ*

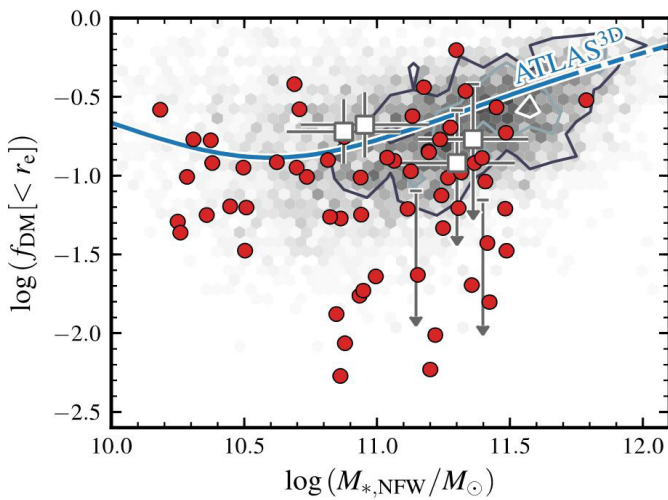


Fig. 3.4.3 The estimated dark matter fraction within the half-light ratio as a function of the dynamical mass in the stellar component. Circles (red) show sample the measured dark matter fractions for our VIRIAL of quiescent galaxies. The blue curve shows the results from the local ATLAS-3D survey; the background shading shows the distribution for galaxies in our GAMA/SDSS sample at $z=0$. Squares and upper limits are from our sample of KMOS-3D massive disk galaxies at $z>1$. Overall, the dark matter fractions in high-redshift galaxies appear lower by $\sim 10\%$ on average compared to galaxies of the same stellar mass at $z=0$.

Roberto Saglia



(Former OPINAS members include: A. Beifiori, J. Chan, M. Fossati, A. Galametz, T. Mendel, D. Wilman)

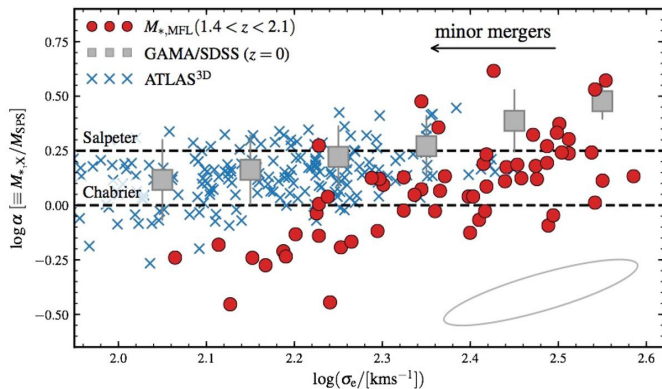


Fig. 3.4.4 The IMF offset parameter α as a function of stellar velocity dispersion.

3.5 Large-Scale Structure and Cosmology

In recent years, a plethora of precise observations has cemented a new cosmological paradigm, the Λ CDM model. Based on general relativity, this model is characterised by the presence of two components, dark matter and dark energy, whose nature remains elusive. The quest for deviations from this remarkable picture of the Universe will be the main objective of observational cosmology during the next decade. The OPINAS group at MPE is contributing to this endeavor by analyzing galaxy clustering measurements. In recent years, we have played a crucial role in the cosmological interpretation of data from the Baryon Oscillations Spectroscopic Survey (BOSS). Building upon this experience, we are now extending our analyses to a new generation of galaxy surveys, in which we are leading participants. These new data sets will measure the large-scale structure of the Universe with exquisite detail, allowing us to put the Λ CDM paradigm to its most stringent test yet.

State of the art: cosmology from galaxy clustering measurements

The basic parameters of the Λ CDM model can be accurately determined by cosmic microwave background (CMB) data. These values can be used to predict the evolution of the Universe from recombination until today. The comparison of these predictions with observations at lower redshifts serves as a powerful test of the Λ CDM paradigm. In this context, the accurate mapping of the expansion and growth of structure histories of the Universe over a wide range of cosmic time is of uttermost importance. Analyses of the large-scale structure (LSS) of the Universe based on galaxy clustering (GC) observations are amongst the most powerful tools to obtain such measurements. The power of these datasets has fuelled the construction of increasingly larger galaxy sur-

veys. The completed Baryon Oscillation Spectroscopic Survey (BOSS) is the best example of the tremendous progress achieved in this field. The OPINAS group has played a leading role within the BOSS collaboration in the analysis of GC data (Alam et al. 2017, Sánchez et al. 2017a,b, Grieb et al. 2017, Salazar-Albornoz et al. 2017).

In most analyses, the large-scale distribution of galaxies is characterised in terms of two-point statistics such as the anisotropic power spectrum, $P(k)$, which represents the variance of the density fluctuations for different Fourier modes. A convenient way of compressing this information is by means of the clustering wedges statistics (Kazin et al. 2012), representing the power spectrum for modes k binned in different angular directions with respect to the line of sight. The left panel of Fig. 3.5.1 shows measurements of three clustering wedges from the final BOSS (Grieb et al. 2017). The wiggles visible in all wedges corresponds to the signature of the baryon acoustic oscillations (BAO), a standard ruler that enables robust measurements of the expansion history of the Universe. The differences in amplitude and shape between the wedges are caused by the gravitationally induced motions of the galaxies, referred to as redshift-space distortions (RSD), which encode key information on the growth of cosmic structures.

Accessing the wealth of cosmological information contained in GC measurements requires accurate models of the effects of the non-linear evolution of density fluctuations, RSD, and the relation between the galaxy and matter density fields (known as galaxy bias). The solid lines in the left panel of Fig. 3.5.1 correspond to a state-of-the-art model of these effects that we developed for the analysis of the final BOSS. Tests of our model against numerical simulations for standard cosmologies,

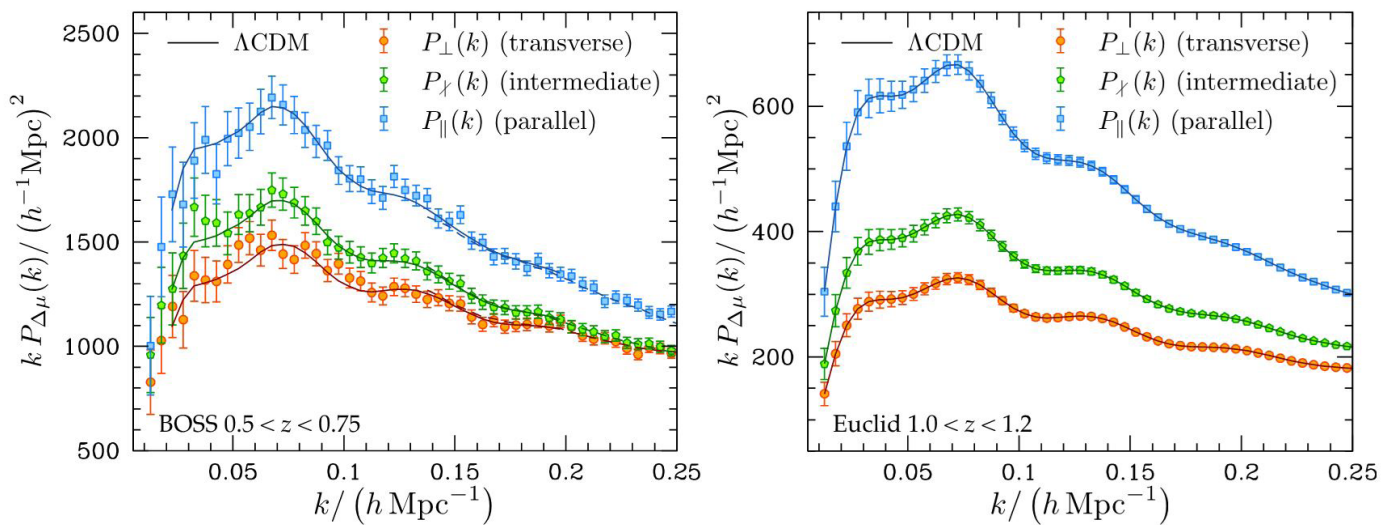


Fig. 3.5.1 Left: power spectra from BOSS for modes k binned in the angular directions transverse (orange), intermediate (green,) and parallel (blue) to the line of sight (Grieb et al. 2017). The lines represent the best-fitting Λ CDM model computed using a state-of-the-art analytic recipe. **Right:** forecast of the same measurements as the left panel attainable by Euclid.

as well as modified gravity models, showed that it provides unbiased results down to smaller scales than in previous analyses, leading to some of the most accurate cosmological constraints to date. To go beyond the limits of individual analyses, we also developed a method to optimally combine the results of applying different analysis techniques to the same data set (Sánchez et al. 2017b) and used it to derive a set of consensus constraints representing the synthesis of all the GC analyses performed on the final BOSS, which constitute the main result of the survey.

The success of BOSS has paved the way for the construction of new large-volume galaxy surveys. Examples of these new projects, in which the OPINAS group is a leading participant, include the ongoing Extended Baryon Oscillation Spectroscopic Survey (eBOSS) and the Hobby-Eberly Telescope Dark Energy Experiment (HETDEX), as well as the future Prime Focus Spectrograph (PFS) survey, the Dark Energy Spectroscopic Instrument (DESI), and the ESA space mission Euclid.

Ongoing surveys: eBOSS and HETDEX

After the completion of BOSS, the Sloan Digital Sky Survey (SDSS) IV continued its science program with the eBOSS project, which is sampling the positions of galaxies and quasars (QSO) as tracers of the LSS of the Universe. As QSO are intrinsically more luminous than galaxies, they can be detected at higher redshifts, opening a new window for clustering analyses. The QSO sample from eBOSS covers the redshift range $0.8 < z < 2.2$, bridging the gap between the BAO distance measurements from BOSS, and those inferred from the Lyman- α forest signal of high-redshift quasars.

The focus of our group as part of eBOSS has been the analysis of the QSO sample by means of clustering measurements in configuration space. For the data release 14 (DR14), we analysed a sample of $\sim 147,000$ objects (PhD project of J. Hou, results published in Hou et al. 2018). We applied the same model of non-linearities, bias, and RSD developed for our analyses of BOSS, extended to account for redshift uncertainties in the QSO

sample. The cosmological information from our clustering measurements can be expressed as constraints on the Hubble parameter, $H(z)$, the comoving angular diameter distance, $D_M(z)$, and the growth-rate parameter, $f\sigma_8(z)$, evaluated at the effective redshift of the sample, $z_{\text{eff}} = 1.52$. The blue contours in Fig. 3.5.2 correspond to the two-dimensional posterior distributions of these quantities. Our results are in excellent agreement with the constraints inferred from the Planck CMB measurements under the assumption of a Λ CDM model, which are shown by the red contours in the same figure.

We are currently leading the configuration-space clustering analysis of the final eBOSS QSO sample (DR16), with almost double the objects compared to DR14. Our contributions to the final analysis are multifold. We performed a series of tests of the spectroscopic weights that are designed to correct for redshift failures. In the previous eBOSS analyses, the redshift failure correction scheme involved up-weighting the nearest neighbour to a missing object. This, however, leaves spurious signals in the line-of-sight dependent quantities. For DR16, we generated new weights based on the efficiency of each individual fibre and the signal-to-noise ratio of the plate. In addition, for the final analysis we are currently testing a new modelling approach that combines perturbation theory with the results of numerical simulations (Nishimichi et al. 2017, Bel et al. 2019). This and other models will be tested against mock catalogues built from high-resolution N-body simulations. The prescription that returns the most unbiased results will be used in the final analysis.

A further exciting project in our group is HETDEX (Hill et al. 2016, Indahl et al. 2016). This is an ongoing survey of emission line galaxies being conducted at the 10m Hobby-Eberly telescope in Texas. An array of 78 integral-field units (IFUs) will carry out a blind spectroscopic search for Lyman- α emitting galaxies (LAEs) at $1.9 < z < 3.5$ over a 450 deg^2 area. HETDEX has begun survey operations, and as of March 2019 has 47 of the 78 IFUs installed. The target is to install the rest at a rate of 2 per month. The observations are currently 7.4% complete,

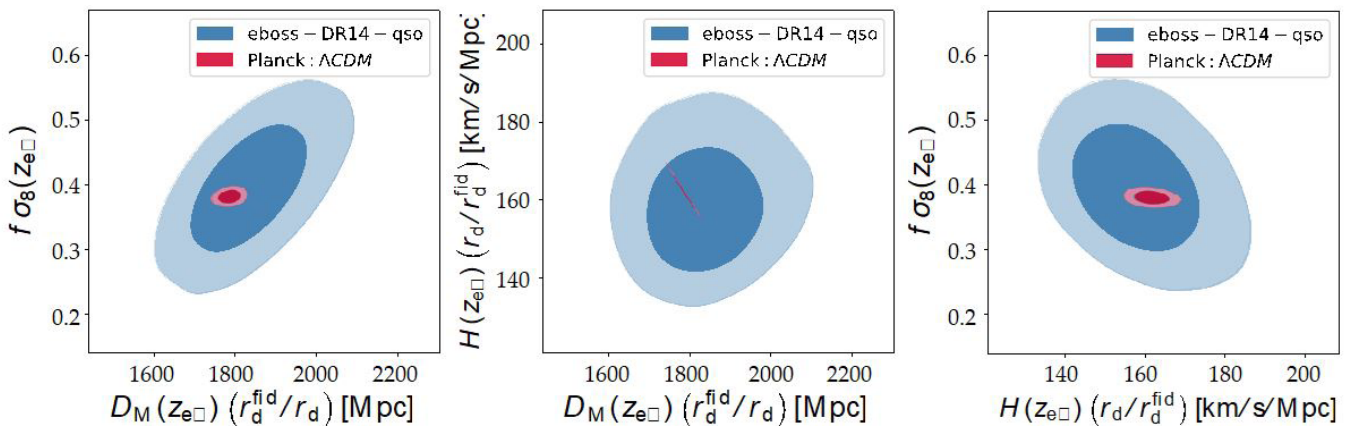


Fig. 3.5.2 Marginalised two-dimensional constraints on $D_M(z)$, $H(z)$, and $f\sigma_8(z)$, at the mean redshift of the eBOSS QSO sample, $z_{\text{eff}} = 1.52$ (blue contours). The factors containing the sound horizon scale at the drag redshift, r_d , account for the difference in the BAO scale in the true and fiducial cosmologies. These results are in agreement with the predictions based on the CMB measurements from Planck under the assumption of a Λ CDM cosmology (red contours).

which already means that HETDEX provides the largest spectroscopic LAE sample to date by far. The first internal data release is expected in April 2019 and we are already engaged in the scientific exploitation of this unique dataset.

OPINAS is playing a vital role in the HETDEX survey, as is underlined by our group holding a position on the HET board (Bender), the HETDEX scientific steering committee (Sánchez) and the positions of window function lead (Farrow), astrometry software lead (Fabricius), and observing tools lead (Snigula) in the HETDEX management structure.

On the software side, the OPINAS-written quality control software 'VIRUS Health Check' mentioned in the last report is now installed and being run at the telescope. As is the 'Observing Conditions Decision Tool', which is being used to automatically carry out HETDEX observations based on the telemetry of the observing conditions. OPINAS is also leading the translation & refactoring of UT Austin written data-reduction-scripts into a version controlled, well tested and maintained pipeline. We have also recently acquired the resources to host a SciServer database for HETDEX, and we look forward to being able to develop a science and collaboration enabling service in this framework.

On the science side OPINAS is leading several projects. We are producing forecasts for the parameter constraints expected from the survey, and are running simulations of how contamination of the LAE catalogue from OII-emitting galaxies can be dealt with by weighting pairs by their LAE probability (Farrow et al, in prep). We are also leading efforts to produce accurate measurements of the selection function, a vital ingredient to LSS measurements. OPINAS is also working towards detecting extended Lyman- α emission regions. HETDEX is well suited to this: it has a large field of view and in the deepest, stacked HETDEX exposures, the data can reach fluxes as low as $5 \times 10^{-19} \text{ erg s}^{-1} \text{ cm}^{-2} \text{ arcsec}^{-2}$, possibly reaching the surface brightness of the neutral hydrogen in the cosmic web itself as it gets excited by the UV background. A further OPINAS project attempts to understand velocity offsets in the Lyman- α emission from the true, systemic redshift of the galaxies. Such offsets cause a change in the inferred distance of the galaxy that needs to be considered in LSS studies. A KMOS follow up of a sample of HETDEX LAEs was conducted under the direction of an OPINAS PI (Fabricius). In the short-term future we plan to use the early data releases to make powerful measurements of the bias, satellite fractions and halo occupation distributions of LAEs, which will provide new constraints on galaxy formation models.

Future surveys: PFS, DESI, and Euclid

The OPINAS group is also involved in some of the most exciting galaxy surveys of the next decade. As of July 2018, we have been participating in DESI, which will probe a large volume of the Universe, sampling the positions of over 20 million luminous red galaxies, emission line galaxies, and QSOs from $0.6 < z < 3.5$ over more

than one third of the sky. MPE also joined the PFS collaboration in November 2016. The PFS cosmology survey will map the positions of 4.2 million [OII] emission-line galaxies over 1400 deg^2 in the redshift range of $0.8 < z < 2.4$. In addition to contributing to the estimation of cosmological forecasts for the survey, we are designing the highly complex fibre assignment algorithm required to match the different sampling strategies of its various surveys (besides the cosmological sample, PFS will contain galaxy evolution and galactic archeology surveys). The focal plane of PFS will be equipped with 2394 individual fibre positioners, each of which can position their fibre within a circular area of about 1.5 arcminutes in radius. Allocating this number of fibres to targets in an efficient manner over the course of multiple observations is a highly non-trivial optimisation problem. An added complication is that individual fibre positioners can collide with each other. We have modelled the fibre assignment as a minimum-cost flow problem that gives the freedom of grouping targets into an arbitrary number of priority classes. We interface this to a physical simulator for the fibre positioners that calculates their trajectories avoiding collisions, while ensuring that a sufficient number of calibration objects are always observed.

The PFS cosmology survey will benefit from overlapping weak lensing (WL) measurements provided by the Hyper Suprime Cam lensing survey (Hikage et al. 2019). As the information content of WL and GC observations are highly complementary, their joint analysis can significantly increase their constraining power. Thus, PFS represents the perfect step between present-day surveys and Euclid, in which our group is also heavily involved. With a launch scheduled for April 2022, Euclid will measure up to 30 million spectroscopic redshifts for GC analyses, and 2 billion galaxy images for WL studies, over an area of $15,000 \text{ deg}^2$ (Laureijs et al. 2011). Besides being involved in the construction of the near-infrared optical system for Euclid (see the specific section on Euclid for more details), OPINAS has a strong presence in the Galaxy Clustering Science Working Group, where we have led the Likelihood Fitting Work Package (2014 - 2017), the Systematic Errors Tiger Team (2017), the Inter Science Working Group Task Force (IST) for Forecasting (2016 - 2019), and the new IST for the Likelihood (since 2018), in charge of producing the likelihood modules for the combined analysis of all Euclid cosmological probes.

The right panel of Fig. 3.5.1 shows a forecast of the power spectrum wedges that will be obtained from Euclid in the redshift range $1.0 < z < 1.2$. The comparison of these predictions with the results from BOSS illustrates the dramatic improvement in the accuracy achievable with Euclid, which represents a unique opportunity for precision cosmology. However, the small statistical uncertainties of Euclid demand a careful control of the systematic error budget. In particular, robust covariance matrix estimates of the clustering measurements are essential for the cosmological analysis.

In most clustering studies, the covariance matrix is estimated from a set of mock catalogues. The noise of these

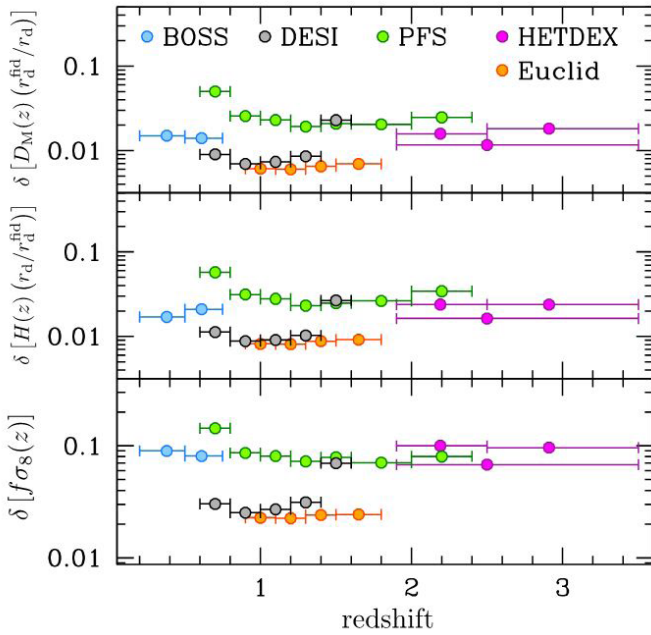


Fig. 3.5.3 relative errors on the measurements of $D_M(z)$ (upper panel), $H(z)$ (middle panel), and $f\sigma_8(z)$ (lower panel) obtained from the final BOSS (blue), and those that could be attainable from the final HETDEX (magenta), PFS (green), DESI (grey), and Euclid (orange). Only estimates based on clustering measurements are shown.

estimates depends on the number of mock catalogues used and must be propagated into the final results. Running a large number of N-body simulations with the required volume and mass resolution for Euclid would be computationally infeasible. Hence we tested the ability of fast approximate methods to correctly reproduce the covariance matrix of clustering measurements. We led a detailed comparison of the various types of currently available methods focusing on two-point correlation function measurements (part of the PhD thesis project of M. Lippich, results published in Lippich et al. 2019), and contributed to similar analyses for the power spectrum (Blot et al. 2019) and bispectrum (Colavincenzo et al. 2019). Our analysis includes seven methods, spanning fully predictive schemes to approaches that require calibration with N-body simulations or assumptions on the probability distribution function of the density fluctuations. For each method we constructed a set of mock catalogues matching the initial conditions of a reference set of 300 large-volume N-body simulations, called Minerva, which were run at MPE. The core of our comparison project is to test the performance of the covariance matrices obtained from the different approximate methods when estimating cosmological parameter constraints. Overall, our results show that most approximate methods are able to reproduce the parameter errors to within 10% or better.

Outlook

Fig. 3.5.3 presents constraints on $D_M(z)$, $H(z)$, and $f\sigma_8(z)$ from different surveys in which the OPINAS group is involved. The BOSS points show the actual constraints from Sánchez et al. (2017a), the rest are Fisher forecasts based on clustering measurements alone, derived using the same model of the final BOSS analyses. HETDEX forecasts are presented in a single redshift bin, or

splitting the survey into two bins. We can see how well the different surveys complement each other to span a wide range of redshifts ($0.2 < z < 3.5$). OPINAS will have a leading role in the scientific exploitation of these data-sets, which have the potential to revolutionise our constraints on the properties of dark energy, deviations from the predictions of general relativity, neutrino masses, and inflationary physics.

Selected References:

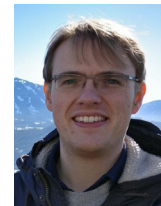
- Alam S., et al., 2017, *MNRAS*, 470, 2617
 Bel J., Pezzotta A., Carbone C., Sefusatti E., Guzzo L., 2019, *A&A*, 622, A109
 Blot L., et al., 2019, *MNRAS*, in press, arXiv:1806.09497
 Colavincenzo M., et al., 2019, *MNRAS*, 482, 4883
 Grieb J. N., et al., 2017, *MNRAS*, 467, 2085
 Hikage C., et al., 2019, *Publications of the Astronomical Society of Japan*, in press, arXiv:1809.09148
 Hill G. J., HETDEX Consortium 2016, in *PASP Conference Series Vol. 507*, p. 393
 Hou J., et al., 2018, *MNRAS*, 480, 2521
 Indahl B. L., et al., 2016, in *Ground-based and Air-borne Instrumentation for Astronomy VI*, p. 990880, doi:10.1117/12.2231915
 Kazin E. A., Sánchez A. G., Blanton M. R., 2012, *MNRAS*, 419, 3223
 Laureijs R., et al., 2011, *arXiv e-prints*, arXiv:1110.3193
 Lippich M., et al., 2019, *MNRAS*, 482, 1786
 Mishimichi T., Bernardeau F., Taruya A., 2017, *PRD*, 96, 123515
 Salazar-Albornoz S., et al., 2017, *MNRAS*, 468, 2938
 Sánchez A. G., et al., 2017a, *MNRAS*, 464, 1493
 Sánchez A. G., et al., 2017b, *MNRAS*, 464, 1640

Additional selected publications on LSS by the OPINAS group during the past three years:

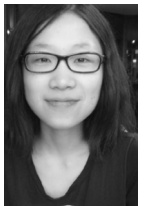
- Ata et al., 2018, *MNRAS*, 473, 4773
 Correa C., Paz D.J., Padilla N.D., Ruiz A.N., Angulo R.E., Sánchez A.G., 2019, *MNRAS*, in press, arXiv:1811.12251
 Hernández-Aguayo C., Hou J., Li B., Baugh C.M., Sánchez A.G., 2019, *MNRAS*, 485, 2194



Ariel Sanchez



Daniel Farrow



Jiamin Hou



Martha Lippich



Maximilian Fabricius

(Other OPINAS group members include: R. Bender, U. Hopp, J. G. Carpio, R. Saglia, J. Snigula, P. Sudek, J. Weller)

3.6 MICADO – Multi AO Imaging Camera for Deep Observations

MICADO is one of the first light instruments for the ESO Extremely Large Telescope (ELT). Combined with the Adaptive Optics Module MAORY, MICADO will deliver diffraction-limited images in the infrared wavelength range. It will equip the ELT with high (1.5 mas/px) and low resolution (4 mas/px) imagers, a medium resolution spectrograph (R~10000) covering a broad wavelength range (J-K Band) and a high contrast imaging mode. The OPINAS/USM group is part of the MICADO Consortium and is responsible for development of the instrument control electronics, control and preparation software and the cryogenic Main Selection Mechanism (MSM). After the KickOff Meeting in 2015 we focused on implementing a baseline design to be presented at the Preliminary Design Review, which took place in November 2018 at ESO. We also performed tests on subcomponent level in ambient and cryogenic environment.

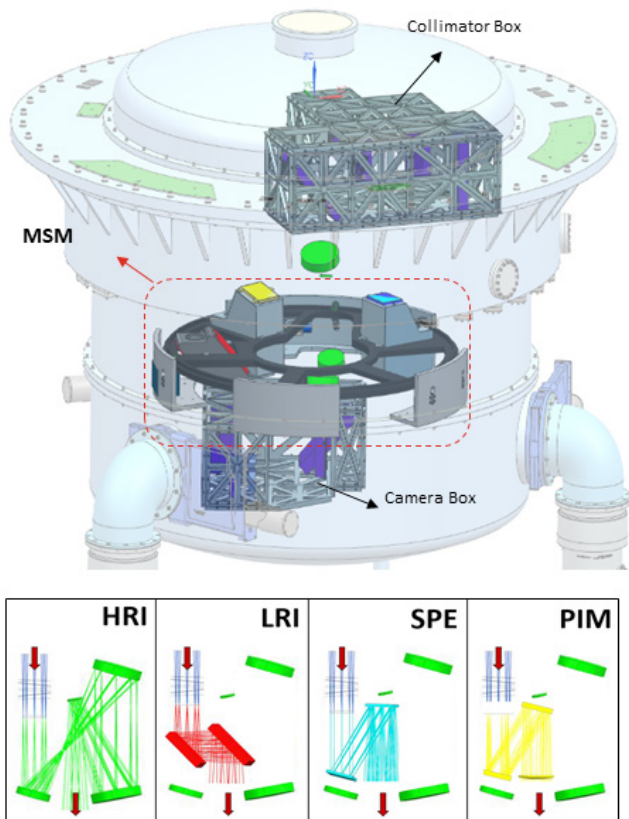


Fig. 3.6.1 MSM inside the MICADO cryostat: The MSM assembly (red frame) is located between the boxes of the Collimator and Camera optics. It consists of a rotating platform with a diameter of ~1.4m (dark gray) and its support structure (light gray). The rotating platform hosts the optical modules of the LRI (in red), PIM (in yellow) and SPE gratings (in blue). To switch between the 4 operational modes, the platform can be rotate in order to locate the respective optical module in between the HRI fixed optics (in green), along the instrument optical path. The upper panel shows a sketch of the 4 optical configurations available for MICADO (the red arrows show the direction of the in- and outcoming beam).

Inside the MICADO consortium, the OPINAS/USM group is responsible for the control electronics, control software and a cryogenic mechanism, the so called Main Selection Mechanism (MSM). The MSM is located inside the MICADO cryostat between the fixed collimator and camera optics. The operating temperature inside the cryostat is 80K. It consists of a rotating platform with an outer diameter of R~1300 mm, supported by individual small bearings to reduce friction and driven by a cryogenic stepper motor (Fig. 3.6.1). Optic modules are mounted on the platform and can be placed into the science beam to select the operational mode (imager, spectrometer) of the instrument. The Low Resolution Imager (LRI) module uses two flat mirrors blocking some of the fixed optical components to change the plate scale on the detector mosaic. The Spectrometer (SPE) consists of two echelle like gratings to use the instrument as a medium resolution (R~10000) spectrograph. Filters are needed to disentangle the overlapping orders. Therefore, two exposures are necessary to cover the full wavelength range. For calibration and alignment purposes, a pupil imager (PIM) will be used to image the pupil plane inside the instrument to the detector array. For positioning and locking the optical modules inside the science beam we intend to use an indent mechanism. The MSM work package includes the design, analysis, assembly, alignment and test of the cryogenic mechanism including all optical components and their mounts located on the rotating platform. Cryogenic testing on subcomponent level (motors, indent mechanism) has already started.

The control electronic tasks under the responsibility of the OPINAS/USM group are shown in Fig. 3.6.2 and highlighted in magenta. ESO decided to use Beckhoff Programmable Logic Controllers (PLC) for all control tasks necessary in ELT instruments. Using this PLC technology the control electronics has to provide all necessary functionality to drive mechanisms inside several subsystems, read sensor signals but also all housekeeping tasks of the MICADO cryostat. All necessary components fill four electronic cabinets that will be located either on the Nasmyth or on the Co-Rotating platform. The PLCs shall in turn be supervised by the MICADO control software subsystem, consisting of observation execution scripts, workstation-level coordination managers, and low-level device control. The overall layout is shown in Fig. 3.6.3. The software tasks under responsibility of the OPINAS/USM group are again highlighted in magenta. It will be implemented on the basis of a generic ELT software framework, tailored to the specific needs of MICADO. In addition, a dedicated preparation tool for AO guide star selection will be provided.

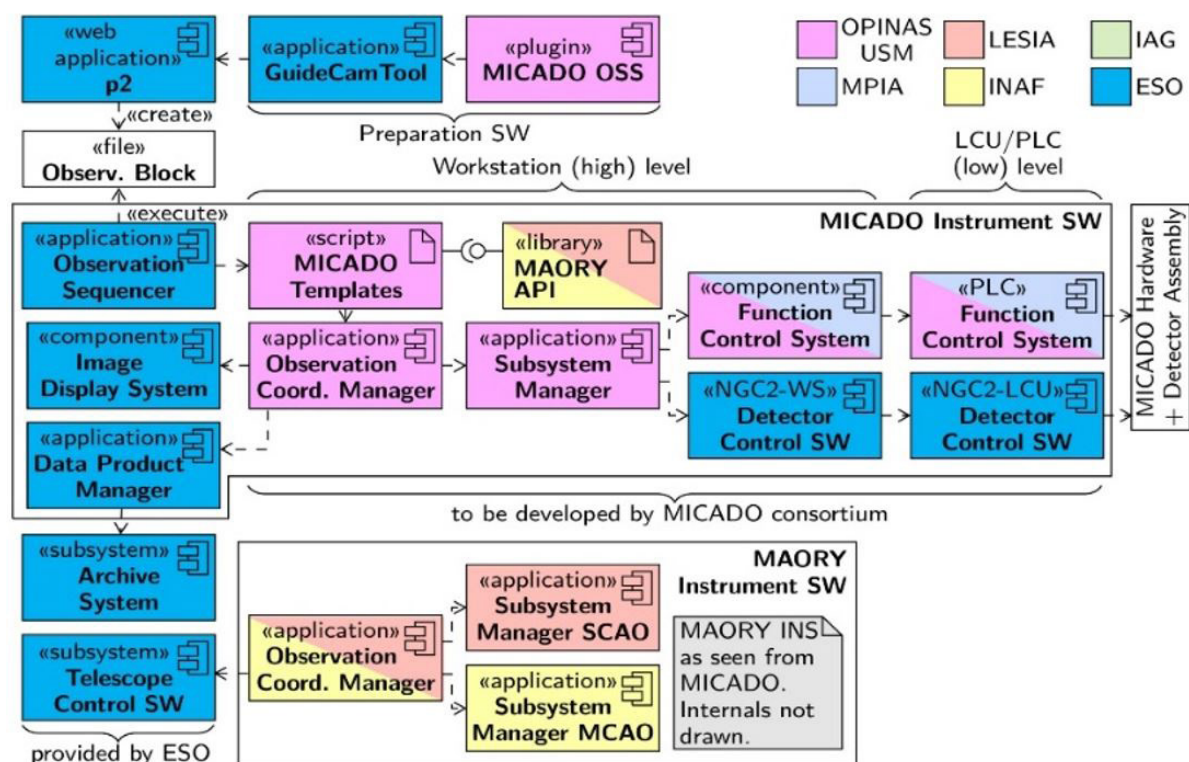


Fig. 3.6.2 Software architecture: Main components and their dependencies in the context of the ELT control system are shown - those under OPINAS/USM responsibility are coloured magenta.

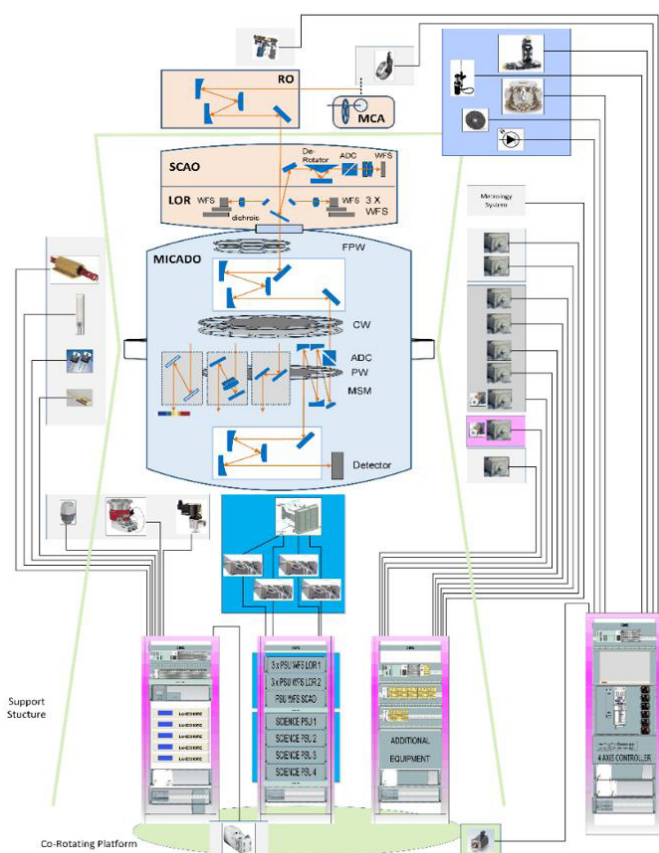
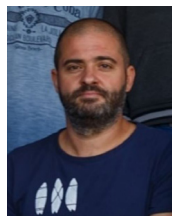


Fig. 3.6.3 Overall control system: Overview of MICADO control electronics components, indicating their purpose, how they are linked, and where they are located. OPINAS/USM components again magenta.

Selected References:

- MPE infrared group science report, Davies, R. et al. 2019
Häuser M. et al., Proc. SPIE 10702, 107028Z (27 July 2018); doi:
10.1117/12.2312048
Wegner M. et al., Proc. SPIE 9913, 99133M (26 July 2016); doi:
10.1117/12.2231332
Lang-Bardl F. et al., Proc. SPIE 10702, 107028Y (11 July 2018); doi:
10.1117/12.2311959
Monna A. et al., Proc. SPIE 10702, 1070295 (11 July 2018); doi:
10.1117/12.2312492



Florian
Lang-Bardl



Anna Monna



Ulrich Hopp

(Other OPINAS group members include: R. Bender, M. Fabricius, F. Grupp, M. Häuser, H.-J., Hess, H. Kravcar, J. Richter, J. Schlichter, J. Thomas, M. Wegner)

3.7 EUCLID Dark Energy Mission

The Euclid space mission will measure the evolution of the cosmic structure in two different, complementary approaches: In a classic redshift survey of the entire extragalactic sky it will map the 3D positions of galaxies and infer the cosmic expansion history through the redshift evolution of their spatial correlation signal. In addition to this, Euclid will measure the weak lensing induced shape distortions of galaxies and in this way directly map the dark matter distribution in the Universe. OPINAS is deeply involved in the development of hardware for the space probe itself, as well as in the science ground segment and in several science working groups. It developed the optical system design of the telescope and built the collimator and camera optics for the Near Infrared Spectrometer and Photometer which were successfully delivered and aligned in June and December 2018. The involved optical lenses are amongst the largest, ever flown in space and reach full diffraction limited performance. OPINAS hosts and operates the German Science Data Center that will not only process the data from the satellite itself, but also large parts of the data from the participating ground based surveys. Finally, our group leads the template fitting and machine learning work packages, that will deliver photometric redshifts of unprecedented precision which are of fundamental importance for the weak lensing measurements of Euclid.

Near Infrared Spectrometer and Photometer NISP

Euclid – ESA's dark matter and dark energy mission, due to be launched in Q2/2022 is addressing the science fields of "fundamental physics" and "the universe" in the Cosmic Vision 2015-2025 space exploration program of the European Space Agency.

OPINAS provides the optical system design for the payload telescope and the optical architecture of the Near Infrared Spectrometer and Photometer NISP. NISP is one of the two instruments on board covering spectroscopic observations with $R = 380$ as well as Y, J and H band photometry out to 24th magnitude on 14000 square degrees of the extra-galactic sky.

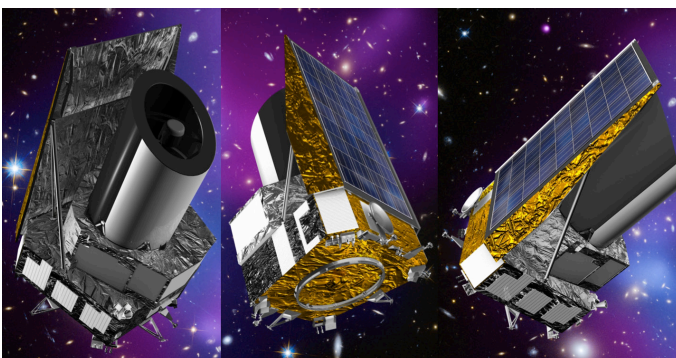


Fig. 3.7.1 An artists view of Euclid (ESA press release).

OPINAS also provided – the flight hardware has been delivered and aligned on instrument level in June and December 2018 – the near infrared optical assembly NI-OA, a highly demanding, cryogenic, four lens focal reducer and spectrometer camera system. The lenses of NI-OA reach diameters of up to 180 mm. They are therefore up to 3 times larger than the largest lenses flown on board of the James Webb Space Telescope.

During the design and development phase of NISP our group at MPE improved and invented methods for lens manufacturing and alignment based on Computer Generated Hologram supported interferometry. With these methods a basic alignment of the NI-OA system to better than five micron in the individual lenses position became possible. In a further step, combining our holographic methods with highly accurate coordinate measuring machine (CMM) tactile metrology we were able to measure the instruments optical properties and focal length simultaneously with unprecedented precision. As an example: Comparing the "as built" optical model simulation of the instruments back focal distance to the "as measured" value in the lab we found: +27 μm for the model compared to the as designed value and +28 μm for the measured value. This at an instrument length of ≈ 1000 mm. The measurement not only needed precise knowledge of the lab temperature, even the air pressure had to be known to a few hPa as 10 hPa pressure change would have resulted in a 5 μm shift of focus. With this new technology of combined interferometric and CMM measurements MPE reached a level of measurement accuracy that no other lab has shown possible for instrument structures of that size.

Having measured the systems properties and performance level under warm conditions in the lab, tests in cryo-vacuum were the final step of confirmation. The total wave front error of the system at the blue end of

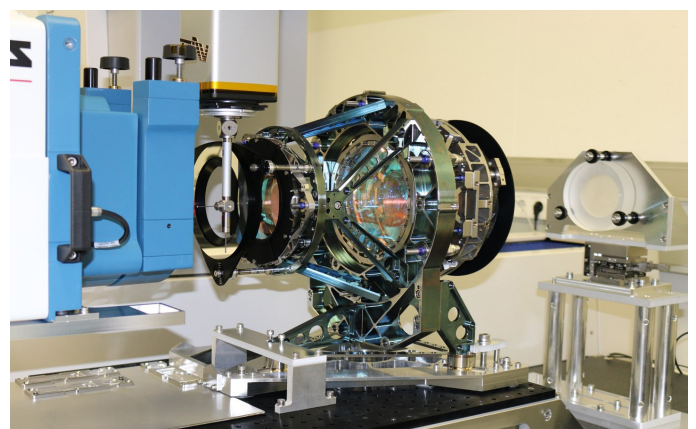


Fig. 3.7.2 The Near Infrared optical assembly NI-OA at the focal length test setup on the CMM with the Interferometer shown on the left hand side. The lens on the right hand side is a test sphere. The focus of the instrument "implements" at the center of this test sphere. This test component is optically measured under auto-collimation condition AND touched by the CMM to get its position in 3D space.

PSF: SHS-Measurement versus Simulation, Field Zero, L = 960 nm

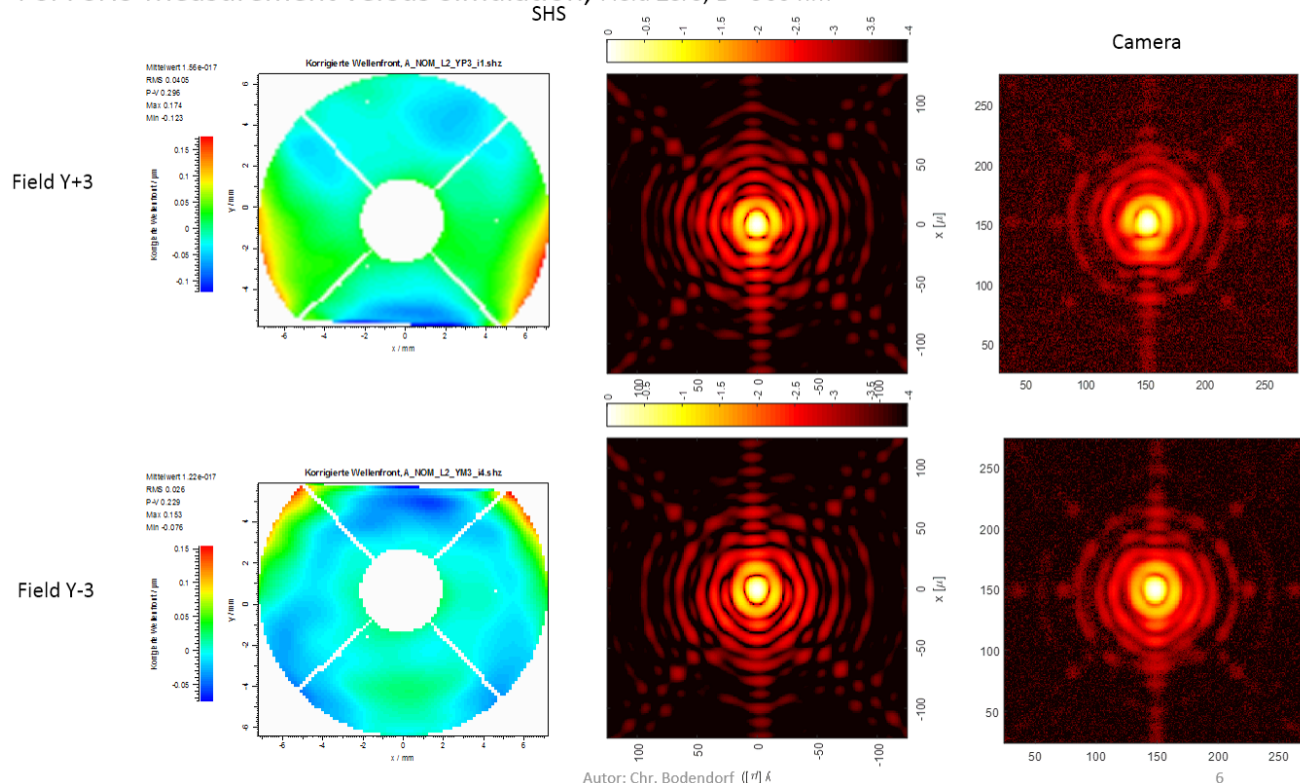


Fig. 3.7.3 Measured wavefront (**left**), simulated point spread function (**middle**) and measured PSF (**right**) of the outermost field points of NI-OA. PSF brightness is plotted on logarithmic scale.

the spectral range where the diffraction limit is smallest provided a fantastic $\lambda/40$ fully diffraction limited performance. Comparing the simulated and the measured Point Spread Function (PSF) in a high resolution recording, model and reality can only be distinguished by measurement noise being present in the real near infrared data. Even the tiniest structures of the PSF (Fig. 3.7.3; shown on logarithmic scale) predicted by the model are found in the measurement.

Having completed these tests for the flight model in December 2017 the system was shipped to LAM Marseille and re-assembled there under interferometric control in two steps in June and December 2018. By the end of 2018 also the flight spare model was fully qualified and is now stored – and hopefully never used. The FS performance is only marginally worse than that of the FM, showing that we have well controlled and repeatable manufacturing processes and alignment methods.

Preparation for massive data: German Science Data Center for the Euclid Space Mission

The SDC-DE is one to the nine science data-centers of the Ground Segment for Euclid. The SDCs receive and reduce

the data from the spacecraft and upload the final data products to the central archive after processing. In addition to the space-based data, a critical component for the Euclid mission is the rich external dataset comprised of imaging data from a number of different ground-based telescopes and surveys such as the Panoramic Survey Telescope and Rapid Response System (Pan-STARRS),

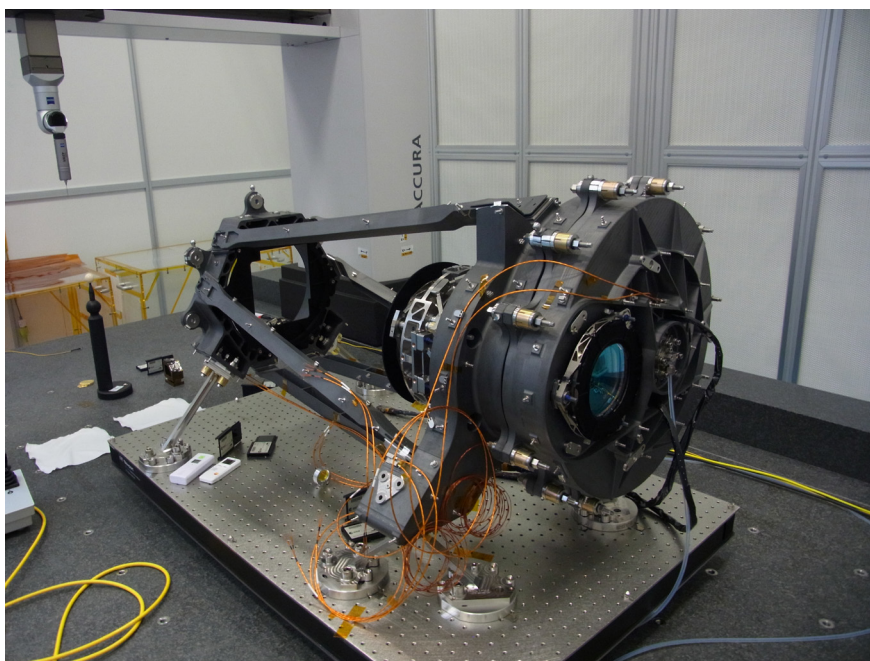


Fig. 3.7.4 NISP with the NI-OA integrated at the LAM Marseille laboratory in December 2018.

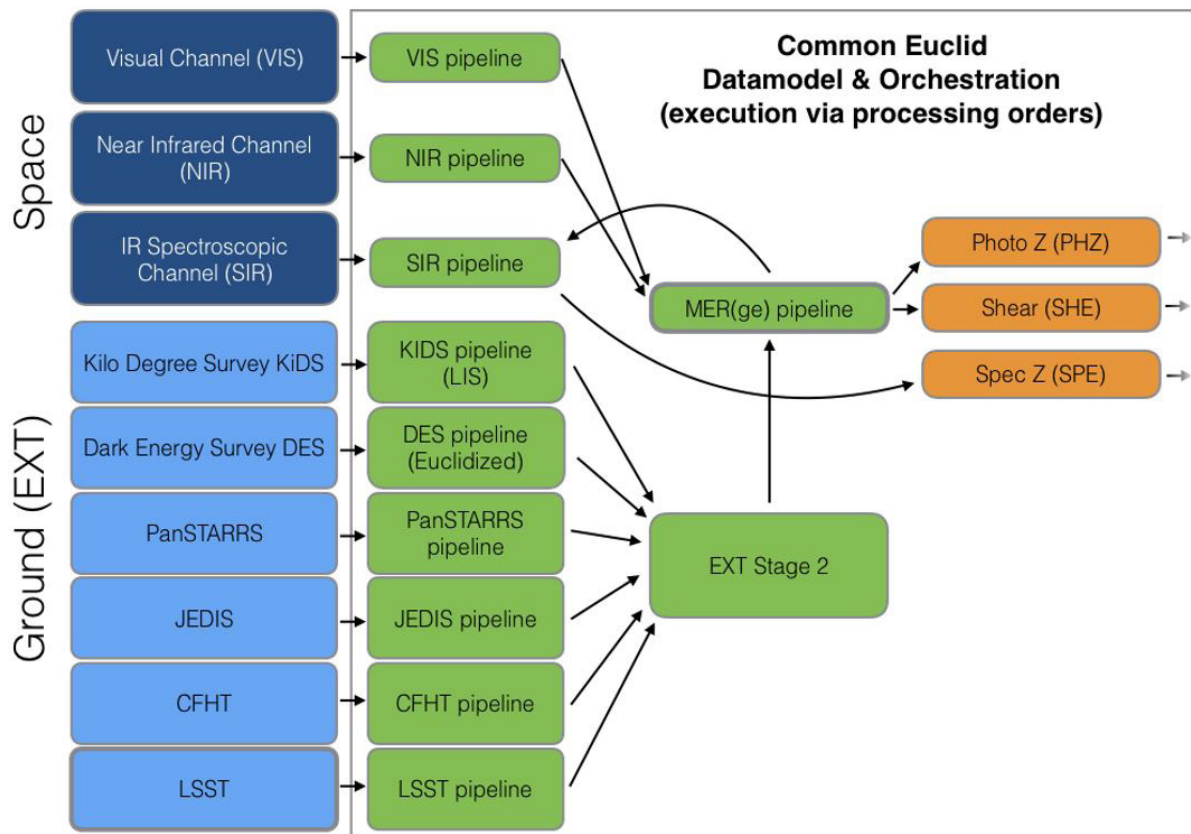


Fig. 3.7.5 Organisation of the pipelines involved in analyzing the data from the Euclid spacecraft and the participating ground based surveys. Each channel, and each survey participates with their own - often - legacy data reduction pipeline. The ground-based surveys deliver their data to Stage 2 that provides a common validation stage and that builds homogenized co-added mosaics that are then passed to MER which derives a common photometry for all detected objects.

the Dark Energy Survey (DES), the Kilo Degree Survey (KiDS), the Canada-France Imaging Survey (CFIS), the Javalambre-Euclid Deep Imaging Survey (JEDIS), and the Large Synoptic Survey Telescope (LSST). These data will allow for the derivation of precise photometric redshifts that in turn are a fundamental ingredient for the analysis and interpretation of the weak lensing measurements from Euclid. The SDC-DE is in charge of the integration of the reduction pipelines for two external surveys: KiDS and DES.

To provide a common interface for all higher level pipelines that deliver for instance photometry and shear measurements, a common homogenization, validation and co-addition component *Stage 2* was introduced in the SGS. SDC-DE is specifically responsible for the co-addition part and will consequently build mosaics for all participating ground-based surveys. Further, SDC-DE is also involved in the integration of the processing function dedicated to the merging of the multi-wavelength data sets (MER). The SGS undergoes regular so-called scientific challenges (SC) of about a one-year duration that in essence represent large software integration tests across all participating pipelines and SDCs in Europe and the USA. At each challenge, successively new pipe-

lines or processing functions are added and the interplay between each of them and the central orchestration system is tested on a large set of simulated data, both from the space craft but also the ground based telescopes. In SC3 for the first time the KiDS, DES and MER pipelines participated. This test was concluded successfully at the end of 2018 and subsequently the SGS passed its Design Review. Currently, the SGS is undergoing SC4/5/6 that tests for the first time the higher level scientific pipelines for the derivation of photometric redshifts, lensing signals and the extraction of spectra. While SC3 simulated about 1 deg^2 on the sky, SC4/5/6 simulates a ten times larger area. By the time of SC8 the simulated sky coverage should be of the same magnitude as the actual Euclid survey ($\sim 10000 \text{ deg}^2$). The storage and processing of the corresponding data volume requires significant investments in computer hardware as well as efficient processing and data management strategies. For this, the SDC-DE hosts a - now 2nd generation - computing cluster with ~ 800 cores and $\sim 1 \text{ PT}$ of disk storage. Finally, SDC-DE is deeply involved in the activities of the system team taking place at the consortium ground segment level, leading in particular the pipelines monitoring and control tasks as well as contributing significantly to the development of the testing strategies.

Photometric redshifts of highest precision: OU-PHZ

Our group (R. Saglia, S. Seitz, V. Guglielmo) leads the Template Fitting and Machine Learning work packages, dealing with the computation of photometric redshifts for Euclid. We perform extensive simulations to test under which conditions the Euclid accuracy and precision requirements of the photometric redshifts could be met for both approaches, finding that a spectroscopic calibration of the color space is essential. We participate to the ESO Large Program to perform this calibration, leading the KMOS near-infrared part of it. We prepare, reduce and analyze all observations, managing to calibrate half of the color cells in the redshift range 1.3 to 2.0 to the required precision. We plan to complete the remaining half in a future spectroscopic campaign using the spectrographs LUCI at the Large Binocular Telescope.



Ralf Bender



Frank Grupp



Roberto Saglia



Maximilian Fabricius

Selected References:

Costille, A.; Carle, Michael; Fabron, Christophe; Prieto, Eric; Beaumont, Florent; Jessen, Niels-Christian; Jakobsen, Peter; Sørensen, Anton N.; Andersen, Michael I.; Grupp, Frank; Maciaszek, Thierry; Ealet, Anne; Gillard, William; Clemens, Jean-Claude *SPIE, Volume 9904, id. 99042U 15 pp, How to test NISP instrument for EUCLID mission in laboratory*

Thiele, H.; Mottaghibonab, A.; Gal, C.; Gawlik, K.; Dubowy, M.; Grupp, F.; Penka, D.; Bode, A.; Bender, R., *SPIE, Volume 10562, id. 105620V 9 pp, Mounting, metrology and verification of Euclid near infrared spectro-photometer optical assembly NI-OA*

Jomni, Cyril; Ealet, Anne; Gillard, William; Prieto, Éric; Grupp, Frank U., *SPIE, Volume 10562, id. 105625M 8 pp., On-ground tests of the NISP infrared spectrometer instrument for Euclid*

Audrey Galametz, Roberto Saglia, Stephane Paltani, Nikolaos Apostolakis, Pierre Dubath, 2017, *SED-dependent Galactic Extinction Prescription for Euclid and Future Cosmological Surveys, A&A, 598, A20-36*

P. Dubath, N. Apostolakis, A. Bonchi, A. Belikov, M. Brescia, S. Caviuoti, P. Capak, J. Coupon, C. Dabin, H. Degaudenzi, S. Desai, F. Dubath, A. Fontana, S. Fotopoulou, M. Frailis, A. Galametz, J. Hoar, M. Holliman, B. Hoyle, P. Hudelot, O. Ilbert, M. Kuemmel, M. Melchior, Y. Mellier, J. Mohr, N. Morisset, S. Paltani, R. Pello, S. Pilo, G. Polenta, M. Poncet, R. Saglia, M. Salvato, M. Sauvage, M. Schefer, S. Serrano, M. Soldati, A. Tramacere, R. Williams, A. Zacchei, 2017, *The Euclid Data Processing Challenges*, M. Brescia, S.G. Djorgovski, E. Feigelson, G. Longo, S. Caviuoti, Eds., *Proc. IAU Symp. 325, 73-82*

(Other OPINAS group members include: C. Bodendorf, V. Guglielmo, J. G. Carpio, D. Penka, F. Raison, J. Snigula, J. Steinwagner, J. Weller, M. Wetzstein. Former members: A. Bode, A. Galametz, I. Hartung, B. Hoyle, J. Kaminski, A. Piemonte, C. Wimmer)

3.8 Dynamics Group - Milky Way and Nearby Galaxies

Observations of nearby galaxies tell us about the current dynamical configuration of stars and dark matter in these systems, and provide a record of their formation and evolution from high redshift until now. The spatial distribution and kinematics of stellar generations in the Milky Way are presently at the focus of extensive space- and ground-based surveys designed to clarify the history

of our Galaxy. Because of the unparalleled resolution and depth, insights into the formation processes of nearby galaxies are important for our understanding of galaxy formation in general ("near-field cosmology"). The following briefly summarizes our recent main research projects.

3.8.1 Structure, Dynamics, and Origin of the Milky Way Galaxy

The Milky Way (MW) is unique in that the kinematics and element abundances of a large number of its stars can be measured individually, allowing us to study the fossil record of its formation history in much greater depth than for any other galaxy. The period 2016-2018 saw the transition of MW science to the Gaia era, in which full phase-space coordinates together with element abundances will be known for many millions of stars and are already transforming our understanding of MW structure and history. Our research concentrates on the dynamics and mass of the bulge and bar, the influence of the bar on the disk, and the mass and shape of the inner dark matter halo to ~ 20 kpc.

The Milky Way as a Galaxy:

The annual review by Bland-Hawthorn & Gerhard (2016) described the structural, kinematic, and integrated properties of the Galaxy prior to Gaia. The MW appears to be a barred galaxy in a fairly advanced stage of evolution (low specific star formation rate), with a mostly old bulge containing $\sim 30\%$ of the stellar mass. The bar reaches significantly further out towards the Sun than traditionally assumed, the disk may have a short scale-length, and the dark matter halo a low virial mass. The new data have spurred many recent studies in which the review is often used. Two major new developments have been the discovery with Gaia data of non-equilibrium signatures related to vertical oscillations in the disk, and signatures of an ancient massive satellite merger building the inner stellar halo of the MW.

The chemo-dynamical history of the Galactic bulge was the subject of a more recent annual review (Barbuy et al. 2018) coauthored by the undersigned. This reaffirmed the bulge as a mostly old, α -overabundant early component of the Galaxy, notwithstanding its mostly barred nature.

Dynamical and chemo-dynamical structure of the Milky Way (MW) bulge and bar:

Our approach has been to understand the Galaxy inside-out, first the distribution of stars, then the dynamical mass distribution, and finally the orbit distributions of different stellar populations in the joint potential. This was greatly facilitated by our made-to-measure modelling

techniques developed in previous years. Using starcounts from VVV, UKIDSS, 2MASS NIR photometric surveys and radial velocities from ARGOS and APOGEE spectroscopic surveys, we constrained the total, stellar, and dark matter mass in the bulge and gave a complete dynamical description of the inner Galaxy, including bulge, long bar, inner disk, and dark halo (Portail et al. 2017a). The most important insights from these models were a slow pattern speed for the bulge-bar, placing corotation near ~ 6 kpc, a likely core or mild cusp in the central dark matter halo, and the large ($\sim 2/3$) fraction of stellar mass in the MW's barred inner regions. Subsequently we constructed separate dynamical models for stars in different metallicity bins, demonstrating explicitly the different orbit distributions of metal-rich and metal-poor bar stars (Portail et al. 2017b). Recently we completed a new analysis of infrared proper motions (PM) from the VIRAC survey, cross-matched to the Gaia absolute astrometric reference frame. The resulting 40 Mio giant star PM all across the bulge clearly show the kinematics of a barred boxy/peanut bulge (Fig. 3.8.1, Clarke et al. 2019). Amazingly, these data are very well described by the best models from Portail et al. This settles the debate about the MW bar's pattern speed and the disk origin of a large fraction of the MW bulge, and enables accurate investigations of the dark matter in the bulge.

MW disk and dark matter halo:

Using the optical depth for gravitational microlensing towards the bulge, we showed that most of the mass within the solar circle must be baryonic ('maximal disk'; Wegg et al. 2016), consistent with the above. With the statistical distribution of distances and transverse velocities provided by the dynamical model, together with the lens mass function, one can furthermore predict the distribution of microlensing time-scales. Thus from the time-scale distribution for some 3000 lens events in the inner Galaxy, we were able to infer the lens mass distribution. This showed, for an old evolved bulge population, that the initial mass function (IMF) in the bulge is indistinguishable from the IMF near the Sun, and is well-described by a Kroupa mass function (Wegg et al. 2017). Using the slower pattern speed of the Galactic bar inferred by our dynamical models, we proposed a new interpretation of the Hercules stream in the solar neighbourhood, as due to orbits visiting from corotation of the bar (Perez-Villegas et al. 2017). This is currently under

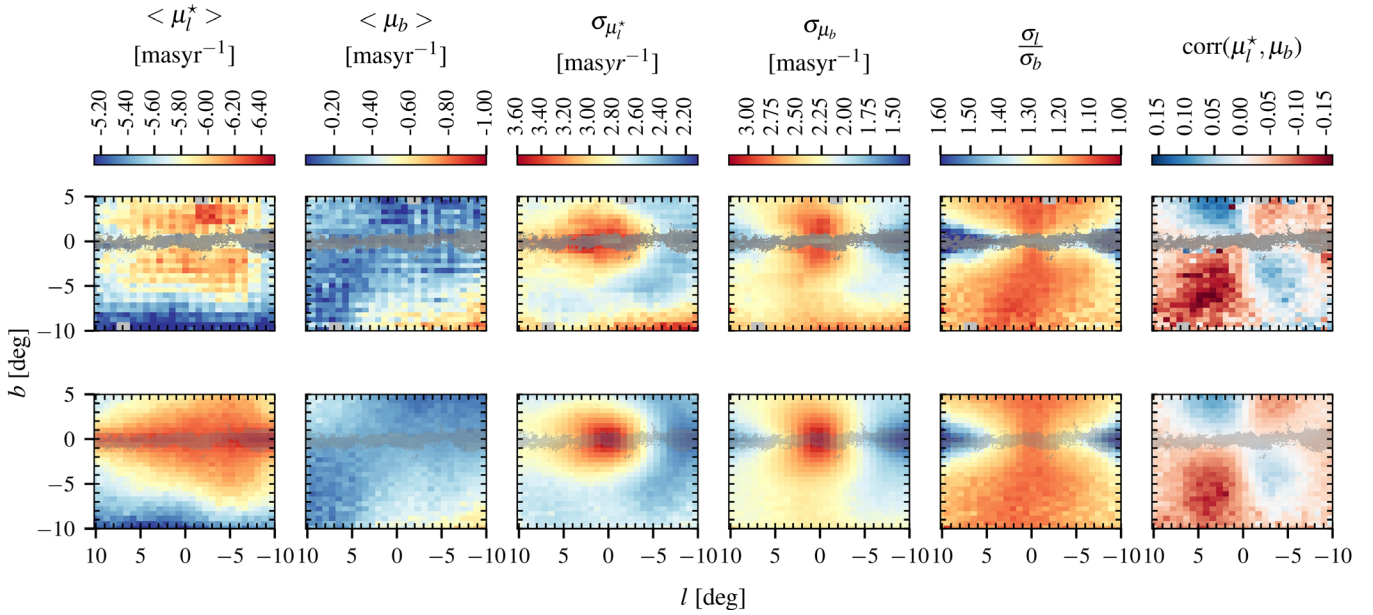


Fig. 3.8.1: Line-of-sight integrated proper motion kinematics of the Galactic bulge. Derived from combined VIRAC and Gaia data for ~ 40 Mio giant stars, we show (**top panels, from left to right**): Mean longitudinal (l) and latitudinal (b) PM μ_l and μ_b , velocity dispersion in l and b , ratio σ_l/σ_b , and σ_b correlation. The shifted quadrupole in μ_b shows the real-time rotation of the bulge, with the near (far) ends of the bulge-bar shrinking and expanding on the sky, the velocity dispersions show the deep central potential, and the correlation reflects the streaming of the bar orbits. **Bottom panels** show equivalent maps for a model with appropriate pattern speed from Portail et al. (2017a), folded with the VIRAC selection function. Note that this model was not fitted to the PM data.

active investigation with the new Gaia data, and may turn out to be the correct explanation given the recent confirmation of the bar's larger corotation radius. Our investigation of the MW's gas flow in Li et al. (2016) has independently shown that such lower pattern speeds are favourable for explaining the molecular gas kinematics (so-called lv -diagram) in the inner Galaxy.

Using the recently published Gaia data release 2, we constructed a cross-matched sample of RR Lyrae stars from PanSTARRS with accurate proper motions, spanning Galactocentric radii of 2-20kpc. Because of the accurate distances to these stars, we were able to statistically infer radial velocities and non-parametrically estimate the gravitational force field of the MW. Subtracting the baryonic force field from the Portail et al. models, we

estimated the dark matter force field and constrained the shape of the MW's dark matter halo to be close to spherical, with error ~ 0.1 in the ellipticity, as well as the circular velocity near the Sun (Wegg et al. 2019).

One of the surprising results from Gaia DR2 was the clear evidence for non-equilibrium corrugation waves in the Galactic disk ("phase-space spiral"). In a high-resolution N-body simulation, we found such corrugation waves lasting for several Gyr, that were originally generated by the buckling of the bulge in the simulation (Khoperskov et al. 2019). Independent of whether this will turn out to be the correct explanation or not, this allows us to obtain a better understanding of these corrugation waves.

3.8.2 Nearby Disk Galaxies

Nearby disk galaxies provide us with a more comprehensive view of galaxy evolution for systems broadly similar to the Milky Way. Studies of their structure, dynamics, chemo-dynamics and dark matter distribution characterize both the uniformity and the cosmic variance of galaxy evolution in a hierarchical universe. Comparison with our Galaxy will also show how typical is the Milky Way.

Dynamics, mass-distribution and chemodynamics of nearby disk galaxies:

Together with a group at Shanghai Astronomical Observatory, we have started to investigate a sample of barred galaxies with data from the CALIFA survey. The goal is to constrain the balance between dark and luminous matter with a combination of modelling the dynamics of stars and gas, as well as to look for similar correlations as in the MW between the orbit distributions and the ages and metallicities of the stellar populations, using the information derived from the spectra. This work will also be complementary to a recent study of the disk and halo mass fractions in nearby face-on disk galaxies in which we participated (Aniyan et al. 2018). With planetary nebula kinematic data, crucial for resolving the kinematics of the young stellar population, these disks were found to have near-maximal disk mass fractions.

The Andromeda galaxy, M31:

Our neighbouring galaxy M31 plays an important role in this context. It is close enough to combine integrated spectra and resolved star information, and it appears to represent the opposite end of the spiral galaxy distribution in terms of its rich stellar halo and recent accretion history. Using Spitzer photometry constraints, we constructed N-body models for M31 including barred and classical bulge (CIB) components, and found that the CIB accounts for only $\sim 1/3$ of the bulge mass in M31 (Blana et al. 2017). We then used the M2M particle technique to adjust these models to VIRUS-W IFU data (see elsewhere in this report) and derived a detailed mass model for the galaxy including the dark matter distribution in the bulge (Blana et al. 2018). Stellar population parameters derived from Lick indices (Saglia et al. 2018) showed that, surprisingly, the bar in M31 stands out in metallicity, but not in age or $[\alpha/\text{Fe}]$, and is only a Gyr or so younger than the innermost CIB. The dynamical models will also be used to obtain a better understanding of the microlensing in M31 (in collaboration with OplnAs at USM/MPE). With colleagues in ESO we have recently started to investigate the larger disk and nearby stellar halo of M31, using the radial velocities of a large number of planetary nebulae (PN). These data confirm that M31 has a quite different age-velocity dispersion relation in its disk, presumably due to its more active interaction history (Bhattacharya et al. 2019).

3.8.3 Stellar Halos and Accretion in Early-type Galaxies

The outer regions of galaxies is where dark matter dominates, and where the signatures of merger and accretion events are preserved longest. We have used planetary nebulas (PN) as tracers to measure the kinematic structure, shape, and angular momentum in the outer halos, and to look for signatures of recently accreted satellites.

Kinematics and shapes of stellar halos in early-type galaxies (ETGs):

Massive ETGs are believed to grow continuously from after their formation at redshift $\sim 2-3$ up until the present time. Observations at different look-back times and cosmological simulations favour a two-stage formation process. An early, dissipative merger-collapse forming a dense centre of in situ stars is followed by a prolonged phase of growth through minor mergers and accretion. While stellar motions and orbits in the inner parts of nearby ETGs are well-studied with integral field (IFU) spectroscopy, much of the “late galaxy formation” happens in their outer halos, where volumes are large and surface brightnesses faint. The study of the outer halos of ETGs has been one of our main research topics. PN

are excellent tracers for this purpose because their radial velocities can be measured from bright [OIII] emission lines at very faint surface brightnesses (IFU absorption line spectroscopy does not reach beyond 2-3 Re).

With the PN spectrograph (PN.S) team, we have assembled PN kinematic in the outer halos of ETGs reaching to median 6 Re. A comprehensive study of 33 ETGs (Pulsoni et al. 2018) showed that the halo kinematics of ETGs is much more diverse than in the centers. A major fraction of massive fast rotators (FR) have halo rotation similar to slow rotators (SR), due to the fading of the rapidly rotating central components in the surrounding halo, and show kinematic as well as photometric indications of triaxial halos. This transition between the dichotomy of FR and SR at small radii to a more diverse kinematics in the halos is as expected in the two-phase model, as the multiple minor merger process could not ‘know’ about the presence or not of a rapidly rotating central component. The inferred transition radii are consistent with some simulation results; a comparison with recent Illustris-TNG simulations is in progress.

Outermost halos:

The accretion processes should be most prominent in the diffuse outer halos of ETGs. A recent paper (Hartke et al. 2018) studied the velocity distribution and specific frequency of PN in the halo of the Virgo group-central M49 in conjunction with published photometry. The results indicate that the galaxy transits into a higher velocity dispersion intragroup halo, consisting of blue stars accreted from a population of low-mass galaxies with inferred metallicity of about 0.1 solar, which are not predicted by current cosmological simulations. A similar population is observed in colour-mag diagrams in the halo of the nearby group-central NGC 3379; a kinematic study with PN is in progress. In the brightest galaxy in the Virgo main cluster, M87, we studied IFU and PN kinematics and, after subtracting the PN in the non-equilibrium Virgo intra-cluster light and in a prominent substructure in projected phase-space, isolated the equilibrium outer halo component. Its kinematics indicates a rapid transition to strong radial anisotropy beyond ~ 100 kpc, as may be expected from an accretion origin, and the dynamics is consistent with the gravitational potential inferred from the hot X-ray emitting gas halo without necessity for non-thermal pressure components. The rapid decrease in density signals the boundary of the equilibrium halo of M87 (Longobardi et al. 2018).

Dynamics Group members and publications:

The group consisted of typically 2-3 PhD students and a post-doctoral fellow from MPE funds, augmented by post-doctoral fellows funded by CONACyT/Mexico (A. Perez-Villegas) and a joint DFG-China proposal (G. Gajda), and PhD students funded by the DAAD (M. Blana, Chile) and the Excellence Cluster Garching (C. Pulsoni). We are collaborating with scientists at MPE, MPA, and ESO, the PN.S team, and other international collaborators. Between 2016-2019, we coauthored two annual reviews and published about 15 first author and 15 non-first author refereed papers.

Selected References:

Aniyan et al. 2018, *MNRAS*, 476, 1909;
 Barbuy, Chiappini, Gerhard, 2018, *ARAA*, 56, 223;
 Bhatta- charya et al., *arxiv:1903.02597*;
 Bland-Hawthorn & Gerhard, 2016, *ARAA*, 54, 529;
 Blana et al., 2017, *MNRAS*, 466, 4279; --- 2018, *MNRAS*, 481, 3210;
 Clarke et al., *arxiv:1903.02003*;
 Hartke et al., 2018, *AA*, 616, A123;
 Khoperskov et al., 2019, *AA*, 622, L6;
 Li et al., 2016, *ApJ*, 824, 13;
 Longobardi et al., 2018, *AA*, 620, A111;
 Perez-Villegas et al. 2017, *ApJ*, 840, L2;
 Portail et al., 2017, *MNRAS*, 465, 1621; --- 2018, *MNRAS*, 470, 1233;
 Pulsoni et al., 2018, *AA*, 618, 94;
 Saglia et al., 2018, *AA*, 618, 156;
 Wegg, Gerhard, Portail 2016, *MNRAS*, 463, 557; --- 2017, *ApJ*, 843, L5;
 Wegg, Gerhard, Bieth 2019, *MNRAS*, 485, 3296



Ortwin Gerhard

(Other MPE team members include: J. Clarke, C. Pulsoni, S. Wylie, G. Gajda, S. Khoperskov. Team members at ESO are M. Arnaboldi, S. Bhattacharya and J. Hartke. Former MPE team members: M. Blana, A. Perez-Villegas, M. Portail, C. Wegg)

4 High-Energy Astrophysics



The integrated Russian-German satellite "Spectrum-Roentgen-Gamma" (SRG) at the company Lavochkin Association near Moscow: the spacecraft navigator, wrapped in golden insulation with the (dark) solar panels, and the mounted telescopes eROSITA (lower) and ART-XC (upper).

4. High-Energy Astrophysics

4.1 Introduction and Overview

The MPE High Energy group's astrophysics program focusses on three main themes: 1) Supermassive Black Hole Evolution 2) Clusters of Galaxies and Large-scale Structure and 3) Compact Objects and Extreme Astrophysics. The science activities of the group have continued to leverage its hardware investments in operating missions such as XMM-Newton, Chandra, INTEGRAL, Swift and Fermi. These facilities continue to reveal significant advances, and surprises, and the group has used a variety of ground-based and multiwavelength programs to augment them. The overall scientific output of the group remains very strong, with approximately 500 refereed papers during the 2016-2018 reporting period, around 100 of which feature an MPE HE group member as first author.

Much of this work has focussed on large-scale surveys, concentrating on and in preparation for the science of eROSITA, and showing the promise of the forthcoming all-sky survey with that instrument. We have assembled large samples of X-ray selected AGN and clusters of galaxies from wide area surveys and used these along with unprecedented spectroscopic coverage to provide new insight into the cosmological evolution of these source classes. For AGN, this includes new and robust determinations of their accretion rate distribution, high redshift evolution, accretion mode, obscuration properties and host galaxy properties. With clusters, the largest samples of X-ray selected objects with spectroscopy and/or accurate photometric redshifts enable cosmological studies via the evolution of the cluster mass function. We are also working towards a better understanding of the thermodynamic properties of the intracluster medium, including non-thermal pressure support and the effects of a multi-phase medium. Clusters also provide an ideal laboratory in which to study the properties of galaxies in the densest large-scale structure environments.

Deeper understanding of accretion and ejection processes around compact objects is possible via the study of nearby systems, be they black holes across the mass scale, or neutron stars. Ultraluminous X-ray (ULX) sources challenge the prevailing paradigm by apparently exceeding the Eddington luminosity for neutron star binaries. In addition to work on these and similar systems in the Magellanic clouds, group members have discovered a new ULX pulsar in the galaxy NGC 300 which confirms unambiguously that the compact companion is a neutron star, with an unprecedented spin-up rate. The group has also been examining energetic processes around the black hole at the centre of our galaxy. In work with the MPE IR group, this has confirmed that synchrotron emission is responsible for the observed bright flares. Predictions for future tests of GR around Sgr A* with the Event Horizon Telescope complement the spectacular current measurements with the IR group's Gravity instrument.

A further highlight from the Galactic centre has been the mapping of the hot gas distribution, which has yielded evidence for large-scale Galactic "chimneys" transporting energy from the Galactic centre into the far reaches of the galaxy, most likely connecting to the so-called Fermi bubbles and with potentially (and literally) wide-reaching implications for Galaxy evolution.

Perhaps the biggest event in the astronomy world in 2017 was the simultaneous discovery of gravitational waves and electromagnetic radiation associated with so-called "kilonova" GW170817 associated with the gamma-ray burst GRB170817A, proving unambiguously that this is a neutron-star merger. The MPE HE group was deeply involved with this, with the GRB itself being discovered by Andreas von Kienlin, using the MPE-built GBM instrument on Fermi. The group played a major role not only in the Fermi work but also Integral and ground-based follow-up with the MPE GROND instrument of this extraordinary event.

In terms of our project work, undoubtedly the biggest news for the HE group since the last SAB has been the completion of the eROSITA instrument, which was delivered to the spacecraft contractor Lavochkin Association in January 2017. At the time of writing eROSITA sits in Khimki, Moscow aboard the fully-integrated Spectrum-RG spacecraft having successfully undergone its final test. Its launch from Baikonur, Kazakhstan, is currently scheduled on June 21st, just a few days after the SAB visit. This is the culmination of an intensive effort by the group in the 10 years since the "detailed agreement" between Roscosmos and DLR that formalised the project. eROSITA is set to revolutionize X-ray astronomy, performing an all-sky survey a factor 30-100 deeper than previous missions, and MPE has been responsible for all aspects of the instrument, under the leadership of the PI, Peter Predehl. The realization of eROSITA has been a remarkable achievement, which has been a project of extraordinary scope even for a group with our strong heritage. In anticipation of the transformative science to be delivered by the all sky survey, and in parallel with our exploitation of existing X-ray observatories, the group has been putting a major effort into preparing for eROSITA from every necessary angle, including ground software, calibration, simulation, science preparation and follow-up resources.

The most important project for the future of the HE group beyond eROSITA is Athena. Our efforts were instrumental in securing the acceptance of Athena as ESA's second large (L2) mission and we have a key role as PI Institute for the Wide Field Imager (WFI), one of the two instruments. The WFI passed two major milestones recently. The first major review of the instrument, by ESA and DLR, was completed successfully in December

2018. In the same month, the consortium responsible for the instrument and led by MPE was recognized formally by ESA. Conceptual design work and technology development for the instrument continues. In the summer, we expect to receive the first full-size, flight-like DEPFET sensors, which are currently being manufactured at the MPG HLL. These bespoke sensors are at the heart of the instrument and enable its ground-breaking capabilities. The HE group is also making major contributions to the Athena optics development via the MPE PANTER facility, where the development of ESA's Silicon Pore Optics (SPO) is tested and validated. The final calibration of the Athena mirror cannot be performed at PANTER, as the beamline is too short and the vacuum chamber too small. Discussions are ongoing with ESA about the construction of a newer, larger facility on the Garching campus to accommodate this. Whether or not to proceed will be a major question for the group – and ESA – in the next couple of years.

Responding to earlier recommendations of the SAB, the HE group has made efforts to complement its “mega-projects” with smaller-scale collaborations. These have the effect of bridging the gap between eROSITA and Athena, and can provide complementary scientific output. The group has recently taken up a significant role in the Chinese Einstein Probe project. This is an exciting small-scale mission focused on transients, featuring a follow-up X-ray telescope closely matching the characteristics of a single eROSITA telescope module. We are working together with ESA to deliver the mirror modules for the telescope, and intend to contribute the detector modules for the focal plane camera.

Looking further to the future, we are performing technology development for the Chinese eXTP project, developing fast Silicon Drift detector modules for use in the spectroscopic telescope array for that mission, which is focused on high throughput spectral-timing studies of AGN and binaries. We continue with our minor partnership on SVOM, the future Sino-French GRB mission, in collaboration with CEA and CNES. At PANTER, we also played a key role in the development and testing of the optics for the innovative NASA Explorer candidate Arcus, an X-ray grating spectroscopy mission using the same SPO technology as Athena. Unfortunately, Arcus was recently downselected. The optics developments we have been supporting are nonetheless still very useful and relevant for Athena, and any re-incarnation of the Arcus concept.

Overall, the MPE High Energy group is in excellent shape. The completion of eROSITA has been a remarkable achievement and has stretched the group to its limits, but is now ready to usher in a new era of X-ray surveys. Our scientific activities in the coming years will be fully devoted to the successful operation and exploitation of this transformative instrument. Looking beyond eROSITA, we continue to leverage our comparative advantages in X-ray detectors and optics, backed up by our PANTER facility, and our relationship with the MPG-HLL, notably for Athena.



Kirpal Nandra for the MPE High Energy Group

4.2 Astrophysics Research

4.2.1 Supermassive Black Hole Evolution

SMBHs are believed to reside at the cores of all massive galaxies, but their evolutionary path and the relation to their hosts is still a matter of intense debate. Understanding these issues, as well as the physics of the central engine of Active Galactic Nuclei (AGN), and their overall contribution to the energy budget of the Universe, are a major focus of the activities of the HE group. We are addressing this using several approaches. Specifically, we are working towards a complete AGN census across cosmic time, using X-ray surveys to understand the obscured and high redshift populations. We also seek to understand the evolution of SMBH with respect to their host galaxies, augmenting the samples of AGN detected in deep, pencil-beam X-ray surveys with the rare, brighter objects that require wider area coverage. The final piece of the puzzle is provided by X-ray spectroscopy, which is used to determine the AGN obscuration and emission properties, and to identify AGN with peculiar spectral and/or variability properties.

Expanding the parameter space of X-ray surveys for AGN demographics:

Deep X-rays surveys have limited area coverage and for this reason, while sampling the faint, host dominated and obscured AGN, they miss the rarer, brighter objects that can be detected only with wide and all-sky surveys. Determining properties such photometric redshifts for these bright objects is extremely challenging (e.g., Salvato et al. 2018b) and for this reason, we have undertaken a major effort to obtain spectroscopic redshifts for the most luminous X-ray selected AGN. This has been made possible thanks to our program within the SDSS-IV survey called SPIDERS (Spectral Identification, of eRosita Sources), originally envisaged to complement the early eROSITA data, as its name suggests. This program allowed us to obtain an unprecedented spectroscopic sample of more than 20,000 AGN detected in the XMM-XXL (Menzel et al. 2016), ROSAT 2RXS (Boller et al 2016), and XMMSLEW (Dwelly et al 2017) surveys. Figure 4.2.1 shows the location of these new sources in the luminosity-redshift parameter space.

While for XMM-XXL the identification of the optical counterparts of the X-ray sources was performed using the standard Maximum Likelihood Ratio technique, the larger positional uncertainties for ROSAT and XMMSLEW required the development of a new procedure, called **NWAY** (Salvato et al 2018a). This algorithm uses Bayesian statistics and our prior knowledge of the properties (colors, magnitudes, etc.) of X-ray emitting AGN from **XMM-Newton** and **Chandra** surveys, to identify X-ray source counterparts even when the positional uncertainty is very large. A further advantage is the ability to match to multiple optical/IR bands simultaneously.

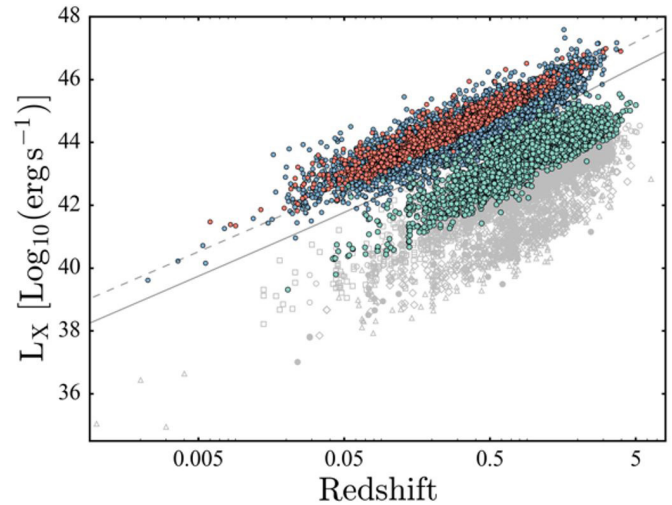


Fig. 4.2.1 Luminosity-redshift distribution of the new sources with spectroscopy that we have gathered in the last three years, following up XMM-XXL (green), ROSAT (blue) and XMMSLEW (red) X-ray sources. The total spectroscopic sample size amassed is larger than all the AGN from previous pencil beam surveys combined (CDFs, CDFN, AEGIS, COSMOS, Lockman Hole, here shown in light grey). Figure adapted from Coffey et al., submitted.

AGN and their host galaxies:

The increase of the sample size and in the coverage of the Luminosity-redshift plane, and the access to spectroscopy, has allowed us to revisit the relation between AGN and their hosts. First, we have explored the incidence of X-ray selected AGN in galaxies as a function of redshift and the stellar mass of their hosts (Georgakakis et al 2017b). The analysis suggests that the so-called downsizing effect that characterises the evolution of AGN relates to subtle changes in the duty-cycle of active BHs with redshift rather than variations in the typical mass of accreting black holes (Fig. 4.2.2).

We have also investigated the incidence of obscured AGN at bright accretion luminosities using one of the largest contiguous surveys available, the XMM-XXL (Georgakakis et al 2017a). Evidence is found for strong luminosity-dependent evolution of the obscured AGN fraction. This may be the result of the interplay between increasing dust/gas-reservoirs in galaxies at higher redshift and AGN feedback processes dominating at bright accretion luminosities. Infrared-based AGN selection methods are critically reviewed and their completeness is found to be predominantly a function of redshift and not obscuration or accretion luminosity.

Using the SDSS/BOSS optical spectra of the broad-line AGN detected in XMM-XXL, we have examined the properties of the enigmatic broad-line AGN which show significant X-ray obscuration (Liu et al 2018). We found that, compared with typical broad-line AGN, the X-ray

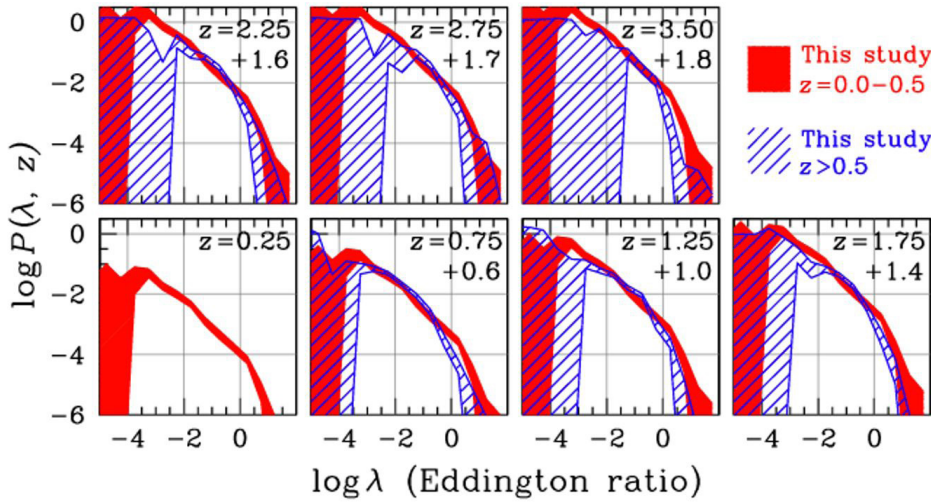


Fig. 4.2.2 Specific accretion-rate distribution of AGN across the stellar mass range $\log(M/M_\odot)=8-13$. Each panel corresponds to a different redshift interval. The red hatched histogram in each panel is the specific accretion-rate distribution of the lowest redshift bin $z=0.0-0.5$. This relation is shifted upwards by the logarithmic offset marked in each panel under the redshift label, to demonstrate that a simple re-normalisation of the distribution at $z=0.0-0.5$ approximates in a rough manner the redshift evolution of the specific accretion-rate distribution of AGN (adapted from Georgakakis et al 2017a).

obscured sources show broader broad lines (and thus higher black-hole mass) and more (but still moderate) optical extinction. These findings can be explained in the framework of a multi-component, clumpy torus model.

The properties of AGN in relation to their host galaxies were also studied combining multi-wavelength data for a sample of AGN and QSO observed with **NuSTAR** (Del Moro et al, 2017), and **Herschel** (Del Moro et al, 2016). Studying the AGN emission in the infrared and X-ray bands, we found a large fraction of infrared-bright quasars out to $z=3$ which are heavily obscured in the X-ray band and are hosted in galaxies with more disturbed morphology compared to unobscured quasars. Moreover, studying the average broadband X-ray spectra of AGN, using **Chandra** and **NuSTAR** data, we found an anti-correlation between the X-ray luminosity and the amount of Compton reflection, which could be linked to the X-ray Baldwin effect.

X-ray spectroscopy of AGN:

While optical and near/mid-IR spectroscopy and photometry probes the link between the AGN and their hosts, X-ray spectroscopy opens up a window onto the physics of the central engine. In Baronchelli et al. (2018), we detected relativistically broadened iron K α emission – the

signature of the inner accretion disk – in the X-ray spectra of a sample of ~ 200 AGN detected in the **Chandra Deep Field South** survey (CDF-S) using the Bayesian X-ray analysis (BXA) package developed in our group (Buchner et al 2014). This suggests that the majority of black holes growth in the Universe proceeds via standard, radiatively efficient disk accretion, and demonstrates the great future potential of X-ray spectroscopy (e.g. with **eROSITA** and **Athena**) to reveal the physics of accretion, out into the high redshift Universe.

X-ray spectroscopy was also used to discover a dramatic and unprecedented X-ray spectral variability event observed in a $z\sim 1$ broad line type-1 QSO (Simm et al 2018). The **XMM-Newton** spectrum from the year 2000 is characterized by an unobscured power-law spectrum with photon index of $\Gamma\sim 2$, a low column density of intervening absorbing material, and no prominent reflection component. Five years later, **Chandra** captured the source in a heavily obscured, reflection-dominated state. The observed X-ray spectral variability could be caused by a Compton-thick cloud eclipsing the direct emission

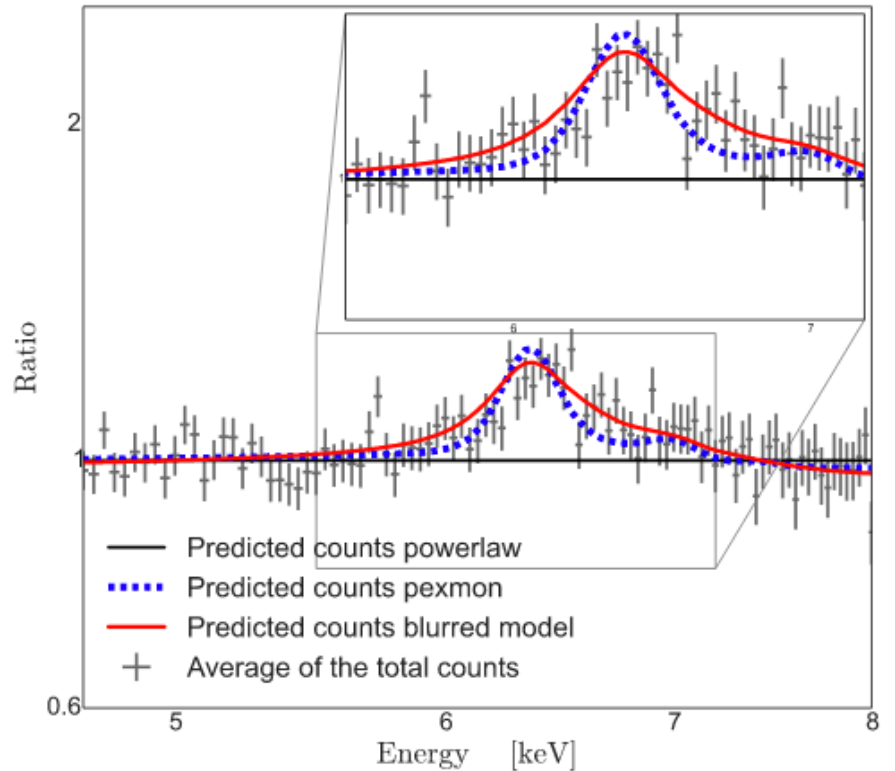


Fig. 4.2.3 Average of the total counts of AGN in the CDF-S, relative to the best fitting power-law model showing a broad and relativistic iron K α line (Baronchelli et al. 2018). The evidence for this feature was determined by fitting the individual spectra using the BXA package, avoiding the problems with spectral stacking that have plagued previous work.

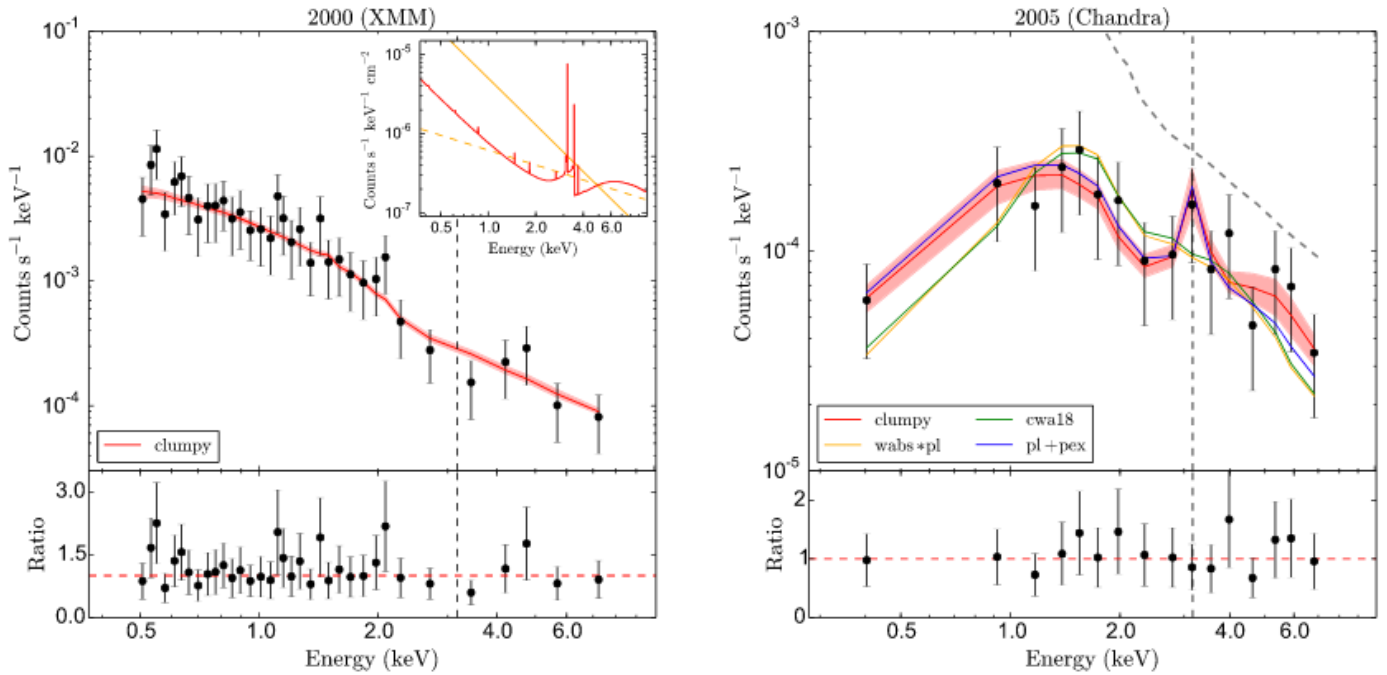


Fig. 4.4.4 The dramatic X-ray spectral change of the type-1 QSO RMID 278. The XMM EPIC-PN spectrum from 2000 (left) is fully consistent with an unobscured power law, while the extremely flat Chandra spectrum from 2005 (right) indicates Compton thick obscuration. The red curves in both panels display the best-fitting clumpy model together with the 1σ error regions (from Simm et al 2018).

of the hot corona, implying an extreme column density variation never before observed in a type-1 QSO. An alternative scenario is a corona that switched off in between the observations. Dramatic X-ray spectral variability of this kind could be quite common in type-1 QSOs, considering the relatively few data sets in which such an event could have been identified. Our analysis implies that there may be a population of type-1 QSOs, which are Compton-thick in the X-rays when observed at any given time. This will be verified with the upcoming multi-epoch **eROSITA** survey data.

Mara Salvato



Andrea Merloni



Selected References:

Baronchelli et al, 2018, *MNRAS*, 480, 2377
 Del Moro et al., 2016, *MNRAS*, 456, 2105
 Del Moro et al., 2017, *ApJ*, 849, 57
 Dwelly, et al, 2017, *MNRAS*, 469, 1075
 Georgakakis et al 2017, *MNRAS* 469, 3232
 Georgakakis et al, 2017, *MNRAS*, 471, 1976
 Liu, T et al 2018 *MNRAS*, 470, 5022
 Liu, Z. et al., 2016, *MNRAS*, 459, 1602
 Menzel et al 2016, 457, 210
 Merloni et al, 2016, *Springer*, 905, 201
 Salvato et al, 2018a, *MNRAS*, 473, 4937
 Salvato et al, *Nature Astron.* 2018b
 Simm et al 2018, *MNRAS*, 480, 4912

Antonios Georgakakis



(Other HE group members include: R. Arcodia, L. Baronchelli, D. Bogensberger, T. Boller, H. Brunner, D. Coffey, A. Fresco, T. Liu, A. del Moro, K. Nandra, G. Ponti. Former members: T. Dwelly, Z. Liu, T. Simm)

4.2.2 Clusters of Galaxies: Large-scale Structure and Cosmology

Clusters of galaxies are the most massive collapsed objects in the Universe. The intra-cluster medium (ICM) is the dominant baryonic component of clusters, emitting in the X-ray waveband. X-ray observations directly probe the physical processes taking place in the ICM, for example mergers and AGN feedback. Observations at other wavelengths provide important additional information, which can be combined with X-ray data. We have performed detailed studies of individual systems and well-selected samples. **eROSITA**, designed as a Stage-IV Cosmology experiment, will soon be launched, and will detect $\sim 100,000$ clusters probing the growth of structures in the Universe. In preparation for its launch, we are undertaking simulations and the analysis of existing surveys, including those from **XMM-Newton** and **Chandra**, while we are also completing the **SDSS-IV/SPIDERS** survey, an extremely large spectroscopic follow up of faint **ROSAT** clusters.

The physics of galaxy clusters:

Cluster physics can have a significant effect on how they are detected in surveys and their measured masses. D. Eckert is leading the X-COP very large project with XMM-Newton to jointly analyse X-ray and **Planck** data to study several aspects of the hot baryons in galaxy clusters. This has included studying the non-thermal pressure support (Eckert et al. 2019; Figure 4.2.5). The results show hydrostatic masses require little correction,

implying a median non-thermal pressure fraction of $\sim 6\%$ and $\sim 10\%$ at R_{500} and R_{200} , respectively, lower than the expectations of hydrodynamical simulations. Ghirardini et al. (2019) studied the thermodynamic profiles of the sample in two decades in radius out to the virial radius. We found gas density and pressure profiles steepening with radius, in agreement with previous results. Entropy profiles beyond R_{500} agree with the predictions of gravitational collapse. The scatter in all quantities is minimized between $0.2-0.8 R_{500}$ and increases outward, with surprisingly more scatter in pressure than temperature or density.

Sanders et al. (2016b) applied the Gaussian Gradient Magnitude edge-sensitive filter to images of three clusters, Perseus, Abell 3667 and M87 (Figure 4.2.6), following its novel application to observations of the Centaurus cluster (Sanders et al 2016a). The filter measures gradients on particular spatial scales. Filtered images with different scales can be combined, producing spectacular images of the edges in clusters. Discussed is the assessment of significance of structures. The method has significant advantages for detecting many kinds of features compared to other analysis techniques, such as unsharp masking. Filtering cluster images in a hard energy band allows shocks to be detected. Freely-available software implementing the technique is also provided.

Sanders et al. (2018) presented a new forward-modelling code for obtaining thermodynamic profiles of clusters from X-ray surface brightness profiles, optionally assuming hydrostatic equilibrium. We applied this to **Chandra** X-ray observations of clusters selected using the Sunyaev-Zel'dovich (SZ) effect with the South Pole Telescope from $z=0.3-1.2$. 60% of the clusters are found to have low entropy material in their cores. No significant evidence for redshift evolution in the profiles beyond that expected from self-similar evolution was found. The average modelled radial density, entropy and cooling-time profiles appear as power laws with breaks around $0.2 R_{200}$.

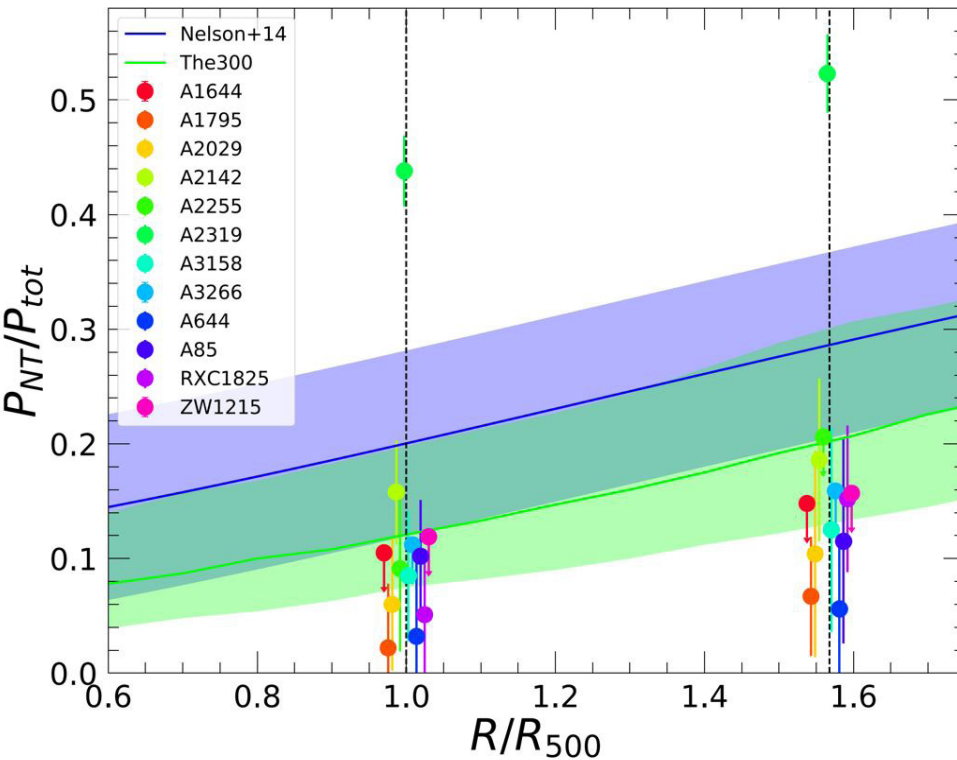


Fig. 4.2.5 Fraction of non-thermal pressure as a function of radius in the X-COP sample (Eckert et al. 2019). The blue and green curves and shaded areas show the mean non-thermal pressure ratio predicted from the numerical simulations of Nelson et al. (2014) and Rasia et al. (in prep.), respectively.

Hofmann et al. (2016) used archival **Chandra** data to obtain independent constraints on a claimed unknown emission line around 3.55 keV, which has been proposed as the signature of decaying sterile neutrinos with a mass of 7.1 keV. For a sample

of 33 high-mass clusters of galaxies all observations from the **Chandra** data archive were merged. In the resulting high signal-to-noise spectra no evidence for an unidentified emission line at 3.55 keV was found. Assuming all dark matter was made of 7.1 keV sterile neutrinos, the upper limits on the mixing angle were $\sin^2(2\Theta) < 10.1 \times 10^{-11}$ from ACIS-I and $< 40.3 \times 10^{-11}$ from ACIS-S data, at 99.7% confidence level.

Surveys of galaxy clusters with eROSITA:

In preparation for **eROSITA**, Clerc et al. (2018) carefully simulated the entire chain of processes from photon emission to source detection and modelling. Using Monte Carlo simulations the selection function was investigated. With an accurate instrument model and state-of-the-art detection technique, we modelled the cluster detection efficiency, finding 10^5 clusters will be detected by **eROSITA** over the whole sky. This work shows how selection effects, for example the cluster size distribution, introduce biases in the obtained cosmological parameters, with those characteristics that require tight monitoring to avoid bias being highlighted. Hofmann et al. (2017) used clusters studied in deep observations with **Chandra** to simulate **eROSITA** detections. Cluster temperature bias and its impact on cluster masses, as well as cosmological parameters derived from the survey were obtained. Temperatures in the survey are biased low by about 5% due to unresolved substructure, compared to emission-weighted average temperatures. This bias would have a significant impact on the **eROSITA** cosmology constraints if not accounted for in the calibration.

Cosmology from existing X-ray surveys:

X-CLASS is a serendipitously detected X-ray-selected sample of 845 clusters based on 2774 **XMM** observations covering ~ 90 deg². Using count-rate and hardness ratios we performed a first cosmological analysis of the sample (J. Ridl, PhD thesis). This forward-modelling approach shows highly improved constraints if individual redshifts are available. We completed the photometric redshift follow-up of a high signal-to-noise subset with GROND, the 7-channel (*grizJHK*) simultaneous imager. We determined photometric redshifts for 232 clusters with an accuracy of $\Delta z = 0.02(1+z)$, publishing a catalogue of the systems (Ridl et al. 2017). We combined a cosmological fitting code with a modern sampler, enhanced to account for cluster redshifts, rewriting to increase its speed, scalability and portability. A blind comparison confirmed consistency with previous results, corroborating a simple Fisher matrix analysis.



Fig. 4.2.6 Edge-filtered Chandra X-ray image of the M87 galaxy cluster using the technique described in Sanders et al. (2016). The image shows the multiple episodes of AGN feedback in the system, seen as X-ray cavities and weak shocks.

Precision cosmology requires reliable redshift estimates for the galaxy clusters discovered as bright extended sources in the X-ray sky. In addition to the AGN program, the SDSS-IV SPIDERS program includes complete spectroscopic follow-up of X-ray-selected, massive ($\sim 10^{14} - 10^{15} M_{\odot}$) galaxy clusters discovered in **ROSAT** and **XMM-Newton** imaging, over a large area (~ 6000 deg²) of the extragalactic sky. Our selection and targeting strategies makes this the largest of such programs before the launch of **eROSITA**. The goal is to determine precise redshifts for 4000-5000 clusters out to $z \sim 0.6$. We demonstrated the efficiency of this selection strategy, and proposed a prototype set of algorithms and a workflow to collate spectra and assign cluster membership, and to deliver catalogues of spectroscopically confirmed clusters. We illustrated our techniques by publishing a catalogue of 230 validated clusters ($0.03 < z < 0.66$) in Clerc et al. (2016). This strategy, now improved, is in use for SPIDERS planned for completion end of 2019.

Galaxy evolution in the densest environments:

Erfanianfar et al. (submitted) published a Brightest Cluster Galaxies (BCGs) catalogue for the SPIDERS DR14 clusters. This contains 416 identified BCGs, along with their stellar mass, star formation rates (SFR), and morphological properties. The BCGs were identified using spectroscopic data from SPIDERS and photometric data from SDSS. Stellar masses and SFRs of the BCGs are computed with SDSS, WISE and **GALEX** photometry, and spectral energy distribution (SED) fitting. Morpho-

logical properties for all BCGs are derived by Sérsic profile fitting in different optical bands (*gri*) (Furnell et al. 2018). We find that stellar mass is the most important factor governing BCG morphology, indicating that our sample consists of a large number of relaxed, mature clusters containing broadly homogeneous BCGs up to $z \sim 0.3$, with little evidence for much ongoing structural evolution in these massive systems. Comparat et al. (2017b) determined the stellar population properties — age, metallicity, dust reddening, stellar mass and the star formation history — for all spectra classified as galaxies that were observed by SDSS-IV SPIDERS (Clerc et al. 2016), making use of high spectral resolution stellar population models of Maraston et al. (2011). The catalogue obtained was also made publicly available within the data release 14 of SDSS.

In Erfanianfar et al. (2016), using data from four deep fields (COSMOS, AEGIS, ECFDS, and CDFN), we studied the correlation between the position of galaxies in the star formation rate (SFR) versus stellar mass plane and local environment at $z < 1.1$. To accurately estimate the galaxy SFR, we use the deepest available Spitzer/MIPS24 and **Herschel/PACS** data sets. We distinguish group environments ($M_{\text{halo}} = 10^{12.5} - 10^{14.2} M_{\odot}$) based on the available deep X-ray data and lower halo mass envi-

ronments based on the local galaxy density. Our results suggest that above a stellar mass threshold ($\sim 10^{10.4} - 10^{10.6} M_{\odot}$), morphology and environment act together in driving the evolution of the star formation activity towards lower level. The presence of a dominating bulge and the associated quenching processes are already in place beyond $z \sim 1$. The environmental effects appear, instead, at lower redshifts and have a long time-scale.

Selected References:

- Comparat et al., 2017a, *MNRAS*, 469, 4157
 Comparat et al., 2017, *A&A*,
 Clerc et al., 2016, *MNRAS* 463, 4490
 Clerc et al., 2018, *A&A*, 617, A92
 Eckert et al. 2019, *A&A*, 621, A40
 Erfanianfar et al. 2016, *MNRAS*, 455, 2839
 Furnell et al. 2018, *MNRAS*, 478, 4952
 Ghirardini et al. 2019, *A&A*, 621, A41
 Hofmann et al. 2016, *A&A*, 592, A112
 Hofmann et al. 2017, *A&A*, 606, A118
 Ridl et al., 2017, *MNRAS* 468, 662
 Ridl, Ph.D. thesis, LMU, München 2017
 Sanders et al. 2016a, *MNRAS*, 457, 82
 Sanders et al. 2016b, *MNRAS*, 460, 1898
 Sanders et al. 2018, *MNRAS*, 474, 1065



Jeremy Sanders



Nicolas Clerc



Alexis Finoguenov

(Other HE group members include: J. Comparat, D. Eckert, G. Erfanianfar, F. Hofmann, F. Kaefer, A. Merloni, K. Nandra, M. Salvato. Former member: J. Ridl,)

4.2.3 Compact Objects and Accretion Physics

One of the main research topics of the HE group at MPE deals with compact objects and the physical processes that power their X-ray emission. This comprises accretion of matter onto objects of different mass like white dwarfs, neutron stars, stellar-mass black holes and supermassive black holes at the center of galaxies. The study of the X-ray emission at different accretion rates allows us to investigate how the matter flow changes and interacts with the radiation, and can reveal the properties and parameters of the central compact object.

Super-Eddington Accretion in Be/X-ray Binary and ULX Systems:

X-ray binaries hosting highly magnetized neutron stars (NS) offer a unique laboratory to study accretion under extreme conditions. At high mass-transfer rates an accretion disk is formed around the NS, while the strong magnetic field of the NS truncates the disk at distances hundreds of times larger than the NS. Be/X-ray binary pulsars are known to exhibit major outbursts with peak luminosities in excess of the Eddington limit expected for isotropic accretion onto a stellar mass compact object. Due to their proximity, well known distances, and low foreground absorption, systems located in the Magellanic Clouds (MCs) offer an ideal environment to study these rare events (Haberl & Sturm 2016, Haberl et al. 2017, Vasilopoulos et al. 2018a). In recent years we have used **XMM-Newton** to observe a number of Be/X-ray binaries located in the MCs (e.g. SMC X-3, SMC X-2, LXP 8.04; Koliopanos & Vasilopoulos 2018; Vasilopoulos 2018) during major outbursts. By performing spectral and temporal analysis at different luminosity levels, we have studied changes in their spectra and pulse profiles that are associated with changes in their emission geometry (Figure 4.2.7). We have shown that for high accretion rates the accretion disk becomes inflated and covers a large solid angle around the NS. As a result it can reprocess a significant part of the radia-

tion originating from the NS. An intriguing consequence is that for ultra-luminous X-ray systems (ULXs) where the luminosity greatly exceeds the Eddington limit, the NS can be engulfed in an optically thick envelope or cocoon, which reprocesses the bulk of the pulsed emission. In the light of this we analysed the spectra of eighteen well-known ULXs to investigate the cocoon hypothesis. We find that the spectral curvature observed above 6 keV in most ULXs, is commensurate with the Wien tail of a hot ($kT > 1$ keV) multicolor black-body component and confirm that a double thermal model (comprised of a "cool" and a "hot" thermal component) with the addition of a faint non-thermal tail describes all ULX spectra in our list. This offers a new physical interpretation for the dual thermal spectrum, which is the result of accretion onto highly magnetized NSs rather than black holes, in agreement with theoretical predictions.

Discovery of the ULX Pulsar NGC 300 ULX1:

Ultra-luminous X-ray sources (ULXs) have been thought to harbor intermediate-mass black holes, but the recent discovery of X-ray pulsations from several ULXs (M82 X-2, NGC 7793 P13, and NGC 5907 ULX1) has shown that these systems powered by accretion onto highly magnetized neutron stars at super-Eddington rates. In a very long and simultaneous **XMM-Newton/NuSTAR** observation, a new ULX was discovered in the nearby galaxy NGC 300, identified as a likely B[e] high-mass X-ray binary (Carpano et al. 2018). Pulsations were found with a pulse period of 31.6 s and a high spin-up rate of -5.56×10^{-7} s/s, which is one of the highest ever reported for an accreting X-ray pulsar. The pulsed fraction, increasing with energy, reached 75% in the NuSTAR band (0.3–30 keV). Archival and further monitoring observations with **XMM-Newton**, **Chandra**, **NuSTAR**, **Swift** and **NICER**, revealed a first significant pulse period detection at 126 s in November 2014, 44 s in April 2016, and reaching 16.5s end of 2018. Since the pulse period continues to decrease, the source is likely still in the so-called accretion regime, where the inner radius of the Keplerian

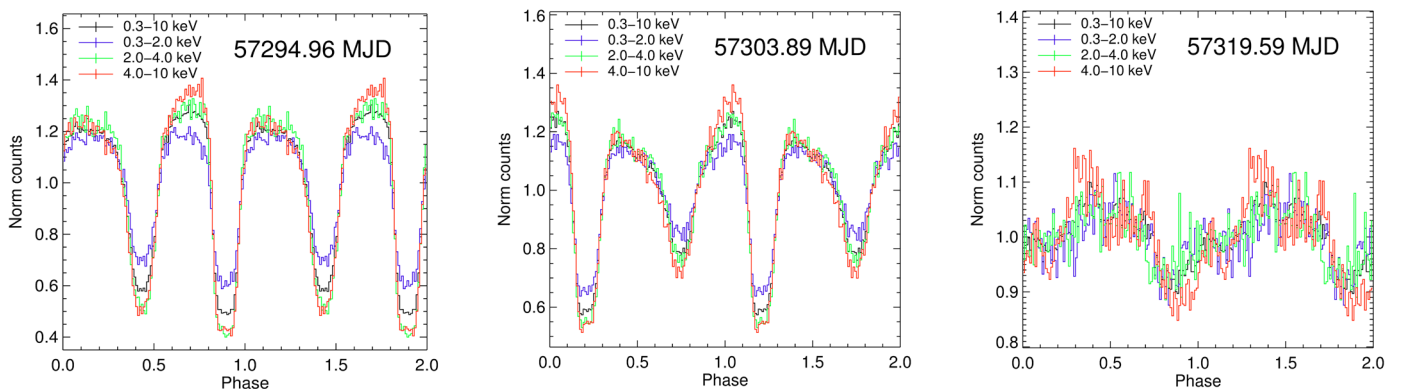


Fig. 4.2.7 Pulse profiles obtained from EPIC-pn data in different energy bands during the September 2015 outburst of SMC X-2.

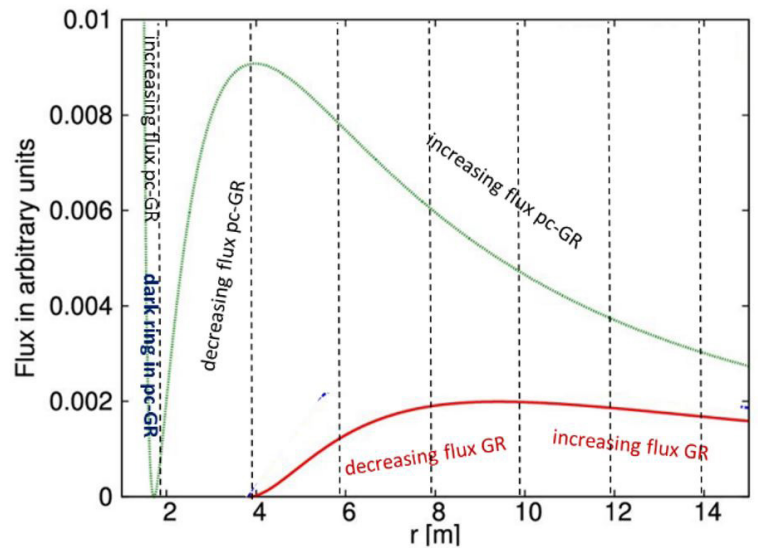
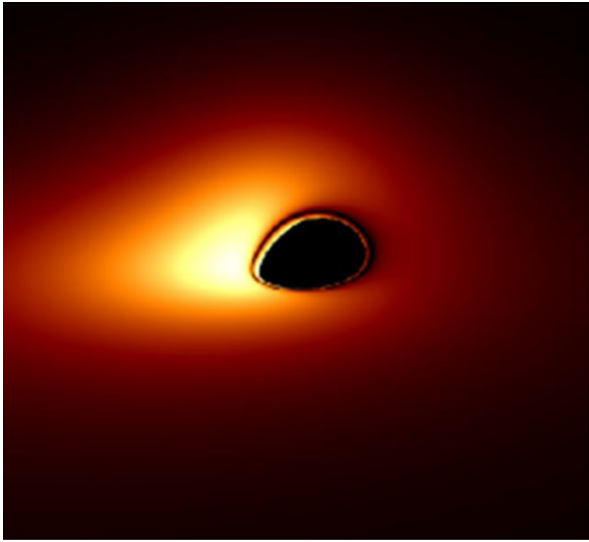


Fig. 4.2.8 Left: PC-GR ray tracing simulation of the emission around a rotating black hole in the Galactic Centre. The new features are the appearance of a black ring at $1.72 r_g$, an inner bright ring, and an outer disc. **Right:** Flux emitted by infalling matter onto the black hole as a function of distance for the standard GR (red line) and the pc-GR theory (green line). The significant differences in flux will allow a robust test of the pc-GR prediction. The curves are calculated for the mass of the black hole in the Galactic Centre and a spin of $a = 0.6$.

disc is smaller than the co-rotation radius, allowing accretion along the magnetic lines. Future observations, when the spin period approaches its equilibrium will be of great importance to test different models of accretion theory (Vasilopoulos et al. 2018b).

Outflows in X-ray Binaries:

A characteristic property X-ray binaries is the presence of equatorial winds during the softer spectral states, while the tracers of such winds typically disappear during the harder states (Bianchi et al. 2017, Ponti et al. 2018a). We recently showed that such “wind disappearance” could be generated by a thermal instability within the outflowing plasma. By studying the ionised accretion disc corona in the eclipsing accreting neutron star X-ray binary MXB 1658-298, we demonstrated that it is possible to measure the radial velocity curve of the neutron star (Ponti et al. 2018b) using X-ray spectroscopy. Measuring the energy shift of the ionised absorption lines of the corona allowed us to measure fundamental parameters (e.g., the masses) of the binary system.

The Black Hole at the Galactic centre:

In collaboration with the MPE IR group, we performed multi-wavelength monitoring campaigns of Sgr A*, the radiative counterpart of the supermassive black hole at the Milky Way centre. In Ponti et al. (2017) we determined the first fully simultaneous measurements of the near-infrared and X-ray spectral slope (and its evolution) during a very bright flare, confirming the synchrotron origin (with a cooling break) of the X-ray emission during flares. Additionally, the temporal evolution of the spectral

energy distribution, during the flare, suggests the presence of a possible evolution of a high energy cut off in the distribution of accelerated electrons.

Observational tests of a modified GR theory using Black Hole imaging with EHT observations:

Einstein’s General Relativity (GR) developed 100 years ago successfully describes gravitation and has withstood all four classical experimental tests. Motivated by the existence of singularities in Einstein’s General Theory of Gravity, e.g. the curvature singularity at $r=0$ m Schwarzschild (1916), and the orbital velocity of $v=c$ at the Schwarzschild radius of infalling matter into the central black hole, Hess & Greiner (2009) published a new algebraic extension of the standard GR, called pseudo-complex General Relativity (pc-GR). A robust test of the pc-GR theory can be made by examining the flux distribution as a function of distance from the central black hole (Figure 4.2.8, Boller et al. 2019). For the standard GR theory, and a BH spin of 0.6, the flux increases up to about $8 r_g$, and decreases towards smaller distances from the black hole due to the increasing gravitational redshift, vanishing at about $4 r_g$. In contrast, pc-GR theory predicts an increasing flux up to about $4 r_g$, due to the reduced gravitational redshift and the repulsive forces. The flux decreases towards the center, reaching zero intensity at $1.72 r_g$. Below this radius, the orbital frequency is sharply decreasing resulting in emission referred to as the inner bright ring. These intensity differences between the two theories are independent on the emission mechanism of infalling matter.

Selected References:

Bianchi et al., 2017, MNRAS, 472, 2454
Boller et al., 2019, MNRAS, in press, arXiv:1812.08417
Carpano et al., 2017, A&A, 602, 81
Carpano et al., 2018 MNRAS, 476, L45
Haberl & Sturm, 2016, A&A, 586, 81
Haberl et al., 2017, A&A, 598, 69
Koliopanos & Vasilopoulos, 2018, A&A, 614, 23
Maitra et al., 2018a, MNRAS, 480, L136
Maitra et al., 2018b, A&A, 612, 87
Ponti et al., 2017, MNRAS, 468, 2447
Ponti et al., 2018a, MNRAS, 473, 2304
Ponti et al., 2018b, MNRAS, 481, L94
Vasilopoulos et al., 2016, MNRAS, 461, 1875
Vasilopoulos et al., 2017a, MNRAS, 470, 1971
Vasilopoulos et al., 2017b, MNRAS, 470, 4354
Vasilopoulos et al., 2018a, MNRAS, 475, 220
Vasilopoulos et al., 2018b, A&A, 620, L12
Vasilopoulos, 2018, PhD thesis, Technical University Munich



Frank Haberl



Thomas Boller



Stefania Carpano



Gabriele Ponti



Georgios Vasilopoulos

(Other HE group members include: W. Becker, J. Greiner, F. Hofmann, C. Maitra, K. Nandra, A. Rau.
 Former members: P. Maggi, R. Sturm)

4.2.4 Transients

The study of transient astronomical events, or short ‘transients’, in the HE group utilizes MPE’s earlier investments in space (Fermi/GBM, INTEGRAL-SPI/ACS) and ground-based (GROND) instrumentation. The scientific focus over the last three years has mainly been on the prompt emission and afterglow modelling of GRBs and their use as probes of the high-redshift Universe, as well as the study of super-luminous supernovae. Moreover, members of the HE group have contributed significantly to opening the new era of multi-messenger astrophysics through the discovery and study of the electromagnetic counterpart to gravitational wave signal of the first confirmed NS-NS merger event.

GW170817 Fermi/GBM prompt emission:

The detection of the gravitational wave event GW170817 by LIGO and Virgo was accompanied by the independent detection of the short GRB170817A by Fermi/GBM, a discovery which was made by MPE’s Andreas von Kienlin. GBM was the first to trigger on this new γ -ray source, 1.7s after the merger of two neutron stars. This kicked off an enormous follow-up campaign which eventually led to the detection of the kilonova and off-axis afterglow and confirmed that binary neutron star mergers are the progenitors of at least some short GRBs. Further analysis of the GBM data provided constraints on the geometry and emission process (Bégué et al. 2017). Members of the HE group were directly involved in the follow-up campaign by releasing the first public Gamma-ray Coordinates Network (GCN) circular, announcing GBMs detection of the GRB and designating it as GRB170817A (von Kienlin et al. 2017). In addition, important contribution to several papers based on the **Fermi**/GBM data from GRB170817A were made, which already accumulated >1000 citations. GBM’s crucial role was recognized also by being awarded the 2018 AAS HEAD Rossi Prize to the **Fermi**/GBM team. A weaker coincident γ -ray signal

was also observed in the data of a second instrument for which MPE played a major role in the hardware development - the Anti-Coincidence Shield (ACS) of Spectrometer SPI onboard ESA’s INTEGRAL mission (Figure 4.2.9).

GW170817 GROND kilonova observations:

The kilonova AT2017gfo associated to GW170817A was intensively monitored with GROND at the MPE 2.2m telescope (Figure 4.2.10). GROND’s capability of observing in 7-bands simultaneously allowed to follow the multi-band temporal evolution, revealing a rapid decline at optical wavelengths by ~ 4 mag in the first 5d. The NIR emission instead remained initially flat before eventually steepening ~ 7 d after the merger event. Fitting semi-analytical models to the bolometric light curve found a power source-function term of $\beta = -1.2 \pm 0.3$, which provides a good match to the theoretical expectations from r-process radioactivity. The best-fit model also suggests a low opacity of $\kappa = 0.1 \text{ cm}^2 \text{ g}^{-1}$, indicating that light r-process elements are dominant within the ejecta, which is about $0.04 M_{\odot}$. The GROND multi-band light curve provides tantalizing evidence that kilonovae are a prime source of heavy elements in the Universe (Smartt, Chen et al. 2017).

The γ -ray - gravitational wave connection:

In addition to the study of the GW170817 members of the HE group have performed a search for short GRBs in the 10-year catalogue of Fermi/GBM that show similar properties. A total of 12 new candidates were found (von Kienlin et al. 2019). The similarity of the candidates is likely caused by the same processes that shaped the gamma-ray signal of GRB 170817, thus providing evidence of a nearby sample of short GRBs resulting from binary NS merger events. From this finding the prediction was made, that Fermi-GBM will trigger on-board on about one burst similar to GW170817A per year. Prior

to the detection of the γ -ray emission from the binary NS merger, Fermi/GBM had hinted at the presence of a weak electromagnetic signal above 50keV related to the binary black hole merger event GW150914. Although this result is still debated (see also Poster Booklet contribution J. Greiner & J.M. Burgess) it shows that Fermi/GBM could add clarification to the question whether a merging black hole/black hole system could produce an electromagnetic emission.

GRB afterglows:

The X-ray to radio afterglows of GRBs are thought to arise from synchrotron emission from a narrow relativistic blast wave deceler-

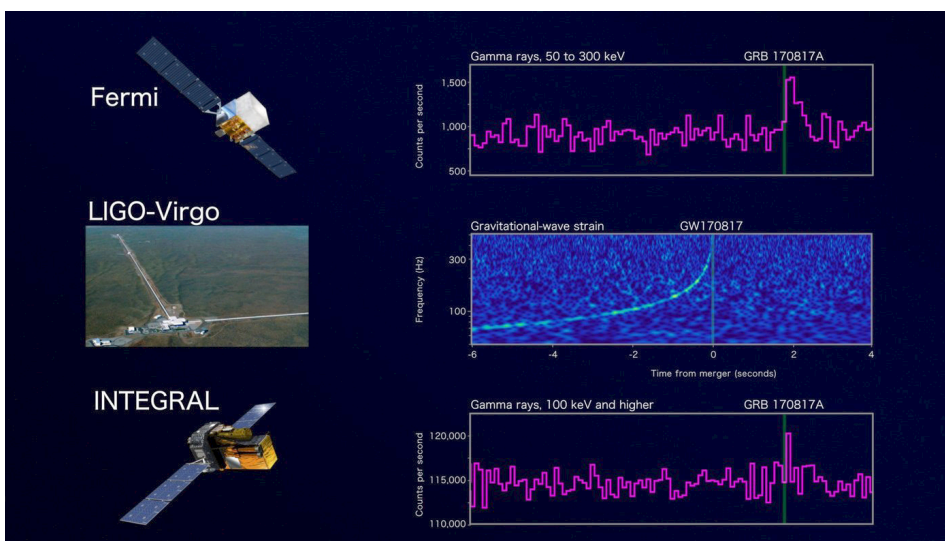


Fig. 4.2.9 Fermi/GBM, LIGO, and INTEGRAL SPI-ACS light curves of GW170817A aka GRB 170817A, discovered by MPE.

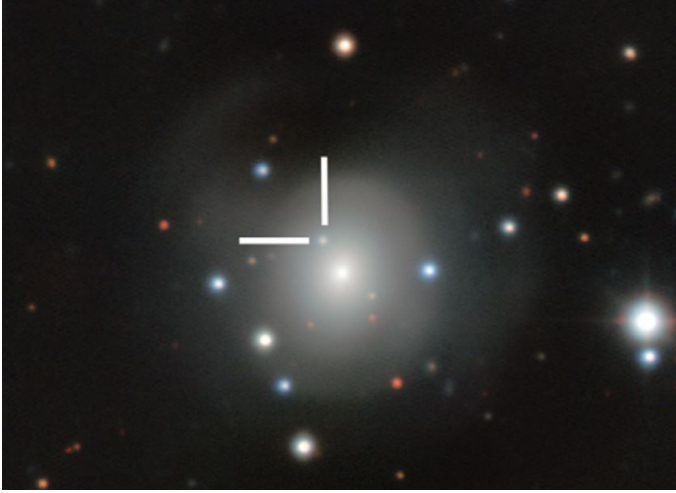


Fig. 4.2.10 GROND color image of the kilonova AT2017gfo and its host galaxy. (Credit: ESO/S.J. Smartt & T.-W. Chen)

ating in the medium surrounding the progenitor. A more sophisticated framework has previously been developed in the group that allows to directly fit the underlying physical parameters to multi-epoch multi-band photometric data of afterglows. Using Swift/XRT and GROND observations of the short GRB 150424A it was demonstrated that its extended emission could be linked to the prolonged energy injection arising from the spin-down of a magnetar that formed during the GRB (Knust et al. 2017). A potentially important role of energy injection was also found in the study of the long duration GRB 121024A. Using X-ray to radio data Varela et al. (2016) showed that the microphysical parameters of the relativistic shocks vary in contrast to the standard theory. The exploitation of multi-band afterglow data (here GROND and Swift/XRT) also played a crucial role in constraining the dust along the line of sight to high-redshift GRB afterglows. For a sample of $z > 4$ GRBs with X-ray and

optical/NIR coverage, Bolmer et al. (2018) found that the high-redshift host galaxies contain on average less dust than their counterparts at $z \sim 2$.

Superluminous Supernovae:

SLSNe are extremely luminous stellar explosions that outshine standard supernovae by over one order of magnitude. The GREAT (GROND-ePESSTO-ATLAS) Survey lead by T.-W. Chen has been designed to rapidly identify hot, blue (in the optical) transients, with the specific goal of finding very young SLSNe and to help constraining their formation models. Here, new transients found in the ATLAS survey, which are associated with dwarf host galaxies (as preferred by SLSN; Chen et al. 2017a), are followed with the GROND instrument. If the black-body temperature derived from the 7-color spectral energy distribution exceeds 15,000K, spectroscopic observations are initiated through the ePESSTO collaboration. This technique led to the discovery of the peculiar transient SN 2017ens. The event showed hydrogen-free spectra during the first month, which surprisingly evolved to H-rich after 150 days (Figure 4.2.11). The unique spectroscopic evolution of SN 2017ens together with its high luminosity poses challenges to all currently known SN scenarios (Chen et al. 2018).

Selected References:

- Bégué, D., et al., 2017, *ApJ*, 851, 19
 Bolmer, J., et al. 2018, *A&A* 609, A62
 Chen, T.-W., et al. 2017a, *MNRAS*, 470, 3566
 Chen, T.-W., et al. 2017b, *A&A*, 602, A9
 Chen, T.-W., et al. 2017c, *ApJL*, 849, 4
 Chen, T.-W., et al. 2018, *ApJ*, 867L, 31
 Knust, F., et al., *A&A* 607, A84
 Smartt, S. J., Chen, T.-W., et al. 2017, *Nature*, 551, 75
 von Kienlin, A., et al. 2019, *arXiv:1901.06158*
 Varela, K., et al. 2016, *A&A*, 589, A3.

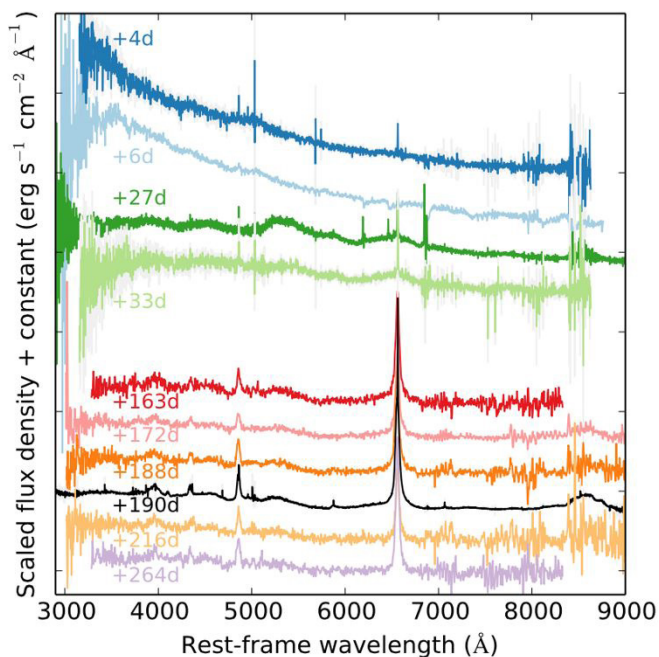


Fig. 2.4.11 Spectroscopic evolution of SN 2017ens (from Chen et al. 2018).



Arne Rau



Ting-Wan Chen



Andreas v. Kienlin

(Other HE group members include: D. Bégué, F. Berlato, J.M. Burgess, J. Bolmer, F. Knust, J. Greiner, A. Malyali, T. Schweyer, K. Varela, H.-F. Yu)

4.2.5 Sofja Kovalevskaja Group: Probing Distant Galaxies with Long Gamma Ray Bursts

Long gamma ray bursts (GRBs) are indisputably linked to massive stars, and their vast distances, and highly luminous emission offer an effective and unique probe of the interstellar properties and chemical composition of galaxies in the young Universe. The research within the Sofja Kovalevskaja (SK) group of Patricia Schady focused on exploiting these cosmic probes, in particular to study the evolution of chemical enrichment, interstellar dust and the conditions of star formation through cosmic time.

The chemical evolution through cosmic time:

Long GRBs offer an alternative way to study the metal enrichment and dust contents of distant, star forming galaxies, acting as a beacon shining through their host galaxy. From the absorption from intervening gas, metals and dust imprinted on their luminous and broadband afterglow, the SK group has studied the origin and composition of high redshift interstellar dust (Schady 2017, Bolmer et al. 2018, Wiseman et al. 2017a), measured accurate gas-phase metallicities (Wiseman et al. 2017a, Bolmer et al. 2019), and probed galactic scale inflows and outflows (Wiseman et al. 2017b) in distant, low mass galaxies that would otherwise remain unseen. To fully exploit GRBs as cosmic probes, the group has also studied other accurate tracers of chemical enrichment, with the ultimate aim of mapping the line-of-sight properties probed by GRBs onto the same scale as more classical, emission-based observations of galaxies (Yates et al. 2019).

The origin of dust in the early Universe:

Interstellar dust acts as a coolant and as a catalyst for molecular gas formation, providing a core-ingredient of star formation. Despite the importance of dust, its formation, composition and environmental dependencies are still poorly understood. Just as GRBs provide a powerful probe of the metals within the interstellar medium of distant galaxies, they offer a detailed view of interstellar dust. It is, however, important to address selection effects that bias against dusty GRB lines of sight. The SK group addressed this issue by using the MPG GRB Optical and Near-IR Detector (GROND) instrument and the UV, optical and near-IR spectrograph, **X-shooter**, to study the host galaxies of dust enshrouded GRB sight-lines that have historically been selected out of GRB afterglow and host galaxy samples. In Wiseman et al. (2017b) and Bolmer et al. (2018) we used these data to investigate the properties and formation channels of dust in the early Universe, finding in-situ dust formation to be a dominant grain growth mechanism in the young Universe.

Tracing star-formation with GRBs:

Long GRBs undeniably trace massive stellar evolution without the drawbacks of more traditional tracers of star-formation that systematically miss lower mass and less luminous galaxies. Nevertheless, a limitation is that the precise details of the properties of their progenitors, and thus the environments that are traced, is still poorly understood. The SK group studied the local environments of the two nearest long GRBs in order to place stringent constraints on the properties of their progenitor stars. This study used the state-of-the-art Multi-Unit Spectroscopic Explorer (MUSE) instrument, which provides sensitive, spatially resolved spectral information. Our analysis suggested two very different progenitor systems; the first likely being a massive, Wolf-Rayet, sub-solar metallicity star, as expected from classical GRB predictions (Krühler et al. 2017), and the second likely originating from a binary system with little dependence on metallicity (Tanga et al. 2018).

Selected References:

Bolmer, J. et al. 2018, *A&A*, 609, 62
 Bolmer, J. et al. 2019, *A&A*, in press (arXiv:1810.06403)
 Krühler, T. et al. 2017, *A&A*, 602, 85
 Schady, P. 2017, *Royal Soc. Open Sci.*, 4, 170304
 Tanga, M. et al. 2018, *A&A*, 615, 136
 Wiseman, P. et al. 2017a, *A&A*, 599, 24
 Wiseman, P. et al. 2017b, *A&A*, 607, 107
 Yates, R. et al. 2019, *A&A*, submitted (arXiv:1901.02890)



Patricia Schady

(Other SK members include: J. Bolmer, T-W. Chen. Former members: J. Graham, T. Krühler, P. Wiseman, R. Yates)

4.2.6 Galactic Structure and the ISM

The dynamics and evolution of the interstellar medium (ISM) develops characteristic interstellar cavities, loops and chimneys. These blow out from the Galaxy's disk into its halo, and provide an important observable part of galactic outflows that feeds the intergalactic medium with metals. It has been recognized that only a proper understanding of galactic processes at the kpc scale, or below, will enable an understanding of the galaxy properties that drive their long-term cosmic evolution, in particular enrichment with metals through star formation and their nucleosynthesis ejecta. Members of the HE group study the structure and dynamics of the interstellar medium (ISM) in the Milky Way and nearby galaxies using a variety of tracers at different wavelengths. Thermal emission can be detected at soft X-ray energies with **XMM-Newton** and **Chandra**, while the emission from relativistic particles, from radioactive nuclei, and positron annihilation can be traced in soft gamma rays with **INTEGRAL**.

The Galactic Centre Chimneys:

Evidence has increasingly mounted in recent decades that outflows of matter and energy from the central parsecs of our Galaxy have shaped the observed structure of the Milky Way on a variety of larger scales. On scales of about 15 pc, the Galactic centre shows bipolar lobes both in X-rays and radio, indicating broadly collimated outflows from the centre, directed perpendicular to the Galactic plane. On far larger scales, approaching the size of the Galaxy itself, gamma-ray observations have identified the "Fermi Bubble" features, implying that our Galactic centre had a period of active energy release leading to the production of relativistic particles that now populate huge cavities on both sides of the Galactic plane. The X-ray maps from the ROSAT all-sky survey showed that the edges of these cavities close to the Galactic plane are bright in X-rays. At intermediate scales (~ 150 pc), radio astronomers have found the Galactic Centre Lobe, an apparent bubble of emission seen only at positive Galactic latitudes. Using XMM-Newton, we found prominent X-ray structures on these intermediate scales above and below the plane (Ponti et al. 2019), which appear to connect the Galactic centre region to the Fermi bubbles (Figure 4.2.12). We propose that these structures, which we term the "Galactic Centre Chimneys", constitute exhaust channels through which energy and mass, injected by a quasi-continuous train of episodic events at the Galactic centre, are transported from the central parsecs to the base of the Fermi bubbles.

The Interstellar Dust:

The main components of the ISM comprise gas, dust and molecules. During the past few decades the properties and distribution of interstellar gas and molecular clouds have been studied in great detail; in comparison, there is

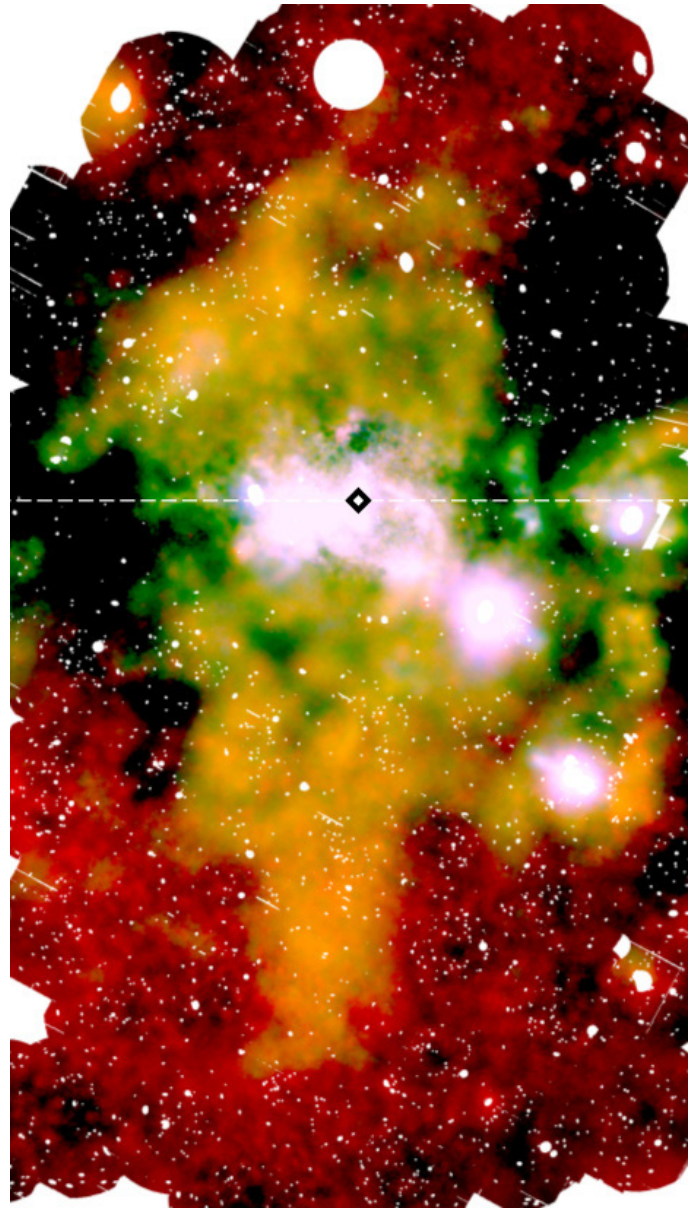


Fig. 4.2.12 XMM-Newton X-ray map of the central 300 pc x 500 pc of the Milky Way with point sources removed. The RGB image shows the integrated emission in the energy range 1.5-2.6 keV (red); 2.35 to 2.56 keV (green), corresponding to the SXV transition; and continuum emission in the 2.7-2.97 keV band (blue). SgrA*, the electromagnetic counterpart of the supermassive black hole, and the central cluster of massive stars are located at the centre. A coherent edge-brightened shell-like feature with a diameter of ~ 160 pc, dubbed the northern Chimney, is present north of SgrA*. A bright and elongated feature is also seen on the opposite side of the Galactic plane, the southern Chimney. The north and south features have comparable brightness, extent and colour, suggesting a similar emission process.

relatively little knowledge about the properties and distribution of the interstellar dust, due to the lack of observational methods. We conducted a study of the X-ray halos around some bright X-ray sources in the direction of the Galactic centre using data from the **XMM-Newton** and **Chandra** observatories (Jin et al. 2017, 2018). Our studies confirm that the observed halos are produced by the

dust grains in the foreground ISM through Mie scattering of X-ray photons. Our detailed investigations of the halo profiles and variability show that most of the dust in the direction of the Galactic Centre should be located in the Galactic disk rather than in the central molecular zone. We also identified a dust layer in the solar neighbourhood, which is in good agreement with previous optical studies of the local ISM using dust extinction. Our research suggests that the investigation of X-ray dust scattering halos is a powerful method for the exploration of the properties and spatial distribution of interstellar dust. It can provide an important high-energy window for the study of the ISM, independent from conventional techniques in low-energy bands. Therefore, this tool can be used in future studies, as a prospect, for the construction of the 3D ISM distribution of the Milky Way.

Modelling the radioactive ISM: Hydrodynamic simulations of interstellar gas evolution challenges even today's computing resources. Typically employed smooth-particle hydrodynamics simulations can only trace many thousands of stars at their resolution limit, thus must incorporate assumptions that need observational verification. Global radioactive afterglow from the decay of ^{26}Al , with its decay time of $\sim 10^6$ years and a gamma-ray line at 1809 keV, is an excellent tracer of interstellar dynamics on these time scales. A recent galaxy-scale simulation of the interstellar dynamics on the million-years time scale, implemented through radioactive tracer isotopes ^{26}Al and ^{60}Fe , has been compared to the gamma-ray data from **INTEGRAL/SPI** (Diehl et al. 2018) observations. We find that the large-scale aspects of such massive-star action as observed, producing a sizeable number of cavities with kpc sizes, are not yet properly represented by the physical models that form the basis of simulations. We therefore build a model from well-observed nearby interstellar morphologies, supplemented on larger scales by characteristics taken from current stellar evolution properties as combined with interstellar dynamics inferred from such simulations. This will allow us to learn about the distributions of massive-star groups and their interstellar impacts throughout our Galaxy, complementing what has been inferred from external galaxies. The action of massive stars with their winds and supernovae on their surroundings eventually provides feedback to the star-formation efficiency of interstellar gas. This has been studied in specific nearby and well-observed regions and their characteristic stellar groups by the INTEGRAL team. Combining this with hydrodynamic simulations, the nearby Scorpius-Centaurus groups of massive stars have been understood to form a sequence of star forming and supernova events reminiscent of a nearby cosmic firework (Krause et al. 2018).

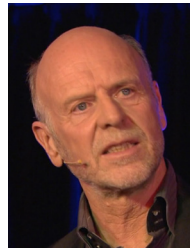
Positrons in the ISM:

Positrons are relativistic particles that stand out through an observational signature with a characteristic gamma-ray line at 511 keV, emitted when positrons annihilate in the ISM. In Siegert et al. (2016a, 2016b), we have

analyzed INTEGRAL/SPI observations to find that the latitude extent of the annihilation emission is much larger than that of Galactic gas or stars, suggesting that chimneys and large cavities also play a significant role in the transport of positrons. We compared the large-scale motion of positron-annihilating phases of the ISM with that observed from radioactive ^{26}Al . This shows that the enhanced Doppler velocity seen for ^{26}Al , which characterizes large-scale Galactic rotation plus expansion in large cavities that extend from spiral arms in forward direction into inter-arm regions, may be compatible with annihilating-positron motion; but positrons tend to show smaller velocities that also could overlap with cold-gas cloud Galactic rotation, and the bright bulge appears to even show absence of any Galactic rotation.

Selected References:

Diehl et al., 2018, *A&A*, 611, 12
 Ponti et al., 2019, *Nature*, in press J
 in et al., 2018, *MNRAS*, 477, 3480
 Jin et al., 2017, *MNRAS*, 468, 2532
 Krause et al., 2018, *A&A*, 619, 120
 Siegert et al., 2016a, *A&A*, 586, 84
 Siegert et al., 2016b, *A&A*, 595, 25.



Roland Diehl



Frank Haberl



Florian Hofmann

(Other HE group members include: J. Greiner, M. Freyberg, C. Jin, C. Maitra, M. Pleintinger, G. Ponti, T. Siegert. Former members: M. Krause, D. Kröll, P. Maggi)

4.3 Projects

4.3.1 eROSITA

eROSITA is the primary telescope on board of the Russian/German **Spectrum-Roentgen-Gamma** Mission (SRG). The main scientific goal is to perform an X-ray all-sky survey, more than 20 times more sensitive than the previous **ROSAT** survey. In addition, eROSITA will provide far better spectroscopic capability. The design of the instrument is driven by the goal to detect 100,000 clusters of galaxies in order to constrain the cosmological parameters. eROSITA was shipped to Russia already in January 2017. Meanwhile the integration and all tests have been completed, and we are awaiting the launch which is scheduled for June 21, 2019. SRG will be launched from the Cosmodrome in Baikonur/Kazakhstan using a Proton-M rocket, the most powerful Russian launch vehicle. After a cruise to the Lagrangian 2 point, eROSITA will start a four years all-sky survey. In addition to clusters of galaxies, eROSITA will detect around three million black holes in the centres of galaxies, and unprecedented samples of all other X-ray source classes, revolutionizing X-ray survey astronomy.

All technical responsibility for eROSITA was taken fully by MPE, limiting sub-contracts to manufacturing. By doing so we kept complete control over the instrument, without the need to make major compromises, and were able to preserve the specifications defined at the start of the project, despite having to overcome many major technical hurdles. As a result of this scheme we have constructed a state-of-the-art instrument at very reasonable cost. A detailed overview of the sub-systems and related technical solutions was already provided within the last report, but we summarise this again here:

eROSITA Instrument: The instrument consists of the optical bench, a carbon fibre structure with two main subassemblies, the optical bench and the hexapod-type interface structure. At its front end seven identical Mirror Assemblies are mounted, each comprising Wolter-I modules with 54 nested shells, an X-ray Baffle in front, and a magnetic deflector at its read end. In the foci of the mirrors at the lower end of the structure, there are seven Camera Assemblies mounted, each consisting of a Filter Wheel, the pnCCD Camera itself, and the associated Camera Electronics. Two

(redundant) Interface and Thermal Controllers (ITC) provides thermal control of the instrument and handles the data flow from and to the Cameras on one side, and the S/C on the other side. The pnCCDs are cooled down to -95°C passively by means of a complicated heatpipe system and large area radiators. Two star-sensors and solar sensors complete the instrument.

Assembly, Integration, and Test:

After its complete assembly, eROSITA underwent the usual acceptance tests. The thermal vacuum test in our PANTER facility lasted for two months. It was followed by vibration and other tests at the end of 2016. In January 2017 eROSITA was finally shipped to the main contractor Lavochkin Association (NPOL) in Khimky near Moscow. Since then a series of tests have been performed until the entirely assembled and tested SRG became ready for packing (as of March 2019). The transport to the Cosmodrome in Baikonur is planned for late April 2019, the launch for June 21/22.

Ground Segment:

Activities ahead of launch are focused on assuring smooth operations of the eROSITA telescope once in orbit, encompassing mission planning, day to day operation of the telescope, timely delivery of high quality calibrated data products, as well as providing user friendly software tools for an in depth analysis of the data. Specific activities include: 1) Further refining and testing communication and data exchange procedures with the Russian project partners. 2) Final integration and exten-



Fig. 4.3.1 Completely assembled SRG with its primary telescope eROSITA and the Russian ART-XC telescope (courtesy Lavochkin Association).

sive testing of the standard data processing pipeline both with simulated data and where applicable with data from ground tests performed with the telescope 3) Further improving and extending the interactive data analysis software package based on user feedback.

Mission planning:

Mission planning activities are performed jointly by the German and Russian project partners. While orbit predictions and times of planned orbit correction maneuvers are provided by the Russian side, optimized all-sky survey scanning patterns and observing time-lines satisfying both Sun and Earth angle constraints due spacecraft geometry, on-board antenna characteristics, and ground antenna visibility are determined by the German mission planning team at MPE and Hamburger Sternwarte.

Ground antennae, operation and data centers:

Communication with SRG will be conducted via ground antennae near Moscow and Vladivostok. Operation centers are located at NPOL for spacecraft operation and at the Space Research Institute IKI for science instrument operation on the Russian side, as well as, for eROSITA, at MPE. Two-way data and communication links between the operation centers are established. Science data centers are maintained at MPE and IKI.

Operations during ground contacts:

The characteristics of the L2 halo orbit of SRG and geographic location of the ground antennas allow for few to up to twelve hours of spacecraft visibility from the ground antenna sites in each 24 hour period, depending on the season. An agreed upon time slot of four hours will be available each day for spacecraft and science instrument commanding and data reception. Up to 600 Mbyte of science and housekeeping data will be downloaded each day. The eROSITA instrument team will initially be located at the Russian SRG operation centers at NPOL and IKI to allow for short reaction times during critical parts of the eROSITA commissioning phase. Routine eROSITA operations will be conducted from an eROSITA control room at MPE.

eROSITA Science Analysis Software System:

The eSASS data analysis package comprises software tasks for pipeline operation and for interactive data analysis. While being specifically developed for eROSITA, the eSASS package is broadly based on experience and in part on the code of the ROSAT and XMM-Newton data analysis software. eSASS tasks function as command line tools providing an FTOOLS-like command line interface, while also supporting a dedicated pipeline parameter system. eSASS tasks intended for interactive analysis comprise event calibration, event selection and binning, exposure, background, and sensitivity map creation, source detection, spectra and light-curve extraction. The interactive eSASS tasks are intended to allow the users to repeat and further refine and extend the standard analysis performed by the data processing pipeline. Work on further code enhancements is ongoing; initial versions of the eSASS package have been made available to the eROSITA user community since 2014.

Calibration database:

The eROSITA data analysis environment makes use of the HEASARC calibration database (CALDB) framework for storing and managing calibration files. An additional versioning layer was implemented on top of the CALDB framework for tying calibration file versions to software releases. The eROSITA CALDB is made available for download to the eROSITA user community and the appropriate calibration files are accessed transparently by the eSASS data analysis tasks with no need for user intervention. The eROSITA CALDB contains calibration datasets for event calibration, detector response and effective areas, detector maps, telescope boresight, vignetting, and point response, among others.

Data analysis pipeline:

The eROSITA data analysis pipeline consists of four main task chains, organized into event calibration, image and exposure map creation, source detection, and the creation of source specific products such as spectra and light-curves. It is fed by a preprocessor which also provides input for a near real-time facility for instrument health monitoring and quick-look time domain science (contributed by Remeis-Sternwarte Bamberg). A pipeline control environment triggers task chain execution and performs housekeeping activities. The pipeline is designed to process data from each of the three principal observing modes of the SRG spacecraft, all-sky survey observations, pointings at individual targets, and scan-mode observations, which cover fields of up to $12.5^\circ \times 12.5^\circ$ with a predefined scanning pattern. All-sky survey data are processed in 4700 overlapping sky tiles of size $3.6^\circ \times 3.6^\circ$. After each ground contact the telemetry data frames received from the spacecraft are processed by the respective pipeline task chains. The telescope task chain collects X-ray event, associated housekeeping and attitude data for each eROSITA telescope, initializes and fills event file data structures, performs an X-ray event pattern analysis and computes calibrated photon energies and sky positions. Good time intervals based on house-keeping quality ranges are added to the event files and the fully calibrated event files are copied to staging areas for further processing.

For sky areas which have received new data, the exposure chain is triggered, which creates a set of merged and per telescope event files and images in each of four standard energy bands. The subsequent detection chain runs a sequence of algorithms, creating exposure, background, and sensitivity maps, as well as X-ray source catalogs. Point sources are characterized both by their best fit parameters employing a sophisticated shapelet-based point response model as well as by aperture photometry in optimized apertures, while extended objects are fit by beta profiles convolved with the point response. Alternative wavelet-based detection schemes are under consideration. In the case of all-sky survey processing, source detection runs will be performed on short-term (single scan), medium-term (six month surveys), and long-term (full cumulative four year surveys) time scales. Finally, the source chain extracts source and background spectra, as well as light-curves for each of the detected

X-ray sources and best fit spectral parameters and variability indicators are determined. Unique source IDs are assigned and data quality checks are performed.

Data access:

Access to calibrated eROSITA data products by eROSITA consortium members is facilitated via a browser-based data access tool. Users may request calibrated data products, such as calibrated X-ray event lists, images and maps, source catalogs and associated source specific data products for sky regions of interest. Requested datasets are retrieved from the archive and made available for password-protected downloading. In addition, an eROSITA source browser allowing registered users to query, browse, inspect and annotate catalogue, source and image level eROSITA data products is under development.

Selected References:

Brunner et al. 2018, Proc. of SPIE, 10699, 5GB
Coutinho et al., 2018 Proc. of SPIE, 10699, 5FC
Eder et al., 2018, Proc. of SPIE, 10699, 1ZE
Predehl et al., 2018, Proc. of SPIE, 10699, 5HP

Josef Eder



Hermann Brunner



Peter Predehl



(Other HE group members include: T. Boller, H. Bräuninger, H. Brunner, V. Burwitz, D. Coutinho, K. Dennerl, M. Freyberg, P. Friedrich, R. Gaida, Chr. Grossberger, F. Haberl, G. Hartner, A. v. Kienlin, N. Meidinger, A. Merloni, K. Nandra, E. Pfeffermann, M. Salvato, J. Sanders. Former members: N. Clerc, T. Dwelly, V. Emberger, T. Er-aerds, M. Fürmetz, A. Georgakakis)

4.3.2 Athena

Athena – the Advanced Telescope for High-ENERgy Astrophysics – is ESA's next large X-ray telescope designed to address the 'The Hot and Energetic Universe' science theme. It is an L-class mission in the Cosmic Vision program with two scientific instruments, the Wide Field Imager (WFI) and X-ray Integral Field Unit (X-IFU). These are complementary interchangeable focal plane cameras behind a novel Silicon Pore Optics mirror system providing unprecedented X-ray survey power and high-resolution spectroscopy, respectively. The WFI is being developed by an international consortium under the leadership of MPE and is the major hardware project of the HE group beyond eROSITA. The group is deeply involved in the Athena mission overall, with K. Nandra being Lead Scientist of the Athena Science Study Team and several group members chairing scientific and infrastructure working groups and topical panels. Furthermore, MPE is making a major contribution to the Athena optics development with the PANTER X-ray test facility.

The Wide Field Imager (WFI) is a powerful new X-ray camera for the Athena X-ray observatory, which has been designed to meet the requirements of the 'Hot and Energetic Universe' science theme. The instrument is based on unique Silicon DEPFET technology developed in the Semiconductor Laboratory of the Max Planck Society. The DEPFET detectors provide the WFI's 40'x40' large field of view, state-of-the-art energy resolution, low noise, fast readout, and high time resolution, with excellent radiation hardness. These properties, in combination with the unprecedented effective area and wide field of the Athena telescope, will provide breakthrough capabilities in wide-field X-ray imaging spectroscopy (see Table 1 for an overview). The WFI will, for example: probe the typical activity of supermassive black holes at $z > 6$; perform a complete and quantitative census of this accretion activity at $z = 1-4$, including the most obscured objects; pinpoint the hot gas occupying the most massive dark matter haloes at $z > 2$ when the first groups and clusters of galaxies formed; measure the temperature and abundances of clusters of galaxies out to their virial radius; perform spectral-timing measurements of bright compact sources to determine the geometry of the innermost accreting regions.

The ambitious WFI science is enabled by a Large Detector Array (LDA) consisting of four large-format (512x512 pixel) DEPFET devices, delivering a field of view of 40'x40'. The pixel size corresponds to 2.3" on the sky, oversampling the expected angular resolution of the Athena mirror (5" HEW) to provide accurate imaging and source positioning. A fifth DEPFET is used for the Fast Detector (FD) that is optimized for bright sources and typically used out-of-focus to improve the count rate capability. The DEPFET devices are controlled and read out by custom ASICs, known as Switcher-A and Veritas-2. The latter feed their signals into a total of five Detector Electronics (DE) boxes that perform the on-board frame processing (see figure 1). The output from the DE boxes is combined and fed to the spacecraft by the Instrument Control and Power-distribution Unit (ICPU), which can also perform additional processing. A conceptual design for the WFI instrument has been developed, demonstrating the basic feasibility of the system. In parallel a number of key technology developments are underway to demonstrate the performance of the detector system (prototype DEPFET and ASICs, see Fig. 4.3.2), the real-time performance of the DE, and the feasibility of the large area, thin optical blocking filter. The delivery of the Flight Instrument to ESA is due in 2028 and the Athena satellite launch to L2 is planned in 2031.

Following the Athena Instruments Consortia Consolidation (ICC) process performed by ESA at the end of 2018, the WFI consortium, consisting of scientific Institutes and

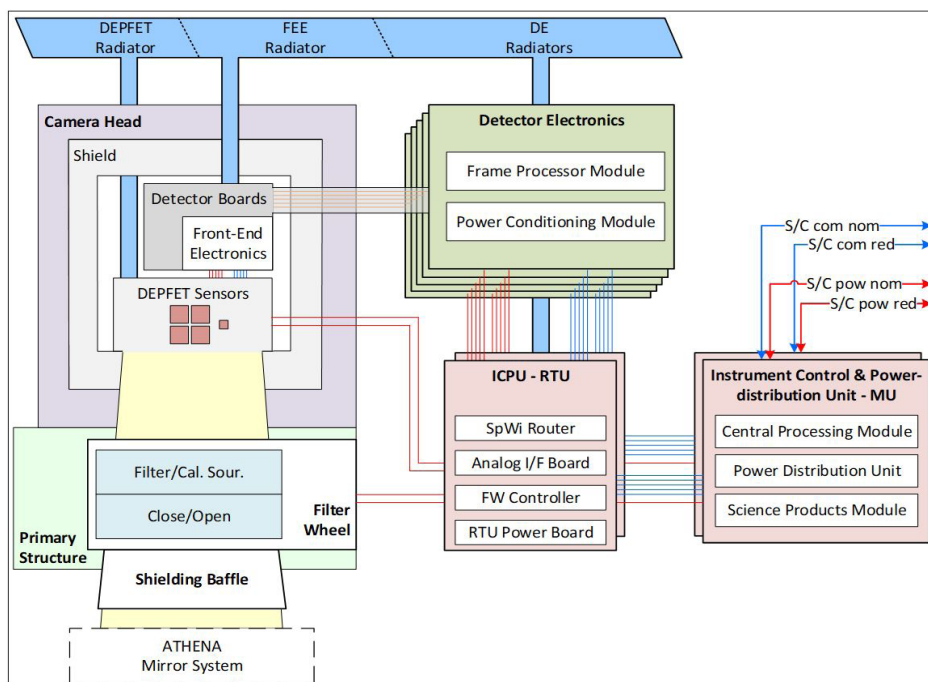


Fig. 4.3.2 Main WFI subsystems: Filter Wheel with baffle, Camera Head with large detector array and fast detector, Detector Electronics (5 units), and Instrument Control and Power-distribution Unit (Main and Remote Terminal Unit, both nominal and redundant). Communication and power interfaces are drawn in blue and red, respectively. Also shown is the thermal system with separate cooling chains for the DEPFET sensor, the Front-End Electronics, and the Detector Electronics.

universities from ten ESA member states and the USA, was officially endorsed. The overall project management is performed by the WFI Project Office at MPE, which hosts the instrument Principal Investigator K. Nandra, Project Manager N. Meidinger, Project Scientist A. Rau, Lead System Engineer M. Plattner, and the Product Assurance Manager A. von Kienlin. Instrument development work packages, including those for the WFI Instrument Science Center (WISC), have been allocated to a responsible partner, supported by their national funding agency and/or institutional resources. Almost simultaneously to the ICC, a Preliminary Requirements Review (PRR) of the WFI instrument was jointly performed by ESA and the German Space Agency DLR. After review and discussion of the provided data pack, the WFI PRR was successfully concluded. Further

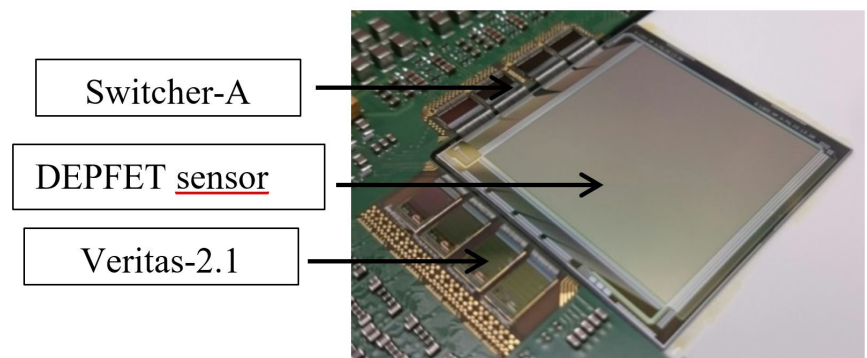


Fig. 4.3.3 Prototype WFI detector with 256x256 pixel sensor. The four readout ASICs are located to the left and the four control ASICs are shown top left on the photo.

details about the WFI instrument development can be found in the 'Abstract Booklet' in the article "The Wide Field Imager Instrument for Athena" and further associated articles.

Parameter	Performance			
Energy Range	0.2-15 <u>keV</u>			
	<u>0.2 keV</u>	<u>1 keV</u>	<u>7 keV</u>	<u>10 keV</u>
Quantum Efficiency; with external filter	5.8 %	83.1 %	95.6 %	92.2 %
Quantum Efficiency; w/o external filter	11.7 %	93.2 %	99.7 %	96.3 %
Eff. Area; on-axis, w/ external filter	0.082 m ²	1.19 m ²	0.17 m ²	0.055 m ²
Eff. Area; on-axis, w/o external filter	0.162 m ²	1.33 m ²	0.18 m ²	0.057 m ²
Energy Resolution (end-of-life)		<80 eV	<170 eV	
Pixel Size	130 μm × 130 μm (i.e. 2.24" × 2.24")			
Positional Accuracy	<1" (99.7 % confidence)			
Field of View	LDA		FD	
	40.17' × 40.17' (outer envelope)		2.38' × 2.38'	
Frame time	5 <u>ms</u>		80 μs	
FD Count Rate Capability*	1 Crab: ~0.3 % pile-up, ~95 % throughput (w/ standard filter) 15 Crab: ~1 % pile-up, ~93 % throughput (w/ 100μm Be filter)			
Instrumental Background	~5x10 ⁻³ cnt/s/cm ² /keV (2-7 keV)			

Table 4.3.1 Instrument Performance Parameters



Norbert Meidinger



Arne Rau



Kirpal Nandra

Selected References:

Meidinger, N., et al., 2018, *Proc. of SPIE*, 10699, 1F
 Meidinger, N., et al., 2015, *JATIS*, 1, 1, 014006-1
 Nandra, K., et al., 2013, *arXiv* 1306.2307
 Rau, A., et al., 2016, *SPIE* 9905-79

(Other HE group members include: R. Andritschke, A. Behrens, M. Bonholzer, V. Emberger, T. Eraerds, G. Hauser, B. Köglmeier, A. Lederhuber, J. Müller-Seidlitz, S. Obergassel, S. Ott, D. Pietschner, A. Rau, J. Reiffers, R. Strecker, J. Tran, W. Treberspurg, A. von Kienlin. Former members: A. Koch, M. Mannhard, M. Fürmetz)

4.3.3 Einstein Probe

Einstein Probe (EP) is a small satellite project of the Chinese Academy of Sciences (CAS) focussed on the detection and follow-up of transient and variable cosmic X-ray sources. The mission is planned for launch at the end of 2022 or early 2023, with a nominal lifetime of three years, with two years possible extension as a goal. The satellite shall operate in a LEO circular orbit of altitude of 600-650 km and inclination of about 30 deg. MPE will contribute to Einstein Probe's Follow-up X-ray Telescope (FXT) in two ways: as a contractor of ESA to the X-ray optics whose design corresponds to an eROSITA Mirror Assembly, and, as its own contribution, to the X-ray camera by providing detector modules.

The Einstein Probe satellite consists of two instruments. The Wide-Field X-ray Telescope (WXT) is based on so-called lobster-eye microchannel plate optics, with a large-area focal plane detector. The WXT provides wide field coverage for the detection of transient sources and wide field monitoring of the X-ray sky in the energy band 0.5–4 keV. The Follow-up X-ray Telescope (FXT) has a narrower field of view but much larger effective area and superior spectral resolution compared to the WXT. The FXT consists of a Wolter-1 type X-ray telescope with a focal length of 1.6 m and a focal-plane camera utilising a pnCCD sensor. The mirror design is essentially identical to that of a single module of MPE's eROSITA instrument, which is due to launch aboard the German-Russian SRG mission in 2019. The FXT pnCCD and front-end readout are also the same as developed for eROSITA. Both the WXT and FXT provide sensitivities more than an order

of magnitude better than previous wide field monitors, or follow-up X-ray telescopes on previous missions devoted to X-ray transient phenomena.

The scientific interests and expertise at MPE mesh well with the EP project, and the collaboration with CAS is considered to be of significant mutual benefit. This is especially the case given the close correspondence between the design and scientific performance of the FXT and of the eROSITA telescope modules, which were designed and realised by MPE and regarding which MPE has unique expertise. Therefore, MPE is willing to provide relevant design information and the existing eROSITA mandrels for the X-ray mirror electroforming.

The Mirror Assembly and the Electron Diverter of the FXT is an ESA contribution to the EP mission. The Mirror Modules (STM, QM and FM) will be manufactured by a mirror contractor of ESA while the Electron Diverters (QM and FM) and X-ray Baffles will be produced at MPE. MPE is also responsible for the unification of Mirror Modules and X-ray Baffles to the Mirror Assemblies and for the full test programme including X-ray tests, vibration and thermal-vacuum tests and, finally, for the shipping to China. Independent from ESA's EP contribution, MPE will provide a number of detector modules (each comprising a pnCCD sensor and CAMEX type front-end readout ASICs mounted on a rigid-flex printed circuit board) for FXT, and relevant information about their operation.



Peter Friedrich



Roland Gaida



Norbert Meidinger

(Other HE group members include: M. Bradshaw, V. Burwitz, J. Eder, K. Nandra)

4.3.4 SVOM

SVOM (Space Variable Objects Monitor) is an approved Chinese-French mission to be launched in 2021. The scientific objectives of the mission evolve around two categories of GRBs: (i) the very distant events at redshift greater than 6, which constitute exceptional cosmological beacons, and (ii) the faint/soft nearby events, which allow probing the nature of the progenitors and the physics at work in the explosion. SVOM will also play a major role in the follow-up of gravitational wave sources. The payload consists of ECLAIRS, a GRB monitor, the MXT soft X-ray follow-up telescope and a 45cm visible light telescope. MPE contributes towards the French payload by providing the pnCCD for the detector of the MXT telescope in collaboration with CEA Saclay and CNES. MPE is also involved in the qualification and calibration of the lightweight square micro channel plate X-ray optics of the MXT and finally in the low energy calibration of the ECLAIRS experiment.



Vadim Burwitz

(Other HE group members include: A. Rau, N. Meidinger)

4.3.5 Operating Missions

XMM-Newton

Stability of the EPIC-pn instrument:

The in-flight calibration of the spectral response of charge-coupled device (CCD) instruments below 1.5 keV is difficult because of the lack of strong lines in the on-board calibration sources typically available. This calibration is also a function of time due to the effects of radiation damage on the CCDs and/or the accumulation of a contamination layer on the filters or CCDs. We used 1E 0102.2-7219, the brightest supernova remnant in the Small Magellanic Cloud, to measure the strength and width of the emission lines of O, Ne and Mg. The remnant is observed regularly by XMM-Newton allowing to investigate long-term changes in the response of the instrument and to do detailed cross-calibration studies with other CCD instruments on board Chandra, XMM-Newton, Suzaku, and Swift. As part of the activities of the International Astronomical Consortium for High Energy Calibration (IACHEC), we have developed a standard spectral model for 1E 0102.2-7219 and fit this model to the spectra extracted from the CCD instruments. The EPIC-pn shows no significant variations of the line strengths over the whole mission duration (see Fig. 4.3.4). No significant decrease in the line intensities

with time is found, which would be an indication for the build-up of a contamination layer, and demonstrates the extraordinary stability of the instrument.

XMM Survey Science Centre:

The SSC collaboration has consolidated its structural changes over the last 3 years, as the lead had moved from Leicester University to IRAP/Toulouse. MPE still contributes to the maintenance and development of EPIC-pn tasks, mainly due to improved and extended calibration, with synergetic effects from eROSITA. Moreover, general EPIC tasks dedicated to multi-observation and archival research have been made available for general use via the XMMSAS software package. MPE has participated in the production of the new 3XMM catalogue (with data releases DR6, DR7, and DR8, Rosen et al. 2016), with the largest number of detections in an X-ray catalog: more than 775,000 detections with more than 530,000 unique sources in ~ 1089 square degrees of sky. The next - completely new - version (4XMM) is in preparation, requiring a full reprocessing of the whole XMM-Newton science data archive.

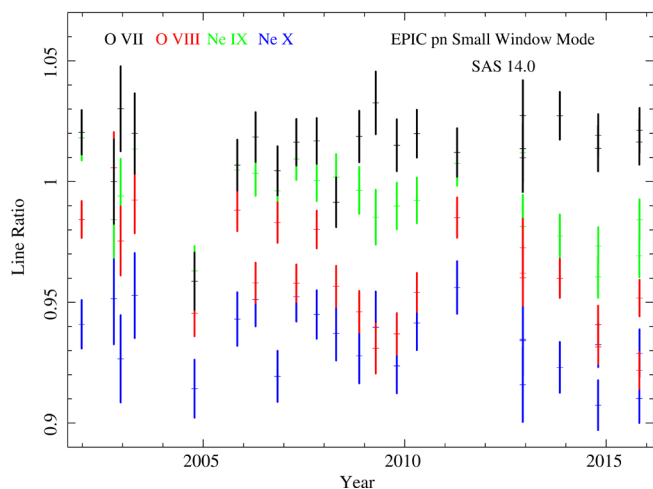


Fig. 4.3.4 Relative line strengths derived from the EPIC-pn spectra of 1E 0102.2-7219 as function of time. Line intensities are normalized to the IACHEC model.

Selected References:

Plucinsky et al., *A&A*, 597, 35 (2017)



Frank Haberl



Michael Freyberg

(Other HEG members include: Konrad Dennerl, Stefania Carpano. Former team member: Nicolas Clerc)

Chandra

The Low Energy Transmission Grating (LETG) on Chandra was built by MPE in cooperation with SRON in the Netherlands. The LETG is equipped with 530 individual grating facets. These gratings are freestanding gold wires with a period of less than $1\text{ }\mu\text{m}$ (1008 lines/mm), a technology that has been developed by MPE together with the company Heidenhain GmbH. After 20 years in space, the LETG works perfectly within its original specification. Our benefit is a continued share of the Chandra guaranteed observing time allocation.



Peter Predehl



Vadim Burwitz

Integral

INTEGRAL continues its extended mission, planned for 3 years while now in orbit for more than 15 years. Its operations are now merged with XMM and Gaia, to maximize synergies among astronomical spacecraft experts at ESOC/ESA. Improved procedures have resulted in lower fuel usage, so that the scientific mission can be continued up to its re-entry in 2029. Also, the concern about increased solar panel degradation as orbit perigee passes through radiation belts have vanished after the recent low-perigee months. In its late mission, INTEGRAL observations emphasize deep exposures (ideal for SPI and its line spectroscopy that is key science for the MPE team), and on rapid reaction to transients, with GRBs and accreting binaries among them, and fitting the MPE HEG science themes.



Andreas von Kienlin

(Other members HE group members include: R. Diehl, M. Pleintinger, T. Siegert, C. Weinberger, X. Zhang)

Fermi

The Gamma-ray Burst Monitor (GBM), the major involvement of the HEG group in NASA's Fermi mission, has successfully continued its operation in the years 2016 - 2018. On the occasion of the 10th anniversary of the Fermi mission on June 11, 2018, the GBM team is currently preparing the 4th general 10 year GBM GRB catalog (von Kienlin et al. 2019, in preparation). Since the launch of Fermi in June 2008, GBM has triggered on-board nearly 6500 times in response to short-lived impulsive bursts lasting from under a second to hundreds of seconds. This collection of triggered events includes nearly 2400 Gamma-Ray Bursts (GRBs), 1200 solar flares, 260 bursts from magnetars, and over 800 Terrestrial Gamma-ray Flashes (TGFs). The GBM team at MPE is still keeping its main responsibilities for instrument calibration, the maintenance of the GBM Team Wiki and its equal share load on the burst advocate shift system, which yielded the discovery by MPE of GRB 170817A, the kilonova associated with GW170817A.

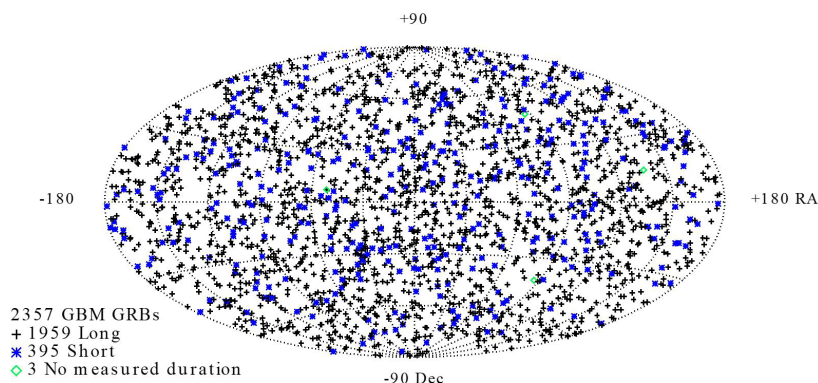


Fig. 4.3.5 FERMI GBM GRBs in first ten years of operation.



Andreas von Kienlin

4.3.6 Ground-based Projects

GROND

The Gamma-Ray Burst Optical Near-ir Detector (GROND) provides simultaneous imaging in seven filters (*g'r'i'z'JH & K*). GROND was developed by the MPE high-energy group in collaboration with the Thüringer Landessternwarte Tautenburg, and is mounted at the MPG 2.2m telescope at the ESO La Silla observatory where it started routine operations in mid-2007. It has been working with a high reliability since then.

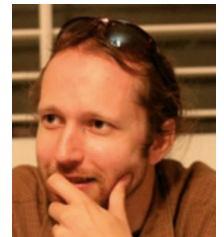
Observing time at the 2.2m telescope is shared by the MPE HE group (~30%) with MPIA Heidelberg (~60%), and the Chilean community (~10%). The HE group allocation is composed of 60 regular observing nights per year and Target of Opportunity (ToO) override access for 15% of all available nights averaged over the year. The telescope is operated locally by personnel at the La Silla observatory and ToO targets are communicated remotely or automatically in case of Rapid Response Mode activations. The latter allow unsupervised control of the telescope to slew to a new high-priority target (e.g., GRBs). Members of the HE group go to Chile for the regular observing nights.

GROND was developed to study the rapidly evolving afterglows of GRBs, measure their spectral energy distributions (SEDs), and constrain their photometric redshifts and physics. As such, it has been extremely successful, observing nearly every GRB detected by the Swift satellite visible from La Silla. The powerful concept of simultaneous observations in seven optical/NIR bands has also been utilized for studying a much broader range of transient and variable sources and GROND's portfolio now covers many research topics of the HE group. At present the ToO program is shared roughly evenly between GRB afterglows and super-luminous supernovae, with a small amount of time being devoted to the follow-up of X-ray-selected transients in preparation for eROSITA.

Following the launch of eROSITA, the usage is expected to heavily shift towards targets from this experiment.

The regular observing nights of the last semesters have been successfully used for the characterization of a large sample of X-ray selected clusters of galaxies as well as for the counterpart search for unidentified ROSAT X-ray sources. The overall scientific impact of GROND is demonstrated by ~15 refereed publications with leadership or contribution from HE. This includes three publications in *Nature* in 2017 alone, covering such diverse topics like the kilonovae of the NS-NS merger GW170817, heavy element pollution in a young supernova remnant, and accretion bursts in a young stellar object.

Access to the 2.2m telescope is regulated through an agreement with MPIA Heidelberg. The current term is coming to an end in September 2019 but a continued operation throughout the eROSITA era is foreseen.



Arne Rau

(Other HE group members include: J. Bolmer, W. Borneman, J. Chen, F. Schrey, T. Schweyer. Former members: J. Graham, T. Krühler, P. Schady)

SDSS-V

The next generation of the Sloan Digital Sky Survey (SDSS-V) will embark on a ground-breaking all-sky spectroscopic survey, anticipated to start in 2020, just after the start of the all-sky survey by MPE's eROSITA X-ray telescope. SDSS-V will be an all-sky, multi-epoch spectroscopic survey of over six million objects. Thanks to its dual-hemisphere strategy, that combines identical instruments on the Northern APO and Southern LCO 2.5m telescopes, SDSS-V is designed to decode the history of the Milky Way Galaxy, trace the emergence of the chemical elements, reveal the inner workings of stars and seek their unseen companions, and investigate the origin of planets. It will also create a contiguous spectroscopic map of the interstellar gas in the Galaxy and the Local Group that is 1,000 times larger than the current state of the art and with sufficient resolution to map the self-regulation mechanisms of galactic ecosystems.

Most importantly for MPE, SDSS-V will be the first world-class facility to perform systematic, large-scale follow-up of the eROSITA survey as part of the so-called "Black Hole Mapper" program. Thanks to that effort, MPE scientists will be able to accurately measure redshifts and physical parameters for hundreds of thousands X-ray sources (mainly AGN and clusters of galaxies) newly discovered by eROSITA.



Andrea Merloni

(Other HE group member: M. Salvato)

4MOST

The 4MOST consortium has been selected by the European Southern Observatory (ESO) to provide the ESO community with a fiber-fed spectroscopic survey facility on the VISTA telescope, as a complement to several all-sky surveys that will span the electromagnetic spectrum. Starting in 2022, 4MOST will simultaneously obtain high- and medium-resolution spectra of ~ 2400 objects distributed over a FoV of $\sim 4 \text{ deg}^2$. Its high multiplex, wavelength coverage and spectral resolution will enable detection of chemical and kinematic substructures in the halo, bulge and disc of the Milky Way, and redshift measurements of millions of distant objects, enabling studies of the evolution of galaxies, QSOs and the large-scale structure. 4MOST's capabilities are designed in particular to complement three space-based observatories of prime European interest: Gaia, eROSITA and Euclid.

Satisfying the ambitious and wide-ranging set of science goals in the allocated time requires that a unified program of observations must be devised. MPE has contributed to the hardware costs of 4MOST, and will also be responsible for its Operations System. This crucial Work Package will enable the success of the project by i) providing sophisticated simulation tools that allow the science team to plan and optimise the survey, ii) carrying out optimised medium-term scheduling using forecasting tools and feedback from previous observations, and iii) producing sets of observation blocks ready for execution at the telescope. In return, MPE will have privileged access to the instrument and data, leading two of the

main 4MOST surveys (Clusters, PI: Comparat; AGN, PI: Merloni). The first goal is to use 4MOST to survey $\sim 50,000$ southern X-ray galaxy clusters that will be discovered by eROSITA, taking spectra of 4–50 galaxies in each cluster. These observations will constrain the evolution of galaxy populations in clusters and groups, yield mass calibration, and provide competitive cosmological constraints by mapping the distribution of massive halos across space and time. The main goal of the AGN survey, instead, is to provide a complete and homogeneous optical spectroscopic follow-up of X-ray AGN detected by eROSITA to study the cosmic evolution of accreting black holes. Our simulations indicate that such a survey will harvest in 5 years ~ 50 times the current number of known X-ray selected AGN with spectroscopic redshifts, amassing a sample ~ 300 times larger than any existing one from equivalent coherent and well-defined surveys.



Andrea Merloni

(Other HE group members include: T. Boller, J. Comparat, A. Gueguen, K. Nandra, M. Salvato, W.-F. Thi. Former member: A. Finoguenov)

4.3.7 Future Space Projects

ARCUS

Over the last three years MPE has been supporting the proposal for the NASA MIDEX mission **Arcus**. The science objectives are to determine how baryons cycle in and out of galaxies including both distant and local systems, probe the feedback power emitted from the dominant ionized outflows in black hole winds and understand how stars, circumstellar disks, and exoplanet atmospheres form and evolve. The heart of the mission is a high-resolution X-ray spectrograph with a spectral resolution of $R \sim 3000$ (in the $12 \text{ \AA} - 50 \text{ \AA}$) and an effective area of 300 cm^2 based on critical angle transmission gratings and silicon pore optics (SPO). MPE has been deeply involved in the technology development for Arcus, procuring the SPOs and testing the optical layout (gratings and SPOs) of the spectrograph on single units to a prototype petal level in the PANTER X-ray test facility. These tests demonstrated the required accuracy for the alignment of the optical elements as well as the spectral resolution necessary to reach the science objectives. In August 2017 the mission was selected for a “phase A” study that was completed in May 2018 with final review

(site visit) in September 2018. In February 2019 NASA announced that Arcus was not selected for a “phase B” study, despite impeccable rankings for the science and technology. The team are exploring ways in which this innovative project can be pursued in the future.



Vadim Burwitz

(Other HE group members include: K. Nandra, J. Sanders)

eXTP

The enhanced X-ray Timing and Polarimetry mission (eXTP) is a Chinese space science mission with European contributions designed to study fundamental physics under extreme conditions of density, gravity and magnetism. The mission aims at determining the equation of state of matter at supra-nuclear density, measuring effects of QED, and understanding the dynamics of matter in strong-field gravity. MPE has been involved in the development of eXTP from a very early stage, in collaboration with colleagues CAS and in particular IHEP in Beijing. The currently-envisaged MPE contribution to eXTP is to the Spectroscopic Focusing Array (SFA), which consists of an array of 9 identical Wolter-I grazing incidence X-ray telescopes, and is mainly used for spectral and timing observations in the energy range $0.5\text{--}10 \text{ keV}$. MPE is currently performing a technology development activity on the focal plane detector for SFA. Key components of the detector are a 19-cell Silicon Drift Detector (SDD) array and a custom Application Specific Integrated Circuit (ASIC) for signal shaping and readout. This combination can deliver the required energy resolution (FWHM) of $<180 \text{ eV}$ at 6 keV in combination with time resolution $<10 \mu\text{s}$. MPE is collaborating with the MPG

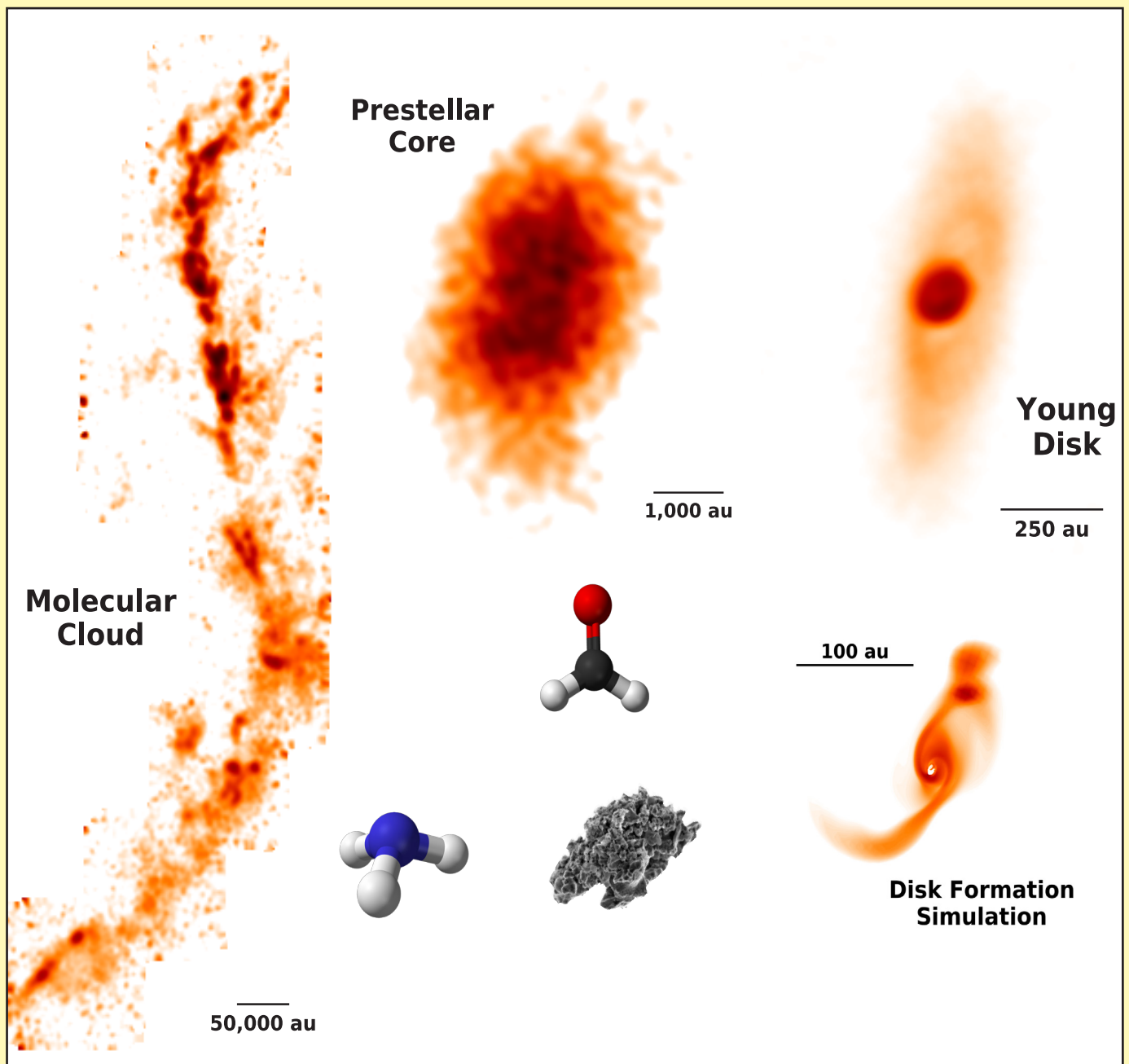
semiconductor lab (HLL) for the SDD sensor development and with Politecnico di Milano for the ASIC development. SDD prototype sensors have been designed and are currently in production, while testing of the ASIC prototype at MPE has already started.



Norbert Meidinger

(Other HE group members include: K. Nandra, S. Yazic)

5 Center for Astrochemical Studies



The left panel shows the NH_3 (1,1) integrated intensity map of the Orion A Molecular cloud obtained with the GBT (Friesen & Pineda et al., 2017), the middle panel shows the N_2D^+ (1-0) integrated intensity map of the L1544 prestellar core with ALMA, the top right panel shows the 1.3mm dust continuum emission map of the Class I object BHB07-11 in the Barnard 59 region obtained with ALMA (Alves et al., 2017), and the bottom right panel shows a non-ideal MHD simulation of disk formation (Zhao et al. 2018). CAS uses molecules to study the link between clouds and protoplanetary disks, while tracing the evolution of gas chemical composition and dust.

5. Center for Astrochemical Studies

5.1 Introduction and Overview

The Center for Astrochemical Studies (CAS) is an interdisciplinary department at MPE, where experts on (i) molecular spectroscopy and quantum chemistry, (ii) astronomical multi-wavelength observations, and (iii) theory (chemical modeling, plasma physics and non-ideal magneto-hydrodynamic simulations) daily interact. The overall goal of CAS is to understand the physical and chemical processes that regulate the formation of stars and planets, while following the chemical evolution of material in the various phases. This requires detailed experiments, sensitive observations and models which can then be tested against observations. Students find in CAS an exciting environment where they can expand their horizons and take advantage of the breadth of expertise in the group. CAS attracts scientists from around the world, interested in astrochemistry, star/planet formation, laboratory astrophysics, plasma physics, origins of life, insuring continuous idea exchanges, keeping us up-to-date, and allowing fruitful collaborations. Since 2016, there have been many developments in CAS in all the activities (Laboratory, Observations and Theory) and this is reported in the next sections.

In the Laboratory, CAS has seen the first light of CASAC (the CAS Absorption Cell), which is now operating at full speed, with several molecular ions and radicals studied in a range of temperatures relevant for interstellar conditions and down to $\sim 80\text{K}$, the temperature of liquid nitrogen, used to cool the system (see Section 5.2.1). To reach lower temperatures (around 10K , relevant for interstellar clouds at the onset of star formation) we have more recently built the supersonic free-jet expansion, which can also be coupled with the Chirped-Pulse Fourier Transform Spectrometer to obtain broad band spectra (Section 5.2.3). These experiments are crucial to be able to use the studied molecule as powerful diagnostic probes of the physical and chemical conditions of interstellar matter. We have also recorded spectra of interstellar ice analogues (in preparation for JWST) and directly measured the complex refractive index and physical structure of CO ices to improve our interpretation of dust continuum emission in dense environments (Section 5.2.2). The last and most challenging experiment (ion traps and nanoparticle) has started to be assembled at the end of 2018 and the first light is foreseen in the second half of 2019; the idea here is to focus on nanoparticles similar to those present in interstellar clouds, by isolating them in ion traps and study their properties in detail, including interaction with radiation, charged and neutral species which can be adsorbed and react on the particle surface – the ultimate aim is to reproduce interstellar conditions more faithfully than using the macroscopic flat surfaces (called “cold fingers”), as done in laboratories around the world, where kinetics and energetics of astrophysically relevant surface processes are investigated. Together with the nanoparticle study, ion

traps will also allow us to measure the rate coefficient of fundamental ion-molecule reactions, such as those regulating the ortho-to-para H_2 ratio and the deuterium fraction in molecular clouds.

A large amount of data has been collected with the IRAM (30m and NOEMA) telescopes, ALMA, JVL, GBT, SOFIA and this has allowed us to study interstellar matter (dust and gas) from pc-scale molecular clouds (Section 5.3.1) to the sub-pc cloud cores (Section 5.3.2) to protoplanetary disks at 10 au resolution (Section 5.3.3). We have also used NIR facilities, such as IRTF and Keck II telescopes to observe ice absorption features toward the Pipe Nebula and study the formation of icy mantles in quiescent environments, away from star formation and protostellar feedback (Goto et al. 2018, A&A, 610, 9); these studies are important to test astrochemical models inclusive of dust-grain interactions and surface chemistry. Theoretical activities include the study of the penetration of cosmic rays in molecular clouds and protoplanetary disks (Section 5.4.1), where their important effect on the ionization fraction in a broad range of densities has been highlighted. Cosmic rays can also influence gas phase and surface chemistry, and this is described in Section 5.4.3, where our astrochemical modeling efforts are presented. A simple astrochemical network, following the ionization fraction and the charging of dust grains has been included in the non-ideal MHD dynamical simulations described in Section 5.4.2, which aim at understanding the formation of protoplanetary disks in different environments. The inclusion of simple chemistry is important not just to follow more accurately the dynamical evolution of contracting magnetized clouds, but also to produce simulated observations at various evolutionary times to be compared with observations. This is especially important in view of the upcoming data from the recently-accepted Cycle VI ALMA Large Project FAUST (Fifty AU Study of the chemistry in the disk/envelope system of Solar-like protostars), of which we are co-investigators, as well as our ongoing IRAM-NOEMA Large Project SOLIS (Seeds of Life in Space; Ceccarelli & Caselli PIs).



Paola Caselli

5.2 CAS Laboratory

5.2.1 Molecular Spectroscopy with CASAC

Most of the gas-phase chemical processes occurring during the early stages of star formation involve small molecules made up by first- and, to a limited extent, second-row elements. Rotational spectra of these species can be observed with millimetre telescopes, and provide a useful mean to probe the physical conditions and the evolution of interstellar gas. The CASAC (CAS Absorption Cell) spectrometer has been developed at the Centre for Astrochemical Study to investigate the millimetre/sub-millimetre spectra of such molecules in the laboratory, with the aim of providing improved spectral data to guide the astronomical searches and to assist the interpretation of the observations. The CASAC has become operative in 2016 and has already produced a number of papers on astrophysically important molecules.

The CASAC spectrometer has been developed to study the rotational spectrum of relatively simple molecules (< 10 atoms) containing light elements (1st/2nd row), and it is specifically designed for the investigation of highly-reactive species. These elusive molecules play an important role in the chemical processes which take place in star forming regions, and their rotational lines (both in absorption and in emission) provide a mean to investigate the conditions and evolution of the interstellar gas.

Such spectral features are typically located at the millimetre/sub-millimetre wavelength regimes and are main targets of observations carried out with single dish telescopes and interferometers (e.g. IRAM 30m, NOEMA, ALMA). A thoughtful knowledge of the spectroscopic properties of the corresponding molecular carriers is clearly a key prerequisite for successful observations, but they are often very unstable in the ordinary terrestrial conditions, thus requiring special techniques to be generated and studied in the laboratory.

The CASAC implements a free space cell especially optimised for the production of unstable molecules: it consists of a 3 m long, 5 cm diameter borosilicate glass tube fitted with high vacuum flanges/connectors and HDPE optical windows at either ends. The cell is connected to a high-vacuum system, consisting of a gas trap, a 20 cm diameter oil-diffusion pump, and a 40 m³/h mechanical pump. Such configuration allows to maintain high flow-rates at the typical pressures used for the study of transient species (5 – 50 μ bar). Two methods are routinely used to generate the gaseous sample: DC low-pressure plasma, and gas-phase high-temperature chemical reactions.

The molecular plasma is generated by triggering a glow discharge in appropriate gas mixtures. To this purpose, two stainless-steel cylindrical electrodes are placed in-

side the absorption cell, which is also cooled by a liquid N₂ circulation system in a crossed-flow arrangement. A 2 m long solenoid provides the axial magnetic field needed for an efficient plasma confinement. This technique is particularly suited for extremely short-lived species, i.e., molecular ions and free radicals.

Semi-unstable molecules (lifetime \sim 1 s) can also be produced with a flow pyrolysis apparatus placed outside the absorption cell. This is a quartz tube placed in a tubular oven capable of temperature up to 1200°C; this side gas-line is directly connected to an inlet port of the CASAC. In this case, the target species are produced by high-temperature chemical reactions of suitable stable precursors and the gaseous products are flown continuously through the cell while the rotational spectrum is recorded.

The CASAC operates in the 80-1600 GHz frequency interval (4 – 0,19 mm) thus covering the full millimetre and sub-millimetre spectral widows and extending up into the far-infrared. The radiation sources are active multiplier chains driven by a cm-wave frequency synthesizer (2-40 GHz). A 4K-cooled hot-electron InSb bolometer is used as detector.

An account of the studies performed in the 2016-2019 period with the CASAC spectrometer is given in the following.

5.2.1.1 Molecular ions

Protonated ions are not only crucial astrophysical tracers, but are also proxies for important interstellar non-polar molecules such as N₂, C₂, CO₂, which are likely to be present to a large extent in the dense gas but escape radio-telescope detection owing to the lack of rotational spectra. With CASAC we have recently studied the ionic species HOCO⁺ (Bizzocchi et al. 2017a) and HSCO⁺ (Lattanzi et al. 2018), together with their deuterated counterparts. These molecules have been produced in DC plasma obtained in a mixture of CO₂/OCS with a small amount of H₂ (D₂) and Ar as buffer gas. The likely formation channel is proton attachment reactions through H₃⁺. Both ions turned out to be particularly elusive and they yielded weak spectra. A careful tuning of the experimental conditions, and the use of the anomalous discharge regime which maximize the ion density in the plasma, enables us to study extensively the rotational spectrum of HOCO⁺ and HSCO⁺ up into the sub-millimetre region; the frequency limits reached by our investigation are 967 GHz, and 405 GHz, respectively.

A recent study performed with CASAC is aimed at the determination of extremely accurate rest-frequencies for the rare carbonylium isotopologues HC¹⁷O⁺ and HC¹⁸O⁺.

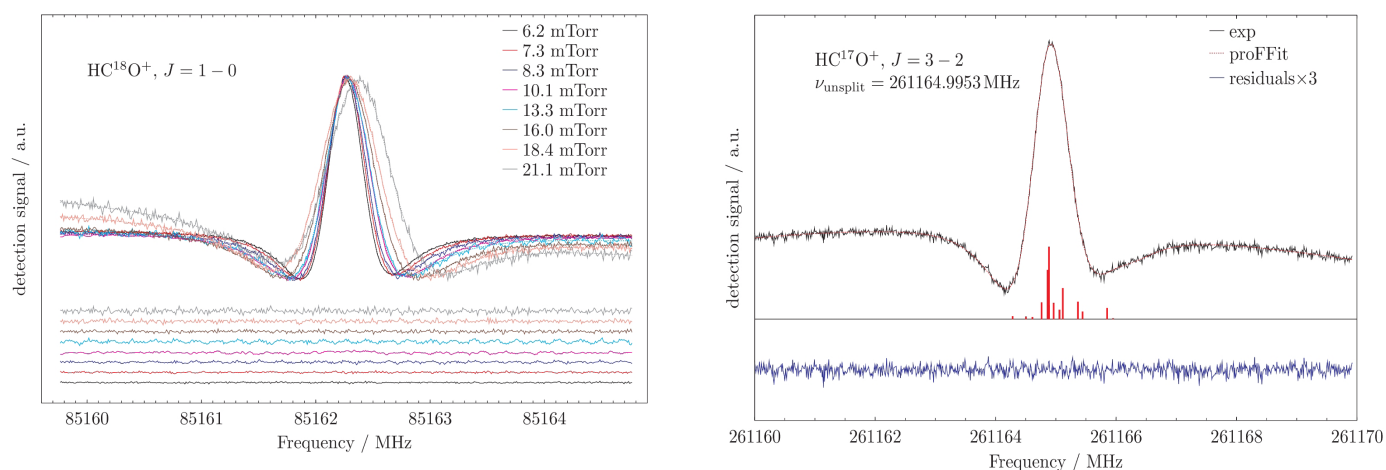


Fig. 5.2.1 (Left): Recordings of the $J = 1 - 0$ transition of HC^{18}O^+ taken at different plasma pressure. The 2nd derivative absorption profile have been analysed using a frequency-modulated speed-dependent Voigt function. The collisional frequency shift of $3.4 \text{ MHz Torr}^{-1}$ is apparent at high pressure. The rest-frequency extrapolated at zero perturber pressure is $85162.2288(21) \text{ MHz}$. **(Right):** Recording of the $J = 3 - 2$ transition of HC^{17}O^+ showing line asymmetry due to the partially blended hyperfine structure (red histogram). The hypothetically unsplit frequency has been derived via line profile analysis. The traces plotted below each lines represent the differences between experimental and modelled spectra.

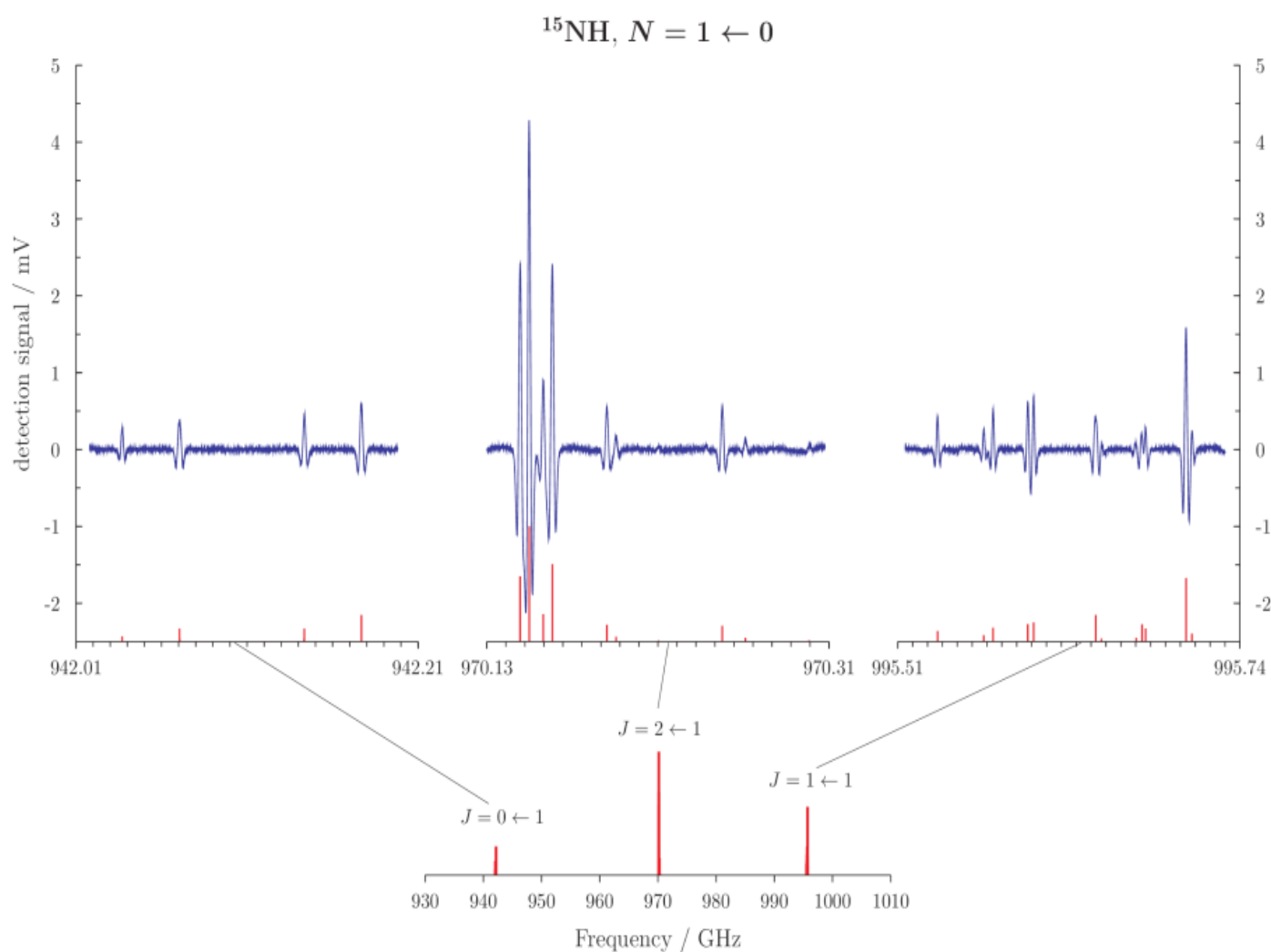


Fig. 5.2.2 Fine and hyperfine structure of the $N = 1 - 0$ rotational transition of ^{15}NH in its ground vibrational state. The bottom plot illustrates a schematic representation of the fine structure splitting. The top plot shows the recordings of the $J = 0 - 1$, $J = 2 - 1$, and $J = 1 - 1$ fine-structure components. The blue traces are the experimental spectra recorded with the time constant $\text{RC} = 3 \text{ ms}$ and accumulation times of ca. 350 s. In both plots, the red bars indicate the line positions and the relative intensities computed from the best-fit parameters.

Such species are extensively used as optically thin tracers for the dense interstellar gas, and a frequency precision of a few parts in 10^8 for their features is desirable in most applications. The ions have been produced in a negative glow discharge of Ar, H_2 , and isotopically enriched CO at 80K, and their spectra have been recorded and analysed by putting a great deal of effort in minimizing the source of systematic errors affecting the determination of the line frequency positions (Bizzocchi et al. in prep). Treatment of the pressure-shift effect (non negligible for low-J transition of light molecular ions) and a careful line profile analysis of the unresolved hyperfine structures (Fig. 5.2.1) have enabled to achieve a frequency precision of ~ 2 parts in 10^{10} at ~ 1 THz.

5.2.1.2 Radicals

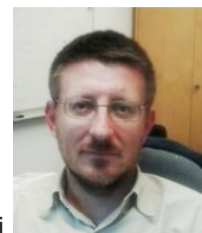
With the CASAC we have recently carried out the spectroscopic study of the free radical ketenyl (HCCO, Chantzios et al. 2018) and ^{15}N -bearing imidogen (^{15}NH , Bizzocchi et al. 2018). HCCO has recently been detected in the interstellar medium for the first time and it might provide useful insights to revise the oxygen chemistry in dark clouds. It is a radical with one unpaired electron and $^2A''$ (bent) ground electronic state. Its rotational spectrum is further complicated by the Renner-Teller effects, i.e., an energy perturbation of the rotational/fine-structure levels due to the interaction with the nearby $^2\Pi$ (linear) excited electronic state. A partially effective treatment of the spin-rotation coupling has been adopted in the spectral analysis in order to reduce the complexity of the problem and to achieve a good fit of the measured line frequencies using a single-state Hamiltonian. This allowed to generate a set of reliable rest-frequencies useful for the astronomical community.

The imidogen radical is an important molecule for the nitrogen chemistry in the interstellar medium and is thought to be a key intermediate in the gas-phase synthesis of ammonia. The full fine structure of the $N = 1 - 0$ rotational transition of ^{15}NH , around 1 THz, has been

observed for the first time with the CASAC. The radical has been produced by means of low-pressure glow discharge of H_2 and ^{15}N -enriched nitrogen. A number of hyperfine components have been observed and accurately measured (Fig. 5.2.2). This study substantially improves the knowledge of the THz spectrum of this rare isotopic variant of imidogen. Accurate values of the central line position ($\sigma \sim 35$ kHz, ≈ 0.01 km s $^{-1}$) were determined via a line profile analysis for 25 components of the ground state and 16 components of the $v = 1$ vibrationally excited state. These improved data can be used for Herschel archival searches, as a guidance for sensitive observations with 4GREAT instrument on board SOFIA, and for future THz telescopes.

Selected References:

- Bizzocchi, L., Lattanzi, V., Laas, J., et al. 2017a, *A&A*, 602, A34
 Bizzocchi, L., Tamassia, F., Laas, J., et al. 2017b, *ApJ*, 233, 11
 Bizzocchi, L., Melosso, M., Dore, L., et al. 2018, *ApJ*, 863, 3
 Chantzios, I., Spezzano, S., Endres, C., et al., 2018, *A&A*, 621, A111
 Lattanzi, V., Spezzano, S., Laas, J., et al. 2018, *A&A*, 620, A184
 Prudenzano, D., Laas, J., Bizzocchi, L., et al. 2018, *A&A*, 612, A56



Luca Bizzocchi

(Other CAS team members include: J. Chantzios, B. M. Giuliano, J. Laas, V. Lattanzi, D. Prudenzano, S. Spezzano, P. Caselli)

5.2.2 Interstellar Ice Analogues in the Laboratory

The cryogenic laboratory developed at the CAS group has reached the operative stage with the publication of the first paper about IR spectroscopy of water and oxygen ice mixtures. The experimental work has been extended to the measurement of the optical constant in the THz regime of CO ice to estimate the dust opacity in dense and cold regions of pre-stellar cores and protoplanetary disks. New projects are under development, regarding the Raman spectroscopy and imaging of ice analogs, and the stability of RNA in early Earth environment.

The chemical and physical processes which are taking place in the icy mantles in many astronomical environments are of key importance to unravel the molecular complexity observed in space. The dust grains properties are significantly influenced by the composition of their ice layers, therefore it is necessary to develop a methodology to investigate how different ices influence observational properties of dust grains.

Laboratory spectroscopic techniques offer an established route to analyze the chemical and physical processes on ices in a controlled environment. The experimental data have supported and guided the interpretation of the observational data throughout the last thirty years, and they continue to serve as a unique tool to untangle the astrophysical processes. In order to provide a solid experimental ground to the observational data and to assist the development of chemical modeling, a laboratory facility specialized in the molecular spectroscopic investigation of astrophysical ice analogs has been designed and developed at CAS.

During the past three years, two main research lines have been explored. On the one side, the focus has been put on the investigation of the spectroscopic properties of water-based ice mixtures. Additionally, the investigation of the optical properties of ice analogs in the THz region has been carried out.

Water is the major component of astrophysical ices, but it is very often mixed with a significant fraction (~20-25%) of carbon monoxide and dioxide, and other minor components such as methanol and ammonia. Most likely, icy mantles could contain a certain amount of infrared inactive species, like oxy-

gen and nitrogen, which cannot be detected directly by means of IR spectroscopy. Nevertheless, the interaction with the water matrix allows the formation of an induced dipole in the molecule which enables the spectroscopic detection. These data are necessary to explore the observing capabilities of new infrared space telescopes, like JWST. The first results of this project have been published by Müller et al. 2018, providing a reference paper for the laboratory setup configuration dedicated to this task. The possibility of detecting solid oxygen toward pre-stellar cores has been explored. When oxygen is mixed with pure water, the intensity of its spectroscopic feature does not allow for a detection using the JWST telescope (see Fig 5.2.3). However, the spectroscopic features can be further investigated in more astronomically realistic ice mixtures, including carbon monoxide and dioxide as matrix components. New estimates for the oxygen detection in water ices mixed with carbon monoxide and dioxide are under investigation.

Experimentally determined optical constants and in particular absorption coefficients of astrophysical ice analogs in the terahertz region are missing. These data are very important to determine how the dust opacity changes when the grains are covered with ice mantles. Thus, more accurate mass determinations can be carried out using the dust continuum emission, especially in cold and dense regions where CO mainly resides in solid form on top of dust grain surfaces, forming thick icy mantles. We have measured the optical and dielectric properties in the THz region of interstellar ice analogs of astrophysi-

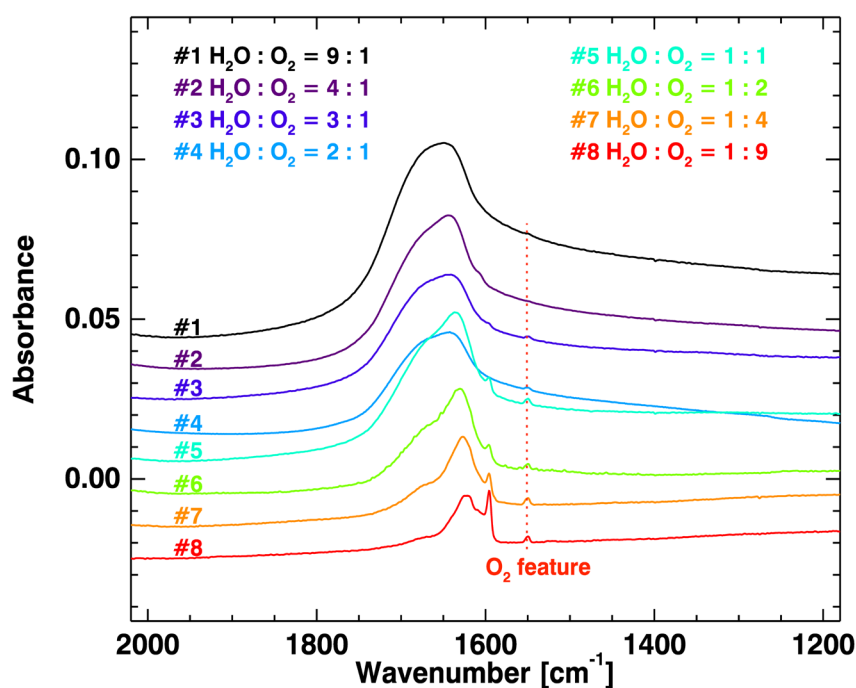


Fig. 5.2.3 Spectra of all H₂O–O₂ composition ratios mixtures investigated, magnified around the O₂ feature (marked by the vertical red dashed line). The spectra for the different compositions are shifted in the absorbance scale for helping their visualization.

cally relevant species, starting with CO, using the time-domain pulsed THz spectroscopic technique (TPS). TPS has the unique advantage of being able to measure both the amplitude and phase of sub-picosecond THz pulses in a wide spectral range in a single measurement and, thus, to reconstruct directly the optical properties without the use of the Kramers-Kronig relations. Making use of a mathematical algorithm developed specifically for this project, we succeeded in the calculation of the CO ice optical properties from the THz spectral data. Based on these results, the dust opacity has been derived afterwards (Giuliano et al, submitted). The analysis of recorded data for other common ice components, such as water and carbon dioxide, is in progress.

Further development in the cryogenic experiments will examine additional research lines. A Raman microscope has been recently purchased and installed in the laboratory. The final aim is to couple the microscope with a customized design cryostat, to investigate the diffusion properties in ice mixtures, and between the ice layers and the substrate. Microspectroscopy is the primary technique to analyse spectroscopic properties in 2D and 3D space, enabling the study of composite materials. With this technique it is thus possible to examine samples like meteorites and interstellar dust, and to assess the role of different substrates in the interaction with the ice mantles. The designed setup will be configured with a tunable sample holder capable to deposit spatially resolved ice sample to address their surface diffusion properties.

Finally, as the CAS group is part of the OLIM (Origins of Life Initiative in Munich) network, which has been recently awarded the “CRC – Emergence of life” project, the cryogenic facility is also dedicated to the investigation of RNA stability, formation and catalysis in simulated prebiotic environments under Solar Nebula and early Earth conditions. These experiments are designed to provide insight on the basic question if genetic systems can survive and evolve in extreme temperature and irradiation conditions. The feasibility study of the project has been the subject of Amine Akermi bachelor thesis, and it will be further developed as part of Max Winkler PhD thesis. The units forming the RNA and DNA structure exhibit a characteristic spectral signature in the infrared range. The change in the shape of the spectroscopic bands can be used to retrieve information on their chemical activity. The aim of these studies is to elucidate the role of the environment on the polymerization properties, and how they can be enhanced or inhibited and ultimately affect the genetic code information transmission.

Selected References:

Müller, B. et al. 2018, A&A, 620, A46



Barbara Michela Giuliano



Birgitta Müller



Max Winkler

(Other CAS team members include: A. Ivlev, P. Caselli)

5.2.3 Spectral and Collisional Characterisation of Astrophysical Molecules

Molecular species in the interstellar gas carry precious information which allow astronomers to understand the physics and chemistry of the different cosmic objects. These studies are based on two main steps, (1) line identification in the radioastronomical spectrum and (2) derivation of the chemical and physical structure using radiative transfer codes which require accurate collisional coefficients. The CAS laboratories are addressing these topics, by means of gas-phase spectrometers, working in the frequency range spanning from the radio to the THz band.

5.2.3.1 The Free-Unit Jet Experiment

Spectroscopic characterisation of reactive species requires the molecules to be produced *in situ* while electromagnetic radiation is probing them, in order to record their spectroscopic fingerprints. These fingerprints serve as a scientific identity card, which allows the astronomer to identify them in interstellar environments.

To extend the capabilities of the CAS laboratory for rotational spectroscopy, and in particular to complement the existing absorption cell (CASAC), two years ago we started to develop a free-jet millimetre and sub-millimetre-wave spectrometer, whose *first light* has been seen in 2018. The molecular beam, a gas generated by the mixture of different chemical samples connected to mass flow controllers, is injected into a high-vacuum expansion chamber ($\sim 10^{-5}$ Torr / 10^{-3} bar) through a 1-mm pin-hole of a pulsed valve. The expansion of the molecular beam into the chamber is supersonic thanks to the high pressure gradient between the valve (few kTorr/ few bar)

and the chamber. This supersonic expansion allows the adiabatic cooling of the molecular beam, yielding temperatures in the range of approximately 7 to 20 K, depending on the buffer gas used, significantly lower than those reachable in the CASAC spectrometer (~ 80 K). The coupling of the molecular beam to the mm- and sub-mm-wave radiation is obtained through a roof-top mirror placed inside the chamber, which also contains the aperture through which the molecular sample is injected. The probing radiation enters the vacuum section through a teflon window on the opposite side of the roof-top mirror, interacts twice with the gas, and finally reflects back outside the chamber. The production of unstable species is achieved by attaching a high-voltage low-current DC nozzle to the front of the valve, through which the molecules pass right after the pulsed valve and prior to free expansion. It is this free expansion (Fig. 5.2.4) where the molecular sample is quickly stabilised in the region dubbed the “zone of silence”; since the gas expansion moves at supersonic velocities, only a few intermolecular collisions are experienced, thus obtaining an efficient isolation of highly-reactive species.

The instrument operates in the 80–1600 GHz range (4–0.2 mm), with some possible extensions down also to the radio band (see later), covering the entire frequency bands accessed by state-of-the-art millimetre observing facilities, such as ALMA, and the lower THz band of the SOFIA aircraft observatory. The radiation source is an active multiplier chain driven by a cm-wave frequency synthesiser (9–50 GHz). Schottky diodes and liquid-helium cooled hot-electron bolometers are used as de-

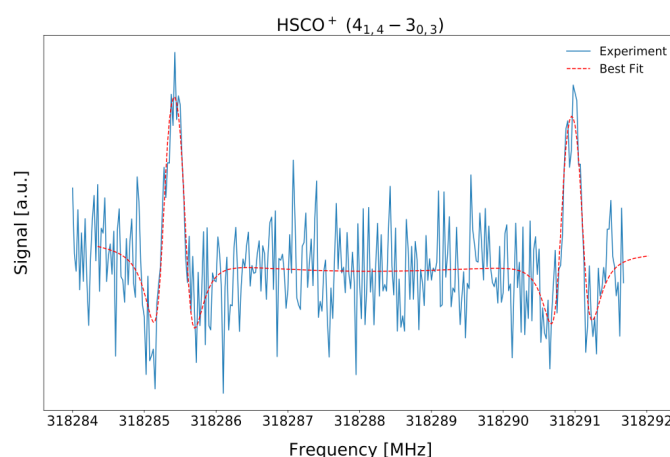
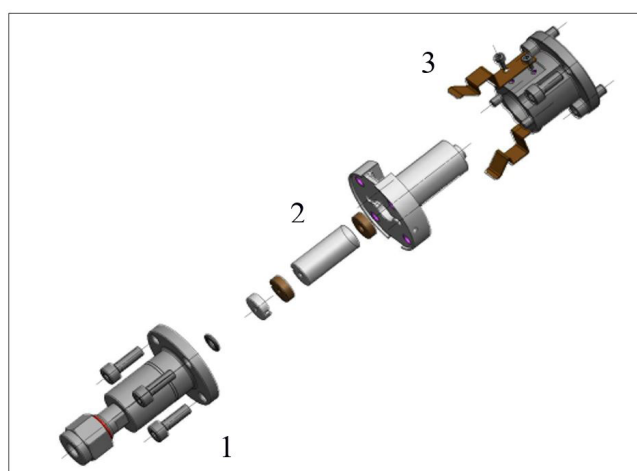


Fig. 5.2.4 Left: Engineering drawing of the coupling of the pulsed valve to the high voltage DC discharge nozzle; the molecular beam first enters the valve housing (1, **bottom left**) and then passes through the combination copper electrodes / teflon spacers (2), where it undergoes a high voltage discharge before expanding into the vacuum cavity (3). **Right:** Laboratory spectrum of the $\text{HSCO}^+ (4_{1,4} - 3_{0,3})$ rotational transition around 318 GHz, acquired with the free-unit jet experiment. The integration time is ~ 15 mins with 30 μs time constant. The red dashed line represents the best fit to a speed-dependent Voigt profile. Each rotational transition has a double-peaked line shape, the result of the Doppler shift of the supersonic molecular beam relative to the two travelling waves that compose the radiation beam.

tectors, with the latter providing higher sensitivity and a lower noise-figure at higher frequencies.

The instrument has been designed with the goal of maximum flexibility to move through projects involving different class of molecular species, such as radicals, ions and also stable molecules (see Fig. 5.2.4, right panel, for an example spectrum). In this latter case, the discharge nozzle can simply be turned off. This case is particularly suited for the so called **interstellar Complex Organic Molecules** (iCOMs). These molecules are key ingredients in several interstellar regions and exhibit a very dense and complex spectra. Thanks to the low rotational temperatures that the molecular beam can reach, considerably less energy levels are populated causing a simplification of the otherwise dense and complex rotational spectrum.

5.2.3.2 The Chirped-Pulse Fourier Transform Spectrometer (CP-FTS)

Molecular spectra at lower frequencies can be studied with a broadband CP-FTS spectrometer, which polarises a molecular sample and records the subsequent free induction decay (FID) with an instantaneous spectral bandwidth of several GHz. The capability to record broad scans with high frequency resolution and high dynamic range on microsecond timescales makes this instrument very suitable for studying the spectra of astrophysically relevant molecules in our molecular jet apparatus, described above, as has been demonstrated by recording spectra of protonated OCS (Fig. 5.2.5, right). Its frequency range has now been extended to the 3mm wave range (Fig. 5.2.5, left) and currently covers the

frequency bands from 6 to 26 GHz, and 80 – 110 GHz. In future projects, we will use this powerful combination to record spectra of molecular species, where besides the accessible frequency range, in particular the large instantaneous bandwidth is required, e.g. if predicted transition frequencies are very uncertain or if molecules exhibit a very line-rich and complex spectrum that is simplified due to the cooling in the molecular jet.

In the past years, the CP-FTS has been used to study inelastic collisions and to establish a new method to derive state-to-state rate coefficients experimentally. In the vast majority of cases, rate coefficients are derived from numerical calculations and experimental studies are often missing. We apply complex pump-probe sequences (see Fig. 5.2.6) to record the kinetics of rotational inelastic $\text{NH}_3\text{-NH}_3$ collisions. The thermal distribution of states is altered by the pump pulse that perturbs the population of the inversion doublet of a single rotational state. The resulting deviation from equilibrium is then propagated to other states due to resonant collisions and interrogated by probe pulses at different pump-probe delay times. State-to-state rate coefficients are estimated via the kinetics and reliably derived from pressure dependent measurements using a global fitting procedure. With these measurements we have not only proven the applicability of the method, but also developed tools to perform the numerical simulations, which are essential for the analysis. Our findings, described in our recently submitted paper, open up the possibility to investigate now also other systems and to derive their rate coefficients including collisions with helium, hydrogen or even pure para- H_2 .

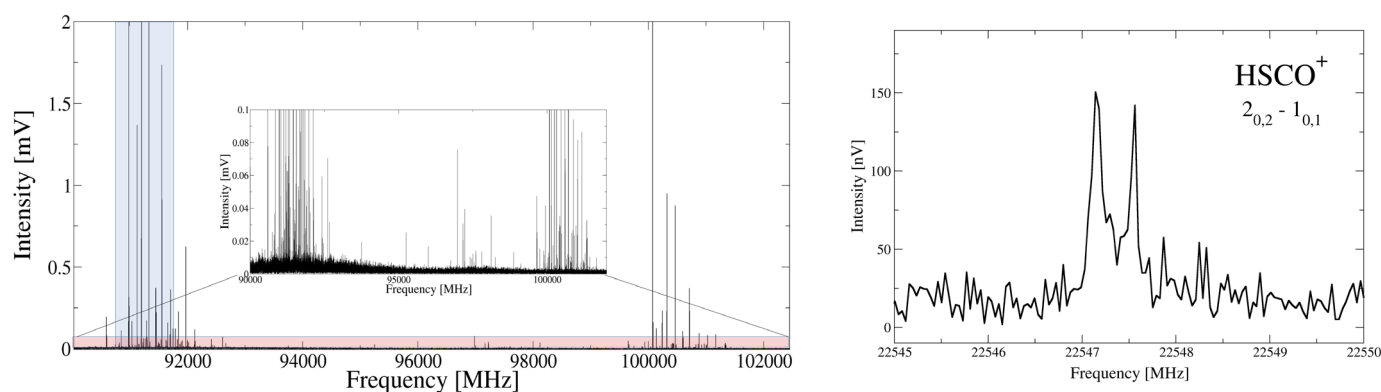


Fig. 5.2.5 Example spectra recorded with the CP-FTS. **Left:** 12 – GHz broad spectrum of HC_3N at 3mm. **Right:** HSCO^+ in the molecular jet expansion.

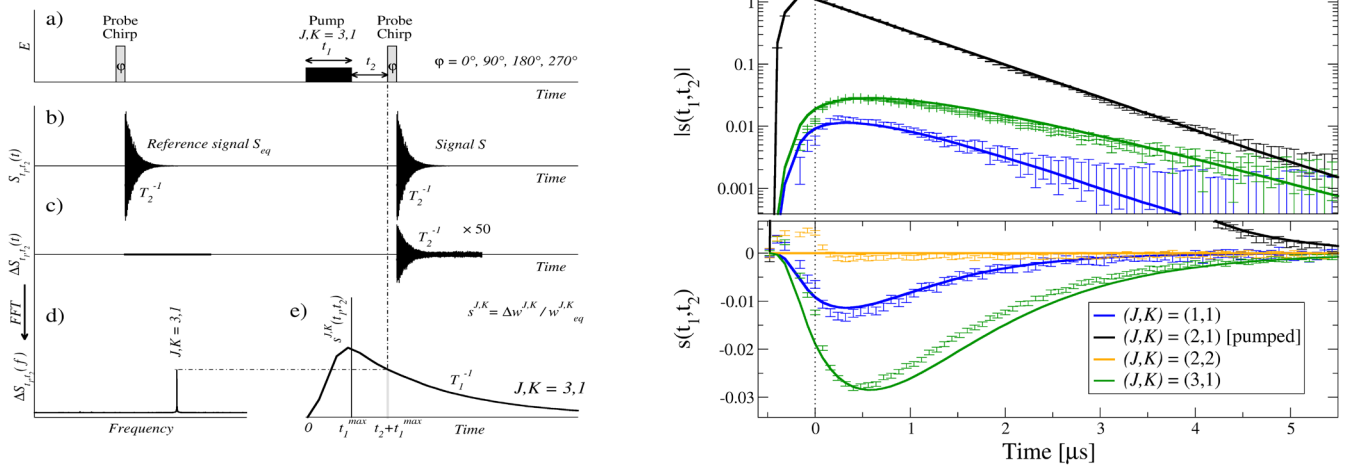


Fig. 5.2.6 Left: Pump-probe pulse sequence and signal processing. a) A sequence of pump pulses followed by 5-GHz broad chirped-pulses (200 ns) are applied and the subsequent FIDs are recorded. Each sequence starts with only a probe pulse to obtain a reference signal at thermal equilibrium conditions, followed by a number of pump-probe combinations. b) The quadrature phase averaged signal $S_{t_1, t_2}(t)$ with the pump pulse length t_1 and delay t_2 . c) difference signal $\Delta S_{t_1, t_2}(t)$. d) Fourier transform to derive the J,K fractional change in signal intensity $\Delta S_{t_1, t_2}(f)$ for each individual transition. e) $s^{J,K}(t_1, t_2)$ plotted as a function of the delay t_2 between pump and probe pulse. **Right:** Temporal evolution of fractional changes of signal intensities (top: log-scale, bottom: normal-scale) for selected transitions. Population of the $(2, 1)$ state, altered by a π - pump-pulse, is transferred to states $(1, 1)$ and $(3, 1)$ ($\Delta J = 0, +1, -1, \Delta K = 0$). The time origin is set to the end of the pump pulse t_1^{\max} and the time axis corresponds to t_2 , the delay time between pump- and probe pulse. Population is still transferred from the pumped doublet to the doublets $(1, 1)$ and $(3, 1)$ after the end of the pump pulse. No population transfer is observed to the doublet $(2, 2)$. The experimental data is shown as error bars and the solid lines correspond to simulations based on the global fit including measurements at different pressures and altering different doublets.

Selected References:

Lattanzi, V. et al. 2018, A&A, 620, A184

Endres, C.P. et al. 2019, submitted



Valerio Lattanzi



Christian Endres

(Other CAS team members include: J. Chantzios, J. Laas, S. Spezzano, P. Caselli)

5.3 CAS Observations

5.3.1 Connecting Molecular Clouds to Dense Cores

We have an active and diverse program to study the properties of molecular clouds and their connection with dense cores. Since molecular clouds provide the initial conditions for dense cores, it is important to determine some of their main properties: the amount of turbulence in the molecular cloud and inside dense cores, the amount of energy radiated by turbulent dissipation, and the role of magnetic fields. We have studied distant Infra-Red Dark Clouds (IRDCs) and nearby molecular clouds in dense gas tracers, using both single dish and interferometers, to reveal a large fraction of dense gas (as traced by NH_3) present in the intra-core medium and to highlight the presence of subsonic turbulence inside dense cores even in the higher-mass star-forming regions traced by IRDCs. The relation between the kinematics and other physical properties of the dense cores and their parental molecular clouds has been explored. In addition, a systematic study of mid-J to high-J CO transitions in IRDCs provided a possible detection of the energy generated by turbulent dissipation. Finally, a comparison between Planck and polarization of background stars was carried out and it showed small differences between both techniques, confirming the validity of the Planck based polarization measurements in molecular clouds.

We investigated the kinematic of the dense gas traced by NH_3 in an IRDC. We used single dish observations with the 100-m Green Bank Telescope (GBT) to determine the gas kinetic temperature. When comparing this temperature to the positions of the embedded young stars we identify local temperature enhancements, which are not evident from the Herschel based dust temperature map (Sokolov et al. 2017). Further higher angular resolution observations with the Very Large Array (VLA) allowed us to spatially resolve multiple velocity components along the line-of-sight, and identify small regions of subsonic turbulence (sonic Mach number <1) thanks to the high spectral resolution of the observations and of the quiescent nature of the targeted IRDC (Sokolov et al. 2018, 2019). These results indicate that early stages of massive star and cluster formation can go through stages more similar to their low-mass counterparts than previously thought.

In the case of nearby molecular clouds, we have completed the NH_3 observations of the GBT Ammonia Survey (GAS, PIs: Pineda and Friesen). This large program at the GBT (>240 hrs) provides large area maps of several nearby star forming molecular clouds with a homogeneous sensitivity, selection criteria, and observing setup. The observations have recently been completed and the first data release (DR1) has been published

(Friesen & Pineda et al., 2017). These data reveal extended dense gas surrounding the dense cores in most regions, with evidence for a large fraction of dense cores with subsonic turbulence surrounded by supersonic molecular clouds material. In particular, Redaelli et al. (2017) found evidence of the protostellar feedback on the GAS derived physical parameters on the Barnard 59 core in the Pipe Nebula. These results, combined with complementary observations, reveal that the B59 core is gravitationally bound. In addition, we also use these large area maps to determine for the first time the gas kinetic temperature and $[\text{NH}_3/\text{H}_2]$ abundance on the lower density material surrounding the subsonic dense cores, by reducing the angular resolution of the data (S. Choudhury et al., in prep.). These observations will be key to constrain the relations between surrounding molecular clouds and dense cores, and to compare to dense core formation simulations.

The new dense gas observations of GAS on OrionA allowed us to combine them with archival VLA data to study the kinematics of the OrionA-OMC1 region, at higher angular resolution and sensitivity than before (Monsch & Pineda et al. 2018). This new data set revealed the presence of narrow filaments, and one of them was missed by the previous studies (Fig. 5.3.1, left). The new filament is surprisingly straight, and when compared to the dust emission polarization observations we identify a small variation on the orientation ($\sim 11^\circ$), which suggests that the filament and the magnetic field are almost parallel to one another. Follow-up observations of the entire OrionA-OMC1, -OMC2, and -OMC3 have just been completed with the VLA, and we will combine to the GAS single dish data to provide a unique kinematic and temperature map of one of the most studied nearby star-forming regions (Maureira & Pineda et al., in prep.).

In another nearby molecular cloud (Taurus), Punanova et al. (2018) studied the L1495 filament using a wide range of molecular transitions and species. These observations allowed us to study the kinematics of the dense gas and the parental filament and explore possible links (Fig. 5.3.1, right). The lower density material traced by C^{18}O (1-0) does not display evidence for perturbations due to protostellar feedback, while all cores show similar velocity patterns in the different transitions: simple in isolated starless cores, and complex in protostellar cores and starless cores close to young stellar objects where gas motions can be affected by outflows. When combining the different tracers observed, we clearly see a decrease in specific angular momentum towards the centers of the cores, which shows the importance of local magnetic fields to the small-scale dynamics of the cores. A NOEMA follow-up project for higher angular resolution observations of the dense gas towards one of these

cores was recently completed to focus on the spatially resolved kinematics.

Since molecular clouds show clear evidence for supersonic turbulence, it is an important question to study where is the energy release of all the expected shocks. The supersonic turbulence can locally heat small fractions of gas to over 100 K, which could be identified as excess in the spectral line energy distributions when compared to PDR models only. A systematic study of low-J to mid-J CO transitions was carried out across IRDCs (Pon et al. 2016a, 2016b). The fitted PDR models to the combined spectral line energy distributions show that they under-predict the mid-J CO emission by orders of magnitude, strongly hinting at a hot gas component within these clumps. The low-J CO data clearly show that the integrated intensities of both the CO J = 8-7 and 9-8 lines are anomalously high, such that the line ratio can be used to characterize the hot gas compo-

nent. Much of the observed mid-J CO emission, however, is also associated with known protostars and therefore they may also be due to protostellar feedback.

Finally, Soler & Alves et al. (2016) compared the polarization orientation towards 4 nearby molecular clouds using polarized thermal emission of Galactic dust observed by Planck at 353 GHz and from the optical and near-infrared polarization of background starlight. The dispersion in the starlight-inferred field orientations within the Planck resolution is less than 20° , and that at these scales the mean field orientation is on average within 5° of that inferred from the sub-millimeter polarization observations in the considered regions. These results show that the polarization orientation determined using Planck does agree with more local estimates, but also that at higher angular resolution the dispersion in polarization orientation does not vary substantially.

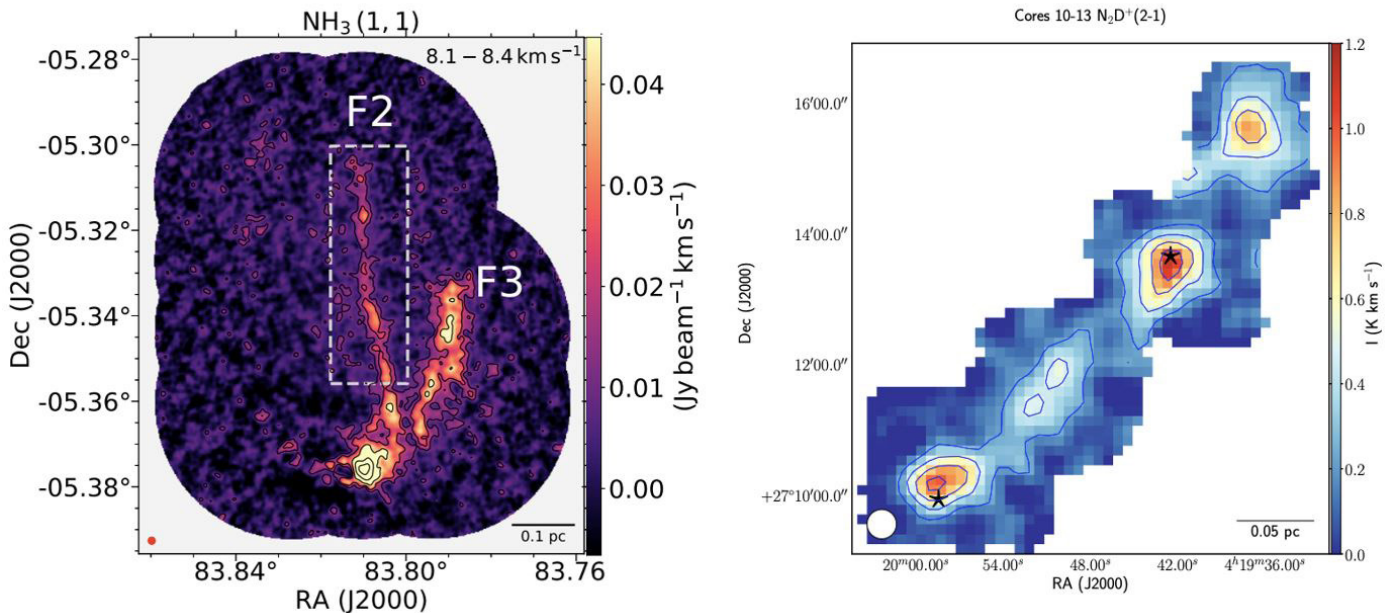


Fig. 5.3.1 Left: Integrated intensity map of the combined GBT and VLA NH_3 (1,1) map in OrionA-OMC1 over a narrow velocity range to highlight the faint emission of the filaments F2 and F3. F2 was not identified in previous works (Monsch & Pineda et al. 2018). **Right:** Integrated intensity map of the N_2D^+ (2-1) line for cores 10-13 in L1495, which show the compact nature of the emission (Punanova et al. 2018).

Selected References:

- Friesen, R. and Pineda, J. E., et al. 2017, *ApJ*, 843, 63
 Monsch & Pineda et al. 2018, *ApJ*, 861, 77
 Punanova, A. et al. 2018, *A&A*, 617, 27
 Pon et al. 2016a, *A&A*, 587, 96
 Pon et al. 2016b, *ApJ*, 827, 107
 Redaelli, E. et al. 2017, *ApJ*, 850, 202
 Sokolov, V. et al. 2017, *A&A*, 606, 133
 Sokolov, V. et al. 2018, *A&A*, 611L, 3
 Sokolov, V. et al. 2019, *ApJ*, 872, 30
 Soler, J & Alves, F. et al. 2016, *A&A*, 596, 93



Jaime E. Pineda

(Other CAS team members include: F. Alves, P. Caselli, S. Choudhury, M. Maureira, E. Redaelli. Former team members include: A. Pon, A. Punanova, V. Sokolov)

5.3.2 Dense Cores

Dense cores are regions within interstellar molecular clouds where stars like our Sun form. In the CAS group a lot of effort is put into studying dense cores with the aim of deriving more constraints for star and planet formation. The collaboration among observers and modellers, as well as the input from laboratory spectroscopists, are crucial to make progress and have a full understanding of the chemical and physical evolution of dense cores. In particular, we focus our attention on the information that can be inferred from isotopic fractionation in dense cores on their physical and chemical evolution. Furthermore, we want to understand and exploit all the information that is carried by the chemical segregation in dense cores, not only to better constrain our chemical networks, but also to derive the physical structure of the core.

Isotopic fractionation:

The isotopic fractionation in star-forming regions carries information on the physical structure of the cores and on their evolution. As an example, by observing deuterated isotopologues we are able to dive in the coldest and densest parts of pre-stellar cores. In Punanova et al. (2016) we explore how the environmental conditions have an influence on the deuterium fractionation and CO freeze-out by observing N_2H^+ (1-0 and 3-2), N_2D^+ (1-0, 2-1, 3-2) and $C^{17}O$ (1-0 and 2-1) towards several cores in the Ophiucus molecular cloud. In order to understand the processes of deuteration at different depths in dense cores, we made a survey to observe the deuterium fractionation of cyclopropenylidene, $c-C_3H_2$, in starless and protostellar cores (Chantzos et al. 2018). Nitrogen-bearing molecules, like N_2H^+ , do not freeze-out onto dust grains as efficiently as C-bearing molecules, like $c-C_3H_2$, so they will trace different layers in the cores. We observed $c-C_3H_2$, $c-C_3HD$, $c-C_3D_2$, and $c-H^{13}CC_2H$ toward 10 starless cores and 5 protostars in the Taurus and Perseus molecular clouds. We examined the correlation between the $N(c-C_3HD)/N(c-C_3H_2)$ ratio and the dust temperature along with the H_2 column density and the CO depletion factor. The deuteration of $c-C_3H_2$ can trace the early phases of the deuteration and is comparable to that of N_2H^+ . However, the largest $c-C_3H_2$ deuteration level is found toward protostellar cores, suggesting that while $c-C_3H_2$ is frozen onto dust grains in the central regions of starless cores, active deuteration is taking place on ice.

We are also studying the deuterium fractionation with molecular emission maps. With respect to single pointing observations, the maps not only give us information about the chemistry, but also about the physical structure of the core. We use emission maps to study the deuteration of molecules happening in the gas phase like N_2H^+ and HCO^+ (Redaelli et al., submitted), as well as on the surface of dust grains, like methanol and formaldehyde (Chacon-Tanarro et al., 2019a) towards the pre-stellar core L1544. Methanol and formaldehyde help us

to understand the chemical processes taking place on the dust grain surfaces and the formation of more complex organic molecules, as well as the deuterium history in the process of star formation. In Chacon-Tanarro et al. (2019a) we show that deuterated methanol peaks closer to the core centre compared to methanol, and this can be simply explained by the larger D/H abundance, so that D atoms compete with H atoms in saturating solid CO to form methanol, see the deuterium fraction map of methanol in Fig. 5.3.2. Formaldehyde follows instead a slightly different distribution compared to CH_3OH . This can be explained by the fact that, unlike CH_3OH , H_2CO can also form via gas phase routes involving hydrocarbons (e.g. CH_2 and CH_3), which are expected to be abundant toward the southern part of the core, where the extinction abruptly drops to relatively low values and where carbon chains are in fact abundant (Spezzano et al. 2016a).

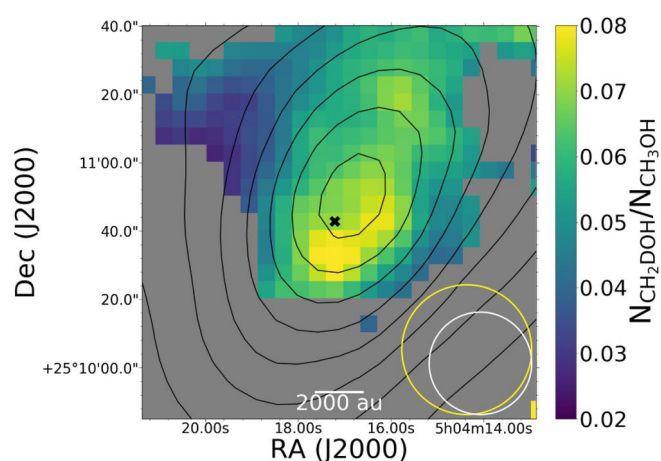


Fig. 5.3.2 Deuterium fraction map of methanol using the column density maps of CH_2DOH and CH_3OH . The black contours represent increasing 10% steps of the peak of the Herschel $N(H_2)$ map, presented by Spezzano et al. (2016).

The isotopic fractionation of Nitrogen is an important diagnostic tool to follow the evolution of material in the Solar System, in particular to follow the evolutionary process from the primitive Solar Nebula (where measurements indicate $^{14}N/^{15}N \approx 440 - 450$) up to present. Earth's atmosphere and meteorites are enriched in ^{15}N . Measurements of N_2 in the terrestrial atmosphere led to the result of $^{14}N/^{15}N \approx 272$, and carbonaceous chondrites show isotopic ratios as low as 50, suggesting that at the origin of the Solar System multiple nitrogen reservoirs were present (Hily-Blant et al. 2017). A particular case is the one of N_2H^+ , whose $^{14}N/^{15}N$ ratio observed towards the pre-stellar core L1544 by Bizzocchi et al. (2013) is ~ 1000 , while the most recent chemical models predict a ratio of about 440, close to the protosolar value. In order to make sure that L1544 is not an outlier, we have observed the ^{15}N fractionation of N_2H^+ in a sample of pre-stellar cores, and the isotopic ratios that we obtain are

in the range 630 – 770, showing that L1544 is not an exception (Redaelli et al. 2018). We use state-of-the-art radiative transfer modelling to retrieve reliable results. Furthermore, a big effort is currently put by Olli Sipilä, one of the chemical modellers in the CAS group, to develop a chemical model that can reproduce the $^{12}\text{C}/^{13}\text{C}$ and $^{14}\text{N}/^{15}\text{N}$ fractionation at the same time.

The most peculiar characteristic of the CAS group, and most definitely one of its biggest strength, is its interdisciplinarity. Especially in a field like astrochemistry, it is of crucial importance to be able to build bridges between different expertises. In Spezzano et al. (2016b) we report the first interstellar detection of HDCCC. We first tentatively detected HDCCC in space, and subsequently confirmed the detection via laboratory measurements. Back then, the CAS laboratories were still under construction, so the spectroscopic part of the work was carried by our collaborators at the CfA. In the meantime our laboratories are fully functioning and we were recently able to tentatively detect for the first time the ground state transition of CH_2OH towards the protostar IRAS4A based on a measurement done ad hoc in our laboratories (Spezzano et al. in prep.). CH_2OH is the only intermediate in the sequence of the methanol formation on grains that has not yet been observed in the ISM ($\text{CO} \rightarrow \text{HCO} \rightarrow \text{H}_2\text{CO} \rightarrow \text{CH}_2\text{OH}/\text{CH}_3\text{O} \rightarrow \text{CH}_3\text{OH}$). Its detection, or upper limits, would put very stringent constraints on a series of interconnected reactions such as the evaporation from grains of intermediates, i.e. before the CO is fully hydrogenated to methanol, the formation of methanol in the gas phase from fragments, and formation of complex molecules from methanol and methanol fragments.

Chemical differentiation:

In Spezzano et al. (2016) we have presented the different spatial distribution of CH_3OH and $c\text{-C}_3\text{H}_2$ towards the pre-stellar core L1544, and we concluded that this is evidence of chemical differentiation driven by different amount of illumination from the interstellar radiation field. To extend this study, we made a survey to observe 7 additional starless cores in Taurus, Perseus and Ophiuchus, in different evolutionary states. We mapped both $c\text{-C}_3\text{H}_2$ and methanol in these cores, and we see the same trend present in L1544 (Spezzano et al., in prep.). Further investigation of the methanol peak in L1544 has been carried out within the SOLIS large project at NOEMA. The interferometric observations show that the methanol peak has a smooth morphology, but reveals a complex velocity field. The increase in velocity dispersion toward

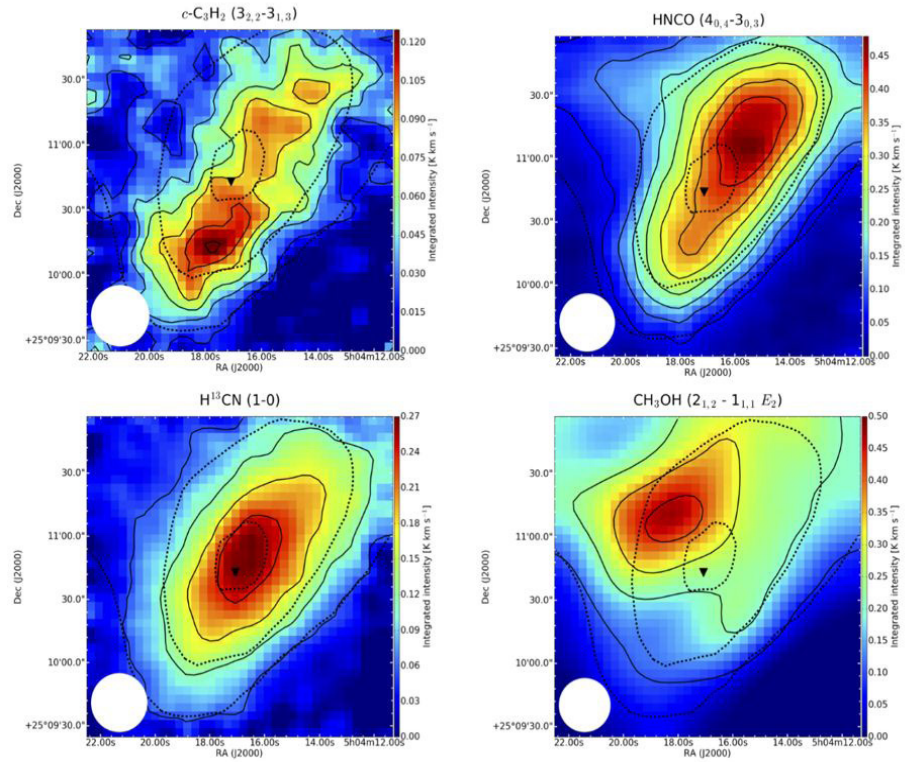


Fig. 5.3.3 Subset of maps observed towards the pre-stellar core L1544 (from Spezzano et al. 2017). The black dashed lines represent the 90%, 50%, and 30% of the H_2 column density peak value derived from Herschel maps. The solid lines represent contours of the molecular integrated emission starting with 3σ with steps of 3σ . The dust peak is indicated by the black triangle. The white circles represent the HPBW of the 30 m telescope.

the northeast edge of the pre-stellar core, where the local velocity gradients also present sharp changes in magnitude and direction, suggests that slow shocks are present. These slow shocks could be produced by either the accretion of cloud material onto the core or by a collision of the two filamentary structures seen in Herschel/SPIRE images.

In Spezzano et al. (2017) we present an extensive study (with maps of over 30 species; see Fig. 5.3.3 for selected maps) on the chemical differentiation in L1544, and its dependencies of chemistry on physical and external conditions. With a first qualitative analysis we have classified the molecules in 4 groups, depending on their emission peak. To systematically study the correlations among different molecules, we have also performed the principal component analysis (PCA) on the integrated emission maps. The PCA allows us to reduce the amount of variables in our dataset. Finally, we compared the maps of the first three principal components with the H_2 column density map, and the T_{dust} map of the core. The principal component maps allow us to confirm the (anti-)correlations among different families that were described in a first qualitative analysis, but also points out the correlation that could not be inferred before. We are currently trying to develop a radiative transfer model able to reproduce the chemical differentiation of the maps that we observed in L1544, with the aim of using the chemistry to put stringent constraints on the physical structure around the core.

The centre of pre-stellar cores:

The role of dust in the processes governing star and planet formation is pivotal. Dust opacities depend on temperature, on grain size, and on frequency-range, and they are usually poorly constrained. In pre-stellar cores, the growth of icy mantles and the coagulation of grains add additional uncertainty on the values on opacity and spectral index of dust. In Chacon-Tanarro et al. (2019b) we have investigated the changes in the optical properties of dust grains as a function of radius for the well-known pre-stellar core L1544 by observing the dust emission at 1.1 and 3.3 mm. With previous models of the core it is not possible to reproduce our observations without invoking opacity variations. With the new data, we have derived new temperature and density profiles for L1544, as well as opacity variations across the core, see Fig. 5.3.4. The opacity variations are consistent with uncoagulated bare grains in the outer part of the core, and grains covered with thick icy mantles towards the centre.

In Caselli et al. (2017) we show for the first time the spectrum of the *ortho*-NH₃ (1_0-0_0) line at 572 GHz observed with Herschel/HIFI across the pre-stellar core L1544. We have used these observations to test current models for the physical and chemical structure of the core. While the observed spectrum can be reproduced well by the empirical ammonia abundance profile derived by Crapsi et al. (2007) from interferometric observations, and by the physical structure used to reproduce other spectra (Keto and Caselli 2010), the comprehensive chemical model of Sipilä et al. (2015), applied to the (static) physical structure of L1544 shows a poorer match. More work needs to be done to gain understanding of the gas-grain chemical processes regulating NH₃ and N-bearing molecules in cold and quiescent objects such as L1544, the precursors of future stellar systems.

Selected References:

Bizzocchi L., Caselli P., Leonardo E., et al. 2013, A&A, 555, A109
 Caselli P., Bizzocchi L., Keto L., et al. 2017, A&A, 603, L1
 Chacon-Tanarro A., Caselli P., Bizzocchi L., et al. 2019a, A&A, 622, 141
 Chacon-Tanarro A., Pineda J. E., Caselli P., et al. 2019b, A&A, 623, 118
 Chantzios J., Spezzano S., Caselli P., et al. 2018, A&A, 863, 126
 Crapsi A., Caselli P., Walmsley M.C., et al. 2007, A&A, 470, 221
 Hily-Blant P., Magalhaes V., Kastner J., et al. 2017, A&A, 603, L3
 Keto E. & Caselli P. 2010, MNRS, 402, 1625
 Punanova A., Caselli P., Pon A., et al. 2016, A&A, 587, A118
 Punanova A., Caselli P., Feng S., et al. 2018, A&A, 815, 112
 Redaelli E., Caselli P., Bizzocchi L., et al. 2018, A&A, 617, A7
 Sipilä O., Harju J., Caselli P., et al. 2015, A&A, 581, A122
 Spezzano, S., Bizzocchi L., Caselli P., et al. 2016a, A&A, 592, L11
 Spezzano, S., Caselli P., Bizzocchi L., et al. 2017, A&A, 606, A82
 Spezzano, S., Gupta, H., Brünken, et al. 2016b, A&A, 586, 110

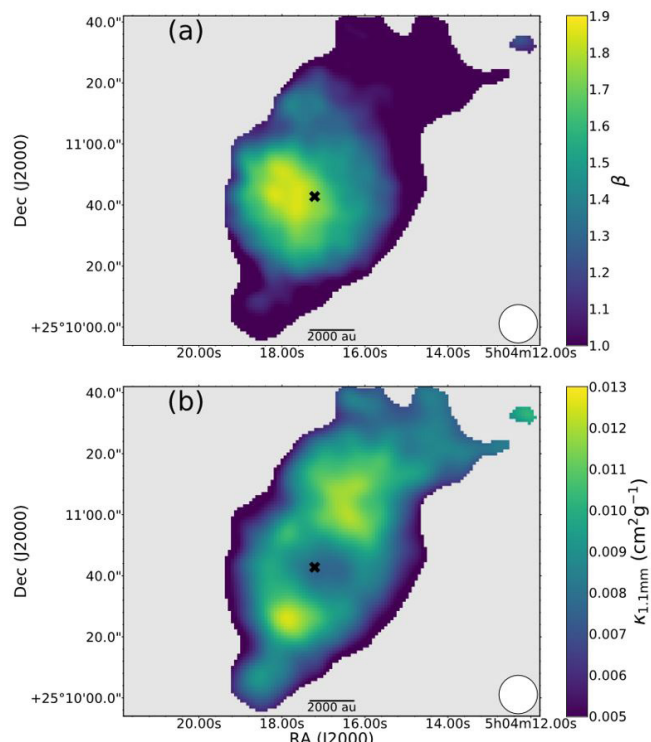


Fig. 5.3.4 Panel a shows the spectral index map and panel b shows the dust opacity map towards L1544 (Chacon-Tanarro et al. 2019). The error in the spectral index is ~ 0.2 and in the opacity is $\sim 10\%$.

Silvia Spezzano



(Other CAS team members include: L. Bizzocchi, P. Caselli, A. Chacon-Tanarro, J. Chantzios, A. Punanova, E. Redaelli)

5.3.3 The Evolution of Circumstellar Disks: From Embedded Seeds to Planet Cradles

Young circumstellar disks regulate the accretion of material from protostellar envelopes to protostars and, in later stages, provide the physical conditions for planet formation. The research done in the CAS group spans several stages of disk evolution, from young embedded disks to more evolved protoplanetary disks. We use state-of-the-art instrumentation including ALMA, NOEMA, and SOFIA which cover a range of observational frequencies and spatial resolutions. Here we present the advancements made by the CAS group using observations of molecular lines, polarization, and dust continuum data.

To study the primordial conditions in which disks form, we must understand how prestellar cores form protostars. When a prestellar core collapses under its own self-gravity, an embedded seed a few au in size is formed, known as a first hydrostatic core (FHSC), which then further collapses to form a protostar and disk. Due to the short duration of the FHSC phase ($\sim 10^2$ – 10^4 years, e.g., Bate et al. 2014), only a few possible FHSCs have been proposed. To continue her hunt for FHSCs (Maureira et al. 2017), CAS member Maria Jose Maureira studies extremely young objects with the ALMA telescope to identify FHSC candidates. Towards L1451-mm, she observed deuterated molecules coincident with the dust peak, an indicator of a very young evolutionary state. She also found a compact methanol (CH_3OH) outflow ~ 640 au in size coincident with other outflow tracers (e.g., CO, Pineda et al. 2011). Compact outflows are key features of FHSCs and help confirm this as the youngest FHSC candidate known (Maureira et al. in prep.). Her granted-time observations with the NOEMA interferometer using C^{18}O and N_2D^+ will further explore the nature of L1451-mm.

Protostellar cores are often magnetized. As envelope matter collapses inwards towards the protostar, magnetic field lines are dragged together with the infalling/rotating material, creating a magnetic pinch and enhancing the magnetic flux in the inner envelope. This leads to magnetic braking, which can suppress the formation of large rotationally supported disks by transferring angular momentum outward (Mellon & Li 2008). Elena Redaelli obtained dust continuum polarization data from the SOFIA telescope as part of her PhD work. The SOFIA data show pinched magnetic field lines in the envelope of the Class 0 young stellar object (YSO) IRAS 15398-3359. She also obtained near-infrared polarimetric data toward the dense core Barnard 59, revealing a very uniform large-scale magnetic field (Redaelli et al. in prep.). For large disks to form, magnetic braking must hence be mitigated in these magnetized environments studied by CAS, usually explained via magnetic diffusion or misalignment between magnetic fields and the core rotation axis.

The youngest protostar of Barnard 59 is the Class I YSO BHB07-11 and has been studied by Felipe Alves. His 36 au resolution dust map (Fig. 5.3.5) shows spiral-shape density enhancements in the inner envelope that, when combined with molecular line data (H_2CO and C^{18}O), trace the transition between infalling envelope and rotationally supported disk. He also detected a bipolar outflow in CO at an offset of ~ 100 au from the disk rotation axis (Alves et al. 2017). The offset in the outflow is caused by the strong pinch in the magnetic field lines in the envelope-disk zone, which provides a magneto-centrifugal mechanism for outflow ejection (e.g., Zhao et al. 2016). ALMA dust polarization observations with 36 au resolution in three bands (3, 1.3, and 0.87 mm) all reveal the same polarization pattern, interpreted as a combination of morphologies produced by envelope collapse and disk rotation (Alves et al. 2018). Higher spatial resolution (7 au) data show a complex network of filaments connecting a circumbinary disk to two small circumstellar disks surrounding each binary component (Fig. 5.3.5, Alves et al. submitted), the first such structure seen in a Class I protostar.

Disks in Class 0 and Class I YSOs are difficult to observe due to the high extinction produced by the dense protostellar envelope. With interferometers whose spatial resolution allows for interferometric filtering of some of the envelope emission, it is possible to study not only the envelope, but also the disk properties and connection between disk and envelopes at young stages. As part of her PhD work, Carolina Agurto-Gangas has used multi-wavelength data from the NOEMA (2.7 mm) and SMA (1.3 mm) interferometers to investigate the dust properties toward the Class I YSO Per-emb-50 with ~ 550 au resolution. With radiative transfer models of the uv-plane visibilities, she found that the envelope significantly affects the emission of the unresolved disk via the backwarming effect, even when the envelope has maximum dust grain sizes < 100 micron (Agurto-Gangas et al. 2019, accepted). As a follow-up project, Carolina is analyzing available higher-resolution VLA continuum data of Per-emb-50 at 8 and 10 mm wavelengths where the disk is resolved to further study the dust grain properties and interplay between envelope and disk in this source.

Using 8 mm dust observations with 15 au resolution from the VLA Nascent Disk and Multiplicity Survey, Dominique Segura-Cox from CAS reported 18 new Class 0 and Class I protostellar disk candidates in the Perseus cloud (Segura-Cox et al. 2016, 2018), where before only ~ 14 confirmed rotationally supported disks in these young phases were known. She is now analyzing her ALMA molecular line follow-up data on the new Class 0/I disk candidates to obtain disk kinematics and study the dynamical and chemical connections between the disks

and envelopes. She is also using ALMA 1.3 mm dust observations to study the Class I disk IRS 63 with 7 au resolution, which reveal concentric dust rings at ~ 25 and 40 au, making IRS 63 the youngest-known protostellar disk with ringed dust substructures (Fig. 5.3.6, Segura-Cox et al. in prep.). Dust rings in disks can provide a stable environment for long enough time scales to grow planets (e.g., Cridland et al. 2019), and the ringed disk of the Class I YSO IRS 63 is the earliest evidence for these planetary cradles.

The more-evolved protoplanetary disk of the Herbig Ae/Be star HD 100546, a disk with two possible embedded planets, was previously studied by Jaime Pineda (Pineda et al. 2014). His new ALMA 0.87 mm dust observations with higher 4 au resolution (Fig. 5.3.7, Pineda et al. 2019) reveal an asymmetric ring peaking at ~ 30 au in radius surrounding a central, unresolved (~ 2 au radius) disk. The ring asymmetry is interpreted as a pressure vortex possibly induced by planet-disk interactions. No compact continuum emission was detected at the locations of either candidate protoplanet. For the candidate protoplanet which was previously directly imaged (e.g.,

Quanz et al. 2015), Jaime derived strong upper limits on the circumplanetary disk mass and radius, showing that these constraints are incongruent with models which require massive circumplanetary disks to grow protoplanets, yet are consistent with other scenarios and numerical simulations. Thus, the high-resolution ALMA study of the disk of HD 100546 proved to be valuable to hone in on probable planet formation pathways.

In the last three years the CAS group has made exciting findings on the nature of circumstellar disks. Our observations of molecular lines, dust, and polarization at different frequencies have made new connections between the earliest seeds of star formation and the disk environments that can harbor planets. By combining data from a wide range of size scales — from core to envelope to disk — new insights on the structure, dynamics, and evolution of circumstellar disks have been revealed. We have studied the impact of magnetic fields in protostellar cores on disk formation, searched for the youngest FHSC candidates, analyzed the disk-envelope connection, examined small-scale disk structures at early times, and hunted for the earliest footprints of planet growth.

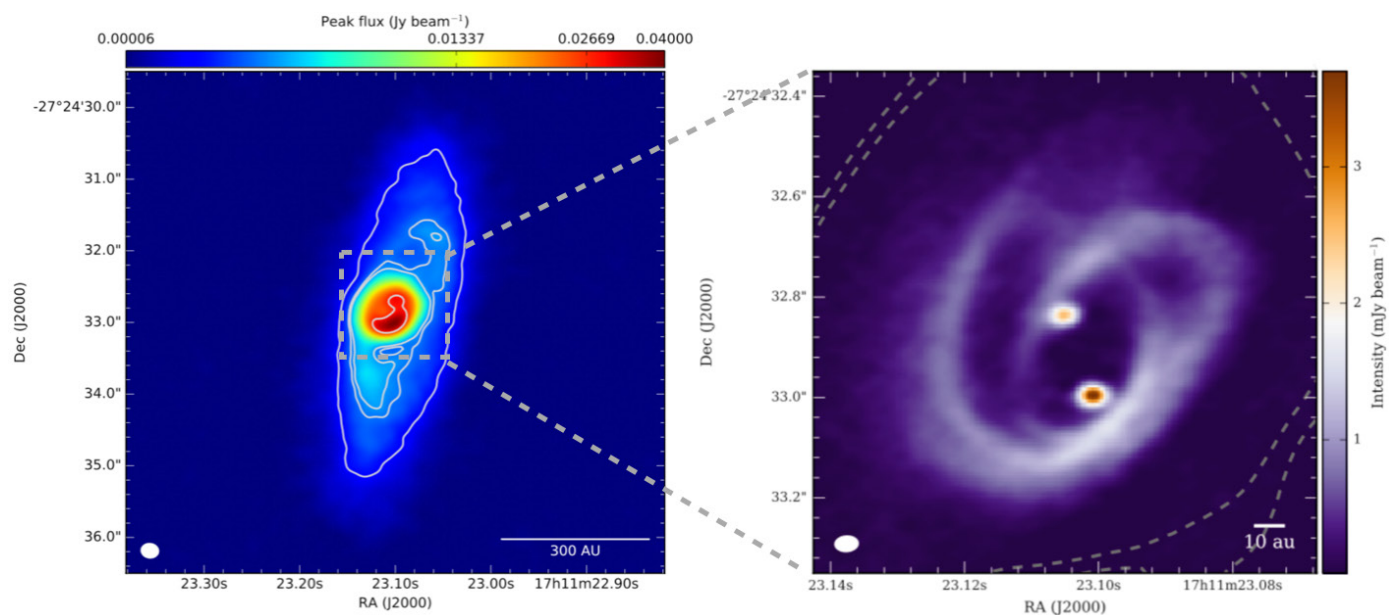


Fig. 5.3.5 *Left panel:* ALMA 1.3 mm continuum image of BHB07-11 at a resolution of 36 au (Alves et al. 2017). *Right panel:* higher-resolution data (7 au) of the inner disk, showing the protobinary system and a network of filaments (Alves et al. 2019, submitted).

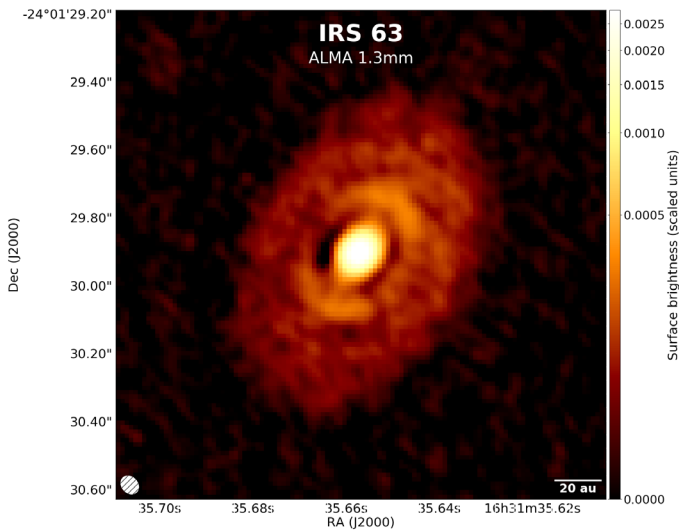


Fig. 5.3.6 The disk of Class I protostar IRS 63, imaged with ~ 7 au resolution with enhanced contrast to highlight the concentric ring pattern (Segura-Cox et al. in prep.).

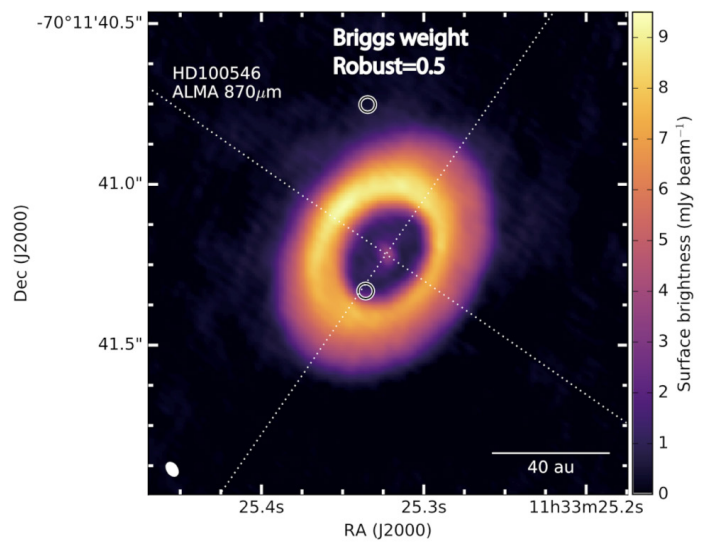


Fig.5.3.7 ALMA 0.87 mm continuum image with ~ 4 au resolution of the disk in HD 100546 displaying the asymmetric ring and small inner disk. The open circles mark the positions of candidate protoplanets (Pineda et al. 2019).

Selected References:

- Agurto-Gangas, C., Pineda, J. E., Szucs, L., et al. 2019, arXiv:1901.05021
 Alves, F. O., Girart, J. M., Caselli, P., et al. 2017, A&A, 603, L3
 Alves, F. O., Girart, J. M., Padovani, M., et al. 2018, A&A, 616, A56
 Alves, F. O., Caselli, P., Girart, J. M., et al. 2018, submitted to Science
 Bate, M. R., Tricco, T. S., & Price, D. J. 2014, MNRAS, 437, 77
 Cridland, A. J., Pudritz, R. E., & Alessi, M. 2019, MNRAS, 484, 345
 Maureira, M. J., Arce, H. G., Dunham, M. M., et al. 2017, ApJ, 838, 60
 Mellon, R. R., & Li, Z.-Y. 2008, ApJ, 681, 1356
 Pineda, J. E., Arce, H. G., Schnee, S., et al. 2011, ApJ, 743, 201
 Pineda, J. E., Quanz, S. P., Meru, F., et al. 2014, ApJL, 788, L34
 Pineda, J. E., Szulagyi, J., Quanz, S. P., et al. 2019, ApJ, 871, 48
 Quanz, S. P., Amara, A., Meyer, M. R., et al. 2015, ApJ, 807, 64
 Segura-Cox, D., Harris, R. J., Tobin, J. J., et al. 2016, ApJ, 817, 14
 Segura-Cox, D., Looney, L. W., Tobin, J. J., et al. 2018, ApJ, 866, 161
 Zhao, B., Caselli, P., Li, Z.-Y., et al. 2016, MNRAS, 460, 2050

Felipe de Olivera Alves



Dominique Segura-Cox



(Other CAS team members include: C. Agurto-Gangas, P. Caselli, M. J. Maureira, J. E. Pineda, E. Redaelli)

5.4 CAS Theory

5.4.1 Penetration of Galactic Cosmic Rays into Clouds and Disks

Galactic cosmic rays (CRs) are a ubiquitous source of ionisation of the interstellar gas. Along with UV and X-ray photons as well as natural radioactivity they determine the fractional abundance of electrons, ions and charged dust grains in molecular clouds and circumstellar discs, and thus substantially impact the dynamical and chemical processes occurring in these objects. The transport regime of the penetration of galactic CRs and their further propagation depend on a variety of conditions. Understanding these conditions is essential in determining whether the CRs can stream freely along the magnetic field lines, or they experience significant scattering on the field fluctuations, leading to diffusive propagation. Below we summarize the recent progress in the theory of CR transport in clouds and disks, and discuss the resulting effect on the gas ionisation for a broad range of densities, from low-density envelopes of molecular clouds to the densest regions of circumstellar disks.

One of the fundamental questions is how interstellar CRs penetrate into clouds and disks, i.e., what mechanisms govern this process and how do they affect the CR spectrum inside the clouds.

In recent papers by Ivlev et al. (2018) and Dogiel et al. (2018) we showed that the Galactic spectrum of CR protons at energies below ~ 30 GeV could be significantly modified while CRs traverse the outer diffuse envelope of a dense cloud, even though the ionisation losses in the envelope are relatively low. The governing mechanism behind the effect is the excitation of MHD waves in the envelope by a flux of penetrating CRs. These self-generated magnetic disturbances efficiently scatter CRs, which inhibits their free streaming into the cloud. We de-

veloped a self-consistent model of this essentially nonlinear phenomenon, describing the energy-dependent transition between a free streaming and diffusive propagation of CRs. One of our key findings is the existence of a certain threshold energy E_{ex} below which the penetrating flux $S(E)$ is modulated. For a broad range of energies below E_{ex} , the magnitude of the modulated flux is inversely proportional to the energy and independent of the Galactic spectrum. Fig. 5.4.1 illustrates the modulation effect, showing that CRs can be significantly depleted in the interior of dense clouds.

Irrespective of their transport regime, CRs propagate along the local magnetic field lines. The magnetic configuration in dense astrophysical objects can be very complicated and the field strength can be much larger than the interstellar value. This leads to efficient mirroring of the penetrating CRs – their pitch angles increase in response to the growing field until reaching 90° , and thus more and more particles are reflected back. On the other hand, the convergence of field lines results in the CR focusing. In Silsbee et al. (2018) we have studied the combined impact of magnetic mirroring and focusing on the ionisation by CRs in dense molecular clouds and circumstellar disks. We rigorously showed that for effective column densities of up to $\sim 10^{25} \text{ cm}^{-2}$ the two effects practically cancel each other out, provided the magnetic field strength has a single peak along field lines. This conclusion implies that the ionisation is independent of the field strength, thus dramatically simplifying the analysis of numerous problems associated with the penetration of CRs (such as the gas ionisation and heating, core and disk dynamics, dust coagulation, etc.).

The processes governing the CR propagation and ionisation become remarkably diversified at column den-

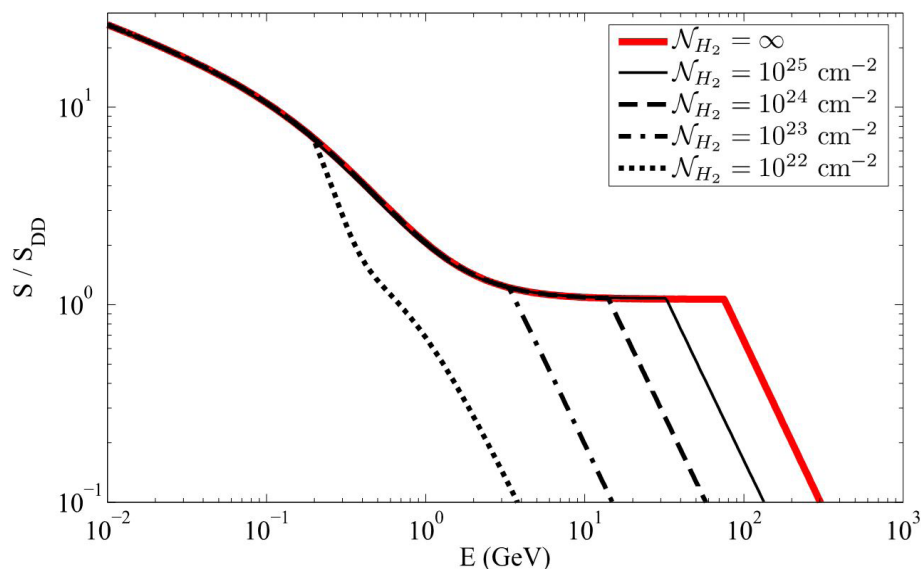


Fig. 5.4.1 Self-modulation of CRs penetrating into a molecular cloud. The CR flux, $S(E)$, is normalized to the universal (diffusion-dominated) relation $S_{\text{DD}}(E) = \text{const}/E$. The modulation occurs below the threshold energy E_{ex} (which depends on the gas column density of the cloud, N , as indicated), at higher energies Galactic CRs freely propagate into the cloud.

ties N above $\sim 10^{25} \text{ cm}^{-2}$, relevant for the inner regions of collapsing clouds and circumstellar discs. Mechanisms of energy loss other than ionisation become dominant in this case. In a paper by Padovani et al. (2018) we carefully investigated attenuation of Galactic CRs at such high column densities, by including both the relevant energy loss and the particle production mechanisms and adopting appropriate models for the transport of primary and secondary CR particles. The top panel of Fig 5.4.2 demonstrates the main ionisation routes associated with various secondary particles produced by primary CRs. We showed that for N above $\approx 3 \times 10^{25} \text{ cm}^{-2}$ the CR ionisation rate rapidly becomes dominated by electron-positron pairs, locally produced by secondary photons. The bottom panel shows contributions of the primary and secondary CRs into the total ionisation rate, demonstrating that the ionisation at very high column densities is expected to be much higher than previously thought.

Selected References:

Dogiel, V. et al. 2018, *ApJ*, 868, 114
 Ivlev, A.V. et al. 2018, *ApJ*, 855, 23
 Padovani, M. et al. 2018, *A&A*, 614, A111
 Silsbee, K. et al. 2018, *ApJ*, 863, 188

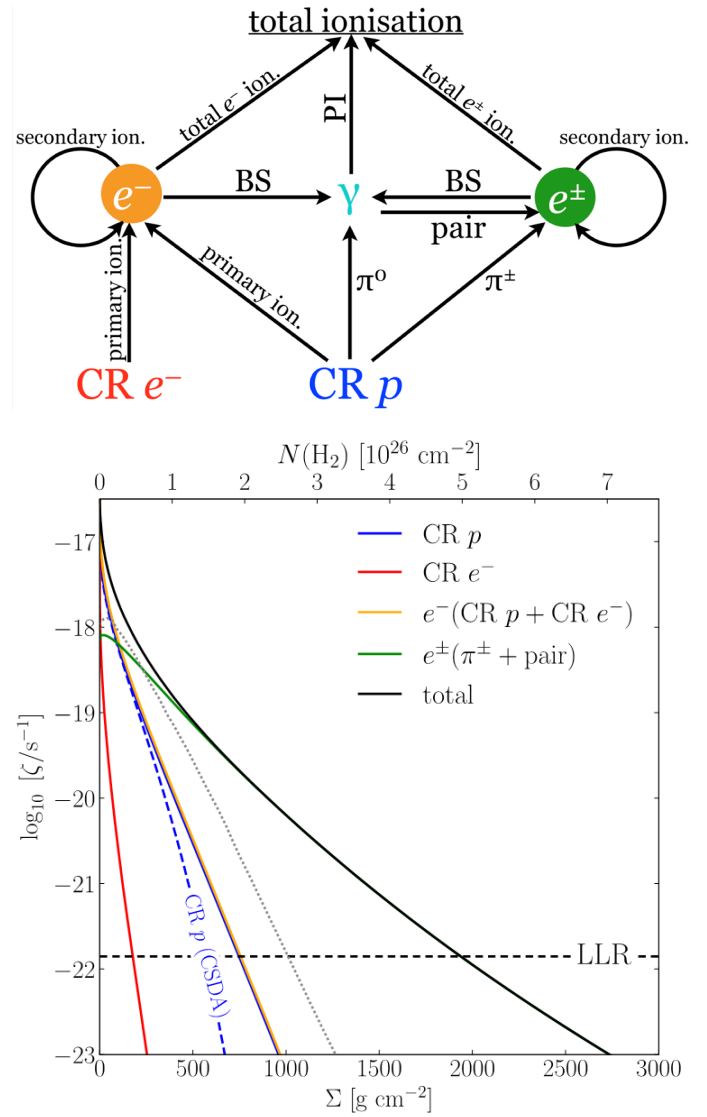


Fig. 5.4.2 Top: Ionisation diagram, explaining the effect of secondary particles that are generated (directly or indirectly) by CR protons and electrons at high column densities through primary ionisation, pion decay (π^0, π^\pm), bremsstrahlung (BS), and pair production (pair). The secondary particles include electrons (e^-), positrons (e^+), and photons (γ). **Bottom:** Ionisation rate per H_2 molecule due to primary and secondary CR species, ζ , plotted vs. the gas column density N . The black solid curve shows the total ionisation rate, the coloured curves represent partial contributions, as indicated in the legend. The horizontal dashed line is the ionisation rate set by long-lived radioactive nuclei (LLR). For comparison, the grey dotted curve shows $\zeta(N)$ which had been commonly used previously.



Alexei Ivlev

(Other CAS team members include: K. Silsbee, P. Caselli)

5.4.2 The Role of Non-ideal MHD in Protoplanetary Disk Formation & Grain Growth

Protoplanetary disks (PPDs) - the cradle of young planets - are the crucial link between the large scale cloud cores and the origin of solar system and life. However, the formation and evolution of PPDs have encountered great challenges in the past decades. Our CAS-Theory group aims to solve the puzzles of early formation of PPDs and the subsequent growth of dust grains in PPDs, in both of which the magnetic field plays a key role. We show through non-ideal magnetohydrodynamic (MHD) simulations that ambipolar diffusion (AD) can efficiently decouple the magnetic field from the bulk neutral matter in the infalling envelope at $\sim 10^2$ AU scale, if a large population of very small grains (VSGs: ~ 10 Å to few 100 Å) is removed from the standard MRN distribution. In the absence of VSGs, the enhanced level of AD enables not only the formation of disks at tens of AU, but also the development of spiral and ring structures at 100 AU scales where binary or multiple systems are born. To follow the subsequent evolution of PPDs and growth of dust grains therein, we now adopt shearing box simulations to obtain a more realistic turbulence spectrum of the magneto-rotation instability (MRI), which lies in the center of grain growth models.

Recent interferometry observations reveal a large number of protoplanetary disks (PPDs) around young stellar objects with Keplerian rotation. To understand how planets form, it is crucial to study closely the formation and evolution of the host PPDs. However, the formation of such rotationally supported PPDs was previously shown to be difficult due to strong magnetic braking which removes most of the angular momentum of the infalling gas (Mellon & Li 2008; Hennebelle & Fromang 2008). This is the so-called magnetic braking “catastrophe” in the ideal

MHD limit when matter is well frozen into the magnetic field. In reality, dense cores are only slightly ionized and magnetic fields are expected to partially decouple from neutral matter through non-ideal MHD effects, including ambipolar diffusion (AD), Ohmic dissipation, and Hall effect, all of which are determined by chemistry and other microscopic physical processes (Nakano et al. 2002).

Ionization Chemical Network for Dense Cores and PPDs:

In order to accurately follow the dynamical evolution of magnetic fields in dense cores and PPDs, we developed a chemical code **ARCHEM** (Zhao et al. 2018b) to pre-compute fractional abundances and non-ideal MHD diffusivities, ready to be tabulated in numerical simulations. Currently, we account for 21 neutral species, 31 ion species, and singly charged (\pm) dust grains, with ~ 500 reactions (can be easily expanded) and a detailed treatment of molecular freeze-out and cosmic ray desorption for different grain size distributions. Similar to Zhao et al. (2016), the complete network also shows that the removal of VSGs greatly enhances the rate of both AD η_{AD} and Hall effect η_{Hall} (Fig. 5.4.3) by 1 - 2 orders of magnitude, which is key for solving both the magnetic flux problem and the magnetic braking “catastrophe” in star formation. We are currently implementing multiple grain charging and more complete ionization mechanisms into **ARCHEM** for global non-ideal MHD simulations of PPDs.

Disk Formation & Fragmentation Enabled by Enhanced Ambipolar Diffusion in the Envelope:

Adopting the tabulated ionization chemistry and non-ideal MHD diffusivities, we carry out 3D simulations of collapsing dense cores using ZeusTW MHD code. We find that in the absence of VSGs, the enhanced AD can

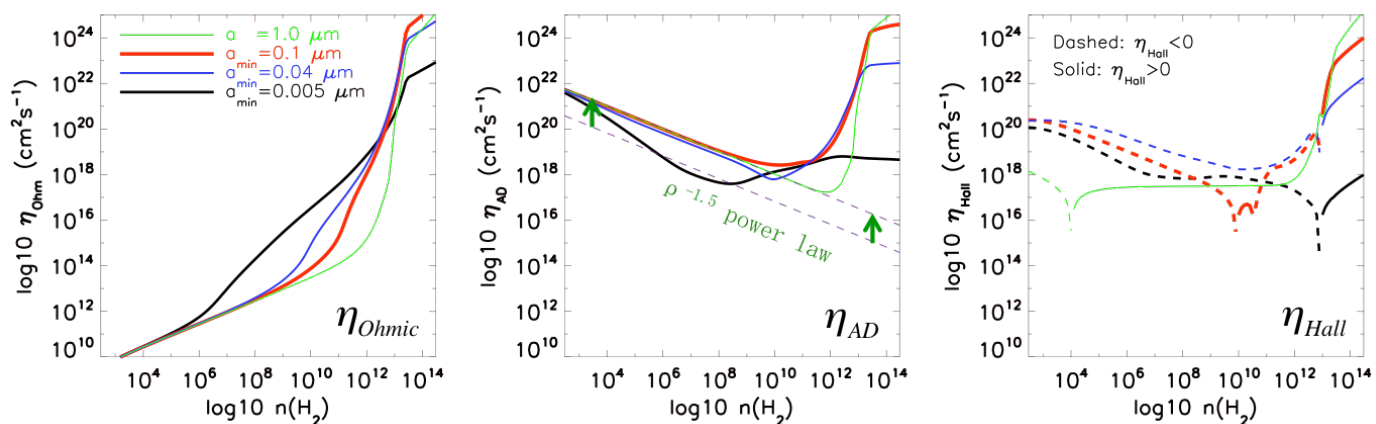


Fig. 5.4.3 Non-ideal MHD diffusivities computed from the ionization chemical network using ARCHEM, for different grain size distributions (with a fixed $a^{-3.5}$ power law and $a_{\max} = 0.25 \mu\text{m}$, but different a_{\min} , except for the single sized case of $a = 1 \mu\text{m}$). **Left:** Ohmic diffusivity η_{Ohmic} . **Middle:** ambipolar diffusivity η_{AD} , the dashed purple line shows the classical $\rho^{-1.5}$ power law. **Right:** Hall diffusivity η_{Hall} . The chemical network can also post-process the simulation output and obtain chemical differentiations from envelope to disk.

efficiently decouple the magnetic flux from the bulk neutral matter in the infalling envelope. Indeed, the outward drift velocity of magnetic field due to AD almost balances the bulk infall velocity at a few 100 AU to 1000 AU scales, indicating that a reduced amount of magnetic flux is dragged into the circumstellar region by the collapsing flow. As a result, the magnetic braking is much less destructive to disk formation and more angular momentum is retained for sustaining disk rotation. With faster initial rotation and/or weaker magnetic field, the initial disks tend to be Toomre-unstable, which leads to the formation of prominent spiral structures that function as centrifugal barriers. The piling-up of infall material near the centrifugal barrier often produces dense fragments of tens of Jupiter masses. Some fragments inspiral towards the central star, producing bursts in mass accretion rate; others are longer lived and have the potential to become companion stellar objects (Zhao et al. 2018a, see Fig. 5.4.4).

Turbulence Spectrum and Grain Growth in PPDs:

As a first step towards the understanding of grain size evolution in PPDs, we investigate the properties of realistic turbulence generated by MRI in the disks and its impact on the grain growth models using shearing box simulations. Conventionally, grain growth models adopt the standard Kolmogorov turbulence for the calculation of relative velocities between colliding particles (Ormel & Cuzzi 2007). However, the turbulence generated by MRI is very different from the Kolmogorov turbulence. The existence of magnetic fields results in a power spectrum proportional to $k^{-4/3}$, flatter than the standard $k^{-5/3}$ in Kolmogorov turbulence. Moreover, the shearing motion induced by the Keplerian rotation and the flat magnetic energy spectrum result in much shorter turbulence turn-over times than the standard estimations. Therefore, the grain collisional velocities from realistic MRI turbulence are very different from that in standard Kolmogorov turbu-

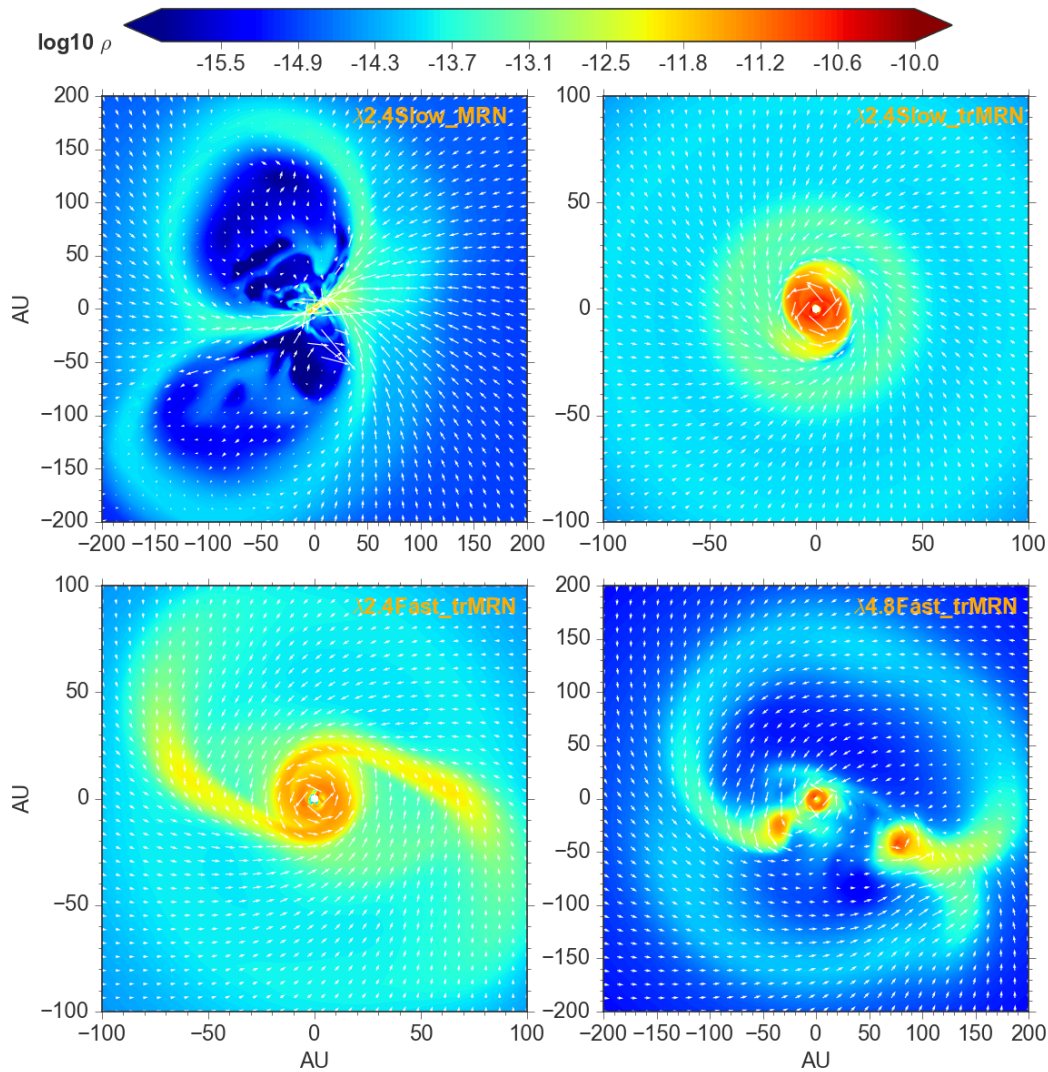


Fig. 5.4.4 Distribution of mass density for different non-ideal MHD models. **Top left:** VSGs present, strong B field (mass-to-flux ratio $\lambda=2.4$), and slow rotation ($\beta_{\text{rot}}=0.025$) model. No rotationally supported disks, only magnetically dominated structure – DEMS (decoupling-enabled magnetic structures). **Top right:** VSGs absent, strong B ($\lambda=2.4$), and slow rotation ($\beta_{\text{rot}}=0.025$) model. Rotationally supported disk. **Bottom left:** VSGs absent, strong B ($\lambda=2.4$), and fast rotation ($\beta_{\text{rot}}=0.1$) model. Large spiral structure. **Bottom right:** VSGs absent, weak B ($\lambda=4.8$), and fast rotation ($\beta_{\text{rot}}=0.1$) Triple stellar system.

lence models: large grains collide at lower velocities, and small grains at much higher velocities (Gong et al. 2019). This can significantly alter the grain size evolution in current standard models. We aim next to investigate the interplay between the grain growth and non-ideal MHD effects in PPDs, and develop self-consistent numerical models, as a pivotal step towards planet formation.



Bo Zhao



Munan Gong

Selected References:

- Gong, M., Ivlev, A., Caselli, P. & Zhao, B. 2019, *in preparation*
 Hennebelle, P., & Fromang, S. 2008, *A&A*, 477, 9
 Mellon, R. R., & Li, Z.-Y. 2008, *ApJ*, 681, 1356
 Nakano, T., Nishi, R., & Umebayashi, T. 2002, *ApJ*, 573, 199
 Ormel, C. W., & Cuzzi, J. N. 2007, *A&A*, 466, 413
 Zhao, B., Caselli, P., Li, Z.-Y., Krasnopolsky, R., Shang, H., & Nakamura, F. 2016, *MNRAS*, 111, 22
 Zhao, B., Caselli, P., Li, Z.-Y., & Krasnopolsky, R. 2018a, *MNRAS*, 473, 4868
 Zhao, B., Caselli, P., & Li, Z.-Y. 2018b, *MNRAS*, 478, 2723

(Other CAS team members include: P. Caselli, A. Ivlev)

5.4.3 Astrochemical Modeling at CAS

Astrochemical models are needed to interpret observations of molecular emission and absorption toward star-forming dense cores, protostellar systems etc., which represent a wide range of physical and chemical conditions. The models must therefore be able to track the chemical evolution of a wide variety of species. These include, but are not limited to, deuterated species which trace the cold and dense centers of pre-stellar cores, and complex organic molecules which are stored on interstellar dust surfaces in the pre-stellar core stage and released into the gas phase during the warm-up phase following protostar formation. The chemical models developed and maintained at CAS encompass these topics and are combined with radiative transfer codes so that molecular emission and/or absorption can be predicted. The chemical models are also used in conjunction with hydrodynamics to study the chemistry in dynamically-evolving systems.

Isotope chemistry: Deuterated species, i.e., species with deuterons substituted in place of protons, become abundant at low temperature ($T \sim 10$ K) and high density ($n_{\text{H}} \sim 10^5 \text{ cm}^{-3}$) where otherwise common molecules such as CO and N_2 freeze onto the surfaces of interstellar dust grains. This opens up new possibilities to trace the gas in cold and dense environments, such as in the centers of star-forming cores. Because both the proton and the deuteron have non-zero spin, species with multiple protons and/or deuterons can exist in different spin states. These spin states can be considered as distinct species at low temperature because radiative decay from one spin state to the other is forbidden by selection rules. Deuterium chemistry is fundamentally connected with spin-state chemistry through the $\text{H}_3^+ + \text{H}_2$ reacting system. Therefore, simultaneous studies of deuterium fractionation and spin-state chemistry yield important information on the properties of star-forming material, and shed light on the initial conditions of star formation. The CAS deuterium chemistry model (developed by O. Sipilä) is used by several members of the CAS group in observational and theoretical studies. A recent research highlight pertains to constraining the chemical age of the envelope surrounding the protostellar system IRAS 16293-2422 A/B to approximately one million years (Harju et al. 2017), made possible by the combination of chemical and radiative transfer models and the simultaneous observation of both the ortho and para spin states of D_2H^+ (Fig. 5.4.5). This also marks the first detection of ortho- D_2H^+ in space.

The isotopes of carbon (^{13}C) and nitrogen (^{15}N) are subject to increasing interest in the star-formation community, because tracing the evolution of isotopes through the star formation process allows us to understand the isotopic abundance ratios observed in the Solar System, for example. ^{13}C has received little attention on the theoretical side, despite its relatively high abundance in

the ISM. Only a handful of models investigating carbon isotopes exist in the literature. A new model for the carbon isotope chemistry is in development at CAS since 2018 (led by O. Sipilä) in collaboration with experts in Paris and Florence. The first publication on this project is currently in the writing stage (Colzi et al., in prep.). The new model – which will be extended to ^{15}N in the future – greatly expands the number of tracer molecules that we can model, providing unique insight into the chemistry in star-forming regions.

Complex organic molecules (COMs): The evolution of organic molecules during the star-formation process is one of the most fundamental questions that astrochemistry aims to answer. However, our understanding of the evolution of molecules such as methanol and methyl formate, which are important precursors of prebiotic molecules, is so far rather limited. The key questions to address are how these molecules are formed in the dark cloud phase preceding star formation, and how they are then distributed in the forming protostellar – and finally planetary – system. Gas-phase and grain-surface formation mechanisms have been explored to explain the formation of COMs in dark cloud conditions, with varying success. The currently most popular mechanism is the so-called warm-up scenario in which COMs are formed on the surfaces of dust grains at low temperature, and then released into the gas phase when the protostar

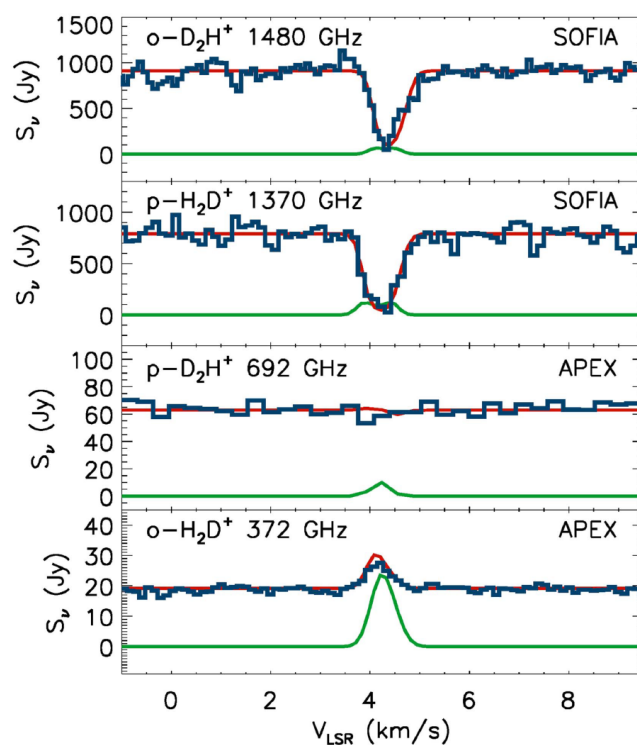


Fig. 5.4.5 Observed (blue) and modeled (red) spectra for ortho and para H_2D^+ and D_2H^+ as presented in Harju et al. (2017). Lines without the effect of dust continuum are shown in green. The match between the observations and the model is very good, and constrains the chemical age of the envelope surrounding IRAS 16293-2422 A/B to $\sim 10^6$ yr.

starts to heat the material around it. This idea is challenged by the observed presence of organic molecules in the gas phase in cold clouds (e.g., Cernicharo et al. 2012).

Vasyunin et al. (2017) presented a new model for the formation of COMs in cold clouds by developing a detailed multilayer ice model that centers around the so-called reactive desorption mechanism as the main driving force responsible for releasing complex molecules in the gas phase also at low temperature. In this scenario, the energy released in a chemical reaction may lead to the immediate desorption of a reaction product on the grain surface. The efficiency of this process depends on the surface composition, and the model of Vasyunin et al. is the first one that couples the reactive desorption scheme with a detailed treatment of time-dependent ice composition. The model predicts relatively high gas-phase abundances for many COMs in dark cloud conditions, and also highlights the important role of the hydroxyl radical OH in the formation pathways of several COMs. Some key results from the work of Vasyunin et al. (2017) are presented in Figure 5.4.6. Like the deuterium model, the COM model is used by several CAS members.

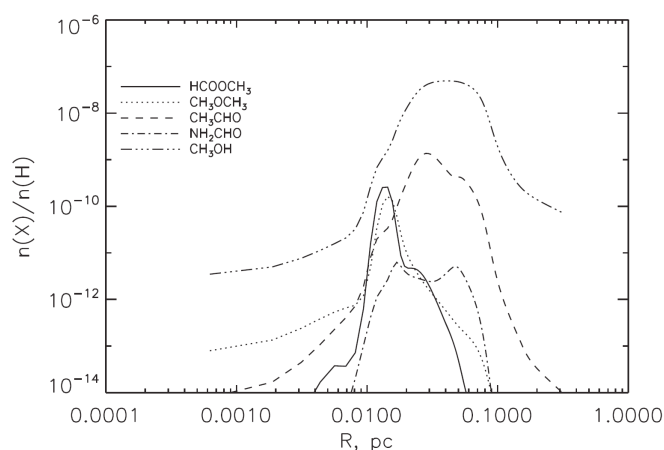


Fig. 5.4.6 Abundance profiles for several COMs in the pre-stellar core L1544 as predicted by the model of Vasyunin et al. (2017). The plot shows that COMs can have appreciable gas-phase abundances if the reactive desorption mechanism is included in the modeling, and that the abundances tend to peak around 0.01-0.03 pc away from the center of the core, in agreement with observations.

Hydrodynamical models: Szűcs et al. (2016) used hydrodynamic giant molecular cloud (GMC) simulations with self-consistent gas phase hydrogen-carbon chemistry and synthetic emission maps in order to evaluate how well CO rotational line emission based observational techniques recover the H_2 masses of GMCs. The X_{CO} and virial analysis based methods recover the H_2 mass of the CO emitting regions within a factor of two, unless the metallicity is low ($\leq 0.3 Z_\odot$) (Fig. 3 in Szűcs et al.). The virial parameter of CO-emitting regions of expanding or dispersing GMCs is systematically lower than that of the overall cloud. The mass derived under the assumption of virial equilibrium corresponds well to the true CO bright H_2 mass of the cloud. At the same time, the CO dark molecular gas fraction increases with the overall

increasing virial parameter. In three-dimensionally irradiated clouds, locally high volume density is needed to reach the few times 10^{21} cm^{-2} column density above which CO is shielded from photodissociation. The high volume density in turn is preferentially associated with stable or collapsing structures.

The large computational cost of chemical models limits the completeness of networks that are practical to implement in hydrodynamic simulations. Szűcs et al. (in prep.) offers a partial solution to the problem by post-processing sub-regions of GMC simulations, taking the density, temperature and irradiation history of gas parcels into account and utilising a gas-grain chemical network comparable to modern pseudo-time-dependent models. Figure 5.4.7 shows abundance profiles in a star forming region in a GMC, post-processed with the above method. The full model includes a gas-grain network with chemical desorption and grain surface quantum tunneling. The comparison to simplified models leads to the following conclusions: 1) dynamics reduces the depletion of gas phase species compared to static models, because gas parcels spend less time at the final density; 2) In the dynamic case the abundance dispersion at a given density increases because parcels reach their final density at different times and their initial abundances at the epoch of core formation differ; 3) dynamic models reproduce the flat abundance profile of NH_3 and N_2H^+ above 10^5 cm^{-3} , seen in observations (e.g. L1544) but problematic in pseudo-time dependent models; 4) the observed range of gas phase methanol abundance cannot be reproduced with only dynamics, non-thermal desorption mechanism and fast surface reactions are more important.

Radiation chemistry: The significant (mostly harmful) effects of ionizing radiation on living organisms are widely known; however, a large body of work in laboratory astrophysics has shown that the bombardment of interstellar ice analogues by energetic ions can lead to the formation of complex organic molecules – even those implicated in the origins of life. Previous attempts to incorporate results from radiation-chemical experiments into astrochemical models has been hampered by the complexity and variety of the underlying physical processes, leading to a glaring deficiency in the physical realism of models of interstellar regions given the ubiquity of cosmic rays and other forms of ionizing radiation there. A new chemical model to simulate the physicochemical effects associated with the irradiation of dust grain ice mantles, with the aim of increasing the physical realism of such models and shrinking the existing gap with experiments, is currently being developed by C. Shingledecker (CAS member since late 2018).

Additional chemical models used at CAS include a dedicated network for computing non-ideal MHD diffusivities in dense cores and protostellar disks (B. Zhao; see also Section 5.4.2), and a chemical network dedicated to sulphur chemistry (J. Laas; Laas and Caselli 2019).

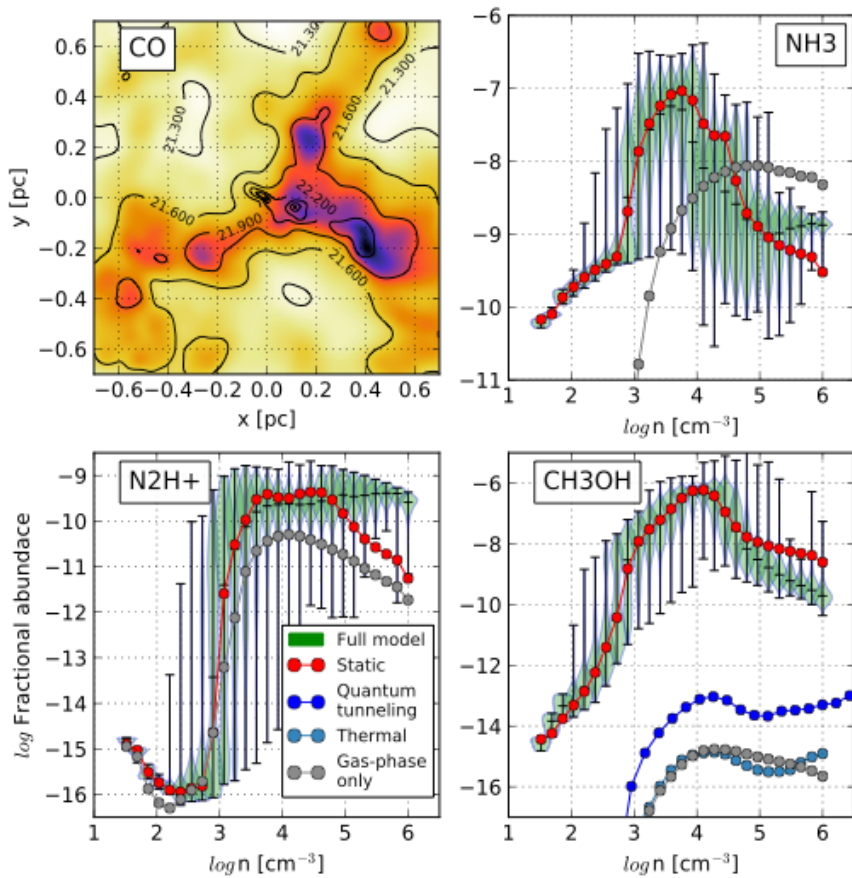


Fig. 5.4.7 Abundance profiles in a simulated star forming region. The green violin plots show the abundance distribution of the full chemical model that takes gas dynamics into account. Colored lines show the median abundance in various simplified models. The red line indicates the static cloud modelled with the full chemical network.

Selected References:

Cernicharo et al. 2012, *ApJL* 759, L43
 Harju, J. et al. 2017, *ApJ* 840, 63
 Laas, J., Caselli, P. 2019, *ApJ* in press
 Sipilä, O. et al. 2017, *A&A* 607, A26
 Szűcs, L. et al. 2016, *MNRAS*, 460, 82
 Vasyunin, A. et al. 2017, *ApJ* 842, 33



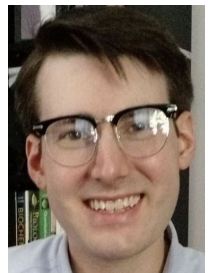
Olli Sipilä



László Szűcs



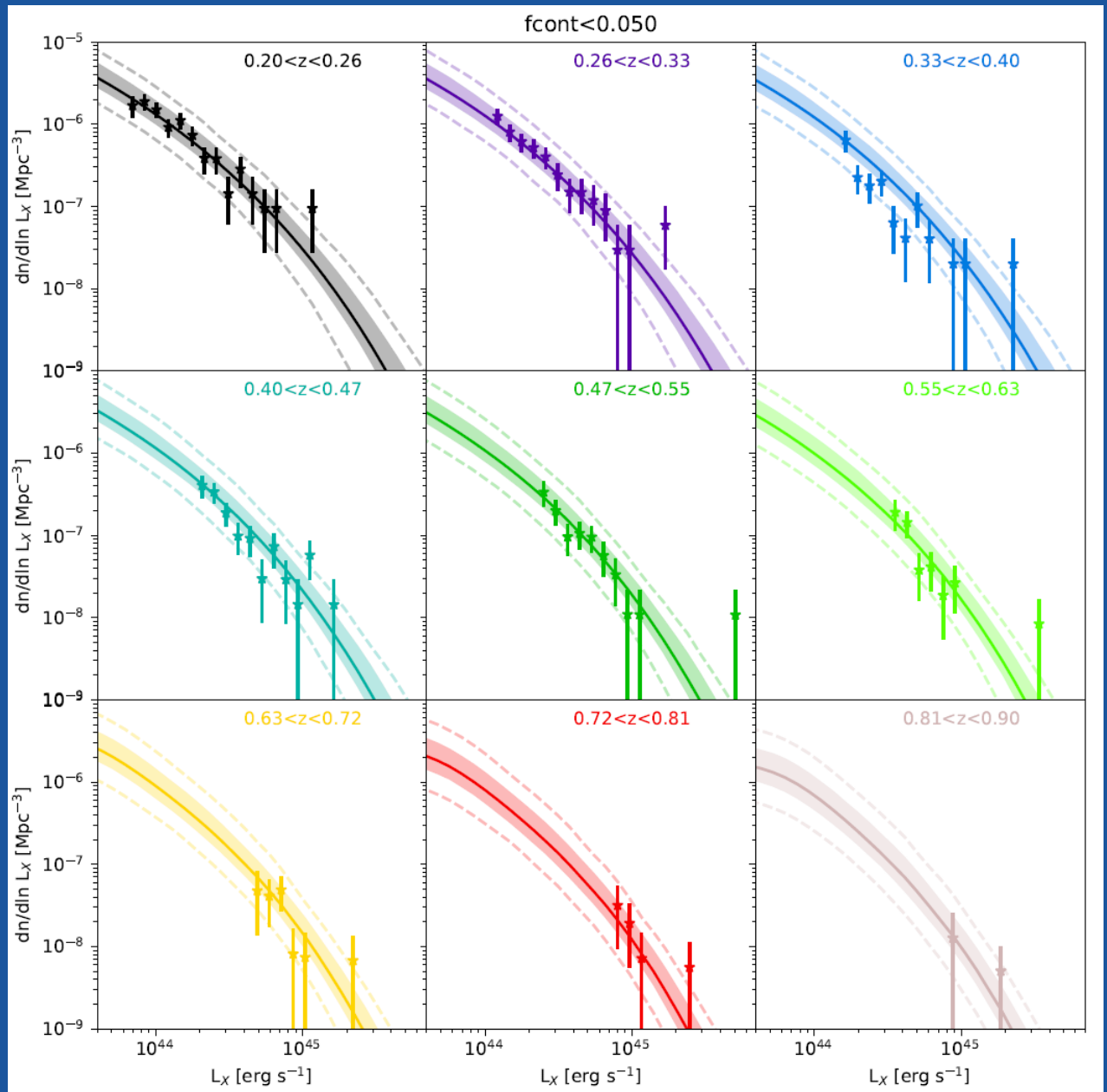
Anton Vasyunin



Christopher Shingledecker

(Other CAS team members include: P. Caselli, A. Ivlev, J. Laas, B. Zhao)

6 Independent Research Groups



The X-ray luminosity function measurements (points) and expectations (lines, shaded regions) within nine redshift bins for a newly defined sample of over 1000 galaxy clusters from RASS+DES. This kind of cluster cosmology analysis is foreseen for application to the X-ray catalogs from the upcoming eROSITA mission.

6. Independent Research Groups

6.1 Developments Toward eROSITA Galaxy Cluster Cosmology

MPG Fellowship Group: Joseph Mohr

The Faculty Fellow group led by Mohr has focused - along with members of the HEG - over the past three years on further preparations for the study of the eROSITA cluster sample. The key elements of this effort include the development and validation of tools for (1) the use of multiband optical imaging data for the definition of the eROSITA cluster sample from the X-ray cluster candidate list, (2) the optimal use of weak lensing and dynamical constraints for the calibration of the masses of the eROSITA clusters and (3) the cosmological analysis of the eROSITA cluster sample with a method that accounts for selection effects and includes marginalization over systematic uncertainties associated with the cluster masses, cluster selection and weak lensing mass calibration.

Optical Confirmation of X-ray Selected Galaxy Cluster Candidates:

The availability of large solid angle, optical multiband surveys like DES, HSC and later LSST for the optical confirmation and redshift estimation of eROSITA selected galaxy clusters is a crucial input for the mission. New tools are needed to combine the eROSITA and ground based optical data efficiently and accurately, pushing beyond what has been done previously in X-ray (and SZE) surveys. Dr. Matthias Klein and Prof. Mohr have developed a red sequence based followup tool that adopts priors on positions and search region from the X-ray properties of an eROSITA cluster candidate and searches through redshift space in the optical dataset to identify overdensities of galaxies (Klein et al. 2018a). This tool builds on our study of the galaxy properties of clusters studied over the full redshift range relevant to eROSITA (Hennig et al. 2017). The new tool, called MCMF (Multi-component Matched Filter cluster followup), also determines the probability that the identified optical source is a random superposition with the X-ray candidate, thereby producing a catalog where the contamination of the final catalog can be tuned according to the application (typically, <1%, for cluster cosmological). As a validation, we apply the new tool to the ROSAT all sky survey (RASS) revised faint source catalog (2RXS- Boller+16), producing a 1000+ X-ray selected cluster catalog over the DES region (Klein et al. 2018b). This catalog has over 100 systems at $z > 0.5$ and has a density that is 7x that of the original RASS selected cluster catalog over the same area. The experience gained in the RASS study has prepared us to deploy this tool for eROSITA.

Weak Lensing and Dynamical Mass Calibration:

Mass uncertainties are the chief systematics challenge in cluster cosmology. To address this, we develop a mass calibration toolkit for cluster observable mass relations that corrects for selection effects, accounts for cos-

mological sensitivities and allows marginalization over systematic uncertainties in the mass constraints. Our Bayesian forward modeling code has been developed and tested both for weak lensing and dynamical mass constraints. For weak lensing, we adopt the observed shear profiles and associated redshift distributions of the shear galaxies as constraints and then predict the expected shear profile for each individual cluster in the sample, iterating to find the best fit mass - observable relation. In contrast to a stacking analysis, our new approach allows us to constrain also the intrinsic scatter in the mass - observable relation (Dietrich et al. 2019), which is crucial input to the cosmological analysis. To use dynamical constraints, we develop a code that uses a Jeans analysis and marginalizes over different models of the orbital anisotropy (Capasso et al. 2019). We have validated our weak lensing code with an initial calibration of SPT selected clusters using the DES dataset (Stern et al. 2019), and we have validated our dynamical code using the kinematic data acquired in the Spiders survey (Capasso et al. 2018). These validation studies have been a success and have prepared us for mass calibration of the eROSITA cluster dataset.

Cosmological Analysis:

A third focus has been the development of a cosmological analysis code that fully integrates mass calibration from weak lensing and is designed to work on the eROSITA cluster dataset (Grandis et al. 2018). This code is a cutting edge Bayesian forward modeling code that allows for the use of multiple observables (e.g., eROSITA count rate, cluster richness, shear profiles). By producing mock catalogs built using characteristics of eROSITA and our measurement of the luminosity - mass relation over the relevant redshift range (Bulbul et al. 2018), we have forecast the eROSITA sample given various selection cuts and studied the expected cosmological constraints on neutrino masses, the cosmic acceleration, the local amplitude of matter fluctuations and the growth rate of cosmic structure (Grandis et al. 2018). We have used a related code for the first weak lensing based cosmological analysis of the SPT cluster sample (Bocquet et al. 2018). We are currently using the eROSITA prototype code for cosmological validation of the RASS+DES cluster sample described above. Therefore, we expect to be ready for the analysis of the eROSITA sample once it has been constructed.

Selected References:

(bold face when papers led or co-led by Mohr group)

- Bocquet et al.**, 2018 *ApJ*, submitted (*astro-ph/1812.01679*).
Boller et al. 2016, *A&A*, **588**, 103.
Bulbul et al., 2019, *ApJ*, **871**, 50.
Capasso et al., 2019, *MNRAS*, **482**, 1043.
Capasso et al., 2018, *MNRAS*, submitted (*astro-ph/1812.06094*)
Chiu et al., 2018 *MNRAS*, **478**, 3072.
Dietrich et al., 2019, *MNRAS*, **483**, 2871.
Grandis et al., 2018, *MNRAS*, submitted (*astro-ph/1810.10553*).
Hennig et al., 2017, *MNRAS*, **467**, 4015.
Klein et al., 2018a, *MNRAS*, **474**, 3324.
Klein et al., 2018b, *MNRAS*, submitted (*astro-ph/1812.09956*).
Stern et al., 2019, *MNRAS*, submitted (*astro-ph/1802.04533*).



Joseph Mohr

(Other members of the Mohr group at MPE include: M. Klein. Other members at the USM are: S. Bocquet, R. Capasso, I. Chiu, J. Dietrich, S. Grandis, C. Hennig, and C. Stern)

6.2 The Physical, Thermal and Compositional Characterization of Small Bodies in the Solar System

Research Group: Thomas Müller

The EU Horizon 2020 funded benchmark study Small Bodies Near and Far (SBNF) addresses critical points in reconstructing physical and thermal properties of near-Earth, main-belt, and trans-Neptunian objects (Müller et al. 2018). We combine visual and thermal data from the ground and from astrophysics space missions to improve our scientific understanding of these objects. We incorporate different methods and techniques to get full information on selected targets: lightcurve inversion, stellar occultations, thermophysical modelling, radiometric methods, radar ranging, and adaptive optics imaging. The development of new tools is crucial for the interpretation of much larger data sets, but also for the operations and scientific exploitation of interplanetary missions. Conversely, the ground-truth information from these missions allows us to assess the limitations of each method and advance the techniques beyond the current state of the art. During the period 2016-2018 the SBNF project created new tools, services and products, for the Planetary Science community and the results are documented in more than sixty refereed publications.

A large part of the SBNF project was devoted to visible and thermal photometric studies of prominent objects like the primitive near-Earth asteroid Ryugu, target of the Hayabusa2 mission (Müller et al. 2017b), or the large Halloween asteroid at lunar distance (Müller et al. 2017a). In the main asteroid belt, we studied the link between (6) Hebe and ordinary H chondrites (Marsset et al. 2017) and the thermal properties of several slowly rotating main-belt asteroids (Marciniak et al. 2018/2019). At larger heliocentric distances, we investigated the physical properties of the Centaur Bienor (Fernández-Valenzuela et al. 2017), the highly elongated trans-Neptunian object (TNO) 2008 OG₁₉ (Fernández-Valenzuela et al. 2016), and large TNOs Haumea, 2003 VS₂ and 2003 AZ₈₄, (Santos-Sanz et al. 2017).

After the very successful Herschel Key Project „TNOs are Cool: A survey of the trans-Neptunian region with Herschel“ (Müller et al. 2009), we started to combine thermal measurements with the newly developed technique of TNO occultations (Ortiz et al. 2019). Size, shape, and even topographic features and spin properties have been revealed by multi-chord occultation events of TNOs 2007 UK₁₂₆ (Schindler et al. 2016) and 2003 AZ₈₄ (Dias-Oliveira et al. 2017). One highlight of the SBNF project (see Fig. 6.2.1) was the discovery of a ring around the dwarf planet Haumea (Ortiz et al. 2017). The occultation results also enabled the reinterpretation of Haumea's thermal emission as measured by Spitzer and Herschel (Müller et al. 2019). Haumea must have a thermal inertia of $\sim 5 \text{ J m}^{-2} \text{ K}^{-1} \text{ s}^{-1/2}$, indicating a compact crystalline water ice surface. The combined data sets led

to geometric albedos above 0.5 for Haumea's satellites and unexpectedly high densities larger than 1.0 g cm^{-3} .

We also took advantage of the Kepler-K2 capabilities to measure high-quality lightcurves of Solar System objects with low apparent sky motions. We were able to determine a wide variety of rotation periods, as well as size and shape information from combined thermal data, for irregular satellites around Uranus (Farkas-Takács et al. 2017) and Neptune (Kiss et al. 2016), for large samples of main-belt asteroids (Szabó et al. 2016) and Trojans (Szabó et al. 2017), and ten Centaurs (Kiss et al. 2019a). We determined the large size and slow rotation of the TNO 2007 OR₁₀ (Pál et al. 2016), discovered a satellite (see Fig. 6.2.1, left) and determined its mass and density (Kiss et al. 2017, 2019b).

The detailed information revealed by target-based characterisation studies can be further exploited by comparison with the statistical properties of different populations. Following up on previous infrared missions AKARI, Spitzer, WISE and Herschel, we characterized sizes and albedos of the Haumea family (Vilenius et al. 2018), currently the only known trans-Neptunian collisional family, of Mars-crossing asteroids (Fig. 6.2.1, right), precursors of some near-Earth asteroids (Alí-Lagoa et al. 2017), and all known asteroid detections in the AKARI survey (Alí-Lagoa et al. 2018). The Herschel radiometric sizes for the 25 known binary or multiple systems in the trans-Neptunian region allowed us to look into the size-density distribution in the outer Solar System (Kovalenko et al. 2017), where densities are typically below 1 g cm^{-3} except for dwarf planets, where we find densities between 1.5 and 3 g cm^{-3} .

The SBNF project (<http://www.mpe.mpg.de/~tmueller/sbnaf/>) also allowed us to improve modelling techniques to reconstruct shape and spin information, to determine accurate sizes, albedos, and to constrain thermal properties for near-Earth, main-belt, and TNOs. Various web tools, databases, and services were developed or improved, a range of new data products were created, and the far-IR calibration activities of Herschel, AKARI, SOFIA, IRAM, APEX, and ALMA were supported by new photometric standards (well characterized main-belt asteroids). All tools and results are publicly available and widely used within the Planetary Science Community.

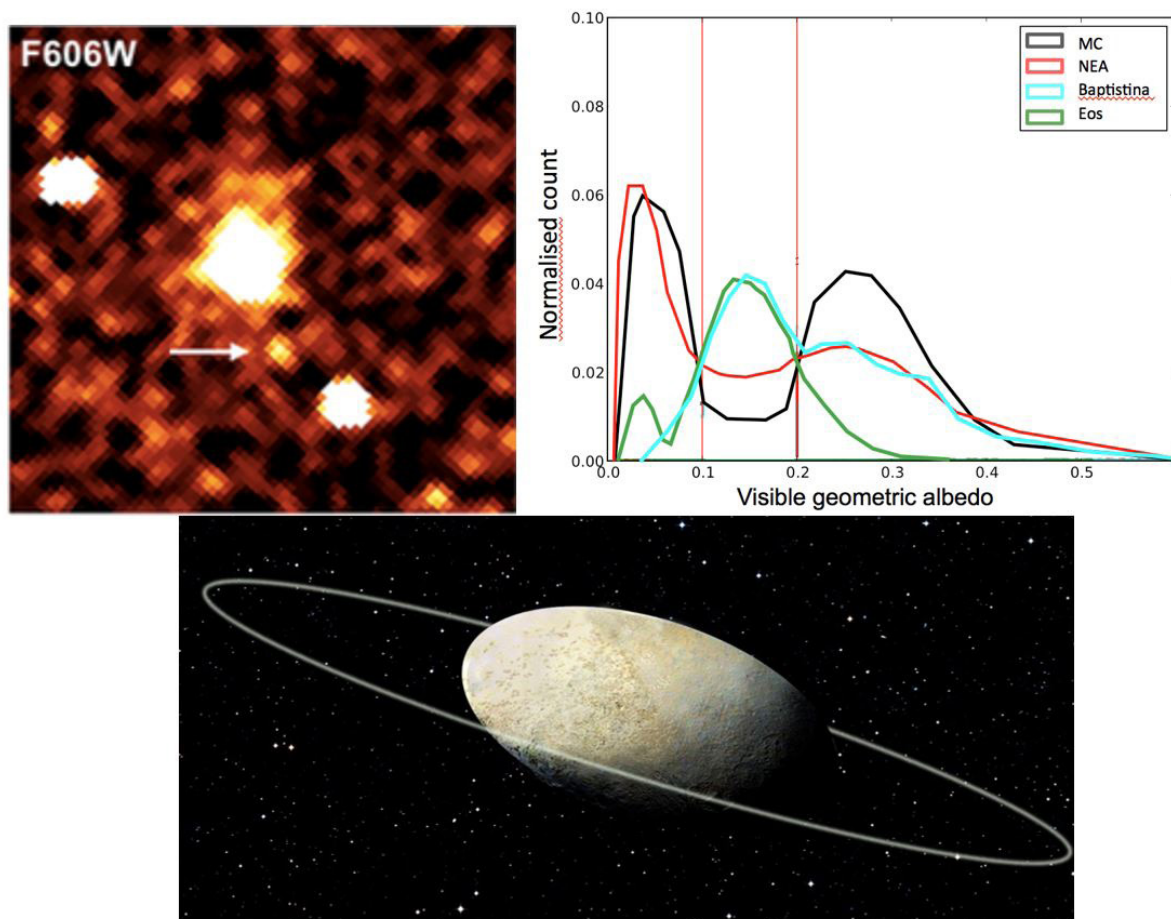


Fig. 6.2.1 Left: The satellite discovery of 2007 OR₁₀ with HST (Kiss et al. 2017). Right: Histogram of geometric albedos of Mars-crossers (MC) and near-Earth asteroids (NEA). NEAs have a higher fraction of 0.1 - 0.2 albedos than the MCs, so other sources like the Baptistina or Eos families must supply such population. Bottom: Artistic rendering of the ring discovered around Haumea (Ortiz et al. 2017).

Selected References:

- Ali-Lagoa et al. 2017, A&A 603, 55A
 Ali-Lagoa et al. 2018, A&A 612, A85
 Dias-Oliveira et al. 2017, AJ 154, 22D
 Farkas-Takács et al. 2017, AJ 154, 119
 Fernández-Valenzuela et al. 2016, MNRAS 456, 2354
 Fernández-Valenzuela et al. 2017, MNRAS 466, 4147
 Kiss et al. 2016, MNRAS 457, 2908
 Kiss et al. 2017, ApJL 838, L1
 Kiss et al. 2019a, MNRAS, subm.
 Kiss et al. 2019b, Icarus, accepted
 Kovalenko et al. 2017, A&A 608, A19
 Marciniak et al. 2018, A&A 610, A7
 Marciniak et al. 2019, A&A, subm.
 Marsset et al. 2017, A&A 604, 64M
 Müller et al. 2009, EM&P 105, 209M
 Müller et al. 2017a, A&A 598, A63
 Müller et al. 2017b, A&A 599, A103
 Müller et al. 2018, Advances in Space Research 62, 2326
 Müller et al. 2019, Icarus in press, arXiv:1811.09476
 Müller et al. 2019, in The Trans-Neptunian Solar System, D. Prialnik, A. Barucci & L. Young (eds.), Elsevier (in press)
 Ortiz et al. 2017, Nature 550, 219
 Ortiz et al. 2019, in The Trans-Neptunian Solar System, D. Prialnik, A. Barucci & L. Young (eds.), Elsevier (in press)
 Pál et al. 2016, AJ 151, 117
 Santos-Sanz et al. 2017, A&A 604, A95
 Schindler et al. 2016, A&A 600, A12
 Szabó et al. 2016, A&A 596, 40
 Szabó et al. 2017, A&A 599, 44
 Vilenius et al. 2018, A&A 618, A136

Thomas Müller



Victor Ali-Lagoa



7 The Institute



7.1 Technical Services

For the realisation of our scientific visions and ideas about the exploration of the Universe with satellites and earthbound instruments, the support of MPE's "general technical services" is indispensable. These services consist of three different groups of specialists:

the department of Electronic Engineering, the department of Mechanical Engineering, each with their workshops, and the IT group. The close collaboration among these engineers and the science groups facilitates efficient development work.

Electronic Engineering

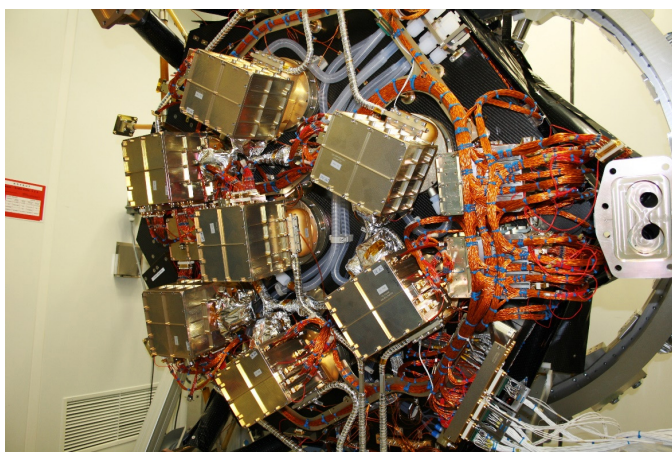


Fig. 7.1.1 eRosita, integrated with all camera electronics boxes and cabling.

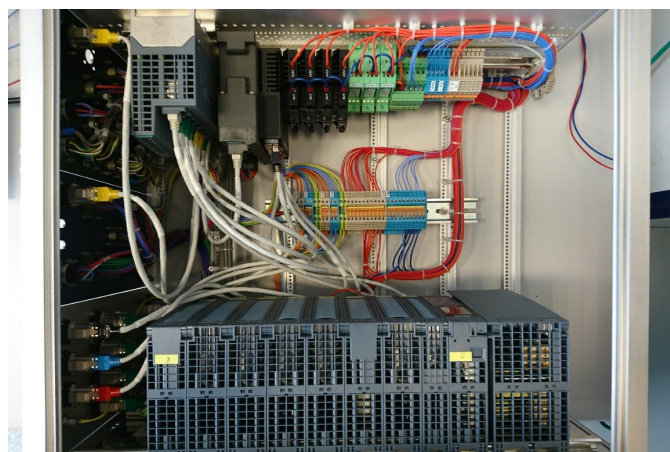


Fig. 7.1.2 PLC-based cryo-vacuum control electronics for ERIS.

The electronics engineering department consists of three groups: electronics development, electronics manufacturing, and building and utilities management. Approximately 30 staff members work in the entire department. In addition, more than ten students are working every year in the group by doing internships, bachelor and master theses.

Electronics engineering at MPE provides all professional skills required for the design, development, manufacturing and testing of scientific instruments. The group's experience covers a broad range, such as PCB (Printed Circuit Board) schematic and layout, electric cabinet construction and wiring, cryo-vacuum technology, PLC (Programmable Logic Controller) programming, processor- or FPGA-based (Field Programmable Gate Array) embedded systems and test setup automation, electronics system engineering, functional or environmental performance verification and circuit simulation.

The electronic equipment is provided for various applications, e.g. instrument control systems in electronics cabinets, highly integrated circuits for space-based electronics or test setups for laboratory experiments. In the years 2016 to 2018 the following MPE projects have benefited

from the technical support of electronics engineers, technicians and other skilled workers in the electronics department: eROSITA, GRAVITY, ARGOS, ERIS, EUCLID, MICADO and ATHENA-WFI. Furthermore, new laboratory facilities and equipment were set up for the science group "Center for Astrochemical Studies".

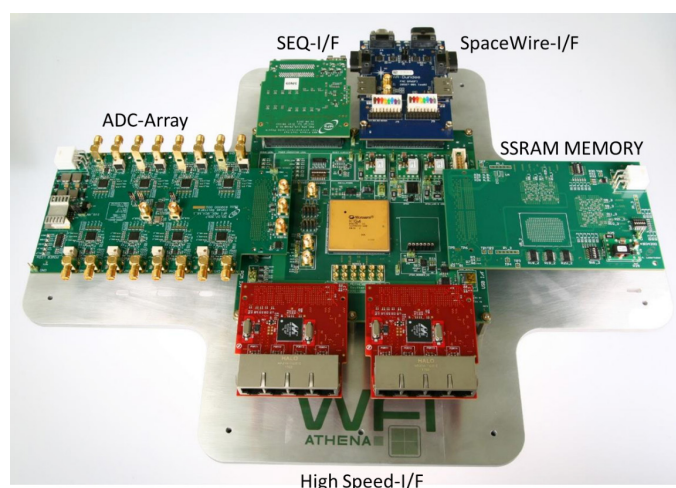


Fig. 7.1.3 ATHENA-WFI Detector Electronics modular breadboard.

Mechanical Engineering

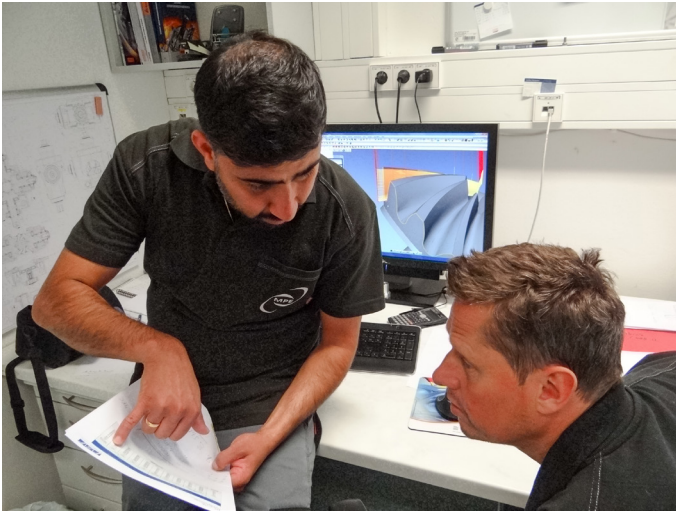


Fig. 7.1.4 Computer-aided design and manufacturing (CAD/CAM) at MPE.

The Mechanical Engineering department develops, manufactures, integrates and tests complex space and ground-based instruments for experimental astronomy. These instruments are based on cutting-edge technologies and innovative concepts and are built in close cooperation with the scientists and project groups, and partly also together with space industry. The department has 37 staff members plus eight apprentices and several student trainees. It is subdivided into three groups: the mechanical design office, the precision mechanical workshop including the training workshop, and the integration and the test facilities.

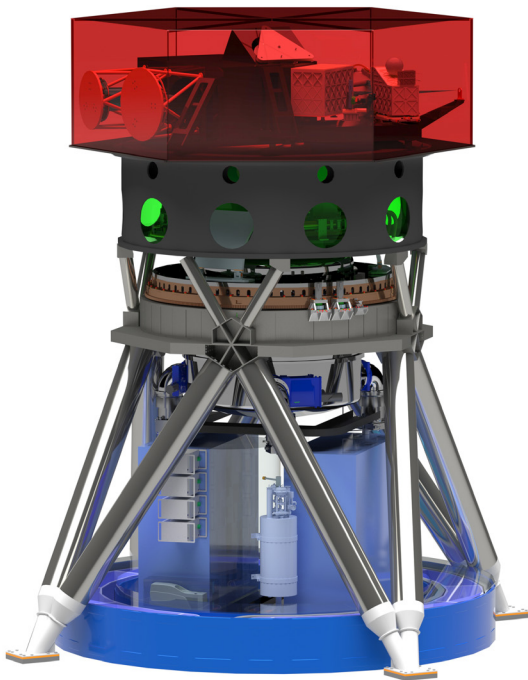


Fig. 7.1.5 CAD view of the MICADO Imaging Camera for the ELT.

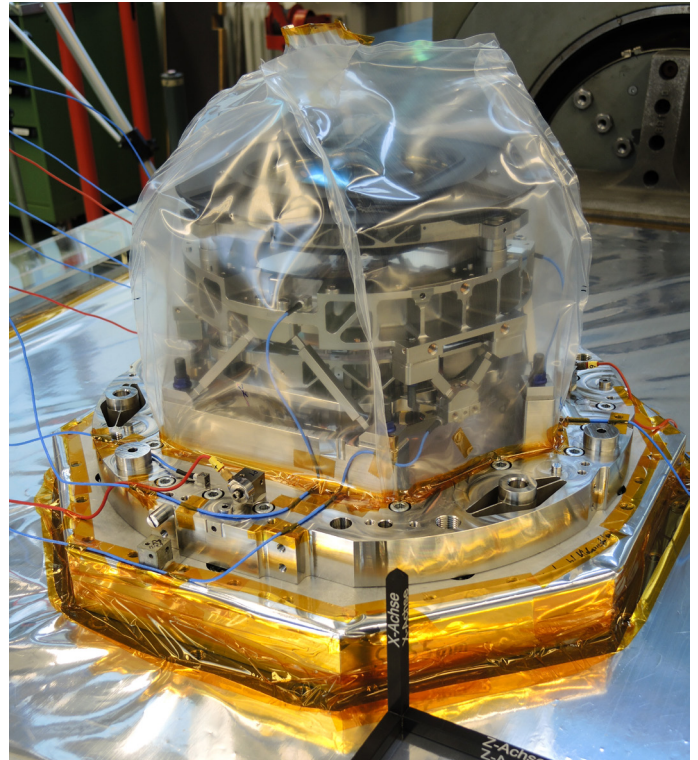


Fig. 7.1.6 EUCLID NISP Optics on the shaker for vibration qualification tests.

The department's qualified specialists deal with a wide range of tasks, reaching from optical- and mechanical design, structural- and thermal analyses to system engineering and product assurance. The complexity in the developments results from the highly demanding requirements, such as extreme cleanliness, stress due to vibration loads during a rocket launch, the required functioning of instruments in vacuum and at very low temperatures. For the mechanical design development and analyses, high-end CAD/CAE/CAM and PLM (Product Lifetime Management) tools are applied. The mechanical workshop then manufactures the sophisticated devices on conventional as well as on state-of-the-art CNC

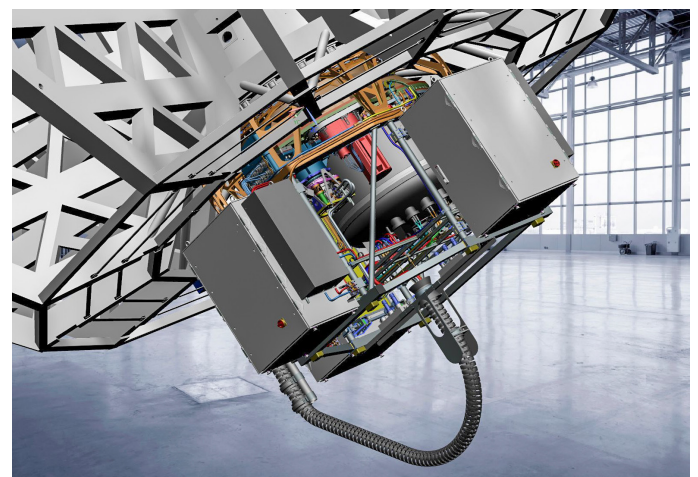


Fig. 7.1.7 CAD view of the ERIS Instrument at the Cassegrain focus of the UT4 telescope of ESO's VLT.

machines. For environmental tests and for space qualification services, a shaker and several thermal vacuum chambers are available in the department.

In the years 2016 to 2018 the mechanical engineering department supported the following main MPE space-

based projects: eROSITA, ATHENA-WFI, EUCLID-NISP, the CASAC millimetre-wave spectrometer, and the cryogenic apertures for ice studies. For ground-based astronomy, mainly the following projects were supported: ERIS, GRAVITY, ARGOS, and MICADO.

Information Technology

Data management and processing is generally a collaborative task of the MPE IT group and the individual research groups. The IT people cover the central tasks and, in addition, support with their IT-knowledge and manpower the science groups in their specific work.

Computing and data processing activities are coordinated and handled by a committee with representatives from all science groups of the Institute. This IT committee plays an important role in steering the Institute's IT strategy, and ensuring that the needs of the scientific groups are being fully accounted for. The main tasks of this committee are to advise on MPE's longer-term IT strategy, to advise and assess central IT projects, to coor-

dinate and to evaluate new hardware as well as software, and the hard- and software procurement. In addition, the committee is co-ordinating the collaboration with the Max Planck Computing and Data Facility (MPCDF).

The members of the central IT support group maintain the central installations, i.e. network, server workstations, printers, and the official WWW pages, with up-to-date information about the Institute. They are also part-time involved in the data processing of and software development for our main science projects like XMM-Newton, eROSITA, GRAVITY, KMOS, PanSTARRS and EUCLID. This guarantees the horizontal flow of information and experience.

7.2 General Services

The Institute's administration supports the scientific management. Organizationally, the administration is divided into four subject areas: Personnel, Finance, Procurement and General Services (including house service, driving and gate/reception services). The administration supports two scientific institutes, the Max-Planck-Institutes for Astrophysics (MPA) and Extraterrestrial Physics (MPE) as well as the Max Planck Computing and Data Facility (MPCDF).

In retrospect, there have been some challenges during the past three years. Several long-time employees retired and had to be replaced. Fortunately, we succeeded in recruiting and integrating appropriate personnel, so the gaps could be closed quickly and smoothly. There were also massive changes with respect to the legal requirements in human resources with the "Wissenschaftszeitvertragsgesetz" (time-limited employment in science). Especially for a research institute with many scientific projects on various time-scales, this new regulation complicates the handling of personnel/employee issues. Furthermore, there were extensive legal changes in the area of procurement (purchasing), in the form of the procurement law reform at national and EU level (VGV procurement regulation and UVG subliminal award regulation), which had to be implemented.



Fig. 7.2.1 Personnel at MPE's administration.

The Print Shop owns all the digital machinery necessary for the production of reports, brochures and preprints for both the MPE and the MPA. In addition, it prints theses of students and reproduces colour copies for MPE and MPA. With the retirement of its personnel, the print shop was closed down in the middle of 2018.



Fig. 7.2.2 The joint MPE/MPA Library.

The Astrobibliothek is the joint library for MPE and MPA. At present it holds a unique collection of about 54000 books and journals, about 7300 reports and observatory publications, as well as print subscriptions for about 140 journals and manages online subscriptions for about 500 periodicals. In addition it maintains an archive of MPA and MPE publications, two slide collections (one for MPA and one for the MPE), a collection of approximately 800 nonprint media, and store copies of the Palomar Observatory Sky Survey (on photographic prints) and of the ESO/SERC Sky Survey (on film). The library catalogue includes books, conference proceedings, periodicals, and theses, in print and online as well.

7.3 Vocational Training and Education

Our **education workshop for apprentices** in the mechanical area of MPE provides apprenticeship training positions. Eight trainees can be educated in a two or three years process for being an industrial mechanics. Occasionally students join the workshop for an internship, preparing for their professional career.

ing departments of the Institute. In the 2016-2018 time frame 39 refugees and migrants completed the courses successfully. They were nationals from Afghanistan, China, Ethiopia, Eritrea, Iraq, Lebanon, Sierra Leone, Somalia, Syria and Tanzania. Also a number of German high school and university students participated in the courses in the frame of required practical trainings or internships as part of their school or university education.

Another important field of education, where we, together with three other renowned scientific institutions located in the Munich-Garching area, support young people to promote their knowledge and careers is (see next page):



Fig. 7.3.1 Mechanical apprentices and their supervisors.

Since recent years, we also organize and conduct **vocational training courses for refugees** at the Institute on a regular basis. The technical courses are intended to provide vocational orientation and to support the professional education and integration in Germany. Most of the participants are young refugees seeking a practical training as part of their general school education. Each course covers a period of typically one to three weeks. The participants are acquainted with basic knowledge and skills in the areas of electrical engineering, electronics, programming, mechanical design and metalworking. The training activities are assisted by the electrical and mechanical workshops and the engineer-

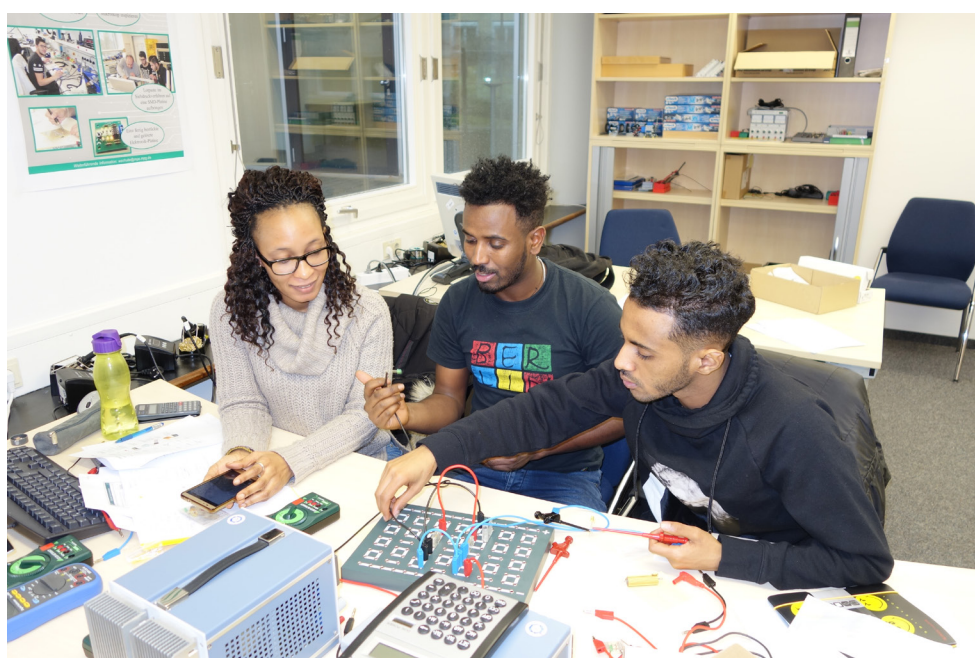


Fig. 7.3.2 Refugees doing an internship at MPE.

The International Max-Planck Research School (IMPRS) on Astrophysics at the Ludwig-Maximilians University of Munich

IMPRS is a graduate school offering a broad PhD program in astrophysics and cosmology. Open for students worldwide, the school provides a world-class teaching and research program with sufficient attraction to compete successfully with other well-known graduate schools. IMPRS comprises all Munich astrophysics institutes, i.e. MPE, MPA and the University Observatory of the Ludwig-Maximilians-University of Munich (USM). ESO participates as an associated partner.

The school was founded in 2001 and was successfully evaluated several times. Right now, it is funded by the

essential elements of astrophysics and cosmology. The joint education of all students in a well-defined set of courses also creates a well-developed esprit de corps throughout the whole student body and forges links that can support them throughout their careers.

There are less than a handful of such places worldwide that can compete in breadth and level of research with our participating institutes. The large number of active scientists who are involved in IMPRS teaching and student supervision guarantees that state-of-the-art knowledge is presented to the students.



Fig. 7.3.3 IMPRS students at the summer excursion 2018 to the Dornier Museum in Friedrichshafen.

341 students from 55 different countries applied for the IMPRS program 2019. In total, the school has received 3322 applications since 2001. Based on their excellence as proven by their university record, by letters of recommendation and by a successful interview during a three-day recruitment workshop in Garching, on average 25 applicants are offered a position every year. The acceptance rate is about 70%.

Since 2001 nearly 285 students finished successfully. Of them about 66% held a post-doc position, about 26% took a job in industry and about 8% started an academic career. We are in contact with the majority of previous IMPRS participants via our alumni program.

Max-Planck-Society (MPG) until September 2025. The MPG funding however, supports only a small minority of our students. The majority is funded through the IMPRS member institutions themselves, either via their own budgets or via external third-party funds.

The training program of our IMPRS is highly structured, aiming for a PhD at the end of three to four years. It is designed to attract young scientists with outstanding qualifications and is advertised worldwide. Coursework, research opportunities, evaluation and mentoring are all managed uniformly across the program, which aims for a broad understanding of the

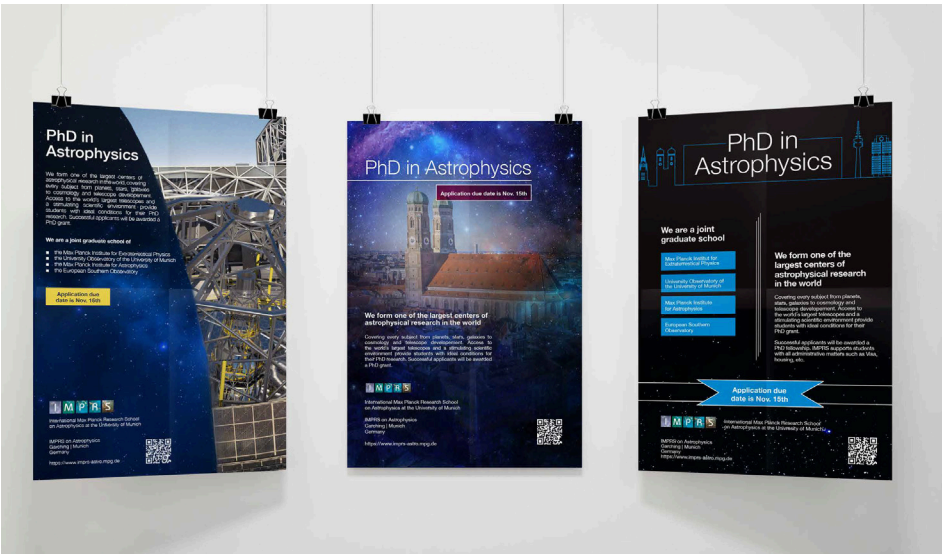


Fig. 7.3.4 Selection of IMPRS Posters used in recent years to advertise our IMPRS program worldwide.

7.4 Public Outreach

A modern technological society needs basic research for a successful future. As fundamental research is mainly funded by tax revenue, it is essential to report our work to and seek the support of the general public. Therefore our Institute actively communicates its activities and results to a broad audience, and makes the argument for science as an integrated and basic part of a vital and developing society, even if the benefits to an individual's daily life are not immediate and obvious.

The MPE public outreach team consists primarily of the press officer and the scientific secretary, who provide a direct link between the Institute and the public. This team, supported by a team assistant and by many MPE members organized several, quite different activities in and outside MPE during the past three years.

Every two years, the Institute actively participates in the **Open House** event on the Garching campus. In October 2017 MPE opened its doors for visitors to present its science as well as its instrumental and technological developments to the public. Popular attractions were as in previous years the public talks by MPE scientists on interesting astrophysical topics, from our solar system to black holes and the beginning of the universe; a tour through the whole institute, where groups and departments showcased their work; and the special children's programme **"Astronomy for Kids"**, where many MPE volunteers prepared attractions such as hands-on experiments, puzzle rallies, and handcraft work. This programme at-

tracted children of all ages, with roughly 300 juniors joining in the activities, while during the whole day about 1800 people visited MPE.

Every year since 2008, the Institute participates in the nationwide **"Girls' Day"**. Sponsored by the European Union, the Federal Ministry of Education and Research



Fig. 7.4.2 Girls visiting a lecture at MPE at the Girls' Day 2018.

(BMBF) and the Federal Ministry for Families, Senior Citizen, Women and Young People (BMFSFJ) the yearly "Girls' Day" initiative has been established in Germany in 2001. Although on average girls do reach a higher level of education at school than their male peers, they still tend to choose traditional female fields of occupation. By providing girls, aged between 14 and 16 years with contact to professionals and an insight to modern working places in the area of technology, IT and natural sciences, it is often possible to catch their interest and encourage them into these fields. 40 to 50 girls visited MPE each year in 2016/17/18 on this day, to learn more about work in astronomy, MPE science, and different career paths in such an academic environment.



Fig. 7.4.1 Impression from the Open House 2017.

The Max-Planck-Society celebrated three anniversaries in 2018: the 70th anniversary of its foundation, the 160th birthday of Max Planck, and the 100th anniversary of Max Planck receiving the Nobel Prize. These anniversaries were celebrated nation-wide by a **"Max-Planck-Day"** in September 2018 with public outreach activities all over Germany. MPE supported



25 to 30 groups per year) and it can be really challenging to meet the requirements of the different visitors as the groups can be as diverse as e.g. high school and university students, senior citizens, interested hobby astronomers or even colleagues from other scientific institutions.

We also support **guided tours in the cosmology exhibition** “Evolution of the Universe” in the “Deutsches Museum” in downtown Munich. This exhibition was designed in the framework of the International Year of Astronomy in 2009 by five astronomical institutes of the Munich area, among them MPE, and – apart from being open for the public - is now regularly used for lectures and guided tours.

Fig. 7.4.3 The MPE exhibition tent in downtown Munich during the Max-Planck-Day 2018.

this “Max-Planck-Day” by contributing to the “Science Marketplace” in downtown Munich. In particular, MPE presented models of the X-ray satellite eROSITA and the optical to near-infrared satellite EUCLID in an exhibition and a PhD student participated in the programme on the central stage with a short presentation. The 66 events in 35 cities all over Germany attracted more than 22.000 visitors.

In addition to such special events and the preparation of singular documents like brochures and flyers, the MPE public outreach team regularly fulfills a number of tasks. MPE offers guided tours for groups through the Institute on request. The tours are available in German and English, as well as some other languages. After a general introduction, scientists of the various groups of the Institute will guide the visitors through their departments. This service is requested quite frequently (about

Together with four other astronomical institutes, MPE organises the monthly **Café & Cosmos** series of discussions. In a restaurant in downtown Munich a scientist briefly introduces an astronomical topic and then takes questions from the audience to discuss his or her current research. This event regularly attracts 80 scientifically interested people.

On a regular basis MPE scientists give **public talks/lectures** for a scientifically interested audience. MPE scientists are invited to e.g. planetariums, schools, or special events to provide their expertise. About 25 such talks/lectures are delivered every year.

MPE's website is regularly updated with research news as well as events like technical achievements or honorary awards. Each year about 20 to 30 new science results of MPE scientists are presented with an eye to the popular press. High-impact science results are issued as press releases, often in cooperation with other scientific institutes. MPE regularly receives journalist inquiries, which range from simple questions to large visits by TV film crews.

Finally, MPE offers the possibility for doing **internships** at the Institute, both for high school and university students. Every year about 10 to 15 high school students (1 to 2 weeks) and 5 to 10 university students (4 to 8 weeks) gain an inside-look at a scientific institute by participating under the supervision of a scientist in a small research project.



Fig. 7.4.4 Presentation of the X-ray exponents for highschool students during a guided tour.

7.5 Social Events

Getting to know one's colleagues not only through formal workplace interaction, but also from joint social activities, can help to form a positive atmosphere in the Institute. These activities help to link people from sometimes quite separate areas, but can also serve to inte-

ings, there is a common event organized during morning hours, which in 2018 was a guided tour through the central city of Augsburg, while the afternoon is „free“ for individual activities. The outing ended - also as usual - with a common dinner in the late afternoon before the buses started back to Garching.



Fig 7.5.1 MPE colleagues are visiting the "Goldene Saal" in Augsburg during the summer outing 2018.

Each year, a large MPE crowd spends a pleasant afternoon - and most also the evening - together at the famous **Munich Oktoberfest**. They may enjoy the fun rides as well as the entertainment in the outdoor festival area but also Bavarian sociability inside the "Wiesn Tents". Many colleagues dress up for this occasion in traditional Bavarian costumes. The unique atmosphere of eating, drinking and celebrating together is very favourable for deepening existing connections between MPE staff members, students and guests, as well as making new ones.

grate new MPE-members. Our social activities range from small group-internal celebrations (e.g. the success of a certain scientific project, a PhD defence, special birthdays etc.) to MPE-wide celebrations like the Christmas party and the three well-established annual trips: the skiing excursion, the summer works outing, and the visit to the Munich Oktoberfest in autumn.

For the **summer outing** in 2018, we visited Augsburg, a nearby Bavarian city. As the 3rd oldest German city, Augsburg was named after the Roman emperor Augustus and has a rich history. It offers many historic and cultural attractions, like the "Fuggerei", the oldest social housing complex in the world, or a number of cathedrals, basilicas and churches of different epochs. Equally prominent is the „Goldene Saal“ in the town hall. Usually in MPE's work out-



Fig 7.5.2 MPE members are enjoying the Oktoberfest atmosphere.